

EFFECTS OF WATER VAPOR ON THE OXIDATION BEHAVIOR OF ALUMINA AND
CHROMIA FORMING SUPERALLOYS AT TEMPERATURES BETWEEN 700°C AND
1000°C

by

Kivilcim Onal Hance

BS, Middle East Technical University, 1995

MS, Middle East Technical University, 1998

Submitted to the Graduate Faculty of

the School of Engineering in partial fulfillment

of the requirements for the degree of

Doctor of Philosophy

University of Pittsburgh

2005

UNIVERSITY OF PITTSBURGH
SCHOOL OF ENGINEERING

This dissertation was presented

by

Kivilcim Onal Hance

It was defended on

April 12, 2005

and approved by

J. L. Smialek, Research Engineer, NASA Glenn Research Center

N. G. Eror, Professor, Department of Materials Science and Engineering

J. A. Barnard, Professor, Department of Materials Science and Engineering

Dissertation Director: G. H. Meier, Professor, Department of Materials Science and Engineering

Dissertation Director: F. S. Pettit, Professor, Department of Materials Science and Engineering

EFFECTS OF WATER VAPOR ON THE OXIDATION BEHAVIOR OF ALUMINA AND
CHROMIA FORMING SUPERALLOYS AT TEMPERATURES BETWEEN 700°C AND
1000°C

Kivilcim Onal Hance, PhD

University of Pittsburgh, 2005

Several superalloys and Ni-Cr alloys were tested at temperatures between 700°C and 1000°C in dry air and in air/H₂O mixtures, whereby the effects of water vapor on the formation of alumina and chromia scales were investigated. The experimental parameters included temperature of testing, composition of the reactive gases, thermal cycling and the composition of the underlying alloy.

Water vapor affected the oxidation characteristics of alumina and chromia in different ways. Selective oxidation of Al was not favored in air/H₂O mixtures and at low reaction temperatures. The alloy composition was critical in developing and maintaining continuous protective scales. For alumina-forming systems, higher Al and Cr contents were found to be beneficial for improved resistance against attack. Significant additions of Hf to the alloys resulted in accelerated internal oxidation at 1000°C. Transient oxidation was more profound in air/H₂O mixtures in comparison to dry air. The adherence of scales was adversely affected by water vapor at 1000°C.

Water vapor did not affect the selective oxidation of Cr. The major impact of H₂O on chromia scales was the accelerated formation of volatile Cr-species which makes the underlying alloy more vulnerable to attack by reactive gases. These reactions were not significant in dry air at 900°C and below. The transient oxidation was not adversely affected by water vapor on Ni-Cr systems. The scale spallation was more profound in dry air. The study showed that the main

degradation mechanism for chromia in wet air was the formation of vapor Cr species. On the contrary, scale spallation was more detrimental in dry air. Additions of the reactive element Ce improved the adherence of chromia scales in dry air as well as in wet air. Ce furthermore decreased the formation rate of chromia in dry air. It was not clear if the element had the same effect in air/H₂O. The presence of water vapor affected the morphology of chromia scales.

The thin external TiO₂ that developed over chromia on IN 738 was found to be beneficial as it reduced the vaporization of chromia. This indicated that the oxidation resistance of chromia formers can be improved by alloying with elements that would diffuse to the oxide/gas interface and develop an external scale, or by applying an appropriate coating.

TABLE OF CONTENTS

ACKNOWLEDGMENTS	xxv
1.0 INTRODUCTION	1
2.0 BACKGROUND	3
2.1 OXIDATION OF METALS	3
2.1.1 Initial Oxidation	4
2.1.2 Transport Mechanisms.....	6
2.1.3 Transient Oxidation	9
2.2 SELECTIVE OXIDATION.....	11
2.2.1 Factors that Affect Selective Oxidation.....	14
2.2.2 Selective Oxidation of Cr, Al and Their Alloys	15
2.3 COMPARISON OF ISOTHERMAL AND CYCLIC OXIDATION CONDITIONS AND THE RESULTING EFFECTS	21
2.4 FACTORS AFFECTING ADHERENCE OF OXIDE LAYERS	22
2.4.1 Reactive Element Effect	23
2.4.2 Sulfur Effect.....	27
2.4.3 Other Factors.....	29
2.5 EFFECTS OF WATER VAPOR ON OXIDATION.....	30
2.6 VOLATILIZATION OF CHROMIA.....	35
3.0 RESEARCH APPROACH	44
4.0 EXPERIMENTAL DETAILS	49

5.0	RESULTS-PART I	54
5.1	SUPERALLOYS THAT ARE CLASSIFIED AS ALUMINA FORMERS	54
5.1.1	Alumina Formers Cyclically Exposed in Dry Air and in Air/Water Vapor Mixtures with $\text{PH}_2\text{O} = 0.3$ atm at a Total Pressure of 1 atm.	54
5.1.1.1	Alumina Formers at 700°C	54
5.1.1.2	Alumina Formers at 900°C	67
5.1.1.3	Alumina Formers at 1000°C	81
5.1.2	Isothermal Exposures of Alumina Formers	99
5.1.2.1	Isothermal Exposures at 700°C	102
5.1.2.2	Isothermal Exposures at 900°C.....	107
5.1.3	Effect of Surface Finish	119
5.2	SUPERALLOYS THAT ARE CLASSIFIED AS CHROMIA FORMERS	120
5.2.1	Chromia Formers Cyclically Exposed in Dry Air and in Air/Water Vapor Mixtures with $\text{PH}_2\text{O} = 0.3$ atm, at a total pressure of 1 atm.....	120
5.2.1.1	Chromia Formers at 700°C	129
5.2.1.2	Chromia Formers at 900°C	130
5.2.1.3	Chromia Formers at 1000°C	135
5.2.2	Comparison of Isothermal Tests to Cyclic Tests	137
5.2.2.1	Tests at 700°C	138
5.2.2.2	Tests at 900°C	139
5.2.3	Effect of Surface Finish	141
6.0	RESULTS PART II	159
6.1	TESTS WITH MODEL ALLOYS	159

6.1.1	Cyclic Tests with Ni-Cr Model Alloys	160
6.1.1.1	Cyclic Tests at 700°C	161
6.1.1.2	Cyclic Tests at 900°C	182
6.1.2	Isothermal tests with Ni-Cr Model Alloys.....	208
6.1.2.1	Isothermal Tests at 900°C.....	209
6.1.2.2	Isothermal Tests at 700°C.....	216
6.2	ISOTHERMAL TESTS WITH OTHER SYSTEMS	217
6.2.1	Isothermal Tests with IN 738 and X-40.....	217
6.2.2	Isothermal Tests with Ni (99.999%).....	220
6.3	FLAKEY-CHROMIA FORMATION IN AIR/WATER-VAPOR MIXTURES	242
7.0	SUMMARY AND DISCUSSION OF RESULTS	248
7.1	ALUMINA FORMATION ON COMPLEX ALLOYS	248
7.1.1	Some Highlights on Selective Oxidation of Al.....	252
7.2	CHROMIA FORMATION.....	254
7.2.1	Chromia Formation on Model Alloys.....	254
7.2.2	Chromia Formation on Complex Superalloys	258
7.2.3	Some Highlights on Chromia Formation.....	261
8.0	CONCLUSIONS.....	269
	BIBLIOGRAPHY.....	273

LIST OF TABLES

Table 3.1: Chemical Compositions of the Superalloys in Weight Percent.....	47
Table 3.2: List of Ni-Cr alloys shows the test conditions and the information expected from each test.	48
Table 5.1: Linear thermal expansion coefficients of select metals and their oxides, [3]......	101

LIST OF FIGURES

Figure 2.1: Simple schematic showing the cross-section of an oxidized sample.	5
Figure 2.2: Schematic showing various stages of oxidation on alloys that develop protective scales.	5
Figure 2.3: The growth rates of most commonly encountered oxides are shown as a function of temperature [3].	13
Figure 2.4: Ellingham diagram showing the relative stabilities of selected oxides.	17
Figure 2.5: Oxide maps of Ni-Cr-Al system at (a)1000°C, (b) 1100°C, and (c) 1200°C developed by Giggins and Pettit [23].	20
Figure 2.6: The equilibrium pressure of the major vapor species over alumina is plotted as a function of temperature (a) in Ar/O ₂ , and (b) in Ar/H ₂ O, [67].	37
Figure 2.7: Partial pressures of vapor Cr-oxides over Cr ₂ O _{3(s)} in air (PO ₂ = 0.21 atm) as a function of time, [65].	39
Figure 2.8: Partial pressures of most abundant Cr containing species over Cr ₂ O _{3(s)} in humid air at different temperatures (PO ₂ = 0.21 atm, PH ₂ O = 0.02 atm), [65].	40
Figure 2.9: Volatile species of the W-O system are shown at 1250K, [3].	43
Figure 4.1: Schematic diagram showing the horizontal tube furnaces used for thermal cycling tests in flowing gases with defined and controlled amounts of water vapor in dry air at a total pressure of 1 atm. Arrows show directions of gas flow. The specimens are hung on silica rods with platinum wires, and are cycled in and out of the hot zone at defined time intervals.	52
Figure 4.2: Schematic diagram showing the apparatus to isothermally oxidize coupon specimens in flowing gases with defined and controlled amounts of water vapor in dry air at a total pressure of 1 atm. Arrows show directions of gas flow. The air flow in the upper region of the reaction tube is to prevent water vapor condensation in the balance area.	53
Figure 5.1: Kinetic plot of the alloy René N5 showing the weight change of the specimens in dry air and in air/H ₂ O mixtures at 700°C as a function of cycle number.	55

Figure 5.2: René N5 at 700°C after cyclic exposures in dry air at 700°C for 3200 cycles. Micrograph shows the cross-section of the sample.	55
Figure 5.3: Back scattered electron images of René N5 showing the sample cross-section after 3200 cycles at 700°C in wet air (a) protrusions of chromia/alumina, (b) islands of Ta-oxide with alumina.....	56
Figure 5.4: SEM images of René N5 showing the microstructure of the alloy in its as-processed condition.	58
Figure 5.5: Kinetic plot of the alloy PWA 1484 showing the weight change of the specimens in dry air and in air/H ₂ O mixtures at 700°C as a function of cycle number.	58
Figure 5.6: SEM images of PWA 1484 showing the cross-section of the oxide scale that formed at 700°C after 3200 cycles (a) in dry air, and (b) in wet air.	59
Figure 5.7: Kinetic plot of the alloy CM 186 showing the weight changes of the specimens in dry air and in air/H ₂ O mixtures at 700°C as a function of cycle number.	60
Figure 5.8: (a) Cross-section of CM 186 at 700°C after 3200 cycles in wet air. Protrusions of transient oxide developed at the specimen surface. (b) Same alloy exposed to dry air at 700°C for 3200 cycles in dry air. (c) Scale that developed in dry air shown at higher magnification.	62
Figure 5.9: Kinetic plot of the alloy MarM 247 showing the weight changes of the specimens in dry air and in air/H ₂ O mixtures at 700°C as a function of cycle number.	63
Figure 5.10: Back scattered electron image of MarM 247 exposed at 700°C. (a) The cross-section of the specimen subjected to cyclic testing for 3200 hours in dry air. (b) Micrograph shows the scale that developed in wet air after 3200 hours of cycling.....	64
Figure 5.11: An oxide map of the Ni-Cr-Al system developed by Giggins and Pettit, [23], showing the regions for continuous formation of the oxides alumina (Region III), chromia (Region II), and non-protective NiO (Region I) at 1000°C. The alloy systems under investigation are marked on this map to show their relative positions.	66
Figure 5.12: Kinetic plot of the alloy René N5 showing the weight change of the specimens in dry air and in air/H ₂ O mixtures at 900°C as a function of cycle number.	68
Figure 5.13: René N5 at 900°C exposed to dry air for 3200 cycles. A duplex scale developed on the specimen surface that consisted of a complex oxide of Cr, Ni and Al at the scale/gas interface, and the slow growing alumina at the matrix/scale interface.....	70
Figure 5.14: SEM image of René N5 showing the scale that formed at 900°C after exposing the alloy to air/H ₂ O mixtures for 3200 cycles.	70

Figure 5.15: Kinetic plot of the alloy PWA 1484 showing the weight change of the specimens in dry air and in air/H ₂ O mixtures at 900°C as a function of cycle number.	71
Figure 5.16: Image shows PWA 1484 at 900°C after tests in wet air for 3200 hours of cyclic exposures.....	72
Figure 5.17: Back scattered electron image of the alloy PWA 1484 showing the oxide layer that formed at 900°C in dry air after 3200 hours of cyclic testing.	72
Figure 5.18: Kinetic plot of the alloy CM 186 showing the weight changes of the specimens in dry air and in air/H ₂ O mixtures at 900°C as a function of cycle number.	74
Figure 5.19: Image of CM 186 showing the alloy after testing at 900°C in air/H ₂ O mixtures for 3200 hours cyclically.	76
Figure 5.20: Back scattered electron image shows the reaction zone that formed on the surface of the alloy CM 186 after experiments at 900°C in dry air. The specimen was subjected to thermal cycling for 3200 hours.	76
Figure 5.21: MarM 247 at 900°C in dry air after 3200 cycles. A thin scale developed on the specimen surface. Oxide protrusions were spotted in some parts along the scale.....	77
Figure 5.22: MarM 247 at 900°C in wet air after 3200 hours of cyclic exposures. The SEM image shows the cross-section of the scale formed on the specimen. An Al-rich scale developed under the testing conditions. Some oxide protrusions with internal alumina were also evident.	78
Figure 5.23: Kinetic plot of the alloy MarM 247 showing the weight changes of the specimens in dry air and in air/H ₂ O mixtures at 900°C as a function of cycle number.	80
Figure 5.24: Kinetic plot of the alloy PWA 1484 showing the weight change of the specimens in dry air and in air/H ₂ O mixtures at 1000°C as a function of cycle number.	82
Figure 5.25: Kinetic plot of the alloy René N5 showing the weight change of the specimens in dry air and in air/H ₂ O mixtures at 1000°C as a function of cycle number.	82
Figure 5.26: PWA 1484 at 1000°C after cyclic exposures for 2435 hours (a) in dry, and (b) in air/H ₂ O mixtures. The back scattered electron images show the spalled areas on specimen surfaces at low magnification. More spalling of oxides occurred after wet tests.	83
Figure 5.27: René N5 at 1000°C after cyclic exposures for 2435 hours (a) in dry air, and (b) in air/H ₂ O mixtures. Images show the spalled areas on specimen surfaces at low magnification.	84

Figure 5.28: (a) PWA 1484 at 1000°C in dry air after 2435 cycles, and (b) René N5 at 1000°C in dry air after 2435 cycles. The surface images of the samples show parts of the scale where spallation occurred. 85

Figure 5.29: Cross-sectional SEM images of René N5 at 1000°C in dry air after 2435 cycles showing (a) the continuous dual scale that developed along the surface of the sample, and (b) the oxide protrusions. 86

Figure 5.30: Cross-sectional SEM images of René N5 at 1000°C in wet air after 2435 cycles. (a) The micrograph shows part of the scale where complex transient oxides developed above the alumina. (b) The image shows formation of the nitride phase (AlN) in the depleted zone. This phase preferentially precipitated below oxide intrusion. However, it is present in other parts of the depleted zone too. 87

Figure 5.31: SEM images of PWA 1484 at 1000°C in dry air after 2435 cycles. (a) A thin layer of oxide developed along the sample surface. Formation of oxide protrusions interrupted the continuity of this thin layer with better protective properties. (b) The micrograph shows the thin protective scale at higher magnification. (c) AlN was also observed to form, preferentially below the oxide protrusions. The image shows such an area at high magnification. 90

Figure 5.32: SEM images of PWA 1484 at 1000°C after exposures in wet air. (a) A scale with substantial amounts of transient oxides covered the surface of the alloy. The transient oxide layer consisted of NiO at the scale/gas interface, a layer of reactive-element oxides, and complex (Ni,Cr,Al,Co)-oxides. Protective alumina scale formed at the substrate/oxide interface. The continuity of the scale was disrupted by scale spallations, which gave rise to formation of oxide protrusions. (b) SEM image shows the nitride phases that developed in the depleted zone at high magnification. 91

Figure 5.33: Kinetic plot of the alloy CM 186 showing the weight changes of the specimens in dry air and in air/H₂O mixtures at 1000°C as a function of cycle number. 92

Figure 5.34: Kinetic plot of the alloy MarM 247 showing the weight changes of the specimens in dry air and in air/H₂O mixtures at 1000°C as a function of cycle number. 92

Figure 5.35: Surface micrographs of CM 186 showing the oxide scale at 1000°C (a) in wet air, and (b) in dry air after 2435 cycles. 94

Figure 5.36: SEM images showing the surface of samples prepared from the alloy MarM 247 after 2435 hours of cyclic exposures at 1000°C (a) in dry air, (b-c) in wet air. 96

Figure 5.37: Cross-section of CM 186 at 1000°C after 2435 cycles. (a) Image shows the scale that formed in dry air. (b) SEM micrograph of CM 186 in wet air. 97

- Figure 5.38: SEM image showing MarM 247 at 1000°C after 2435 cycles. A zone of internal oxides developed after exposures. (a) Cross-section of the scale that developed in dry air. (b) MarM 247 in wet air. Image shows the zone of HfO₂ coated with alumina. 98
- Figure 5.39: Surface images of CM 186 at 700°C. (a) EDX analysis showed that mixed oxides formed on the alloy after exposing the system to high pressure steam after 4320 hours. (b) Cyclic exposures to air/water vapor mixtures at ambient caused formation of large NiO islands over mixed oxides (3200 cycles). 103
- Figure 5.40: SEM micrographs showing the cross-section of CM 186 at 700°C. (a) Specimen isothermally exposed to high pressure steam in an autoclave for 4320 hours. (b) The scale that developed after cyclic exposures in wet air at ambient pressure after 3200 cycles..... 104
- Figure 5.41: PWA 1484 at 700°C. Micrographs show the cross-section of the scale the system developed at this temperature. (a) Isothermal tests in steam at high pressure for 4320 hours resulted in the formation of a thin scale on the surface of the specimen. (b) A thick multi-layered scale of transient oxides formed after cyclic tests in wet air for 3200 hours. 105
- Figure 5.42: PWA 1484 at 700°C. (a) Isothermal tests in high pressure steam for 4320 hours caused formation of a thin layer of mixed oxides that covered the whole surface area of the specimen. (b) The micrograph shows the scale that formed after cyclic tests in wet air at 1 atm total pressure with P(H₂O) = 0.3 atm after 3200 cycles. The major part of the scale was covered by a continuous and thick layer of (Ni,Co)-oxide. In very limited parts of the scale, non-continuous islands of NiO were detected. 106
- Figure 5.43: MarM 247 at 700°C. (a) The image shows the cross-section of the scale that formed on the specimen after exposure to high pressure steam isothermally for 4320 hours. (b) Same alloy after cyclic exposures in air/H₂O mixtures at a total pressure of 1 atm, where P(H₂O) = 0.3 atm. 109
- Figure 5.44: Surface images of CM 186 at 900°C after isothermal tests (a) in air/H₂O for 2400 hours at 1 atm total pressure [P(H₂O) = 0.3 atm.], and (b) in high pressure steam for 4320 hours..... 110
- Figure 5.45: CM 186 at 900°C. (a) Cross-sectional image showing the scale that formed after isothermal steam tests for 4320 hours. (b) Scale that formed on the specimen surface after isothermal tests in wet air where P_{total} = 1 atm for 2400 hours. 111
- Figure 5.46: MarM 247 at 900°C after isothermal tests at high pressure in 100% steam. A Cr-rich scale covered the surface of the specimen. Some NiO islands with underlying Co-oxide were spotted along the surface on some limited locations..... 112
- Figure 5.47: MarM 247 at 900°C after isothermal tests at high pressure in 100% steam. The image shows the cross-section of the reaction zone. Internally formed alumina was detected below the external scale. 112

Figure 5.48: MarM 247 at 900°C isothermally exposed to air/H₂O mixtures at P_{total} = 1 atm (PH₂O = 0.3 atm). Micrographs show the cross-section of the scale. The alloy developed an Al-rich thin dual layer along the surface with a slow growth rate. However, many locations with oxide protrusions were present on the surface too. These locations were the areas where the system could not form the oxide with better protective properties. Instead, faster growing phases developed. 113

Figure 5.49: MarM 247 at 900°C cyclically exposed to hot gases at atmospheric pressure (a) in wet air, and (b) in dry air. The back scattered electron images show the cross-section of the oxide scale..... 114

Figure 5.50: Cross-section of PWA 1484 isothermally exposed to wet air at 900°C, Ptotal=1 atm. 116

Figure 5.51: SEM images of PWA 1484 showing the specimen cross-sections after tests at 900°C. The testing conditions for each sample were (a) isothermal in 100% steam at high pressure for 4320 hours, (b) isothermal in wet air at ambient pressure for 2400 hours (equivalent to 3200 cyclic hours), and (c) cyclic in wet air at ambient pressure for 3200 cycles..... 117

Figure 5.52: Surface images of PWA 1484 at 900°C showing the external oxide scale that formed after (a) and (b) isothermal exposures in high pressure steam and in wet air at ambient pressure respectively, (c) cyclic exposures at atmospheric pressure in air/H₂O mixtures..... 118

Figure 5.53: SEM micrographs of PWA 1484 at 700°C after exposures in wet air (a) for 1 hr, (b) for 2 hours, and (c) for 4 hour. The sample surfaces were polished down to 0.05 micron alumina..... 121

Figure 5.54: SEM images of PWA 1484 at 700°C after exposing the alloy to wet air, (a) for 1 hr, (b) for 2 hours, and (c) for 4 hours. The surfaces were ground down to 600-grit with abrasive paper. 122

Figure 5.55: SEM micrographs of PWA 1484 showing the cross-section of the oxidation zone at 700°C in dry air (a) after 1 hr, (b) after 2 hours, (c) after 4 hours. The surfaces of the alloy were polished down to 0.05 micron alumina. 123

Figure 5.56: SEM images of PWA 1484 showing the scale that formed at 700°C in dry air after (a) 1 hr, (b) 2 hours, and (c) 4 hours. Sample surfaces were ground down to 600 grade abrasive paper prior to testing exposure. 124

Figure 5.57: SEM image of René N5 that shows the cross-section of the scale at 900°C after 4 hours of isothermal exposures in dry air. (a) The surface of the sample was ground down to 600-grade SiC abrasive paper. (b) Pre-exposed surface was polished with 0.05 micron alumina..... 125

Figure 5.58: SEM images of René N5 at 900°C in wet air after 4 hours. Micrographs show the cross-section of the scale. (a) Sample surface was ground with abrasive paper down to 600 grade before exposure. (b) Sample surface was polished with 0.05 micron alumina prior to exposure.	126
Figure 5.59: René N5 at 700°C in dry air after 4 hours of isothermal testing. SEM images show the scale in cross-section. (a) Surface finish of the unexposed sample was 600-grade abrasive paper. (b) The surface of the alloy was polished with 0.05 micron alumina prior to testing.	127
Figure 5.60: SEM micrographs showing René N5 at 700°C in wet air after 4 hours of isothermal exposure. (a) Surface finish was 600-grade SiC abrasive paper. (b) Polishing the surface with 0.05 micron alumina increased the oxygen diffusion rate remarkably.	128
Figure 5.61: IN 738 at 700°C (a) in dry air, and (b) in wet air after 2520 hours of cyclic testing.	131
Figure 5.62: Kinetic plot of the alloy IN 738 showing the weight changes of the specimens in dry air and in air/H ₂ O mixtures at 700°C as a function of cycle number.	132
Figure 5.63: Kinetic plot of the alloy X-40 showing the weight changes of the specimens in dry air and in air/H ₂ O mixtures at 700°C as a function of cycle number.	132
Figure 5.64: X-40 at 700°C (a) in dry air, and (b) in wet air. Similar scales formed in both environments. The oxide layer was identified as chromia.	133
Figure 5.65: Kinetic plot of the alloy IN 738 showing the weight changes of the specimens in dry air and in air/H ₂ O mixtures at 900°C as a function of cycle number.	142
Figure 5.66: IN 738 at 900°C after cyclic exposures for 2520 hours (a) in dry air, and (b) in wet air, (c) TiN formed in the depleted zone in dry as well as in wet air. The micrograph shown displays the formation of the phase for the dry-exposed specimen.	144
Figure 5.67: Kinetic plot of the alloy X-40 showing the weight changes of the specimens in dry air and in air/H ₂ O mixtures at 900°C as a function of cycle number.	144
Figure 5.68: SEM images of X-40 at 900°C after exposures to hot gases for 2050 hours. (a) Substantial scale spallation occurred in dry air. (b) Micrograph shows the oxide layer that formed in air/water vapor mixtures at atmospheric pressure.	145
Figure 5.69: X-40 at 900°C after 4250 hours of cyclic testing. (a) Image shows the cross-section of the specimen exposed to dry air at low magnification. (b) Same alloy after tests in wet air. (c) Cross-section of X-40 at 900°C in wet air after 4250 cycles shown at higher magnification. Alloy lost its protectiveness. Co-oxide developed at the top of the scale. (d) Cross-section of X-40 at 900°C in dry air after 4250 cycles shown at higher magnification.	147

Figure 5.70: Kinetic plot of the alloy X-40 showing the weight changes of the specimens in dry air and in air/H ₂ O mixtures at 1000°C as a function of cycle number.	148
Figure 5.71: X-40 at 1000°C in wet air after 615 cycles. (a) The micrograph shows the scale that formed on the specimen surface in dry air at a low magnification. (b) The image shows the reaction zone that developed after tests in air/H ₂ O mixtures.....	149
Figure 5.72: X-40 at 1000°C after cyclic exposures in hot gases for 615 hours. (a) The SEM image shows the cross-section of the specimen exposed to dry air. (b) Micrograph showing the scale that formed after tests in wet.....	150
Figure 5.73: Kinetic plot of the alloy IN 738 showing the weight changes of the specimens in dry air and in air/H ₂ O mixtures at 1000°C as a function of cycle number.	151
Figure 5.74: IN 738 at 1000°C after 500 cycles. (a) SEM image shows the cross-section of the sample exposed to wet air at low magnification. (b) Specimen cross-section after tests in dry air. (c) Micrograph shows a pore with internally formed oxide around its periphery in wet air.....	153
Figure 5.75: SEM images showing the oxide scales that formed on IN 738 at 700°C. (a) Image shows the reaction zone after exposing the alloy to high pressure steam isothermally for 4320 hours. (b) The oxide layer that formed in air/H ₂ O mixtures atmospheric pressure after cyclic tests for 2520 hours.....	154
Figure 5.76: Back scattered electron image shows X-40 at 700°C. (a) Alloy was subjected to isothermal tests in high pressure steam for 4320 hours. (b) Same system after cyclic tests in wet air for 3200 hours.....	155
Figure 5.77: SEM images of IN 738 at 900°C. (a) Specimen tested isothermally in high pressure steam for 4320 hours. A dense chromia scale developed on the surface. TiO ₂ formed a thin external layer. (b) Same alloy tested isothermally in air/H ₂ O mixtures at atmospheric pressure for 4320 hours. (c) Image shows the scale that formed after cyclic tests in wet air at ambient pressure after 2520 cycles.....	156
Figure 5.78: Back scattered electron images of X-40 at 900°C after isothermal tests. (a) Cross-section of the scale that formed in pure steam environment at high pressure. (b-c) Scale that developed in wet air at ambient pressure. All specimens were tested for 4320 hours.	158
Figure 6.1: Kinetic plot of Ni-Cr alloys cyclically exposed to dry air at 700°C at a total pressure of 1 atm. The diagram shows differences in weight gains for different alloy compositions.	162
Figure 6.2: Kinetic plot of Ni-Cr alloys cyclically exposed to wet air at 700°C, where P(H ₂ O) = 0.1 atm and P _{total} = 1 atm. The diagram shows differences in weight gains for different alloy compositions.	162

Figure 6.3: SEM image shows surface of Ni-15Cr at 700°C after tests in dry air. Lighter-colored grains were the areas where NiO formed as an external scale. The darker colored grains were where chromia developed.	163
Figure 6.4: Image shows the formation of NiO islands on Ni-15Cr at 700°C in dry air where chromia formed as the primary oxide. These areas were defined as the darker colored grains in Figure 6.3,	163
Figure 6.5: SEM image showing the cross-section of the scale that developed over Ni-15Cr in dry air at 700°C after 240 cycles. (a) Chromia scale (b) Transient oxidation.	164
Figure 6.6: Ni-15Cr at 700°C after cyclic tests in wet air. The specimen was subjected to thermal cycling for 240 hours.	165
Figure 6.7: SEM image of Ni-15Cr showing the scale in cross-section that developed at 700°C after cyclic tests in wet air for 240 cyclic hours.	166
Figure 6.8: Low-magnification SEM image of Ni-15Cr-0.1Ce showing the NiO (light-colored) and chromia formation over the surface at 700°C after exposing the alloy to dry (a) for 240 cycles, and (b) for 700 cycles.	168
Figure 6.9: Ni-15Cr0.1Ce at 700°C in dry air (a-c) after 240 hours of cyclic testing, and (b-d) after 700 hours of cyclic testing. (a-b) NiO, (c-d) Chromia.	169
Figure 6.10: Back-scattered electron image of Ni15Cr0.1Ce showing the cross-section of the scale that formed at 700°C in dry air after 700 cycles. (a) Continuous chromia, (b) Transient oxides.	170
Figure 6.11: Back-scattered SEM image of Ni-15Cr-0.1Ce at 700°C after 240 cycles in wet air. Micrographs show the surface of the oxide scale that developed.....	171
Figure 6.12: SEM image of Ni-15Cr-0.1Ce showing the oxide layer that developed at 700°C in wet air after 700 cycles in cross-section.	171
Figure 6.13: Back-scattered electron images show the surface of the Ni-20Cr specimen after cyclic tests in dry air at 700°C. (a) Ni-20Cr at 700°C after 240 cycles, and (b) Ni-20Cr at 700°C after 700 cycles in dry air.	173
Figure 6.14: Cross-section of Ni-20Cr at 700°C after 700 cycles in dry air (a) Chromia scale (b-c) transient oxides.	174
Figure 6.15: Ni-20Cr in wet air at 700°C after 240 cycles.	175
Figure 6.16: SEM image of Ni-20Cr at 700°C in wet air after 700 cycles. Micrograph shows the cross-section of the specimen.	175

Figure 6.17: Ni-30Cr at 700°C in dry air after 240 cycles. (a) Micrograph shows the chromia that developed over the specimen surface. (b) Back scattered electron image showing the cross-section of the chromia scale. The oxide/alloy interface was observed to be flat. 178

Figure 6.18: SEM image shows Ni-30Cr at 700°C in wet air after 240 cycles. (a) The surface image of the scale. Flakey Cr₂O₃ crystals developed over the continuous chromia layer. (b) Micrograph shows the oxide layer in cross-section. 179

Figure 6.19: Ni30Cr0.1Ce in dry air at 700°C after 240 cycles. (a) Topographic image of the oxide layer. (b) Cross-section of the specimen showing the mono-layered chromia. 180

Figure 6.20: Ni-30Cr-0.1Ce at 700°C in wet air after cyclic tests for 240 hours. (a) Image shows the surface of the chromia layer that developed on the specimen. (b) Cross-sectional micrograph of the specimen. 181

Figure 6.21: The weight changes of Ni-Cr alloys at 900°C in dry air are plotted as a function of cycle number (a) on a large scale, and (b) on a smaller scale to show the details. 183

Figure 6.22: The weight changes of Ni-Cr alloys at 900°C in wet air are shown as a function of cycle number. Each cycle was a 1 hour period with 45 minutes in the hot zone and 15 minutes in the cool zone of the furnace. 184

Figure 6.23: Secondary electron images show the surface of Ni-15Cr after cyclic tests in dry air at 900°C (a) for 124 hours, and (b) for 240 hours. 184

Figure 6.24: Back scattered electron images of the scale cross-section that developed on Ni-15Cr at 900°C in dry air after cyclic tests for 240 hours. 185

Figure 6.25: Secondary electron images show the surface of Ni-15Cr after cyclic tests in wet air at 900°C (a) for 206 hours, and (b) for 650 hours. 186

Figure 6.26: Back scattered electron images of the scale cross-section that developed on Ni-15Cr at 900°C in wet air after cyclic tests for 350 hours. 187

Figure 6.27: In wet air, fast diffusion of Cr through the grain boundaries results in the formation of Cr₂O₃ at and around the boundary. Chromia grows laterally and eventually develops a continuous layer at the substrate/oxide interface. In dry air, although Cr diffuses through the grain boundaries, it can not develop continuity. Instead, it forms as an internal oxide. 189

Figure 6.28: Ni-15Cr-0.1Ce at 900°C in dry air after 124 cycles. Image shows the surface of the alloy. Chromia was the main oxide phase that developed on the alloy surface. However, formation of NiO was also observed. 189

Figure 6.29: Ni-15Cr-0.1Ce at 900°C in dry (a) after 500 cycles, and (b) after 1000 cycles. Images show formation of NiO blisters over chromia. In time their size and number increased. Note that the scales for each micrograph are different.	190
Figure 6.30: Ni-15Cr-0.1Ce at 900°C in dry air after 1000 cycles.....	190
Figure 6.31: Ni-15Cr-0.1Ce in wet air after 206 cycles at 900°C.	191
Figure 6.32: Ni-15Cr 0.1Ce at 900°C in wet air after 700 cycles.....	191
Figure 6.33: Ni-15Cr-0.1Ce in wet air at 900°C after 700 cycles.	192
Figure 6.34: Ni-20Cr at 900°C in dry air (a) after 124 cycles, and (b) after 500 cycles.	192
Figure 6.35: Ni-20Cr in dry air at 900°C.....	193
Figure 6.36: Ni-20Cr at 900°C in dry air after 1000 cycles.	193
Figure 6.37: Ni-20Cr in wet air at 900°C (a) after 100 cycles, (b) after 200 cycles. Lighter colored areas are where NiO developed. Darker colored oxide was chromia. NiO did not spread over the surface with continued exposures.....	195
Figure 6.38: Ni-20Cr in wet air at 900°C 165 cycles.	195
Figure 6.39: Ni-20Cr at 900°C in wet air after 700 cycles.....	196
Figure 6.40: Ni-30Cr-0.1Ce at 900°C in dry air after (a) 99 cycles, and (b) 224 cycles. Scale spallation was evident, which became more pronounced with longer exposure times.	197
Figure 6.41: Ni-30Cr-0.1Ce at 900°C in dry air after 224 cycles. Image shows formation of NiO as small islands. Scale spallation is also evident in the micrograph.....	197
Figure 6.42: Secondary electron images of the alloy Ni-30Cr-0.1Ce at 900°C in dry air after 1210 cycles.....	198
Figure 6.43: Ni-30Cr-0.1Ce at 900°C in dry air (a) after 224 cycles, and (b) after 1210 cycles.	200
Figure 6.44: The kinetic data of the alloys Ni-30Cr and Ni-30Cr-0.1Ce at 900°C in dry and wet air.	201
Figure 6.45: Ni-30Cr-0.1Ce at 900°C in wet air (a) after 99 cycles, (b) after 224 cycles, and (c) after 500 cycles.	202
Figure 6.46: Images show the surface of the oxide scale that developed on Ni-30Cr-0.1Ce at 900°C in wet air (a) after 44 cycles, and (b) after 700 cycles.....	203

Figure 6.47: Cross-sectional images of Ni-30Cr-0.1Ce at 900°C (a) after 224 cycles, and (b) after 700 cycles in wet air.	204
Figure 6.48: SEM images show the oxide surfaces that developed on Ni-30Cr in dry air at 900°C after (a) 99, (b) 224, and (c) 1210 cycles.....	205
Figure 6.49: Images show the cross-section of Ni-30Cr at 900°C in dry air after 224 cycles. ..	206
Figure 6.50: Cross-section of Ni-30Cr at 900°C in dry air after 1210 cycles.	207
Figure 6.51: Images show the oxide surface that developed over Ni-30Cr at 900°C in wet air after (a) 117 cycles, (b) 500 cycles, and (c) 700 cycles.....	210
Figure 6.52: Cross-section of Ni-30Cr at 900°C (a) after 224 cycles, and (b-c) after 700 cycles in wet air.....	211
Figure 6.53: (a) Kinetic plot of Ni-30Cr at 900°C in dry air shows the weight changes as a function of exposure time during isothermal testing. Tests were done in two different types of equipment. (b) The plot of weight change as a function of time on a log-log scale (c) Estimated weight change data for long term exposures plotted together with experimental data.....	222
Figure 6.54: The weight changes of Ni-30Cr and Ni-30Cr-0.1Ce after isothermal tests are compared to the same systems after cycling testing. All tests were done at 900°C in dry air.	223
Figure 6.55: The empirical weight change data of Ni-30Cr-0.1Ce at 900C in dry air was used to estimate the long term behavior of the system assuming the chromia growth obeys the parabolic rate law, and the vaporization is linear.	223
Figure 6.56: The TGA data of Ni-30Cr-(0.1Ce) at 900°C in wet air shows that the system(s) lose weight due to the formation of vapor species. (PH ₂ O = 0.1 atm, Ptotal = 1 atm).	224
Figure 6.57: The comparison of the weight changes during isothermal tests to cyclic experiments for Ni-30Cr system at 900°C in wet air shows that scale spallation is not very substantial. The weight losses originate essentially from the formation of vapor species.	224
Figure 6.58: The diagram shows the weight changes of Ni-30Cr and Ni-30Cr-0.1Ce at 900°C in wet air. The data obtained from TGA tests is compared to cyclic exposures and to isothermal tests using multiple specimens, each of which was exposed to wet air for a predetermined time in ceramic boats. Results show good agreement between isothermal boat tests and TGA. The cyclic exposures do not result in more pronounced weight losses for Ni-30Cr or Ni-30Cr-0.1Ce. This indicates that the weight losses in this environment are due to vapor species formation rather than scale spallation.	225

Figure 6.59: The surface, (a-b), and the cross-sectional, (c-d), images of the alloy Ni-30Cr are shown at 900°C after isothermal TGA tests for 168 hours in wet and dry air. (a) In air/H₂O flakey Cr₂O₃ developed over the continuous chromia layer. (b) High magnification image of chromia that developed in dry air is shown. The chromia flakes were not observed in this environment. (c) SEM image shows the scale that developed in wet air in cross-section. Void formation at the oxide/gas interface was evident. (d) Image shows chromia scale that developed in dry air. The thickness of the layer was twice larger in comparison to wet air. Voids developed at the substrate/oxide interface in this environment as well. 227

Figure 6.60: The comparison of the TGA data for Ni-30Cr(0.1Ce) in dry air to wet air at 900°C showed that the weight losses were more pronounced for the latter environment. In dry air, the growth rate of chromia was slower for the Ce-doped specimen. The presence of the reactive element did not affect the vaporization rate significantly. These results are in agreement with literature. The deviation between Ni-30Cr and Ni-30Cr-0.1Ce in wet air is experimental..... 228

Figure 6.61: Ni-30Cr at 900°C after isothermal TGA tests for 168 hours. Back scattered electron images show the formation of voids at the alloy grain boundaries (a) in wet air, and (b) in dry air..... 229

Figure 6.62: Ni-30Cr-0.1Ce at 900°C (a) in wet air, and (b) in dry air after isothermal tests for 168 hours..... 230

Figure 6.63: The comparison of the TGA data to the cyclic tests at 700°C was in agreement with the results obtained at 900°C. Scale spallation was more pronounced for the tests in dry air, (a), in comparison to wet air (b). The formation of vapor species was evident at this temperature as well. The weight changes in air/H₂O mixtures were more negative compared to dry air, (c)..... 232

Figure 6.64: Weight losses related to vapor species formation were not evident for IN 738 at 900°C. The comparison of isothermal tests to cyclic experiments showed that the weight changes were smaller for the latter condition. This is related to scale spallation that arises during thermal cycling..... 232

Figure 6.65: The TGA data for IN 738 at 900°C in wet air was compared to the model alloys (i.e. Ni-30Cr and Ni-30Cr-0.1Ce), which were tested under the same conditions. The weight losses associated with the formation of vapor species were not evident for the superalloy. 233

Figure 6.66: Comparison of the isothermal weight change data of IN 738 to the simple alloys at 900°C in dry air showed that the behavior of the superalloy was similar to Ni-30Cr..... 233

Figure 6.67: The microscopic examination of IN 738 which was tested isothermally at 900°C showed that Ti developed a thin oxide layer at the oxide/gas interface. This layer was detected in wet air (a), as well as in dry air (b). The existence of this layer put a physical barrier between the chromia scale and the reactive gases. This avoided the loss of the

protective layer by the formation of vapor species, which was observed to be more aggressive in air/H ₂ O mixtures.	234
Figure 6.68: The isothermal tests with the superalloy X-40 at 900°C showed that volatile species formation was evident in wet air. The weight changes during cyclic tests were significantly lower for exposures in dry air. This was less pronounced in air/H ₂ O mixtures.	235
Figure 6.69: The SEM images of X-40 show the surface of the alloy after isothermal tests, (a), in wet air, and, (b) , in dry air for 168 hours at 900°C. EDX analysis indicated the presence of Co and W along with chromia. Co- and W-oxides were more abundant on the specimen tested in dry air. Additionally, the surface morphologies were observed to be different for each environment. The scale was smoother after experiments in wet air, whereas it was rougher for the sample exposed to dry air.	236
Figure 6.70: The back scattered electron microscopy images show the cross-section of the X-40 specimens which were tested isothermally at 900°C for 168 hours, (a) in wet air, and, (b), in dry air. Wet air resulted in the formation of thinner scales with uniform thickness. The scale that developed after exposures in dry air was identified as chromia with transient Co(W)-oxides at the oxide/gas interface. The internal oxidation was more pronounced in dry air. Formation of voids at the oxide/gas interface was evident in wet, as well as in dry air.	237
Figure 6.71: The kinetic plot shows the weight changes for model systems and the superalloy X-40 as a function of time at 900°C after TGA tests in dry air and in air/H ₂ O mixtures.	238
Figure 6.72: The weight change data for Ni(99.999%) at 900°C is shown as a function of exposure time. The metal was subjected to isothermal tests in dry air and in air/H ₂ O mixtures for 168 hours.	238
Figure 6.73: SEM images show the cross-section of pure Ni (99.999%) after isothermal tests at 900°C (a) in air-10% H ₂ O, and (b) in dry air after 168 hours. The thickness of the NiO layer was found to be slightly larger after exposures in dry air.	239
Figure 6.74: Low magnification SEM images of the Ni(99.999%) sample cross-sections after isothermal tests for 168 hours at 900°C (a) in dry air, and (b) in wet air [P(H ₂ O) = 0.1 atm, P _{total} = 1atm).	240
Figure 6.75: The images show the surface of NiO that developed on pure Ni(99.999%) after isothermal exposures for 168 hours at 900°C (a) in dry air, and, (b), in wet air. In dry air, equiaxed grains were evident. In wet air faceted surface development was observed.	241
Figure 6.76: SEM images showing the morphology of the chromia scale that developed on Ni-30Cr at 900°C in wet air (P _{H₂O} = 0.1 atm, P _{total} = 1 atm) at different exposure times.	244
Figure 6.77: Formation of flakey chromia over Ni-30Cr-0.1Ce at 900°C is shown after exposures in air/H ₂ O mixtures (P _{H₂O} = 0.1 atm, P _{total} = 1 atm) for different hold times.	245

- Figure 6.78: SEM image shows Ni-30Cr-0.1Ce after isothermal tests at 900°C for 168 hours in wet air. Formation of abnormally big flakes with a different morphology was detected in addition to the smaller sized flakes with the hexagonal geometry. 245
- Figure 6.79: The chromia flakes that are observed on the Ni-Cr alloys after tests in air/H₂O mixtures at 900°C are shown at high magnification..... 246
- Figure 6.80: SEM images of Ni-30Cr at 900°C in wet air after 16.5 hours. The pattern of the grain boundaries and the pores over the spalled areas displays similarities with the pattern for the formation of chromia flakes. 247
- Figure 6.81: Ni-30Cr in dry air at 900°C after 535 hours of isothermal testing. Substantial amounts of scale spallation took place during cooling. Spalled areas revealed pore formation in the substrate..... 247
- Figure 7.1: PWA 1484 at 700°C after 4 hours of isothermal exposure in wet air, where $P_{H_2O} = 0.3$ atm and $P_{total} = 1$ atm. EDX analysis indicated a concentration gradient in terms of the oxygen in the internal oxidation zone. The atomic percent of oxygen decreased from 50% at the NiO/internal-oxide interface, (labeled as “a”), to 17% at the internal-oxide/alloy interface, (labeled as “b”). Moreover, the Ni concentration was observed to decrease by moving from “b” towards ‘a’. No detectable amounts of oxygen were present below this interface, i.e. in the alloy..... 262
- Figure 7.2: Kinetic plots of René N5, PWA 1484 and CM 186 indicate that at 900°C the transition from transient oxidation to steady state oxidation takes places after same exposure times in wet air and in dry air. For MarM 247 no specific transition point is evident. However, the oxidation kinetics follows the same trend in either environment for this system as well. 264
- Figure 7.3: In air/H₂O mixtures anion transport in the oxide proceeds faster in comparison to dry air. At time $t > 0$ the depth of the oxygen affected zone is larger in the wet environment. As a result, the protective scale forms deeper in the alloy. Thicker layers of transient oxides develop above the protective alumina scale..... 265
- Figure 7.4: When the Ni-Cr alloys are exposed to dry air or to air/H₂O mixtures, chromia scales develop at the substrate surface considering the %Cr in the substrate is sufficiently high. After the formation of the initial thin chromia layer, the scale continues to grow by the outward diffusion of Cr cations. In the mean time, the composition of the substrate changes gradually. The concentration of Cr close to the reaction zone decreases with time. During wet exposures, substantially thinner scales develop due to the loss of the protective Cr₂O₃ by the formation of the vapor oxide species. Therefore, the strain energy for these specimens is less than the ones exposed to dry air. As a result scale detachments and spallations start earlier in the dry environment. When the Cr₂O₃ layer spalls off, the unexposed surface of the substrate material reacts with oxygen. Since the substrate is depleted in Cr, oxides other than chromia form in these spalled areas. Oxygen also diffuses

through the cracks and micro-channels in the oxide. The reactions at the oxide/alloy interface give rise to internal oxidation. 266

Figure 7.5: SEM image shows Ni-30Cr exposed in dry air at 900°C for 168 hours isothermally. Chromia developed in the substrate by the alternate oxidation and reduction processes... 267

Figure 7.6: Kinetic plots of IN 738 and X-40 at 900°C indicate that the onset of breakaway oxidation is approximately the same time in dry air and in wet air for each system..... 268

ACKNOWLEDGMENTS

First, I would like to express my sincere gratitude to my advisors Dr. Pettit and Dr. Meier for their encouragement, guidance, support and advice throughout this study. I feel very lucky to have the opportunity of working with them and learning from them.

I would like to thank to my committee members Dr. Eror, Dr. Barnard, and Dr. Smialek for their participation and input in this study.

I would also like to express my gratitude to the High Temperature Oxidation Group members Monica Maris-Sida, Scott Laney, Matt Stiger, Igor Garcia, Kee-Young Jung, Wes Jackson, Julie Hammer and David Helmick for their friendship and collaboration.

I appreciate the technical assistance and the friendship of Al Stewart and George McManus. It was always nice to be around them. The technical support of Earl Hewitt is also acknowledged. Our administrative staff members Carolynn Wilson, Nora Siewiorek and Carol McFadden are not to be forgotten. Thank you for your help in administrative issues and, more importantly for your friendship.

I would like to acknowledge South Carolina Energy Research and Development Center for their financial support. I would also like to thank to the Oak Ridge National Laboratories for performing the high pressure steam tests for us.

Meltem and Cagatay, my special friends... I cannot thank you enough. It was and will always be a treasured friendship. I am very lucky to have such wonderful people in my life.

Mom and dad, I am the luckiest person for having you as my parents. And Koray, the best brother one can have. You always believed in me, encouraged me and supported me under any circumstances. I love you so much. You were always right next to me even though we lived miles apart from each other.

And of course, Brandon, my sweetheart... Thank you very much for your patience, support, selfless friendship and unconditional love.

1.0 INTRODUCTION

The free surfaces of all metals and alloys react with the elements in their surrounding environments, and develop an interlayer at the gas/metal interface. The type of bonding and the extent of reaction vary depending on several parameters including the composition of the gas phase and the metal/alloy, as well as the temperature of the environment. The rate of reaction is typically accelerated with temperature increases. Therefore, oxide formation is an important consideration in high temperature applications. Such applications require the formation of thin, protective oxide scales at the metal/gas interface. Understanding the mechanism(s) of protective scale development is therefore of utmost importance, because the useful lifetime of components is very much dependent on the type of the oxide scale(s) and the rate of reaction(s).

Studies have shown that the presence of water vapor in the oxidizing environment influences metal/gas reactions. Some of the observations on the effect of $\text{H}_2\text{O}(\text{g})$ on oxide development include changes (acceleration/deceleration) in reaction rates, changes in selective oxidation processes, modifications in transport mechanisms, increased tendency to cracking and spalling of oxides. However, the mechanism(s) for the observed differences are not very well understood. Therefore, there is still a need to investigate the phenomena in more detail.

The two oxides that are of most interest for high temperature applications are alumina (Al_2O_3) and chromia (Cr_2O_3). These oxides are considered as “protective oxides” because of their slow growth rates at elevated temperatures. In this study, the mechanism(s) that are

effective during the development of alumina and/or chromia scales were investigated when water vapor is involved in the oxidizing reactions. Several commercial superalloys and binary Ni-Cr alloys were tested at various temperatures and pressures in dry air and in air/water-vapor mixtures. Specific aspects of water vapor induced degradation of chromia and alumina scales including the transient oxidation, the spallation of oxide scales, selective oxidation of Al and/or Cr, the growth rate of chromia scales, and the formation of volatile species were investigated in detail.

2.0 BACKGROUND

2.1 OXIDATION OF METALS

Virtually all metals and alloys are subject to deterioration by oxidation upon exposure to environments containing oxygen and/or oxygen bearing species such as air, $\text{H}_2\text{O}_{(g)}$, $\text{CO}_{2(g)}$, or their mixtures (i.e. air/ H_2O , $\text{H}_2/\text{H}_2\text{O}$, Ar/ O_2 etc.). The basic metal/gas oxidation reaction can be represented by the equation



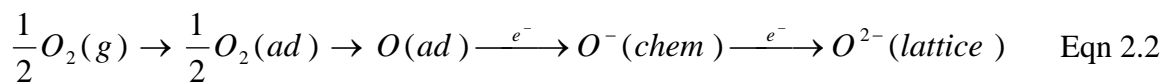
Although the given representation resembles a simple chemical reaction, the actual phenomenon is usually a complex set of reactions, involving mechanisms that are still not clearly understood. The reaction paths and the oxidation behavior of metals, and especially their alloys are affected by a large variety of factors. The list includes compositional make-up of the system, partial pressures of oxidizing gases, gas stream velocity, surface conditions, grain size of the substrate, total pressure of the oxidizing atmosphere and many more.

Under most conditions, the reaction products are solid oxide films that develop on the substrate surface. Figure 2.1 is a simple schematic showing the cross-sectional view of an oxidized component.

Generally, there are three consecutive stages that are observed during alloy oxidation. The initial period, which is called the transient stage, involves the simultaneous formation of all possible oxides that can be developed by the particular system. The rate of reaction is typically high at this stage. The steady state stage is associated with the formation and maintenance of a continuous, slow growing “protective scale”. During this period, significant reductions in reaction rates are observed. The onset of accelerated attack as a result of the loss of protectiveness is termed the “breakaway stage” [1]. A plot showing the oxidation stages is given in Figure 2.2.

2.1.1 Initial Oxidation

When a fresh and clean substrate surface is exposed to an oxygen-containing environment, the very first step will be the adsorption of O₂ molecules to the metal surface. After the chemisorption of the gas molecule, it will dissociate and adsorb atomically on the substrate. The steps of the adsorption process can be represented as follows



If the metal surface, which is saturated with adsorbed oxygen atoms, is further exposed to oxygen, oxide nuclei will develop on the substrate surface. These nuclei may grow laterally and establish a thin continuous film on the surface; or they may nucleate as separate oxide particles. Surface preparation, impurity content, crystal defects at the surface and surface orientation are among the factors that affect the extent of oxygen adsorption and initial oxide formation [2].

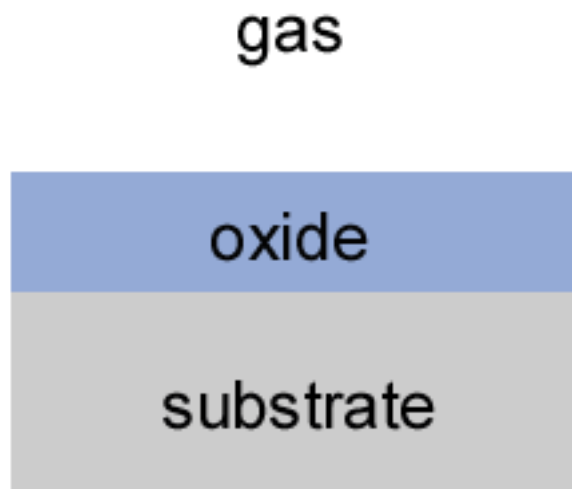


Figure 2.1: Simple schematic showing the cross-section of an oxidized sample.

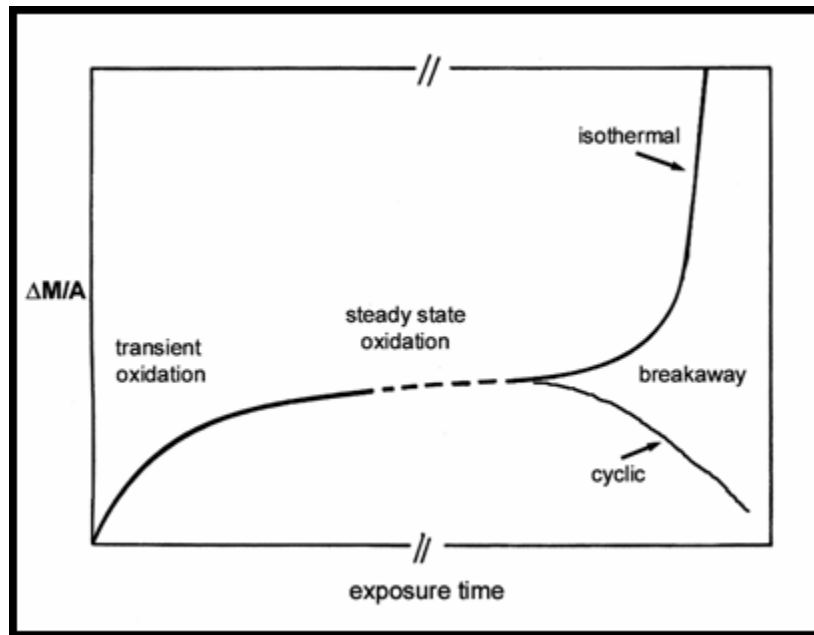


Figure 2.2: Schematic showing various stages of oxidation on alloys that develop protective scales.

As the oxidation reaction proceeds, the oxide phase spreads over the metal surface, and, in most cases, a continuous scale covers the metal/gas interface. The reaction mechanism changes at this point. The film builds a barrier between the metal and the oxidizing gases. Now, the reaction can proceed only via the transport of one or both of the reactants through the scale [2].

2.1.2 Transport Mechanisms

The transport mechanism(s) of reactants have a complex nature. An ionic compound is a compound where the atoms are charged, and the cations and anions are assigned a valence. The sum of all positive and negative charges is equal to zero in such compounds to maintain electroneutrality [2]. Most metal oxides are ionic in nature. Therefore, both metallic and non-metallic constituents are expected to migrate in their ionized states rather than as neutral atoms [3]. Several mechanisms are derived to explain ionic transport through ionic solids, both for stoichiometric and non-stoichiometric crystals. In all compounds, all types of defects are possibly present to some extent, certain types being dominant. Predominant defects in highly stoichiometric crystals are Schottky defects, and Frenkel defects.

In Schottky disorder ionic mobility is provided via ionic vacancies. A crystal with Schottky defects contains equivalent concentrations of cation and anion vacancies to preserve neutrality ($\text{Null} \rightarrow V'_M + V^\bullet_X$). In this structure both cations and anions are mobile, because the oxide contains vacancies in both sublattices [2].

In a Frenkel defect structure, the defects are limited to either the cation sublattice or the anion sublattice. A Frenkel pair consists of vacancies and interstitials of the same species. The concentration of vacancies and interstitials in the crystal are equivalent to each other so that

electroneutrality requirements can be satisfied ($M_M^x + V_i^x \rightarrow M_i^\bullet + V'_M$, or $X_X^x + V_i^x \rightarrow X''_i + V^{\bullet\bullet}_X$) [2].

Unfortunately, neither of these defects can be used to develop a model for oxidation reaction mechanisms, because they do not provide a mechanism for electron migration¹. In order to develop an oxide scale, either cation and electron mobility, or anion and electron mobility is required. The first case results in oxide growth at the oxide/gas interface, whereas the latter case causes new oxide formation at the metal/oxide interface [3].

Simultaneous ion and electron mobility can be explained by considering the oxidation products to be non-stoichiometric compounds. In a non-stoichiometric oxide, electroneutrality is still preserved, although the metal/oxygen ratio does not exactly match the chemical formula of the compound. This criterion is met by considering variable cation sub-lattice valencies [3].

In principle, metal oxides have exact stoichiometry only under very specific conditions (i.e. at certain temperatures with certain partial pressures of components). Therefore, as a general rule, metal oxides deviate from stoichiometry [2].

Non-stoichiometric compounds may be metal or oxygen deficient; or they may have an excess of oxygen or metal relative to their stoichiometric compositions. Each possibility refers to different defect structures [2].

An oxygen deficient nonstoichiometric oxide such as MO_{1-x} or an oxide with excess metal such as $M_{1+y}O$ will have defects with positive effective charges. These positive charges will be compensated with negative electrons to preserve electrical neutrality. Such non-stoichiometric oxides are considered as n-type compounds. In n-type oxides the concentration of electrons and oxygen vacancies in oxygen deficient structures, or metal interstitials and electrons in metal

¹ Wagner's oxidation theory, which explains the important basic oxidation principles for metals, requires the migration of both ions and electrons across the scale.

excess structures will be proportional to $P_{O_2}^{-1/n}$ [2]. The value of the coefficient n depends on the degree of ionization in the system [3].

In a metal deficit oxide such as $M_{1-y}O$ or an oxide with oxygen excess such as MO_{1+x} , the predominant defects will be metal vacancies and oxygen interstitials, respectively. The negative effective charges resulting from the defect structure will be compensated by positive electron holes due to electroneutrality requirements. Such oxides are known as p-type semiconductors. If the oxide is metal deficit, the relative concentration of electron holes and metal vacancies will be proportional to $P_{O_2}^{1/n}$ [2].

The defect structure of a compound could also be changed from p-type to n-type, or visa versa, by using proper dopants. However, the examples of this case are rather rare [2].

Experimental studies on Ni have identified NiO as a p-type oxide. It is a metal deficient oxide, where the metal vacancies are the major defects. The oxygen pressure dependency ranges between $PO_2^{1/6}$ to $PO_2^{1/4}$ which suggests that the Ni vacancies are singly and doubly ionized [2-4]. CoO forming on Co is another example of a p-type oxide. Experimental studies identified this compound as metal deficient at oxygen activities higher than its decomposition pressure (10^{-12} atm at 950°C, and 10^{-6} atm at 1450°C) [4]. The concentration of cobalt vacancies increases with oxygen pressure. The non-stoichiometry in Cr_2O_3 is very small [4]. The defect structure of this oxide has not been identified with certainty. However, most studies report an intrinsic behavior at temperatures above 1000°C-1200°C [4-6]. It is believed that at lower temperatures it is an extrinsic oxide. Observations of p-type and n-type behavior exist. This is found to be dependent on the type of the dopant in the system. Acceptor doped (impurity with negative effective charges) Cr_2O_3 displays p-type behavior [4, 5, 7]. The behavior is pressure dependent when the dopant is the donor type (i.e. with positive effective charges). Under these conditions, the

behavior is n-type at very low oxygen pressures and changes into p-type as the oxygen pressure increases [5]. Therefore, it is generally accepted as a p-type oxide below 1000°C [4, 6]. The defect structure of Al₂O₃ is not fully understood. The concentration of electronic and ionic defects in the oxide is extremely small. This is believed to be due to the large energy band gap and the high lattice energy of the system. According to Kröger, [5], the conductivity is electronic at high oxygen activities, and ionic at low PO₂ in an acceptor dominated oxide. For donor-dominated compounds the reverse is observed.

2.1.3 Transient Oxidation

When the fresh surface of an alloy is exposed to oxygen containing atmospheres, the surface atoms of all components will react with oxygen. This will result in the formation of a thin oxide film. As a general rule, the growth rates of all oxide phases are different. Therefore, the oxide with higher growth rate will overgrow the slower ones. At the same time, displacement reactions between the atoms of the less noble elements in the substrate and the fast growing oxide phases will occur. These reactions at the scale/alloy interface will cause depletion of some elements in the alloy next to the scale.



Different oxygen affinities and different diffusion rates of the alloy constituents will result in continuous and gradual compositional changes in the scale and in the alloy close to the scale. This stage of oxidation is termed “transient oxidation”.

Transient oxidation is very dependent on the physical properties of the material such as specimen pretreatment, specimen geometry, crystal orientation, and exposure conditions [2, 8-11], as well as the internal properties including the alloy composition, the diffusivities of the elements that develop protective scales, and the stabilities of different oxides [12]. Surface finishing technique (mechanical polishing vs. electrochemical etching) [13-15], as well as the method of bringing the sample to the exposure temperature leads to significant differences in scale development (i.e., loading the specimen at room temperature into the established hot zone vs. preheating the sample in vacuum in an inert gas atmosphere and then exposing it to the experimental environment) [2].

It is not possible to draw a general relation between surface roughness and oxidation rate. Most studies report tendencies towards more prominent transient oxidation on smoother surfaces [10, 13-15]. However, there are studies that report decelerations in oxidation rates on finer pre-exposed surfaces as well. One such investigation was conducted by Tolpygo, [8], where a decline in the reaction rate was observed with finer surface finishes on a Cr rich Fe-Cr-Al system in He-O₂ mixtures. The work by Wlodek, [15], using René 41 and Udimet 700 showed that the former alloy developed less transient oxides on smoother surfaces, while the latter system displayed the opposite behavior. Some investigations suggest that there might be an optimum surface condition where the reaction rates are at a minimum. For example, in the study by Uran et al., [9], it was reported that the reaction kinetics of the Al rich Fe-Cr-Al system in air decreased as the surface finish changed from 30 μ m to 3 μ m. However, at 1 μ m they observed a sudden increase in scale thickness, accompanied by compositional changes in the oxide layer.

Goedjen and Shores [10] examined the effect of alloy grain size on the oxidation behavior of NiCrAl alloys. They observed that smaller grain sizes decreased the transient oxidation rate. On

the other hand, long-term oxidation was found to be independent of alloy grain size. They attributed the lower transient oxidation rate to rapid grain boundary transport of Al and Cr to the oxide/metal interface that promoted Cr_2O_3 and Al_2O_3 formation during early stages of oxidation. Similar observations were reported also by Giggins and Pettit on Ni-Cr alloys [14].

The very delicate nature of transient oxidation usually results in diverse scatter of the observations by different researchers working even with the same system. The oxide development during the transient stage is important as it might have significant influences on the properties of further stages, i.e. selective oxidation and breakaway oxidation.

2.2 SELECTIVE OXIDATION

As the name implies, selective oxidation is the preferential oxidation of one of the alloy components. It takes place only above a critical concentration of the active element. In an A-B alloy system with sufficiently high N_B , a continuous BO_v scale is expected to form, where B is the less noble element. During this reaction, A diffuses into the alloy from the alloy/scale interface. As a result, the substrate becomes enriched in A. In the mean time, the concentration of B in the alloy decreases. However, if the concentration of B in the alloy system is less than N_B at which B oxidizes selectively, then the scale will contain oxides of A and B. The following equation defines the conditions for transition from internal-to-external oxidation.

$$N_B^{(o)} > \{ (\pi g^*/2v) N_O^{(s)} [(D_O V_m)/(D_B V_{ox})] \}^{1/2} \quad \text{Eqn. 2.4}$$

where $N_B^{(o)}$ is the initial concentration of B in the bulk, $N_O^{(s)}$ is the surface concentration of oxygen, D_O and D_B are the diffusivities of oxygen and B, respectively. V_m and V_{ox} are the molar volumes of the bulk alloy and the oxide, respectively. g^* is the critical volume fraction of oxide ($g = f(V_{OX}/V_m)$), whereby lateral growth of BO_v occurs.

The concentration of B in the A-B system to maintain the external BO_v scale once it formed was estimated by Wagner as;

$$N_B = (V/Z_B M_O)(\pi k_p/D)^{1/2} \quad \text{Eqn. 2.5}$$

assuming a model where the scale was pore free and compact. In this equation N_B is the critical concentration of B, V is the molar volume of the alloy, Z_B is the valence of B atoms, M_O is atomic weight of oxygen, D is the diffusion coefficient of B in the alloy, and k_p is the parabolic rate constant for the growth of BO_v scale [2].

The same basic principles mentioned above apply also for multi-component systems. However, the addition of each element affects the interactions within the system which increases the complexity of the reaction dynamics.

The selective oxidation of elements such as Cr, Al, and Si in an alloy system yields to the formation of Cr_2O_3 , Al_2O_3 , and SiO_2 as continuous scales. These oxides provide enhanced oxidation resistance to commercial alloys as a result of their low growth rates [2]. Therefore, systems with the ability of developing and maintaining such scales are of great interest for high temperature applications. A diagram showing the relative growth rates of most commonly encountered oxides during such applications is presented in Figure 2.3.

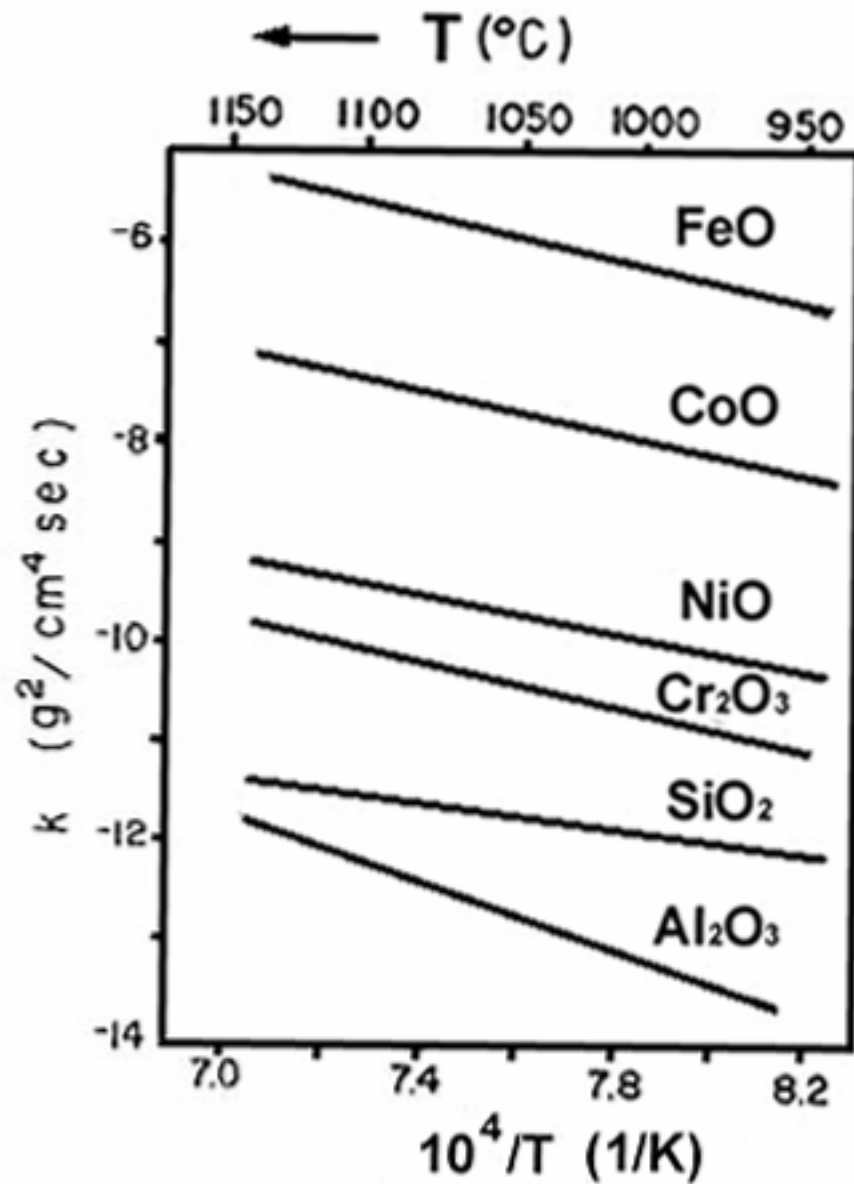


Figure 2.3: The growth rates of most commonly encountered oxides are shown as a function of temperature [3].

2.2.1 Factors that Affect Selective Oxidation

The key factors that determine the extent of selective oxidation and the depth of the internal oxidation zone are oxygen solubility and diffusivity in the alloy, active metal concentrations and their relative mobility in the substrate. Therefore, any other parameter that influences the mentioned properties will affect the reaction kinetics.

As the temperature changes, the diffusion rates and the solubilities of oxygen and other alloy elements will change. These changes will affect the critical concentration for selective oxidation. A good example of such cases would be systems that contain both Al and Cr.

Elevated temperatures generally favor selective oxidation of aluminum. The oxide scale characteristics of an alloy that develops protective chromia layers with internal alumina at low temperatures may change at higher temperatures. Alumina no longer precipitates internally; it rather forms external continuous scales [16, 17]. Maximum protection via alumina formation is generally obtained in a temperature range between 1000°C-1200°C [2]. Therefore, for applications at or above 1000°C, alumina formers are preferred. However, temperature elevations beyond 1300°C will accelerate diffusional transport through alumina, which would lead to rapid formation of alumina scales. This will cause faster degradation of the substrate due to Al depletion in the bulk.

The reaction rate is also sensitive to compositional changes in the scale. Since alumina is a slower growing oxide compared to chromia, a deceleration in oxide growth rate upon the formation of the latter accompanies the transition from internal precipitation to formation of continuous alumina layers.

Selective oxidation is affected by surface preparation and by sample geometry as well [15]. The flat surfaces of a sample may display selective oxidation while the corners and edges form

duplex scales. This is related to surface-to-volume ratio of the specimen, which is larger at the corners and edges [2]. Grain size is another aspect that influences the conditions for preferential oxidation. Studies have shown that, alloys of the same composition but of different grain sizes require different levels of element additions for selective oxidation. In alloys that are exposed to high temperatures in air, oxygen, and steam it is observed that selective oxidation takes place at lower concentrations as the grain size decreases. The same conclusion applies also to alloys that are cold worked prior to exposure [2, 14]. The widely agreed upon explanation is that grain boundaries and short circuit paths enable faster cation transport, which makes the complete coverage of the surface with protective scale easier.

Incorporation of reactive elements such as Y or their oxide dispersions are proposed to promote selective oxidation and establishment of continuous scales at lower solute concentrations. As quoted by Prescott and Graham [18], oxide particles of oxygen active elements may influence transient oxidation by providing preferential nucleation sites for chromia, which in turn helps to establish continuity during selective oxidation[19]. Similar mechanisms are proposed also for alumina formers [20, 21].

2.2.2 Selective Oxidation of Cr, Al and Their Alloys

The alloys that are most widely used in commercial high temperature applications are usually Ni- or Fe-based alloys with Cr and Al additions to ensure the formation of the slow growing oxides chromia and alumina. Since this study involves mainly Ni-based superalloys, emphasis will be given to selective oxidation in Ni-based systems.

In the previous section it was mentioned that grain size is an important factor in terms of selective oxidation. Giggins and Pettit [14] investigated this issue in detail in the Ni-Cr system

for a wide composition range at 900°C and 1100°C. They observed that selective oxidation of Cr in this system took place preferentially at the grain boundaries. Cr₂O₃, which precipitated along the grain boundaries, emerged into the grain interiors by lateral diffusion. As a consequence of this mechanism, the oxidation rate became sensitive to grain size. Since the diffusion distance for lateral movement was shorter for finer grains, the continuous scale establishment process was accelerated. The oxidation rate dropped to smaller values by leaving out any necessity to adjust the bulk composition. The critical Cr concentration in the bulk for continuous and protective scale formation shifted to lower values by surface grain size refinement.

In most industrial applications, Ni-based alloys containing both Al and Cr constitute the larger fraction of the alloy spectrum. The thermodynamically stable oxide phases in Ni-Al and Ni-Cr phases are Al₂O₃ and Cr₂O₃ respectively, Figure 2.4. Therefore, the same oxides are expected to form in Ni-Cr-Al systems. In terms of oxidation resistance, Al₂O₃ is a considerably better oxide compared to Cr₂O₃. In general, alumina formation is favored to chromia because of its higher thermodynamic stability, Figure 2.4. It also provides better oxidation resistance due to its lower growth rate, Figure 2.3. The minimum solute concentrations required for continuous oxide film formation are reported as app. 13-25% for chromia, and 1-8% for alumina in oxygen at atmospheric pressures [1]. The use of Cr together with Al decreases the critical concentration for selective Al oxidation. This mechanism is called “oxygen getter effect”, where the rapid development of a surface oxide film reduces the oxygen activity at the oxide/alloy interface. This helps outward transport of the solute element, so that it can establish a continuous layer. In Ni-Cr-Al alloys, precipitation of Cr₂O₃ during initial oxidation puts a barrier to oxygen inward transport from the surface. This allows alumina more time to develop continuity. Oxygen

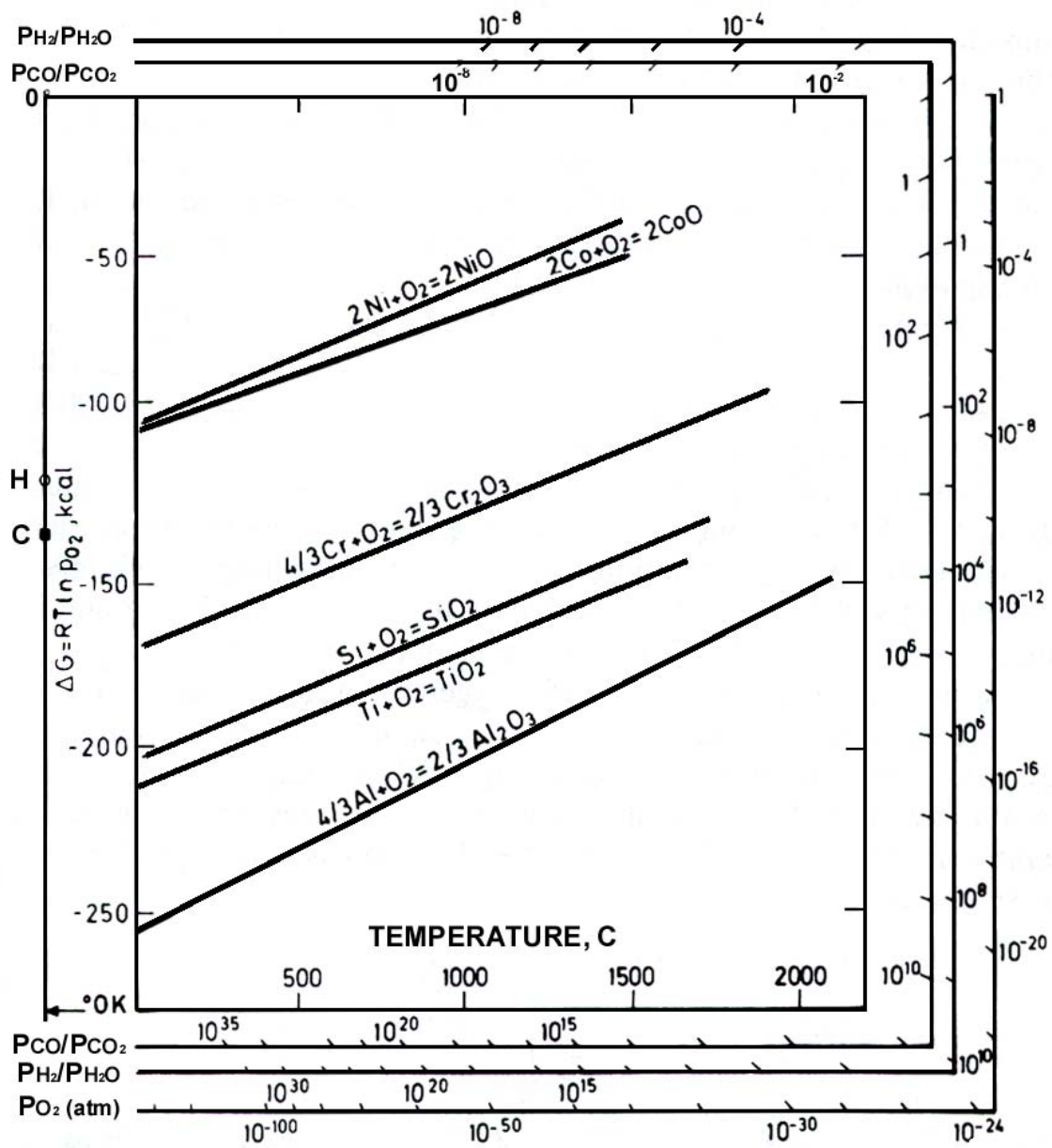


Figure 2.4: Ellingham diagram showing the relative stabilities of selected oxides.

gettering in the Ni-Cr-Al system is beneficial also in terms of alloy design, because large aluminum additions result in increased brittleness and depress the melting point of the system [22].

If conditions for selective Al oxidation are not satisfied, alumina precipitates as an internal oxide below the chromia scale.

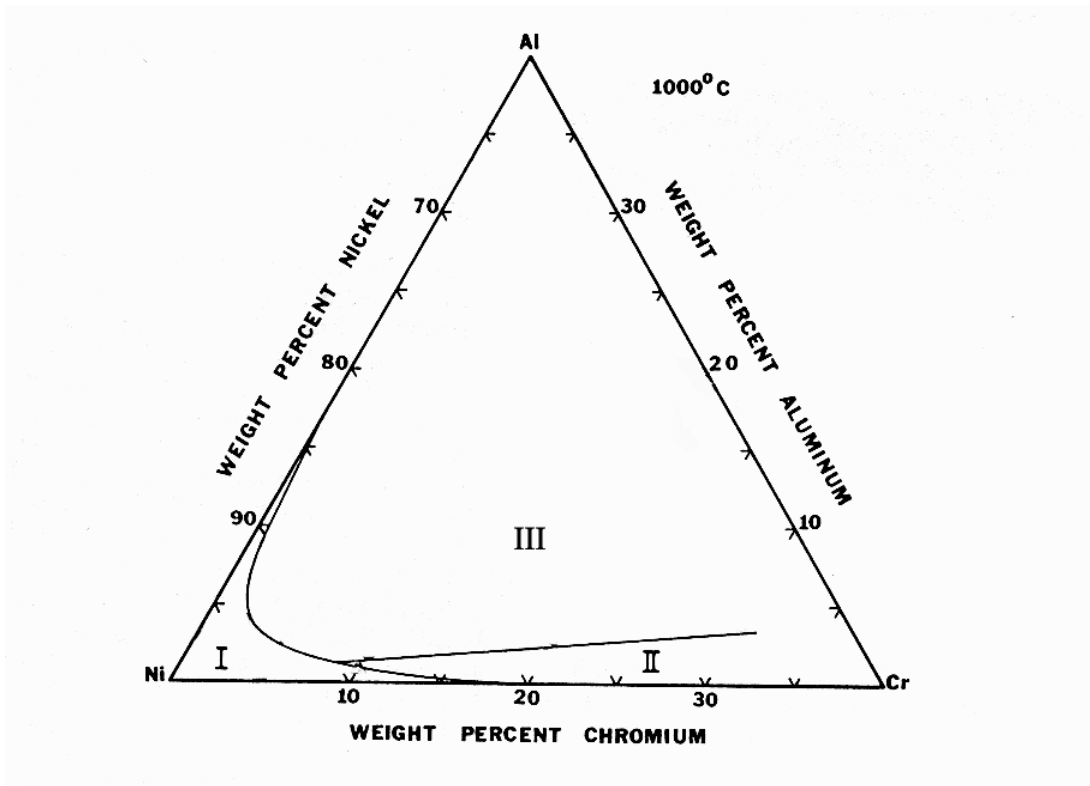
Giggins and Pettit [23] investigated the Ni-Cr-Al system in detail, and developed oxide maps for the system at temperatures 1000°C, 1100°C and 1200°C (Figure 2.5). The main features of oxidation in this temperature regime can be classified as follows:

In *Regime I*, where the alloy composition does not allow continuous chromia or alumina scaling, NiO will form at the scale/gas interface. Cr- and Al-oxides will develop a discontinuous subscale below this external oxide by precipitating internally. The rate-determining step will be Ni diffusion through the NiO scale.

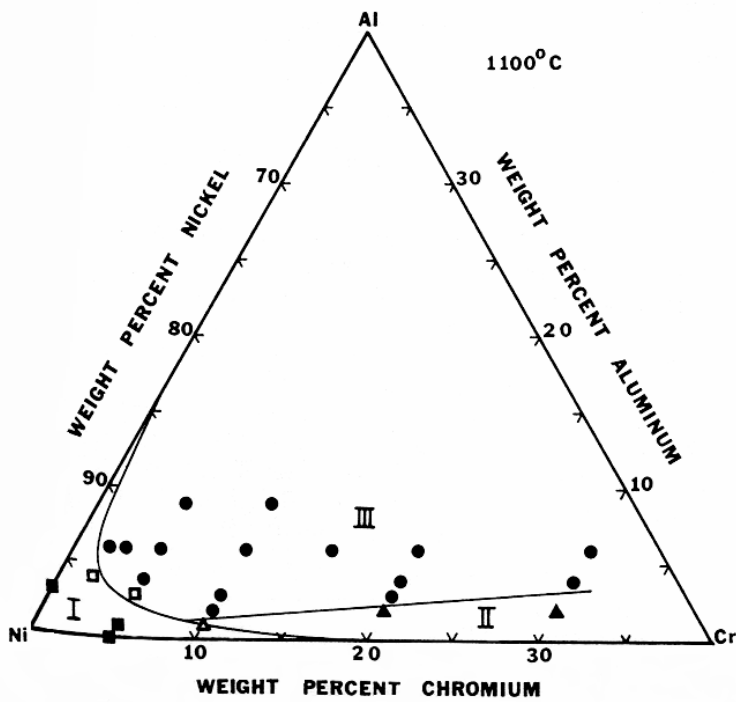
If the alloy has sufficient amounts of Cr but not Al, as in *Regime II*, Cr will oxidize preferentially. The external scale will consist of continuous chromia. Al-oxide will precipitate into the alloy below the scale. The oxidation rate will be controlled by diffusional growth of chromia.

In cases where the alloy composition exceeds the minimum critical Al concentration (*Regime III*), protective Al₂O₃ scale with a small amount of dissolved Cr will develop. This time, diffusional growth of alumina will govern the overall oxidation rate.

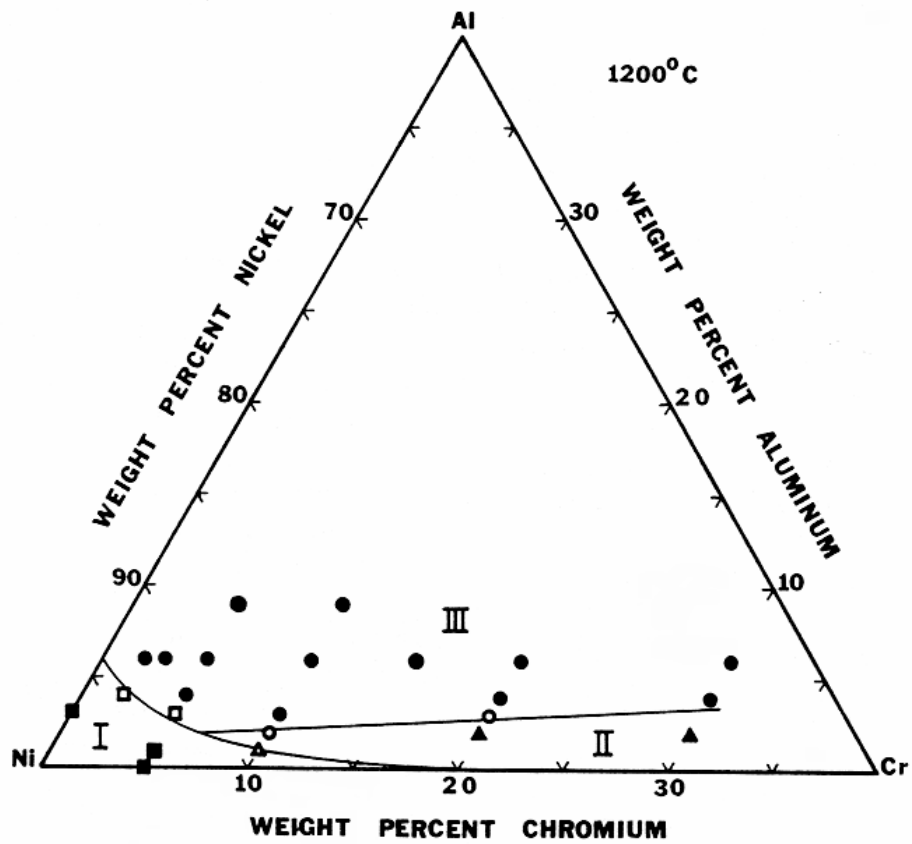
Birks et al. [12] observed favorable selective oxidation of Al₂O₃ along alloy grain boundaries. They stated that aluminum transport to the metal surface might be faster at grain boundaries than in the bulk alloy, and Al₂O₃ nucleation might also be affected. They observed a relation between selective oxidation and the surface condition as well. Protective Al₂O₃ scales



(a)



(b)



(c)

Figure 2.5: Oxide maps of Ni-Cr-Al system at (a)1000°C, (b) 1100°C, and (c) 1200°C developed by Giggins and Pettit [23].

were detected on samples with 600 grit finish, but not on the 0.5 μm polished surfaces [24, 25]. These results are similar to the observations reported for Cr_2O_3 scales as discussed earlier in this section [14].

2.3 COMPARISON OF ISOTHERMAL AND CYCLIC OXIDATION CONDITIONS AND THE RESULTING EFFECTS

In general, cyclic oxidation is a more destructive process than isothermal applications. The useful life of the alloys is limited to much shorter times. The main reason for this is the incorporation of thermal stresses into the scale together with the growth stresses. Temperature changes that arise during cooling and heating the material between each cycle give rise to additional compressive stresses in the scale during cooling because of the mismatch of thermal expansion coefficients between the alloy and the substrate. Thermal stresses are much larger than growth stresses [26]. They induce spalling of scales. Repeated surface spallation accelerates substrate degradation. The subsurface alloy becomes depleted in elements that provide protectiveness to the system. In some cases, external scale destruction may allow gas access to the material, and induce internal oxidation and/or nitridation [27]. Depletion of the alloy in terms of potential protective oxide formers makes it also more susceptible to breakaway oxidation [28].

Several different models such as COREST and COSP were developed in an attempt to define the response of alloy systems to cyclic oxidation by simplified equations, as quoted by Murriss [26]. However trying to describe the phenomenon semi-quantitatively by models is a big

challenge. Cyclic oxidation is sensitive to even very small variations in experimental methods and material properties. Surface preparation techniques, or different hold times at the hot zone and cool zone location, rate of heating/cooling may significantly affect cyclic oxidation kinetics. Typically, the degradation is more severe at higher temperatures [26, 29]. Larger grain size may also contribute to enhanced scale spallation by inducing higher creep resistance in the alloy, which decreases stress relief within the oxide [26].

The discontinuities in weight change plots for thermally cycled systems, which are quite common, indicate that the material cannot deform plastically anymore. Cracks develop in the scale. They create new surfaces, which react rapidly with the oxygen. As a result, a sequence of stages with parabolic oxidation kinetics occurs [26].

2.4 FACTORS AFFECTING ADHERENCE OF OXIDE LAYERS

Oxide scales that form on metal or alloy surfaces display different degrees of adherence to the substrate material. There are cases where a uniform scale is perfectly attached to the exposed surface. But in most practical applications varying degrees of detachment are common. This is an important issue in terms of the resistance of an alloy system to oxidation. A protective scale should be thermodynamically stable, pore free, slow growing and perfectly adherent to the substrate. Partial or complete spallation of the scale, convolutions along the oxide layer and similar physical discontinuities, which arise due to residual compressive stresses in the scale as a result of growth and thermal stresses, decrease the useful life of the material.

Researchers put considerable effort on the subject for decades. Several different mechanisms are suggested. Some of them will be discussed in the following sections.

2.4.1 Reactive Element Effect

Reactive -or oxygen active- elements are metals, which form oxides that have higher stabilities than the protective oxides “alumina” or “chromia”. The high temperature oxidation literature is very rich in terms of reports on the effects of reactive element additions. Several, and usually conflicting theories have been proposed to identify the mechanisms that operate when these elements are present in the alloy. However, there is agreement that the additions of yttrium, zirconium, hafnium, cerium or their oxide dispersions to the alumina- and chromia-forming systems improve the adherence of the protective scale to the underlying material. Studies showed that both alumina and chromia scales benefited from these additions in similar ways in terms of some aspects. However, there were also certain features, which were observed on one system only. Some of the studies available in the literature will be summarized here to give brief information on the subject.

Investigations on alumina formers by several research groups showed a substantial improvement in scale adherence. One of the common conclusions was the observation of a change in the cation and anion diffusivities. There is agreement that the aluminum transport was suppressed relative to oxygen diffusivity by the addition of the reactive elements. The transport path was believed to be the oxide grain boundaries [2, 20, 30-32].

Studies also showed reactive element related morphological changes in alumina scales. Transitions from equiaxed to fine-and-columnar grains were reported by some researchers [30, 33, 34]. It was suggested that this transition improved the mechanical properties of the oxide

phase. Scale deformation by diffusional plastic flow or by grain boundary sliding became easier, which enabled accommodation of growth stresses.

Alumina grows by counter-current diffusion of aluminum and oxygen in systems that are not treated with reactive elements. This results in new oxide formation in the scale and increases compressive growth stresses [20, 30]. This may sometimes lead to interface imperfections such as convolutions [20]. Golightly et al. [20] proposed that Y additions prevented new oxide formation within the scale by suppressing Al transport. This avoided convolutions by decreasing the extent of compressive stress generation in the scale and improved scale adherence. Similar conclusions were also drawn by Ramanarayanan et al. [30].

Segregation of reactive elements to grain boundaries is also a common observation. According to Kofstad [2] the extremely small solid solubility of Y (referring to the study by Petot-Evans et al. [35, 36] on maximum Y solubility in alumina) and probably also of the other reactive elements causes segregation of these elements to grain boundaries and changes the grain boundary transport.

Another mechanism that is proposed to explain improved scale adherence is the formation of oxide pegs, which grow into the alloy around the internal oxide particles of reactive elements and mechanically key the scale. Allam et al. [37] stated that an optimized oxide peg distribution by internal oxidation pretreatment would decrease scale spallation. The method was successful on Hf and Ce, but it did not work on Y. Birks et al. [12], on the other hand, observed increased oxidation rates with increased yttrium oxide pegs. They said that Y_2O_3 incorporated into the growing alumina provided faster transport paths for oxygen than the alumina grain boundaries. They stated that optimum levels of Y (i.e. levels just below the concentration at which oxide pegs start to develop) are important for improved protectiveness. There are also studies where

improved adherence was obtained without peg formation. For example, Ramanarayanan et al. [30] reported that they did not observe any peg formation, although there was a substantial improvement in scale adherence. They suggested that peg formation may lead to an improvement, but is not necessary to obtain significant adherence.

The effectiveness of the reactive elements was also found to be dependent on the properties of the substrate material. The comparative study by Smialek et al [29] on NiAl and FeAl alloys with Hf and Zr showed that the growth rates in FeAl were higher in comparison to NiAl system. They attributed the less effective oxidation resistance of FeAl to the larger thermal expansion mismatch stresses in that system, and also to the non-optimal levels of dopants. They concluded that Hf and Zr were not the most effective elements in terms of improved oxidation resistance.

As mentioned earlier in this section, optimum levels of reactive element addition appear to be important. The study by Czyska-Filemonowicz et al. [31] is another example of this case. Their tests on FeCrAl-based ODS alloys showed that increased yttria contents caused accelerated oxidation rates. They reported that the higher growth rate was related to the increased number of oxygen diffusion paths by formation of alumina with very fine grain sizes.

Although the big picture of the response of alumina and chromia to oxygen active elements looks similar, the oxidation rates are affected differently in each oxide. Studies clearly showed that reactive elements decreased the rate of oxidation of chromia scales, whereas this conclusion does not apply to alumina. Ramanarayanan et al [21], tested both alumina and chromia formers for comparison purposes. They observed large differences in the oxidation rate of chromia after Y addition. The parabolic rate constants were 12-14 times larger for Y-free alloys. On the other hand, yttrium did not appear to influence the growth rate of alumina. The Pt marker tests showed that although the inward growth by oxygen diffusion was the predominant mechanism in

both cases after Y additions, in chromia there was also evidence for some outward chromium migration through the oxide. This suggested that the degree of suppression of the cation transport rate was less in this compound. Green and Bastow [38] reported that addition of reactive elements (0.5% Y, Hf, Ce and Zr) into Ni-20Cr and Ni-20Cr-6Al system did not change interdiffusion coefficients in the alloys, but decreased the oxide growth rate in Ni-Cr, improved maintenance of contact between alloy and scale, and reduced the degree of chromium depletion in the alloy beneath the growing scale. They reported that Y was the most effective addition for reducing depletion in Ni-Cr, while Ce had a smaller effect. Zr and Hf were the least effective elements, but still caused some reduction in chromium depletion compared to the reactive element free alloy. They proposed that the reactive element effect could be correlated with a decrease in Cr ion diffusion rates in chromia scales. Depletion of Al with and without reactive elements was negligible. It was due to slower alumina scale growth rate compared to chromia. According to Ramanarayanan et al [21], the effect of yttrium or thorium on oxide growth was particularly dominant in chromia formers. They made tests both on alumina and chromia formers.

Cotell et al. [39] tested pure Cr and Y-implanted Cr at 900°C. They reported that grain boundary segregation of Y changed the transport mechanism from outward cation diffusion to predominant anion diffusion.

Ecer and Meier [40] tested Ni-50Cr with Ce between 800-1100°C in oxygen, air and oxygen at reduced partial pressures. Their study showed that the rate of oxidation decreased with increased Ce content. Additionally, they observed slower oxide grain growth. They attributed these effects to the interaction of Ce ions and Ce-oxide particles with oxide grain boundaries in reducing grain boundary diffusion and oxide boundary mobility. Another significant effect of

Ce-addition was less oxide spallation upon cooling, which they believed resulted from thinner, finer-grained scales formed on Ce-containing alloys.

Another important observation is reported by Weinbruch et al. [41]. They tested both chromia and alumina formers between 900°C-1300°C. They observed yttrium diffusion to the surface of the oxide. Y was completely depleted in the oxide in both alloys after long exposures. Then, scale growth proceeded by simultaneous inward and outward diffusion of anions and cations, respectively. At this stage, the oxide growth mechanisms of both ODS and non-ODS alloys were the same. At a certain temperature yttrium depletion was found to be faster in chromia than alumina.

2.4.2 Sulfur Effect

Studies on alumina- and chromia formers suggest that there exists a relation between the scale adherence and the presence of sulfur. Although there is a debate on the responsible mechanism, all studies agree in that decreased sulfur levels provide better scale adherence. The methods to minimize the interaction of sulfur with the oxide scale vary from desulfurizing the bulk material by hydrogen annealing in controlled atmospheres, to tying up sulfur with Y to avoid its segregation.

Smeggil et al. [42] proposed that segregation of indigenous impurities such as sulfur to the metal/scale interface could markedly affect the scale adherence by weakening the bond between the protective scale and the substrate. According to the researchers the role of Y is to interact with sulfur and form a refractory sulfide in the alloy, which decreases the degree of surface segregation. Later studies by others showed similar results. For example, the report by Hou and Stringer [43] stated that Y was able to tie up S, inhibiting sulfur segregation, which is a possible

cause for scale failure. Siegers et al. [44] showed that Y suppressed sulfur segregation to the surface, and promoted Al-oxide formation, and also improved adhesion. Jayne and Smialek [45] state that interfacial sulfur segregation was related to spalling of protective alumina scales. They observed a significant improvement in cyclic oxidation behaviour of PWA 1480 by hydrogen annealing which decreased both bulk sulfur content and segregated sulfur content. Janakiraman et al. [46] also observed beneficial effects of decreased sulfur levels on alumina scales under cyclic conditions.

Studies on chromia yielded similar results. Lees [47] stated that improved adhesion and chemical composition were correlated with the sulfur content rather than reactive elements. Removal of sulfur from chromium increased scale adherence. Melas and Lees [48] reported that chromium could develop non-convoluted scales in the absence of reactive elements. Decreased impurity levels by hydrogen annealing the substrate enhanced flat and more adherent scale development. Fox et al. [49] observed similar results with commercial chromium of very low sulfur contents ($< 5\text{ppm}$). They reported that the same system developed convoluted and less adherent scales after contamination with sulfur. Similar results were observed on alumina scales in a Fe-5%Al alloy by these researchers. Dong et al. [50] proposed a change in the transport mechanism in chromia. They stated that sulfur promoted outward migration of cations. Removal of the element from the bulk enhanced inward oxygen transport. It also improved scale adherence.

Hou and Stringer [43] observed differences in the behavior of alumina and chromia in that, for alumina the accumulation of impurities at the metal/oxide interface was believed to be the primary reason for failure. However, the main effect on chromia was the interfacial morphology. Scale failures occurred on areas with large amounts of voids, which resulted from the oxidation

process. S segregation was also observed. However, the amount of sulfur on failed and adherent areas were found to be the same.

Although the mechanisms cannot be clearly defined, all the studies show that reactive element additions and sulfur removal improve scale adherence, or delay oxide spallation during isothermal as well as cyclic exposures. There is evidence that a certain ratio of reactive element to sulfur gives the best results [51]. Y was found to be the most effective reactive element in superalloys [38]. The lower effectiveness of Hf, Zr and Ti in complex alloys was attributed to their high solubility in Ni; and also to their higher tendency to form carbides in the alloy [51]. As a conclusion, the use of reactive elements with decreased sulfur levels is recommended [12, 51].

2.4.3 Other Factors

Hou and Stringer [52] did some tests with samples pretreated in quartz capsules with a Rhines pack. Their purpose was to develop internal oxides before exposure, and study their effect on oxidation kinetics. During chemical analysis they realized that the samples were contaminated with Si. Surprisingly, they observed lower oxidation rates, better scale adherence and more protective scale development on contaminated samples compared to the clean ones. More detailed investigation showed that small additions of Si were as beneficial as Y additions. Later on, similar results were observed with Si and Ti additions in NiCrAlY alloys [53].

The degree of surface smoothness is also known to play a role on scale adherence. Higher total mass gains and gradually increasing oxide spallation are reported with increased roughnesses on pre-oxidized alloy surfaces. However, Y doping the alloy changed the observed

differences. Alloys that contained Y demonstrated very good oxide adhesion irrespective of surface preparation [8].

2.5 EFFECTS OF WATER VAPOR ON OXIDATION

The majority of oxidation studies are conducted under controlled atmospheres with predetermined compositions of purified gases. However, in real applications, oxidizing atmospheres usually contain some amounts of N, S, and also water vapor, which sometimes have subtle effects on the reaction kinetics, but in certain cases may change the behavior significantly. Therefore, it is necessary to investigate the effect(s) of water vapor on the oxidation kinetics.

It is well known that most technical steels and superalloys oxidize in a different manner in atmospheres containing water vapor in comparison to dry air or oxygen. Many researchers have been working on the subject for several decades [41, 46, 54-83]. However, the mechanism(s) responsible for the observed behavior is(are) still not fully understood.

Early studies on Fe-systems showed increased oxidation rates in environments containing water vapor [55-58]. Rahmel and Tobolski [56], and Tuck et al. [57] observed perfectly adherent, but porous scale development in wet environments. Fuji and Meussner [55], and Kvernes et al. [58] also agreed that wet atmospheres induced porous scale formation.

Rahmel and Tobolski [56], Fuji and Meussner [55], and Kvernes et al. [58] proposed gaseous transport of H_2O , H_2 and O_2 via pores, and a dissociative scale development mechanism, where the reduction of the scale oxide and oxidation of metal/alloy take place in the vicinity of the pore.

Tuck et al. [57] proposed that the oxide scales, which developed in water vapor, had a higher plasticity, possibly due to the incorporation of hydrogen into the lattice, which may enhance the mobility of dislocations. They also reported that oxidation behavior depended on impurity level and sample geometry.

In time, research on this topic has spread over a larger selection of materials. As a result, the reported effects of water vapor started to display significant deviations from system to system. The most commonly encountered observation on such studies is water vapor related accelerations in the reaction kinetics [60, 63, 64, 69, 71, 73, 75, 77, 79, 81, 84, 85]. However, there exist studies where the reverse effects are reported as well [62, 76, 80]. Many times it is suggested that the oxidation is governed by diffusion controlled reactions, where the reaction kinetics display good matches with the parabolic rate law [60, 63, 73, 80]. However, some studies state otherwise [62, 84].

One of the observed effects of water vapor is morphological differences related to its presence. Several researchers reported the development of blade-like or whisker-type oxides in H₂O containing environments for different systems including the oxides of Fe, Cr, Cu, Ni, and Al [63, 64, 82, 85-87]. In the absence of water vapor the oxides had smoother surfaces. In such instances, other parameters including the exposure temperature, the oxygen partial pressure, or the flow rate of the reactive gases are believed to be critical as well. Asteman et al. [71] observed formation of needle-like oxide islands at low concentration of water vapor or at low gas flow rates on the alloy 304L. Smooth surfaces developed when the concentration or the flow rate was increased. Honda et al. reported a preferential growth of α -Fe₂O₃ whiskers along the [110] and [300] directions on SUS 430 stainless steel.

H₂O(g) can influence the composition and/or the crystal structure of oxide scales as well [54, 80]. For example, the study by Boualam et al. [54] with alumina scales reported a transition from metastable θ -Al₂O₃ to the stable α -Al₂O₃ in water vapor. The same study showed that the oxide which developed in the dry environment was θ -Al₂O₃. The transition from the metastable to the stable phase reflected itself as a minimum in the reaction kinetics.

It is widely believed that water vapor enhances oxide spallation, especially during cyclic exposures. Janakiraman et al. [46] tested alumina formers cyclically at 1100°C in dry air and in air with water vapor. They reported twice higher degradation rates in water vapor compared to dry air for the cracked and spalled scales. They proposed that water vapor causes stress corrosion cracking during cyclic oxidation at the alumina/alloy interface by changing the oxide/substrate interface bonding. In Fe-base systems, water vapor both enhances oxide spallation and shortens the incubation period before the onset of breakaway oxidation [71, 75, 77, 79]. However, there are also some cases where improved adherence is observed in wet atmospheres. Quadackers et al. [64] reported less buckling and better adherence on pure Cr and Cr-5Fe during oxidation in Ar-H₂-H₂O than in air, accompanied by morphological changes. Similar observations were reported by Henry et al. [78] for chromia layers grown on pure Cr in oxygen and in water vapor. Scales that developed in oxygen spalled off upon cooling, while even thicker scales that formed in water vapor did not.

Quadackers et al. [64] proposed a model, which correlates oxidation in H₂ containing environments to desulfurization by hydrogen annealing. As mentioned in the previous sections, low sulfur levels improve scale adherence. The unintentional desulfurization to some degree in H₂ containing atmospheres may be responsible for the improved scale adherence.

A research group from Sweden, which investigates the relation between hydrogen dissolved in the metal (or alloy) and the oxidation behavior of chromia forming systems, has another approach that correlates RE and hydrogen effects [68-70, 83]. Their tests with yttria treated and H charged Cr and Cr-5Fe showed that, in the absence of H, yttria did not have any influence on oxidation rates. On the other hand, H by itself caused early breakdown in samples, which were not yttria treated. Separate tests with H charged and dehydrogenated samples showed that H caused spallation and wrinkling, whereas removal of the element resulted in flat and adherent scale development, which they related to substantial outward cation migration accelerated by H [83]. (This observation resembles the observations in S studies by others). Moderate amounts of hydrogen combined with Y_2O_3 , however, displayed a decrease in oxidation rate. Their model suggests that yttria increases the O_2 dissociation rate, and hence, inward oxygen transport, while H enhances cation diffusion. A balance between anion and cation diffusion rates gives the best protection to the system. Similar results were obtained using Pt. They proposed that adjusting the transport of metal and oxygen ions by the use of RE additions or Pt to counteract the H effect, which increases the transport of metal ions by segregating to grain boundaries, pores, and micro cracks, would improve the resistance of the systems.

These studies suggest that there might be a similarity between the S effect and the dissolved H in the alloy. It is possible that hydrogen is the responsible agent for the differences in oxidation in H_2O containing atmospheres.

As discussed in an earlier section, it is well established that RE additions improve scale adherence in air, or $O_2(g)$ environments. Similar beneficial effects of oxygen active elements are also reported in H_2O containing environments. Jianian et al. [75] observed delayed breakaway oxidation on CeO_2 treated Fe-Cr alloys. They proposed that the transport of water vapor was

taking place in molecular form through the channels and cracks in the oxide. H₂O reacted with Fe in the Cr depleted zone and gave rise to formation of Fe-oxides. The additions of ceria decreased the number of defects at the oxide/gas interface, which in turn inhibited breakaway oxidation of FeCr alloys in O₂/H₂O mixtures. The study by Quadackers et al. [64] with Cr5Fe and Cr5Fe1Y₂O₃ showed that the presence of yttria in the alloy decreased the reaction rate in Ar/H₂/H₂O. They reported that the formation of whiskers in wet environments was less pronounced on the ODS treated alloy.

Water vapor may also have an impact on the defect structure of the oxide phases. Fritscher and Lee [81] observed a transformation from p-type conduction in air to n-type in H₂O-O₂ mixtures on chromia scales. Liu et al. [59] reported that chromia scales were intrinsic electronic conductors above 700°C, and mixed ionic-and-electronic conductors below this temperature. They showed that H doping of chromia could reduce both electronic and ionic conductivities. They proposed that proton dissolution in the lattice reduced concentrations of electron holes and chromium interstitials. Treatment of the alloy with yttria displayed similar effects, which they related to segregation of RE to grain boundaries and cutting off short circuit paths for ionic transport.

Henry et al. [77] proposed a mechanism based on ionic radii of the possible oxidizing species, i.e. O²⁻ (ionic radius = 140 pm) vs OH⁻ (ionic radius = 95 pm). They suggested that OH⁻, being the smaller agent, migrates faster, which explains the higher oxidation rates in wet atmospheres. Galerie et al. [76] stated that OH⁻ ions could be incorporated into the oxide lattice as substitutional defects only, because their radii are too large for interstitial positions (100-120 pm depending on coordination number vs a few pm)², and move exactly the same way as oxygen

² Reference does not specify the oxide.

ions do. Another possibility for the mobility of the species in the lattice they suggested was that hydrogen jumped from a blocked OH^- site to an oxide ion position. They concluded that the reaction rate of H_2O with metals would be faster than O_2 provided that hydroxyl ion transport is possible in the oxide phase (p-type oxides). The alternative model for cases, where OH^- transport was not possible, was based on another parameter which they called “the surface acidity”. Surface acidity is related to the bond properties of the H_2O molecule. In their paper, they stated that the energy required to break the second O-H bond is twice as much as that required to break the first O-H bond. Therefore, the surfaces of species exposed to H_2O were easily covered with hydroxyl ions, but to form oxygen species was not that easy. This was where surface acidity became important. As quoted from their paper “Acidic surfaces can fix the OH particles tightly by their oxygen electron pairs, which leads to great polarization and easier breaking of the second O-H bonds” [76]. The reaction rates were expected to be higher the more acidic the oxide was.

A model is proposed by Passier et al. [62] for the oxidation of Nb and Ti in H_2O . They suggest that the limiting step is the surface reaction of oxygen incorporation into the oxide scale, without formation of hydroxide defects.

2.6 VOLATILIZATION OF CHROMIA

Volatile oxide formation is a problem mainly for alloys that depend on chromia for oxidation resistance. In general, alumina formers are less susceptible to degradation of this type. Alumina is highly stable in pure oxygen. The decomposition of Al_2O_3 into Al, oxygen or gaseous

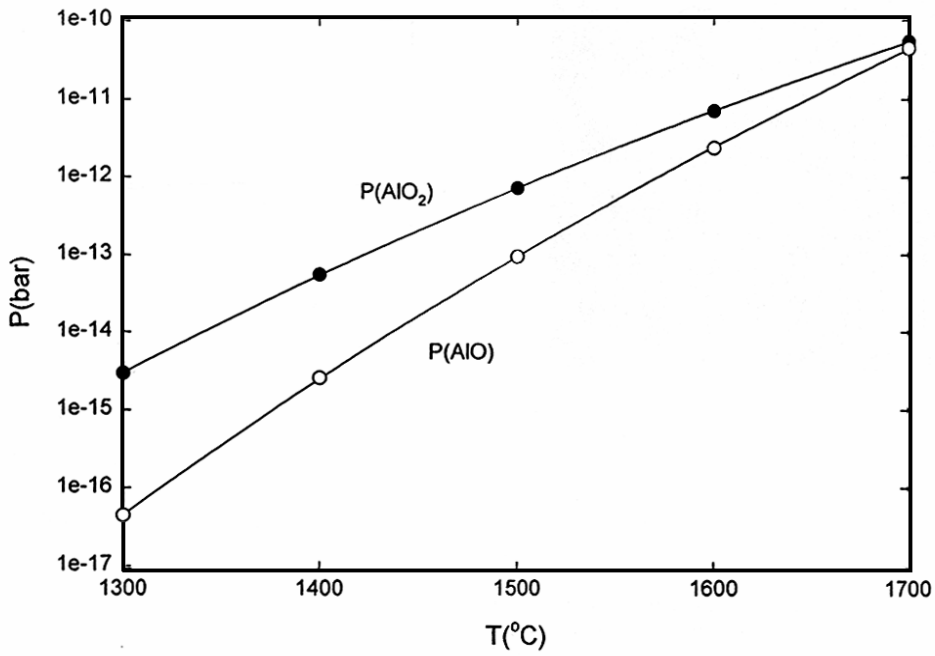
aluminum oxides occurs at very high temperatures and at very low oxygen pressures. Increased pressures suppress vaporization of the oxide. According to Tai et al., [67], the vaporization of alumina would be enhanced in H₂O due to the formation of Al-O-H vapor species. However, even then this effect is not significant at temperatures of 1500°C and below. The plots of partial pressures for the major vapor species over Al₂O₃ are shown in Figure 2.6 as presented by Tai et al., [67].

Alloys that rely on the formation and maintenance of chromia layers are subject to deterioration by the loss of the protective scale as vapor species at temperatures as low as 600°C [72, 88]. The problem becomes more pronounced at elevated temperatures. This issue was addressed by early studies when significant weight losses were noticed by the researchers [89]. These weight losses were too large to be solely due to the formation of vapor Cr₂O₃, since the equilibrium vapor pressure of chromia was too low [90].

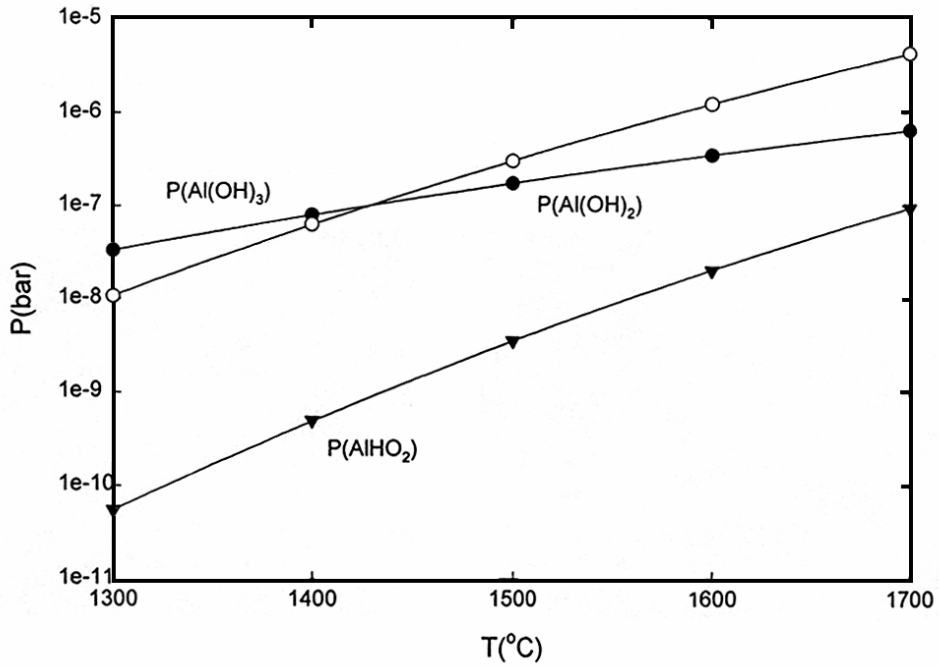
Studies have shown that the most stable vapor oxide over Cr₂O_{3(s)} in air or in O₂ is CrO_{3(v)} for the temperatures of interest. A plot showing the equilibrium vapor species of some Cr-oxides is given in Figure 2.7. In environments where the source for oxidation is O₂, Cr₂O_{3(s)} may convert to CrO_{3(v)} according to the reaction;



if thermodynamic and kinetic conditions are favorable. However, when water vapor is involved in the reaction, different vapor species are stable. Investigations have shown that the most stable Cr-species in humid air is CrO₂(OH)_{2(v)}, [65, 91]. Under such conditions, the reaction is defined as



(a)



(b)

Figure 2.6: The equilibrium pressure of the major vapor species over alumina is plotted as a function of temperature (a) in Ar/O₂, and (b) in Ar/H₂O, [67].



A diagram showing the equilibrium pressures of Cr-species in O₂/H₂O mixtures is available in Figure 2.8.

The growth kinetics of chromia scales is believed to be parabolic. The oxygen pick-up during oxide formation results in an increase in the total weight of the system. This is represented as

$$\left(\frac{\Delta m}{A}\right)^2 = k_p t + C \quad \text{Eqn 2.8}$$

where $\frac{\Delta m}{A}$ is the weight change in the system per unit surface area, k_p is the parabolic rate constant, and t is time [89]. The reactions between chromia and O₂/H₂O are surface controlled reactions which follow the linear reaction kinetics. During the formation of the volatile species the system loses weight. Tedmon [90] analyzed the oxidation kinetics of chromia, and derived the following equation;

$$\frac{dx}{dt} = \frac{k'_p}{x} - k'_s \quad \text{Eqn 2.9}$$

where $\frac{dx}{dt}$ is the change in the thickness of the scale as a function of time, k'_p is the constant describing the diffusive growth of chromia, and k'_s is the constant defining the volatilization.

The integration of this equation gives

$$\frac{-x}{k_s} - \frac{k_p}{k_s^2} \ln(k_p - k_s x) + C = t \quad \text{Eqn 2.10}$$

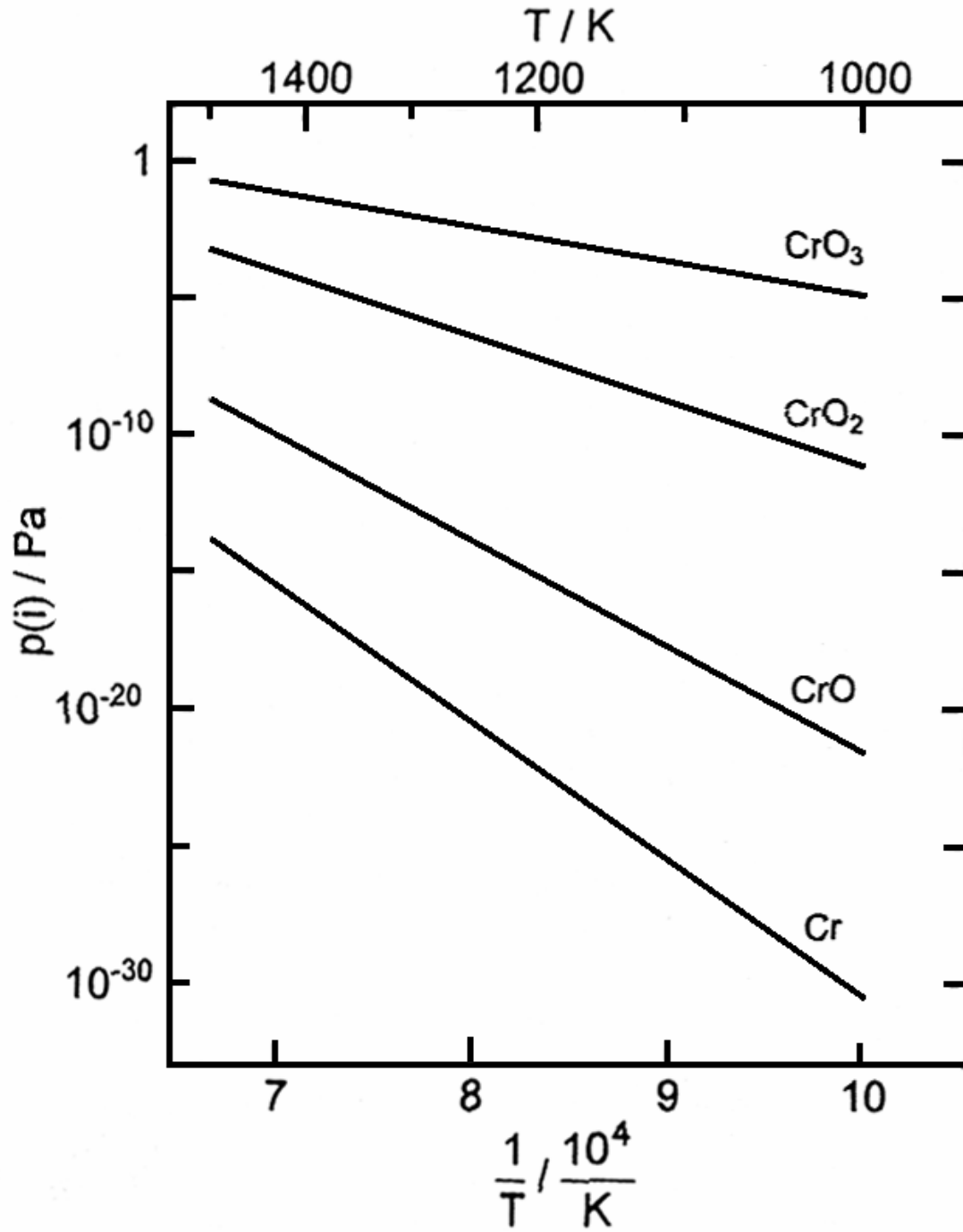


Figure 2.7: Partial pressures of vapor Cr-oxides over $\text{Cr}_2\text{O}_3(\text{s})$ in air ($\text{PO}_2 = 0.21 \text{ atm}$) as a function of time, [65].

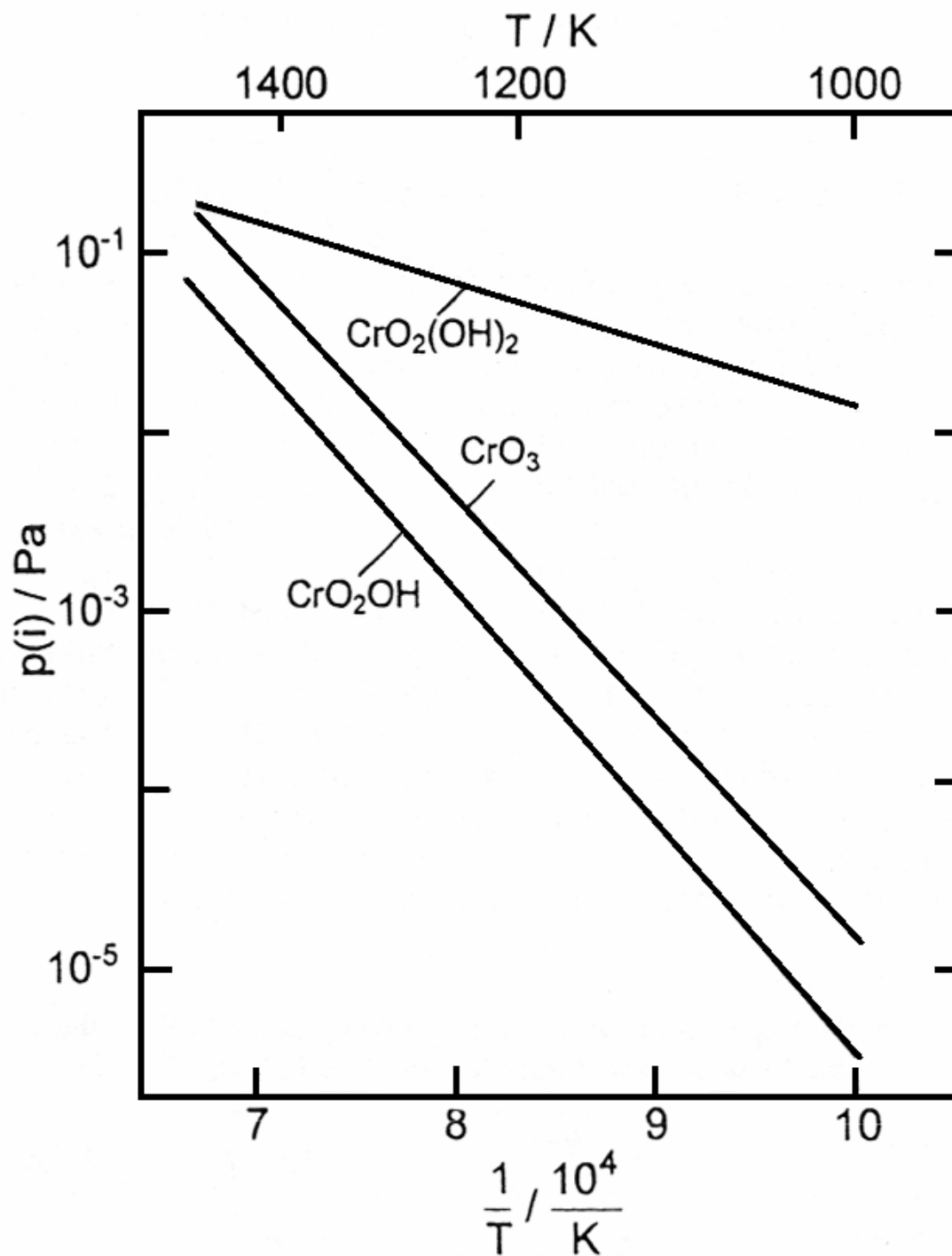


Figure 2.8: Partial pressures of most abundant Cr containing species over $\text{Cr}_2\text{O}_3(\text{s})$ in humid air at different temperatures ($P_{\text{O}_2} = 0.21$ atm, $P_{\text{H}_2\text{O}} = 0.02$ atm), [65].

During the early periods of oxidation the effect of chromia volatilization is not very significant. The formation of chromia is more rapid due to the faster diffusion of the ions through the initially thin oxide layer. However, as the scale thickens, the volatilization rate becomes important. The limiting thickness, x_0 , is reached when the growth rate equals the volatilization rate. This is defined as

$$x_0 = \frac{k'_p}{k'_s} \quad \text{Eqn 2.11}$$

from equation 2.9 by setting $\frac{dx}{dt} = 0$, [3].

The formation of vapor species is typically more aggressive in O₂-H₂O mixtures than in oxygen. Studies in air or in oxygen have shown that the vaporization effects are not very significant at temperatures below 1000°C, [92]. However, tests in H₂O containing environments showed that alloy degradation due to formation of volatile species is a concern even at 600°C [93].

According to the studies by Gindorf et al., [66], and Hilpert et al., [65], the temperature dependence of vaporization rate in wet air is not as strong as in dry air, considering the vapor species are CrO₂(OH)₂(v) and CrO₃(v) in wet and in dry oxygen, respectively. This can be seen also in Figure 2.8.

When the oxidation process involves oxide vaporization, gas flow rate should be watched closely. As the evaporation rate is surface controlled, flow rate of the reactive gases influences the reaction kinetics significantly. Volatile oxides diffuse from the surface through a stagnant gas phase layer, which builds a boundary between the bulk gas and the substrate surface. Increased flow rates will cause substantial evaporation by decreasing the thickness of the boundary layer.

Asteman et al. [72] observed mass losses related to volatile oxyhydroxide formation in $\text{H}_2\text{O} + \text{O}_2$ environments, and not to scale spallation. Their further studies showed a strong dependence of oxidation characteristics on water vapor concentration and on flow rate [71, 93]. They reported that ‘chemical etching’ was responsible for non-homogeneous and non-protective oxidation. As chromium diffuses faster along grain boundaries it reacts in the first place with water vapor to form $\text{CrO}_2(\text{OH})_2$. Flowing gases carry away the volatile species and re-expose the grain boundaries to H_2O . Because Cr diffusion in the grain interiors is not fast enough, non-protective oxides form over these areas. The result is a surface with grooves along grain boundaries and hills of non-protective oxides. They suggested that surface applications, which provide easy diffusion paths such as shot peening, would be beneficial.

Studies have shown that the presence of reactive elements does not affect the volatilization rate. However, the growth rate of the chromia is observed to decrease significantly, [19].

Volatilization in the W-O system is important at high temperatures and high oxygen pressures. The volatilization in this system does not follow the parabolic reaction kinetics, where a limiting thickness is reached. Instead, complete volatilization of the oxide can occur. The vapor species diagram of the system at 1250 K is presented in Figure 2.9, [3].

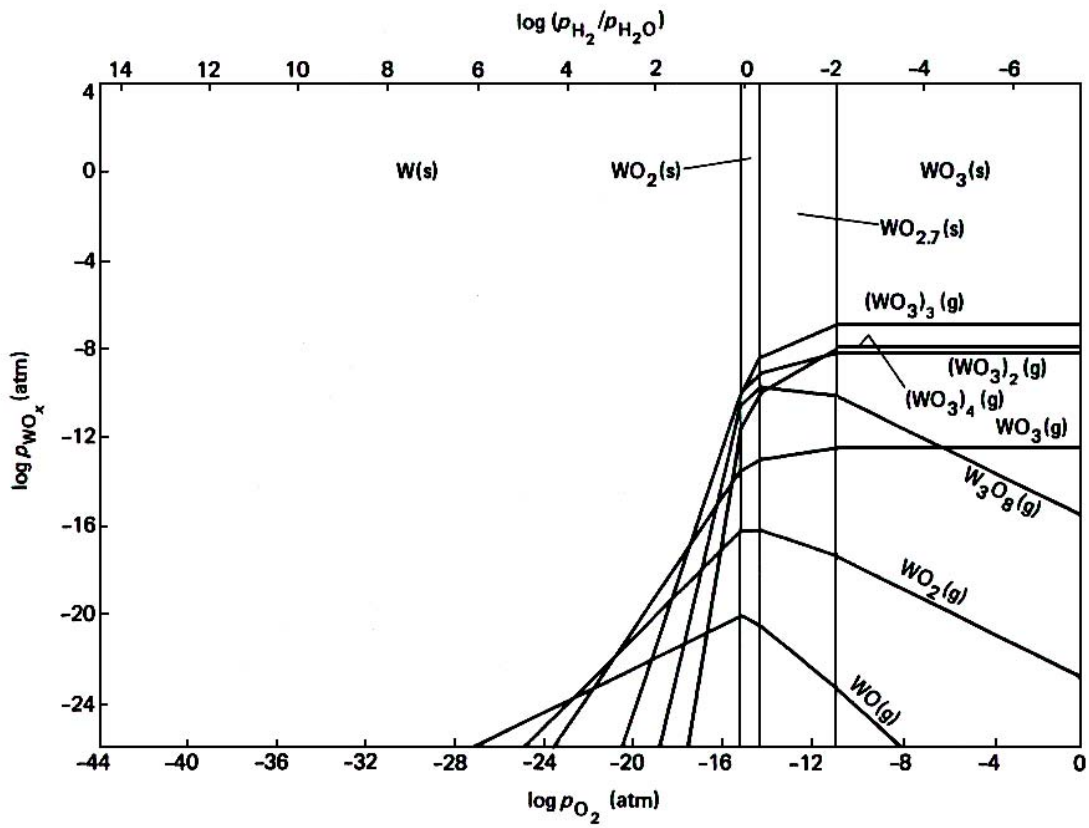


Figure 2.9: Volatile species of the W-O system are shown at 1250K, [3].

3.0 RESEARCH APPROACH

The metals and alloys that are used in some industrial applications might become exposed to H₂O during operation. For such cases, the involvement of water vapor could be intentional or unintentional. In some applications, such as the solid oxide fuel cells, H₂O is present in the environment as a by-product of some reactions. Some other industrial applications require the use of water vapor such as the gas turbines where steam injection is used to augment power and reduce emissions. For these applications, field experience has shown that hot section distress in the gas turbine is more severe when steam injection is employed. However, the interaction of steam/air mixtures with the turbine airfoil materials is not very well understood, [94].

As reviewed in the background chapter, water vapor could have a variety of effects on the oxidation of metals and alloys. These effects depend on several factors including, but not being exclusive to, the alloy under consideration, the oxidation temperature, the water vapor pressure, the gas flow rate, and the surface conditions of the unexposed alloy. Although substantial work has been done for decades, the responsible mechanism(s) for the observed differences in the oxidation behavior of materials in environments with and without H₂O(g) are not identified with certainty. This brings in the necessity for further investigation of the subject.

The aim of this work was to gain a thorough understanding regarding the behavior of superalloys which were considered as candidate materials for applications involving water vapor.

Experimental planning targeted observing the response of these materials to different temperatures, steam pressures and surface conditions. The information obtained from the preliminary testing was then used to narrow down the experimental parameters and get a more basic understanding of the phenomena using simpler systems as model alloys.

During the preliminary work, Ni- and Co-based superalloys with various Al and Cr concentrations were tested. The alloy selection involved both chromia and alumina formers. The list of the alloys along with their chemical compositions is presented in Table 3.1. Chromia is a stable oxide at low temperatures. However, as the temperature increases, formation of volatile oxides and/or oxyhydroxides arise which result in the rapid degradation of the protective scale. On the other hand, alumina forms preferentially at these elevated temperatures. Therefore, tests were designed to enable observing the temperature-dependent transition from protective to non-protective behavior of the alloys.

All superalloys were subjected to tests in air/H₂O mixtures (wet air) and in dry air at a constant gas flow rate. The study compared the oxidation behavior of each system to itself and to others. Comparisons were based on the following criteria:

- testing environment, i.e. wet air versus dry air
- temperature
- alloy composition
- testing mode, i.e. cyclic versus isothermal

The response of the systems to temperature changes was documented by exposing the alloys to the reactive gases between 700°C and 1000°C. In industrial use, the components are often being subjected to temperature fluctuations. Therefore, the specimens tested in this work were also

thermally cycled to simulate the real-life applications more closely. These tests were done at 1 atm. total pressure. In air/water-vapor mixtures, the partial pressure of H₂O was set to 0.3 atm. In general, cyclic exposures cause more rapid degradation of the alloys due to the additional thermal stresses under such conditions, which enhance spallation of the protective oxide scales. To understand the contribution of thermal cycling to the failure of the systems, some isothermal tests were also included in the planning of the experiments. These tests were done at 900°C in air/steam mixtures (P_{H₂O} = 0.3 atm).

In the gas turbine, the alloy system is being exposed to high-pressure gases. During the course of this study, it was attempted to observe the effects of high pressure steam on the oxidation behavior of the alloys under investigation. For this purpose, coupons of each alloy were exposed to 100% steam at 17 atm. at 700°C and 900°C. These tests were done at the Oak Ridge National Laboratories.

The data obtained from the preliminary work provided basic understanding about the effects of water vapor on the oxidation behavior of the alumina and chromia forming superalloys. During the second part of the study, tests were done with simpler systems as models to overcome the compositional complexity of the superalloys. This time the focus was narrowed down to chromia formation and the effects of water vapor on this phase. The experiments were designed to investigate the following aspects of the phenomenon;

- selective oxidation of Cr
- growth rate of Cr₂O₃ scales
- spallation of the protective chromia scales
- formation of the vapor species, i.e. CrO_{3(v)}/CrO₂(OH)_{2(v)}

Work was done on alloys of Ni-Cr with various compositions. Each composition targeted to identify a certain aspect of the problem as shown in Table 3.2. Tests involved thermal cycling and isothermal exposures at 700°C and 900°C. The data accumulated were analyzed, and the information obtained was used to develop mechanisms in an attempt to explain the phenomena.

Table 3.1: Chemical Compositions of the Superalloys in Weight Percent

<i>Alloy</i>	<i>Ni</i>	<i>Cr</i>	<i>Al</i>	<i>Co</i>	<i>Ta</i>	<i>W</i>	<i>Mo</i>	<i>Ti</i>	<i>B</i>	<i>C</i>	<i>Hf</i>	<i>Zr</i>	<i>Nb</i>	<i>Re</i>
PWA 1484	Bal.	5.0	5.6	10.0	8.7	6.0	2.0				0.1			3.0
René N5	Bal.	7.0	6.2	7.5	6.5	6.0	0.6				0.1			3.0
CM 186	Bal.	6.6	5.7	9.2	3.2	8.5	0.5	0.7	0.01	0.07	1.4			
MarM 247	Bal.	8.2	5.4	9.9	3.0	9.8	0.7	1.05	0.01	0.13	1.3	0.4	0.2	
IN 738	Bal.	16.0	3.4	8.5	1.7	2.6	7.1	3.4	0.001	0.11		0.05	0.9	
X-40	10	25.5		Bal.		7.5				0.5				

Table 3.2: List of Ni-Cr alloys shows the test conditions and the information expected from each test.

Alloy Composition	Test Details		Targeted Aspect
	Test Condition	Temperature	
Ni-15Cr	Cyclic (wet and dry)	700°C	Selective oxidation of Cr
		900°C	
Ni-15Cr-0.1Ce	Cyclic (wet and dry)	700°C	Selective oxidation of Cr, Spallation of chromia scales (R.E. effects)
		900°C	
Ni-20Cr	Cyclic (wet and dry)	700°C	Selective oxidation of Cr
		900°C	
Ni-30Cr	Cyclic (wet and dry)	700°C	Spalling of chromia scales
		900°C	
	Isothermal (wet and dry)	700°C	Formation of vapor species, Growth rate of Cr ₂ O ₃
		900°C	
Ni-30Cr-0.1Ce	Cyclic (wet and dry)	700°C	Spalling of chromia scales (R.E. effects)
		900°C	
	Isothermal (wet and dry)	700°C	Formation of vapor species, Growth rate of Cr ₂ O ₃
		900°C	

4.0 EXPERIMENTAL DETAILS

The materials that were used during this study are grouped into two classes: the superalloys and the Ni-Cr binary system. The experimental work considering the superalloys is investigated under the title Part I, while the work with the model alloys is discussed as Part II.

The list of the superalloys under investigation was presented in the previous chapter (Table 3.1). All of these alloys are Ni-based systems with the exception of X-40, which is a Co-based material. PWA 1484 and René N5 are single crystals while the rest are polycrystalline. On this list, the first four systems, i.e. PWA 1484, René N5, CM 186 and MarM 247 are designed such that they develop the slowly growing alumina scales upon exposures to reactive gases at high temperatures. Hence, they are classified as alumina formers. IN 738 and X-40 are known as chromia formers. The Cr content of these systems is significantly higher than the other alloys under investigation. The alloy list that was used during the second part of the study was also provided earlier in the previous chapter (Table 3.2).

For the tests, either disc-shaped or rectangular specimens were prepared depending on the geometry of the bulk material. The approximate dimensions of the rectangular specimens were 10x15x1.5 mm. The discs were approximately 10-16 mm in diameter, and 1.5 mm in thickness. Suspension holes were drilled in each specimen to enable hanging them on silica rods. All surfaces were mechanically polished with abrasive paper down to 600-grit, and then cleaned with

soap-water mixtures under running water, followed by ultrasonic cleaning in acetone before exposure to temperature.

The experiments with the superalloys were performed mostly in horizontal tube furnaces. A schematic of the apparatus is provided in Figure 4.1. These furnaces were used for cyclic exposures in dry air as well as in air/water-vapor mixtures. All cyclic experiments were done at atmospheric pressure. To establish the wet air environment, extra-dry grade tank air was passed through water containers which were kept at a certain temperature to satisfy the desired saturation level. During the experiments in Part I, the partial pressure of water vapor was chosen as 0.3 atm. To establish this environment, the temperature of the water bath was maintained at 72°C. During Part II exposures, this value was decreased to 0.1 atm. This time, the water bath temperature was 46°C. For the dry exposures, the tank air was directly sent to the furnace.

The cyclic experiments were designed as 1 hour periods where the specimens were exposed to hot gases for 45 minutes, and then cooled down to lower temperatures (200-208°C) for 15 minutes outside the hot zone. The exposures were interrupted periodically (approximately every 50 cycles) to record the weight changes of the specimens as a function of time, along with the visual examination of the oxide surfaces. The weight change data were used to document the oxidation kinetics of the systems under investigation. The cyclic tests with the superalloys were performed at 700°C, 900°C and 1000°C. For the model alloys the 1000°C exposures were omitted.

The horizontal tube furnaces were also utilized for isothermal tests in wet air. During these experiments, the mechanism which moved the specimens into and out of the furnace was turned off. These isothermal experiments were performed with the superalloys and at 900°C only. The partial pressure of H₂O was again 0.3 atm. under a total pressure of 1 atm. These tests were

performed to document the microstructural differences that arise between thermally cycled and isothermally exposed alloys subjected to the same environment for the same duration.

Another set of isothermal exposures with the superalloys was done in 100% steam at high pressures (250 psi). These experiments were performed in autoclaves at 700°C and 900°C at the Oak Ridge National Laboratory.

The third group of isothermal tests was done with the systems that develop chromia scales for oxidation resistance. The technique utilized was thermogravimetric analysis (TGA). This method enables continuous recording of the weight changes that occur during oxidation reactions. The schematic of the experimental set-up is provided in Figure 4.2. The weight change data were recorded digitally via a Cahn D200 model microbalance that was connected to the vertical quartz tube. The specimens were suspended into the flowing gases via a platinum wire. The gas flow rate was approximately 0.05 cm/sec. These tests were done in dry air and in air/H₂O mixtures at 1 atm total pressure. The H₂O partial pressure of the wet environment was set to 0.1 atm. Exposures were done at 700°C and 900°C.

All specimens were subjected to microstructural and chemical characterization. Optical and scanning electron microscopy techniques were utilized for the analysis and documentation of the reaction zone microstructures. The chemical analysis was done by the energy dispersive analysis method. Normalized weight change data of the specimens as a function of exposure time were used to examine the kinetics of oxidation.

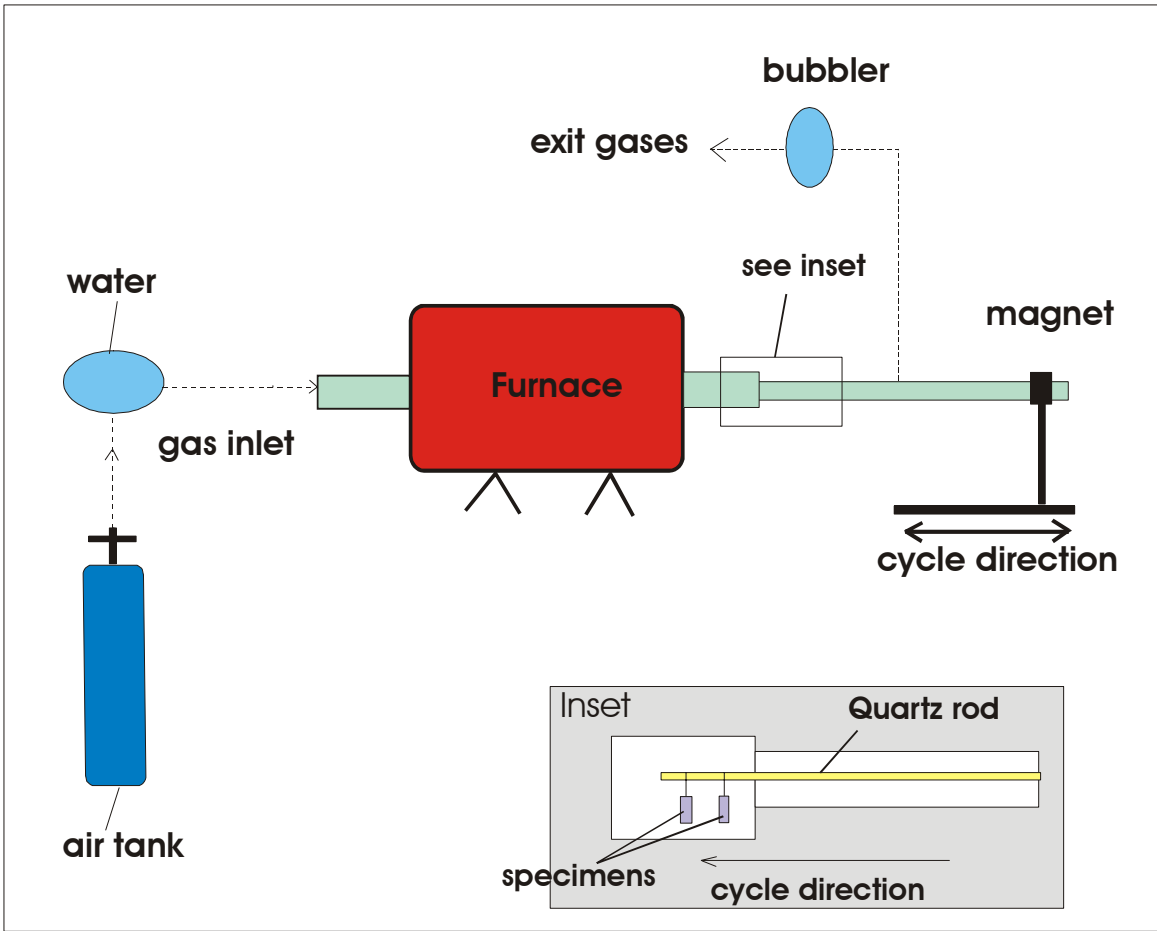


Figure 4.1: Schematic diagram showing the horizontal tube furnaces used for thermal cycling tests in flowing gases with defined and controlled amounts of water vapor in dry air at a total pressure of 1 atm. Arrows show directions of gas flow. The specimens are hung on silica rods with platinum wires, and are cycled in and out of the hot zone at defined time intervals.

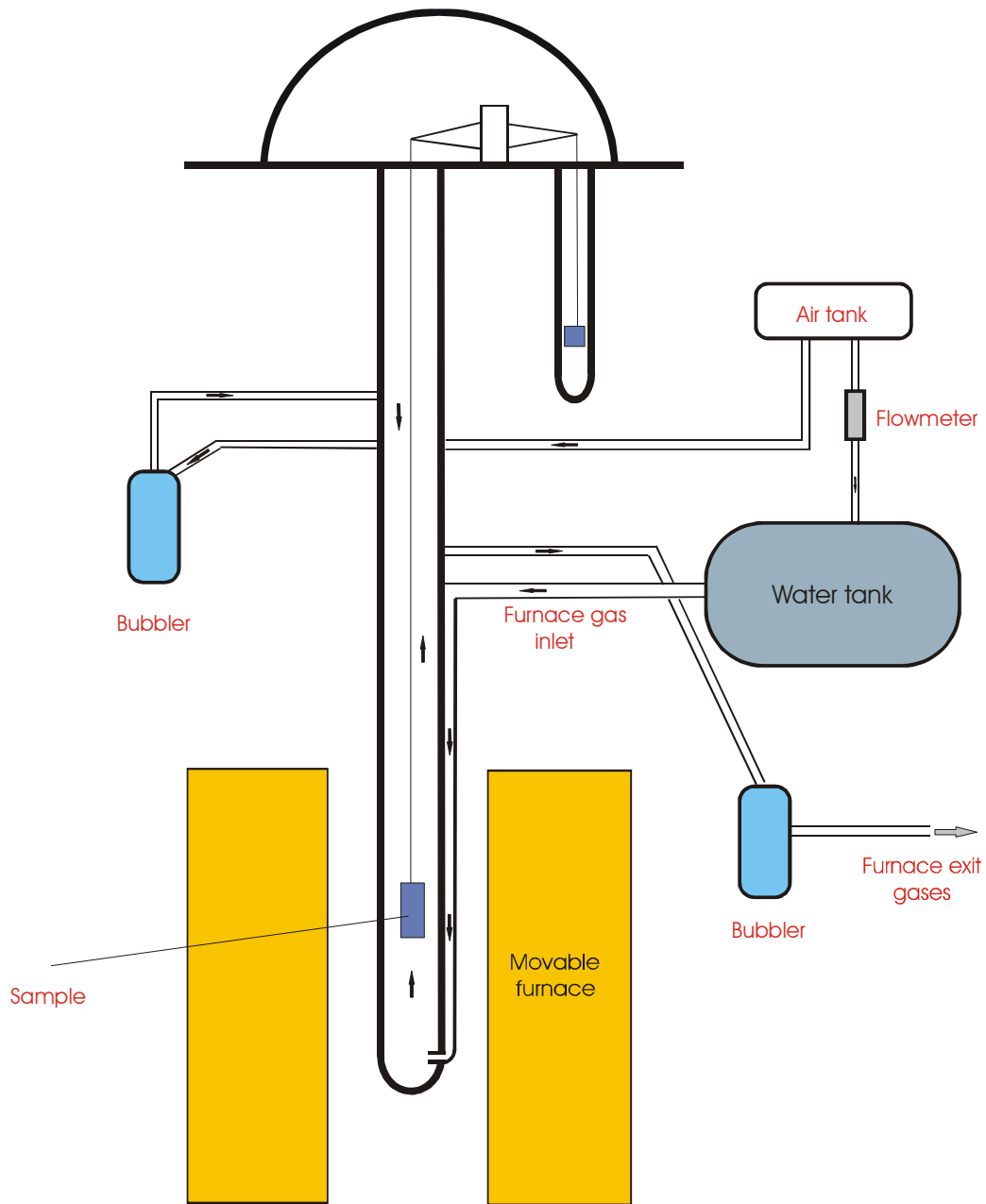


Figure 4.2: Schematic diagram showing the apparatus to isothermally oxidize coupon specimens in flowing gases with defined and controlled amounts of water vapor in dry air at a total pressure of 1 atm. Arrows show directions of gas flow. The air flow in the upper region of the reaction tube is to prevent water vapor condensation in the balance area.

5.0 RESULTS-PART I

5.1 SUPERALLOYS THAT ARE CLASSIFIED AS ALUMINA FORMERS

5.1.1 Alumina Formers Cyclically Exposed in Dry Air and in Air/Water Vapor Mixtures with $P_{H_2O} = 0.3$ atm at a Total Pressure of 1 atm.

5.1.1.1 Alumina Formers at 700°C: The tests at 700°C using René N5, CM 186, PWA 1484 and MarM 247 indicated that the response of the alloys to attack was strongly dependent on their composition. This was especially significant in wet air. In this section, first the results obtained will be discussed for each alloy. Later, comparisons and general comments will be made.

Tests with René N5 indicated that the alloy was not severely attacked at 700°C. The kinetic data suggested that the oxidation reactions were very slow in both environments, Figure 5.1. The system did not display significant weight changes even after 3200 hours of cyclic exposures to hot gases. The back scattered electron images of sample cross-sections after 3200 cycles are shown in Figures 5.2-5.3. The EDX examination of the scale that developed after exposures in dry air indicated the presence of a thin chromia layer at the oxide gas interface accompanied by internally formed alumina. The alumina was able to develop partial continuity in some locations. In other parts it was present as fine precipitates underneath the chromia layer. In wet air there was no evidence for the formation of a continuous layer. Instead, many locations were spotted

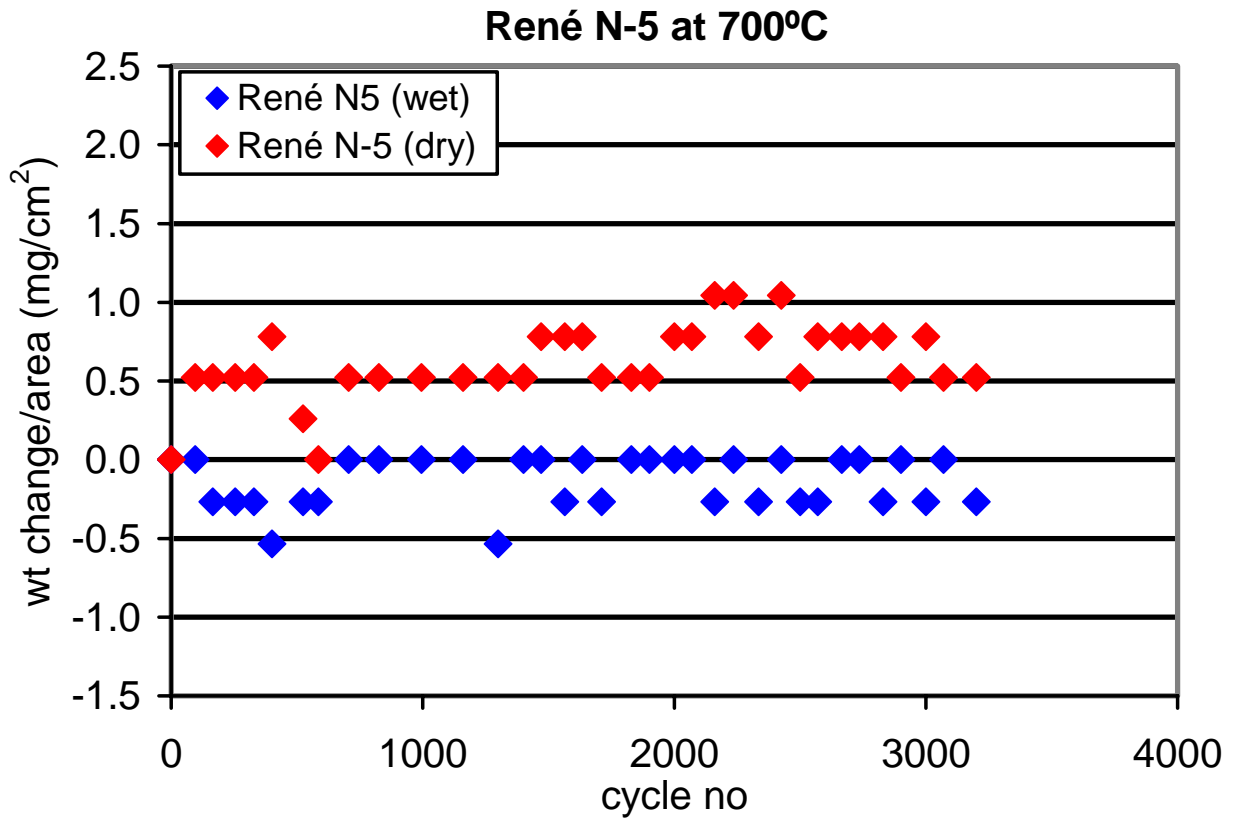


Figure 5.1: Kinetic plot of the alloy René N5 showing the weight change of the specimens in dry air and in air/H₂O mixtures at 700°C as a function of cycle number.

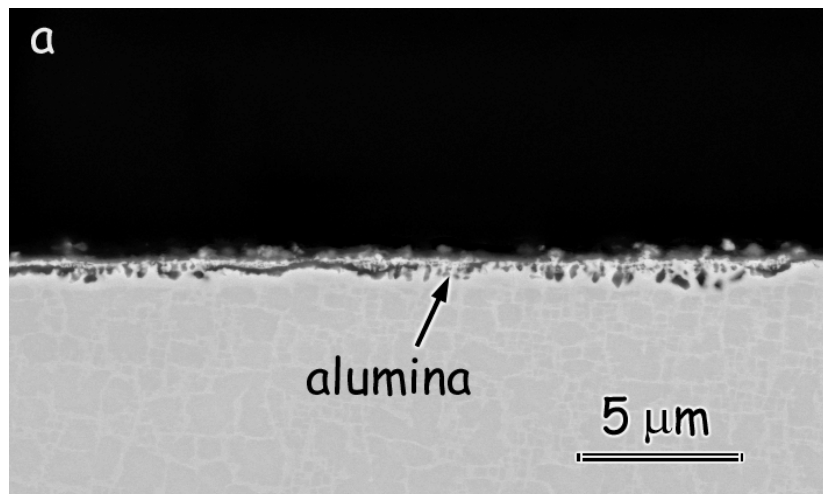


Figure 5.2: René N5 at 700°C after cyclic exposures in dry air at 700°C for 3200 cycles. Micrograph shows the cross-section of the sample.

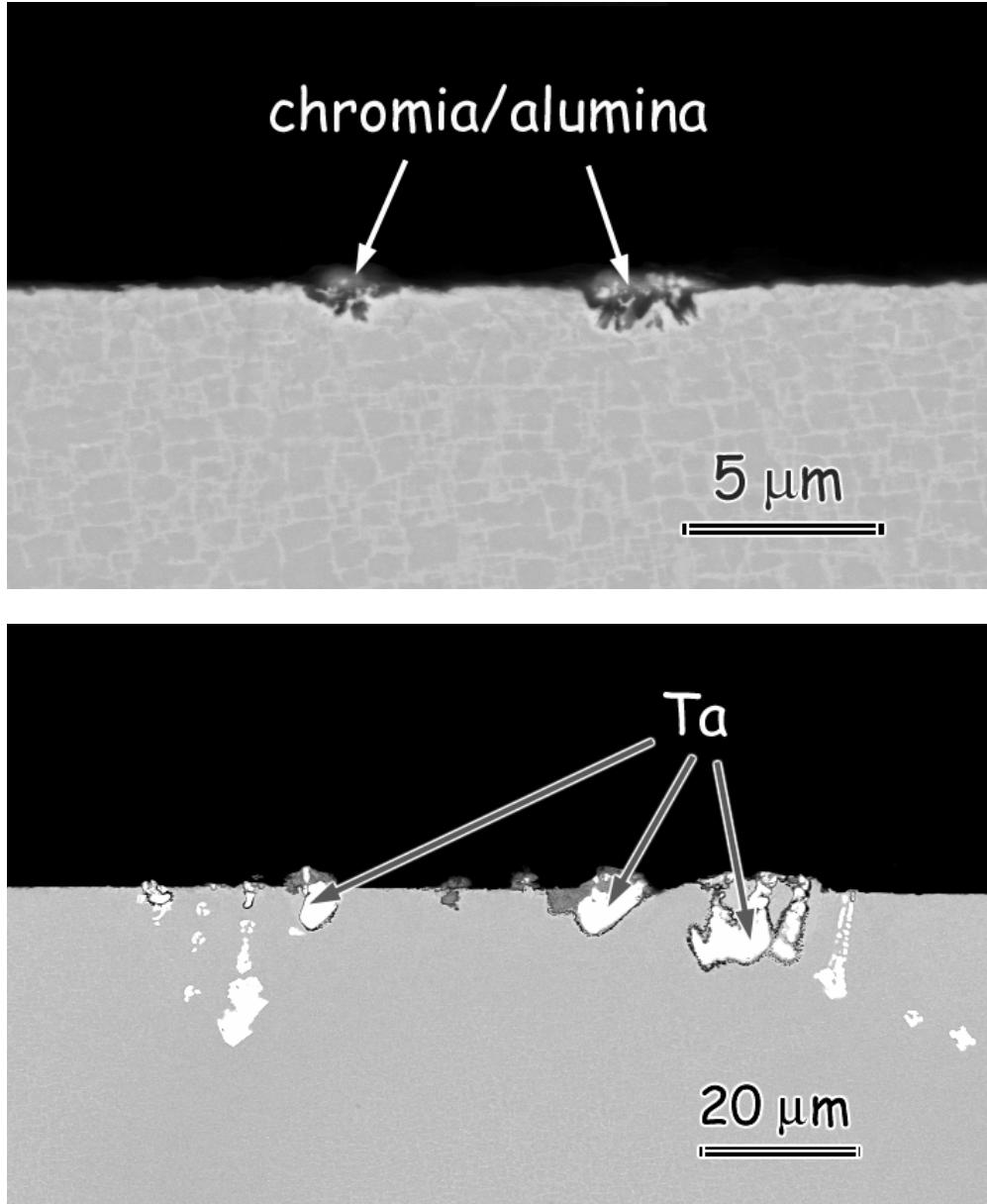


Figure 5.3: Back scattered electron images of René N5 showing the sample cross-section after 3200 cycles at 700°C in wet air (a) protrusions of chromia/alumina, (b) islands of Ta-oxide with alumina.

where protrusions of oxides developed, Figure 5.3. Some of these protrusions were small islands of chromia/alumina. However, a major fraction of them consisted of Ta-oxide islands surrounded by a thin layer of alumina. The examination of the as-processed specimens showed that these Ta islands were present in the pre-exposed condition, Figure 5.4. It appeared that the Ta/matrix interface acted as a fast diffusion path and accelerated internal oxidation in the vicinity of the reactive element particles.

The test results of PWA 1484 at 700°C indicated that the oxidation behavior of the alloy differed drastically in environments with and without water vapor. The kinetic plots pointed to exceptionally high oxidation rates in wet air, as Figure 5.5 shows. On the other hand, the kinetics in dry air was comparable to other alloys that were under investigation. The cross-sections of the samples were examined with scanning electron microscopy. The image of the dry exposed specimen is shown in Figure 5.6 (a). As is apparent in the figure, the alloy developed a thin Cr-rich outer scale. Aluminum oxidized internally. Al_2O_3 could not develop a continuous layer under the test conditions. The cross-sectional SEM image of the wet exposed sample is given in Figure 5.6 (b). As the micrograph indicates, this time the system developed an undesirably thick oxide layer. The degree of attack was very severe. The thickness of the layer was approximately 30 times larger compared to the one that developed in dry air after exposures for the same number of cycles. The entire scale consisted of several layers of fast-growing non-protective transient oxides. The presence of water vapor caused oxygen to move rapidly into the alloy. Therefore, a continuous chromia scale could not develop as occurred in dry air.

The weight change rates of CM 186 during early oxidation were also significantly different in air/ H_2O mixtures and in dry air as indicated in the kinetic plot, Figure 5.7. Larger weight gains were observed in wet air which is an indicator of more profuse transient oxidation.

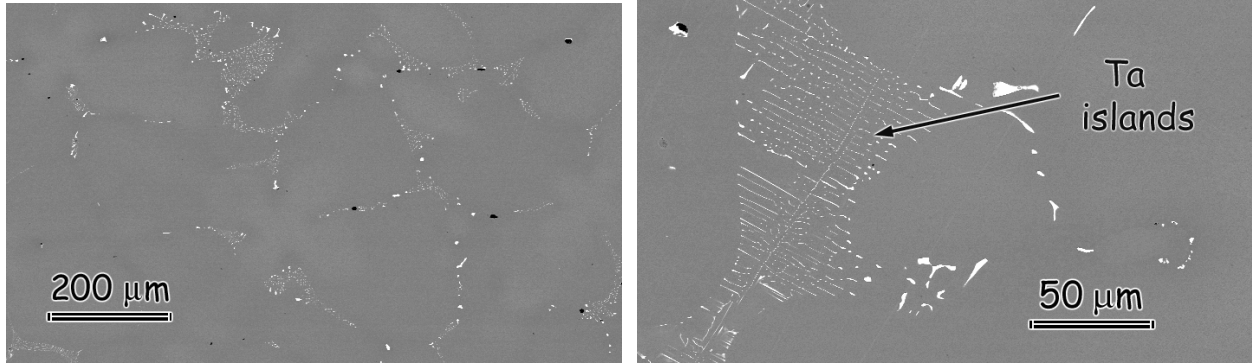


Figure 5.4: SEM images of René N5 showing the microstructure of the alloy in its as-processed condition.

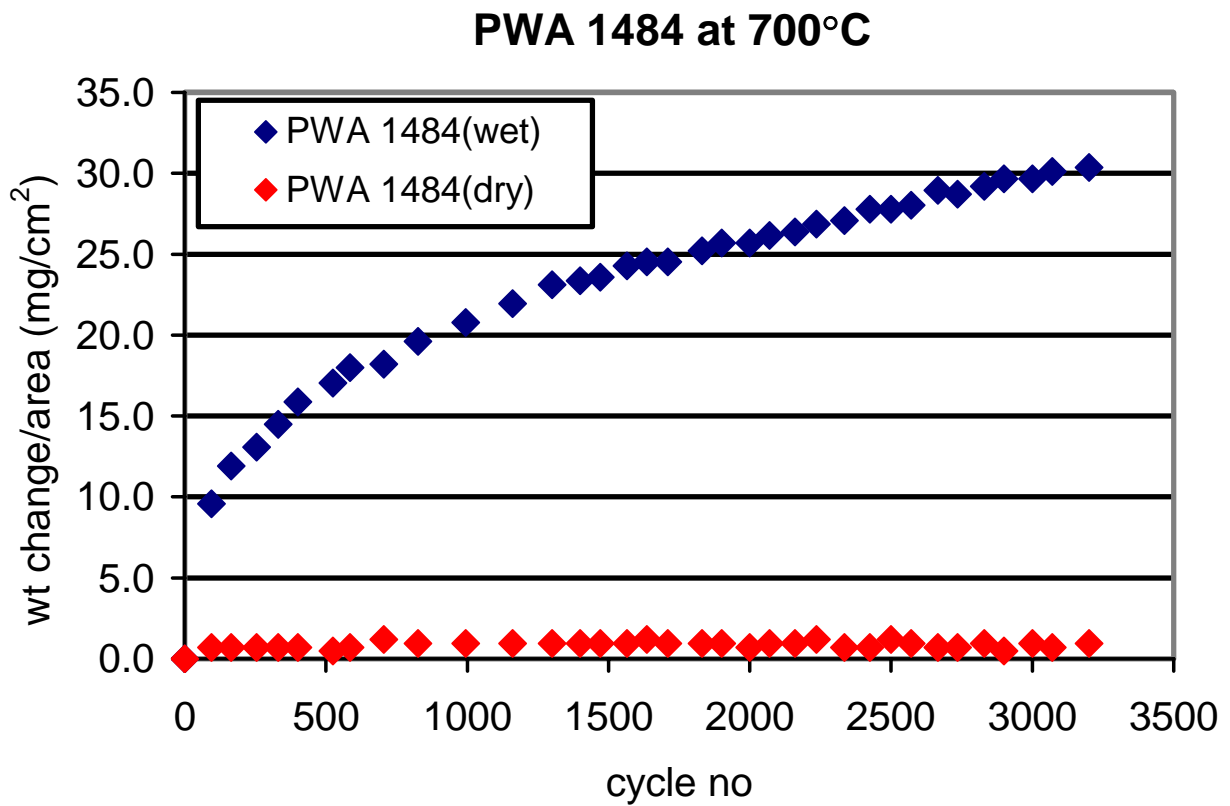
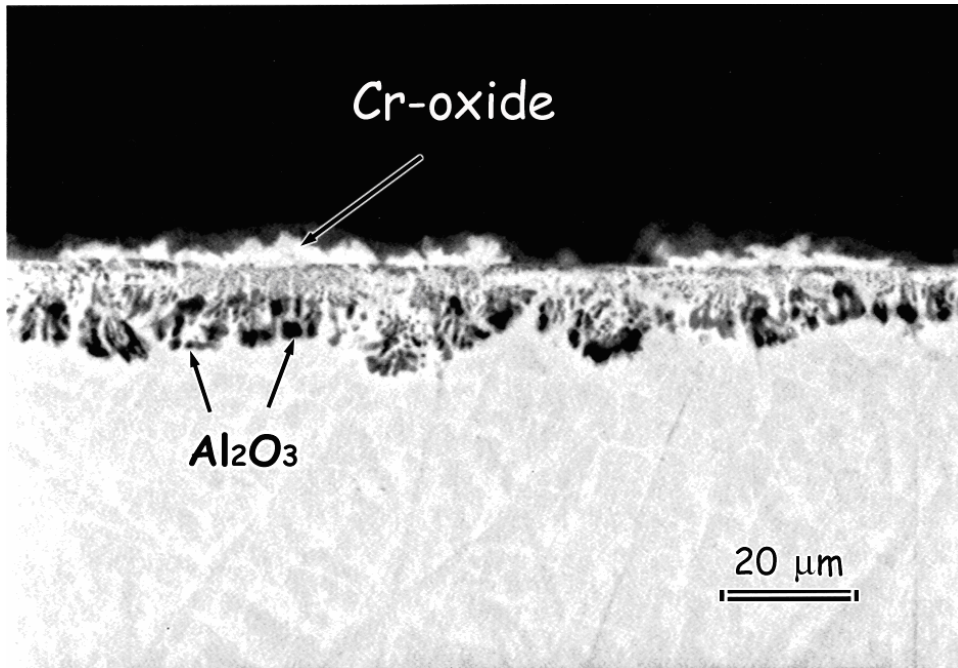
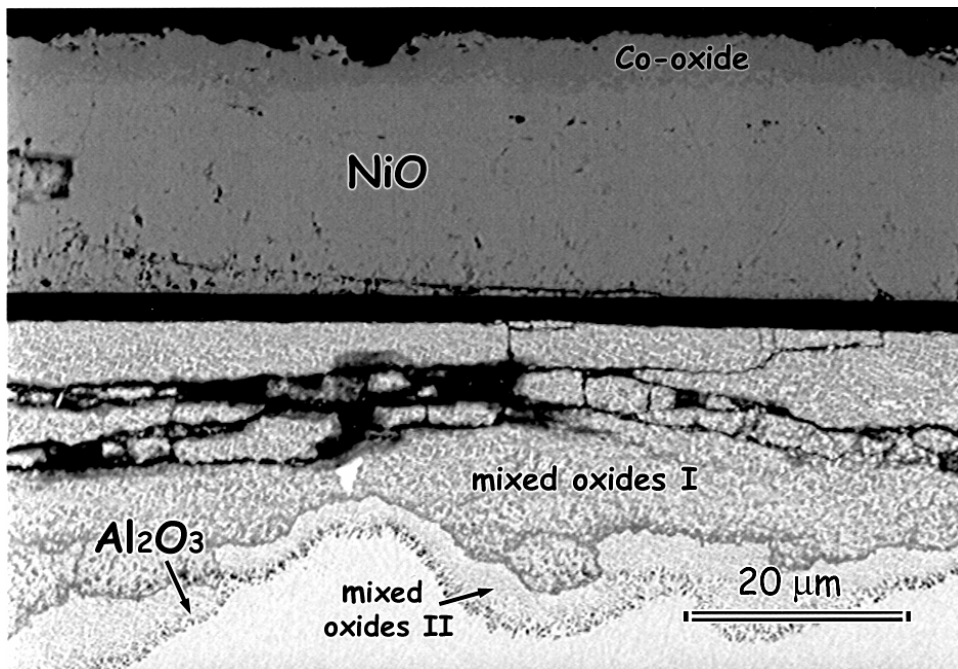


Figure 5.5: Kinetic plot of the alloy PWA 1484 showing the weight change of the specimens in dry air and in air/H₂O mixtures at 700°C as a function of cycle number.



(a)



(b)

Figure 5.6: SEM images of PWA 1484 showing the cross-section of the oxide scale that formed at 700°C after 3200 cycles (a) in dry air, and (b) in wet air.

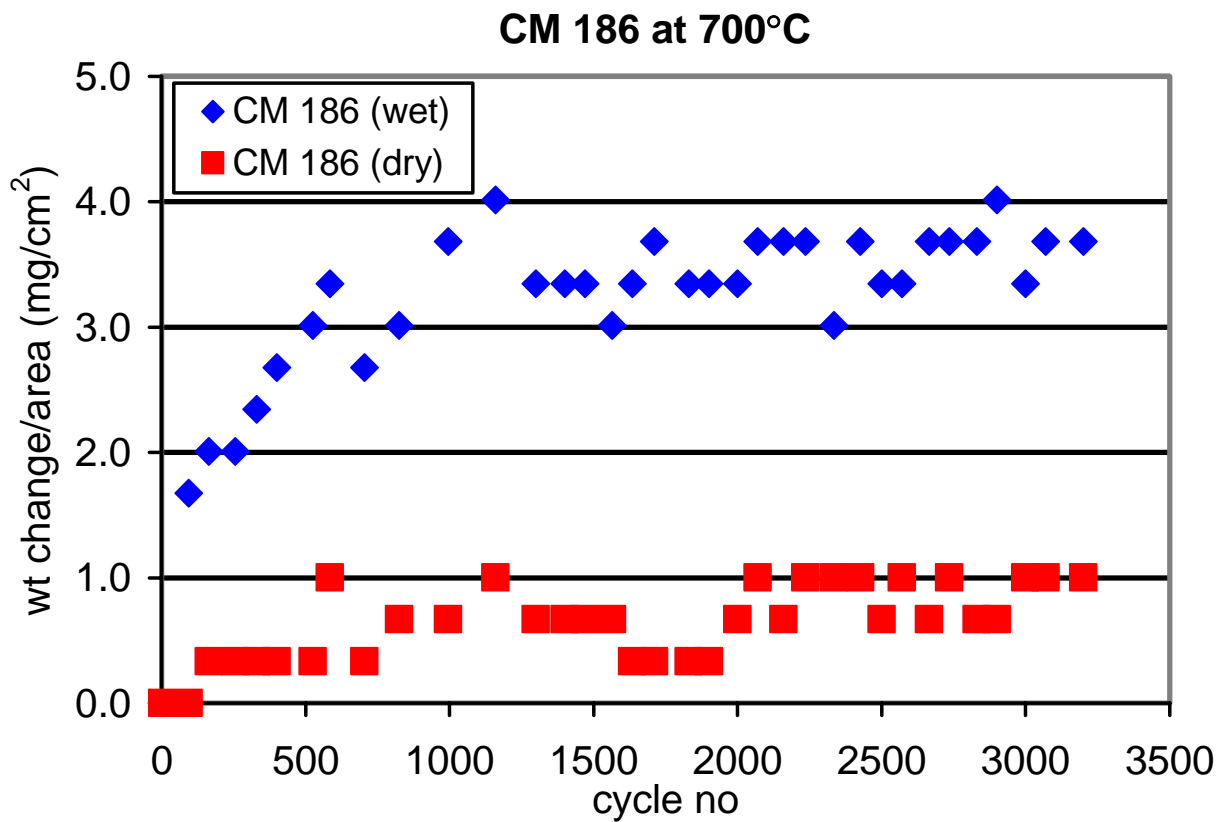
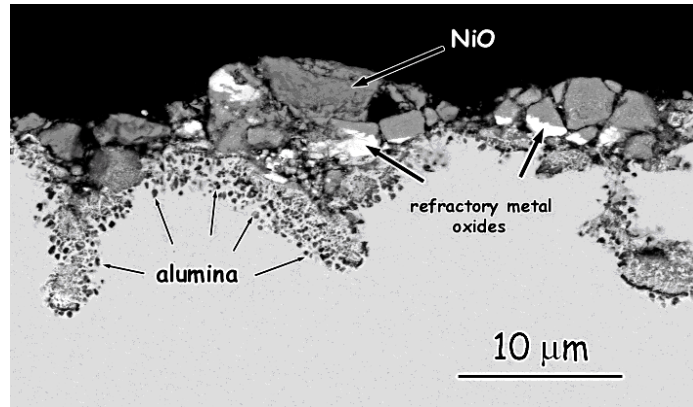


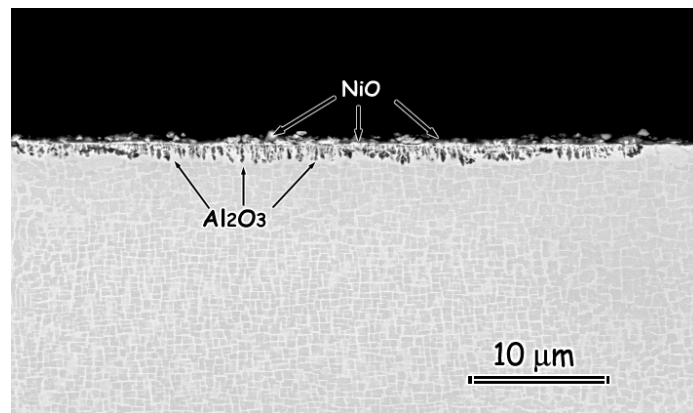
Figure 5.7: Kinetic plot of the alloy CM 186 showing the weight changes of the specimens in dry air and in air/H₂O mixtures at 700°C as a function of cycle number.

Comparison of specimen cross sections revealed that the thicknesses and the morphologies of the scales were different in the wet and dry environments, Figure 5.8. Much thinner scales formed in dry air, which consisted of chromia mixed with NiO at the oxide/gas interface. Aluminum was not selectively oxidized. It reacted with oxygen and formed alumina internally below the chromia layer. The morphology of the scale was similar to the one observed with René N5. However, in contrast to the latter alloy, CM 186 did not display partial continuity of alumina. In air/H₂O mixtures a thick scale formed on the sample surface. This scale consisted of non- protective, fast growing oxides. The major phase was NiO. Oxides of refractory elements were also present. Alumina formed fine internal precipitates. The scale morphology was consistent with the kinetic data, which suggested that more extensive transient oxidation occurred in wet air. The results suggested that the oxidation mechanisms operating in dry air and in air saturated with water vapor were not the same.

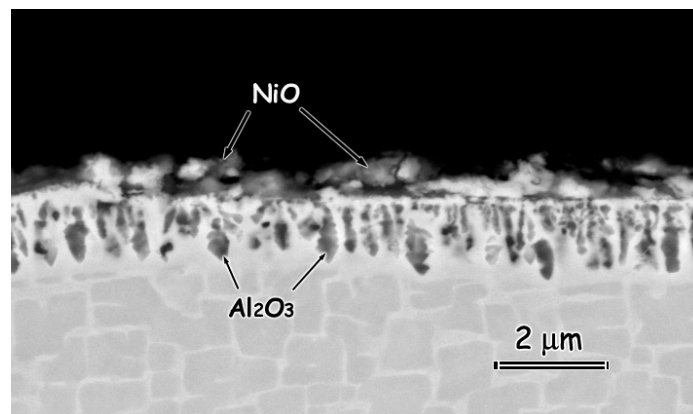
Analysis of the data accumulated concerning MarM 247 showed that, the differences between wet and dry exposures were more subtle compared to PWA 1484 or CM 186. Similar scales developed in each environment. A Cr-rich oxide with Al and Ni in solution formed at the alloy/gas interface. Aluminum oxidized internally in the substrate. Alumina developed continuity in dry air along a considerably large fraction of the subscale. In wet air, some locations were spotted which indicated the beginning of partial continuity in the alumina. The observations suggested that, the resistance of the alloy to attack was better in dry air. These results were consistent with the kinetic data which showed that the weight gain in the air/H₂O mixture was greater than in dry air, Figure 5.9. Figure 5.10 shows the cross sections of the specimens.



(a)



(b)



(c)

Figure 5.8: (a) Cross-section of CM 186 at 700°C after 3200 cycles in wet air. Protrusions of transient oxide developed at the specimen surface. (b) Same alloy exposed to dry air at 700°C for 3200 cycles in dry air. (c) Scale that developed in dry air shown at higher magnification.

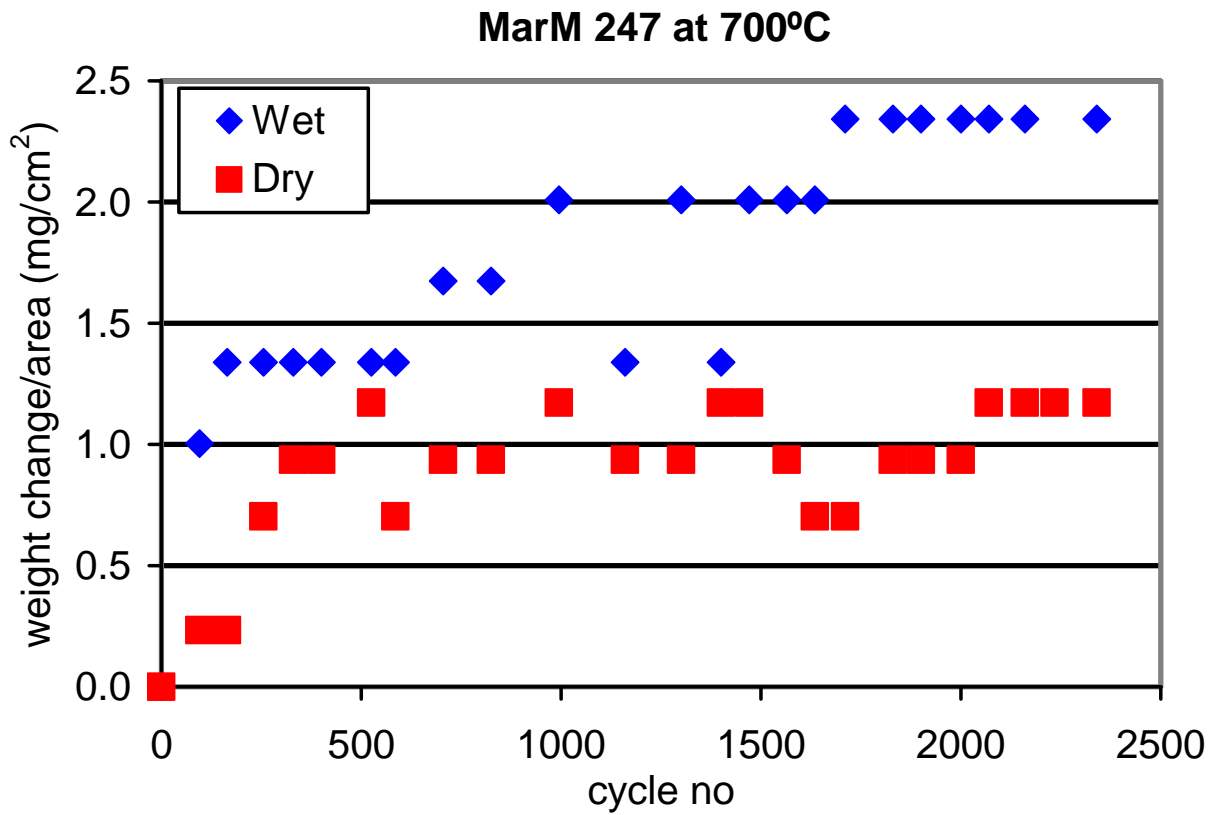
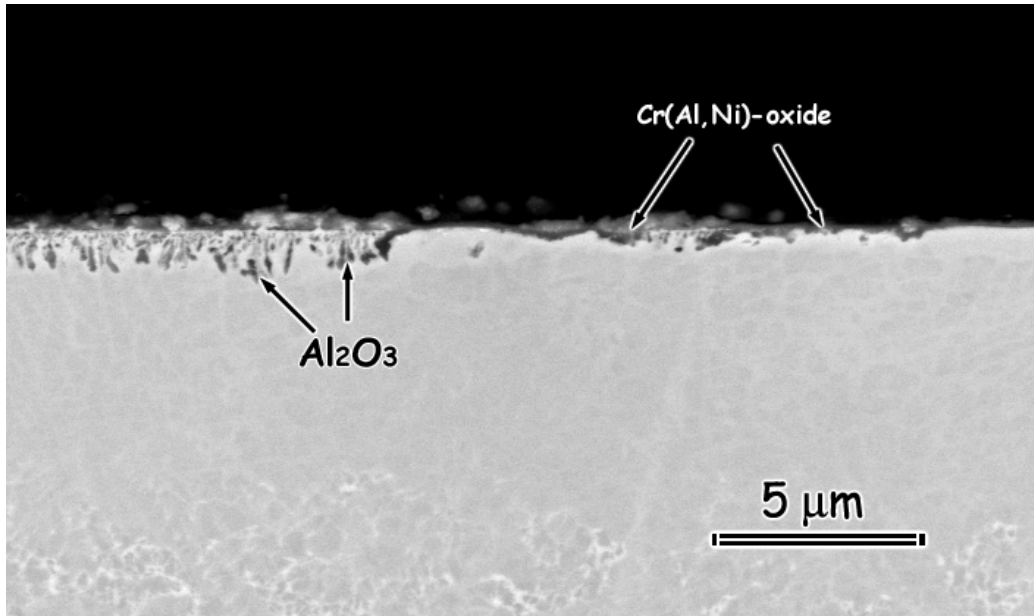
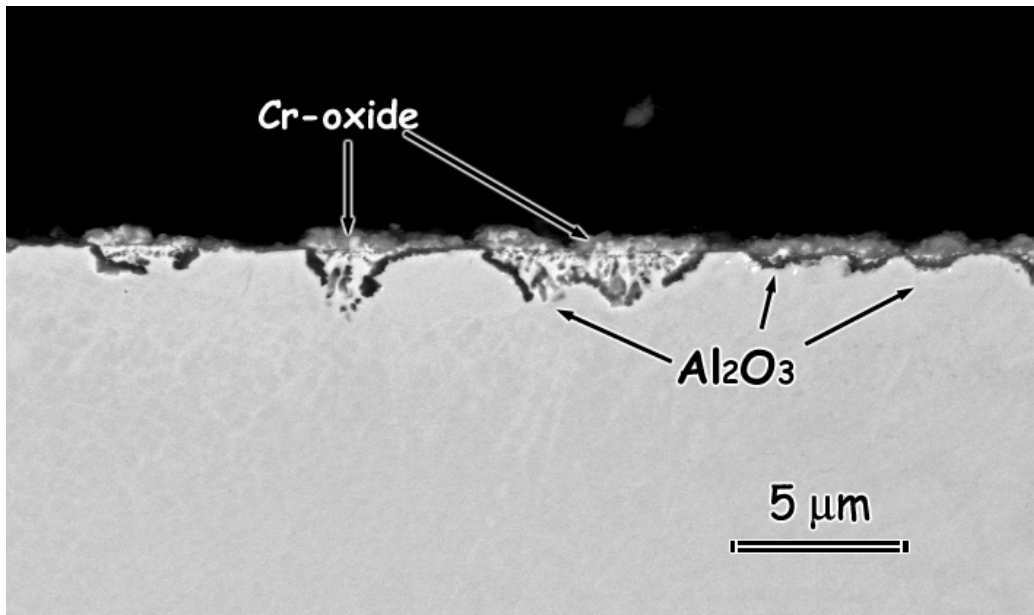


Figure 5.9: Kinetic plot of the alloy MarM 247 showing the weight changes of the specimens in dry air and in air/H₂O mixtures at 700°C as a function of cycle number.



(a)



(b)

Figure 5.10: Back scattered electron image of MarM 247 exposed at 700°C. (a) The cross-section of the specimen subjected to cyclic testing for 3200 hours in dry air. (b) Micrograph shows the scale that developed in wet air after 3200 hours of cycling.

Tests at 700°C showed that the alloys under investigation were not alumina formers at 700°C. Furthermore, they were more susceptible to attack in air/H₂O mixtures compared to exposures in air only. The major effect of water vapor was the acceleration of reactions leading to the formation of transient oxides. Another important observation was that water vapor adversely affected selective oxidation of aluminum. Continuous alumina formation was suppressed in the wet environment. Al oxidized internally in the subscale. These observations suggested that oxygen diffused more rapidly into the alloy when the reaction environment contained H₂O mixed with air. How this happened is not understood. However, the possibility that the nature of the surface oxides allows more oxygen in by changing the oxygen activity in the presence of H₂O is considered. René N5, which is the alloy with the highest Al and Cr content, (Table 4.1), displayed the best performance. Observations pointed towards an inverse relation between the alloy composition and the resistance of that particular system to attack. The alloys with richer Al and Cr compositions displayed smaller differences in weight changes in dry air and in air/H₂O mixtures. More specifically, the proportion of weight gains in wet to dry was around 30:1 for PWA 1484, 4:1 for CM 186, 2.5:1 for MarM 247, and even smaller for René N5.

The oxide map for 1000°C developed by Giggins and Pettit, [23], for the Ni-Cr-Al system is reprinted here, Figure 11. (This map was used as a reference although the tests under discussion were done at 700°C, since oxide maps for lower temperatures were not available). Each alloy under investigation is marked on this map tentatively to see which region they fall into. As the plot shows, PWA 1484 is the system that lies closest to the boundary. CM 186 is the second closest alloy. This explains why these systems were more vulnerable to transient oxidation. It is believed that these alloys approach Region I at lower temperatures as the boundaries of the map would move towards higher aluminum and chromium concentrations. It is also believed that

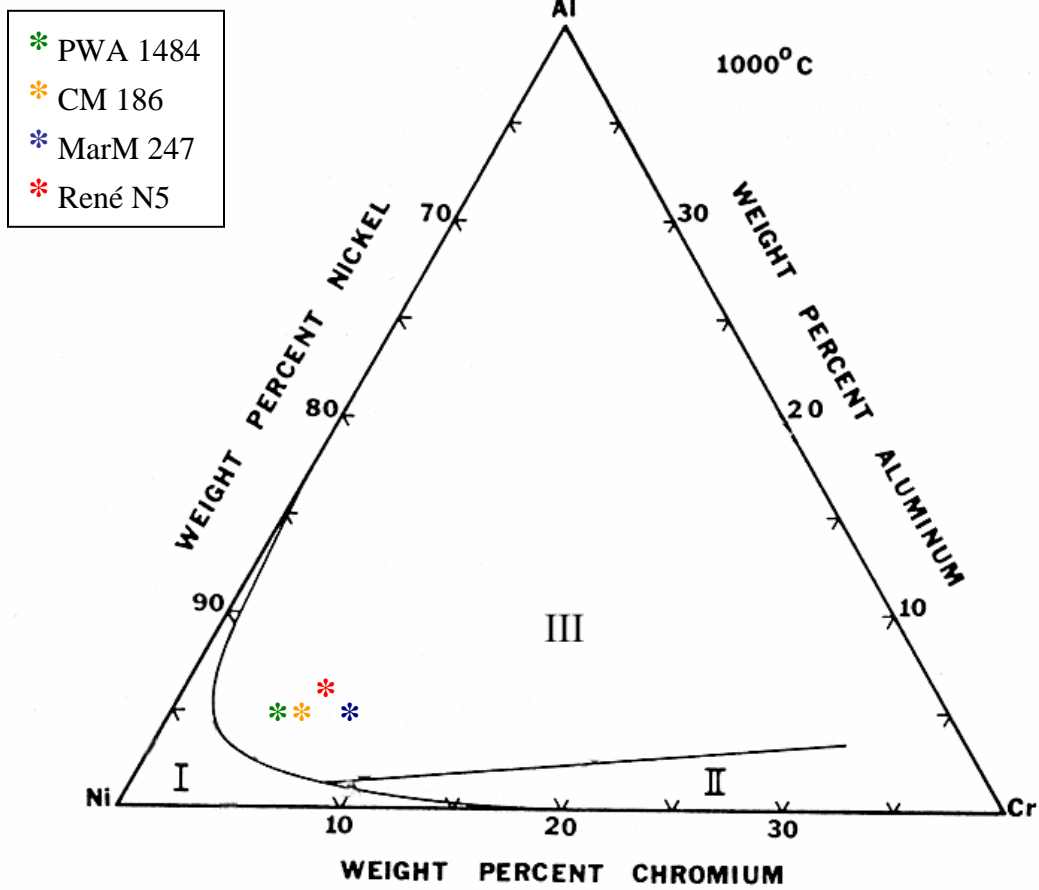


Figure 5.11: An oxide map of the Ni-Cr-Al system developed by Giggins and Pettit, [23], showing the regions for continuous formation of the oxides alumina (Region III), chromia (Region II), and non-protective NiO (Region I) at 1000°C. The alloy systems under investigation are marked on this map to show their relative positions.

water vapor causes further shifts on the map in favor of transient oxidation. Therefore, development of continuous alumina scales becomes even more difficult.

5.1.1.2 Alumina Formers at 900°C: The kinetic data for René N5 indicated that the total weight gain in air/H₂O mixtures was higher compared to dry air, Figure 5.12. The source of the difference was the early stages of oxidation. In wet air, faster oxygen pick-up started with the onset of exposure to high temperature, and leveled off upon entering steady state oxidation. As a result, the rate of reaction in wet air was above that in dry air during the transient oxidation period. As the steady state stage started, the reactions in both environments proceeded with similar rates until the end of the test. Similar observations were also evident for exposures at 700°C.

Examination of the reaction zones by scanning electron microscopy showed that the types of oxides that formed were different for each environment. A continuous and duplex scale with a uniform thickness developed on the surface of the dry exposed specimen, Figure 5.13. Chemical analysis by EDS identified the external scale as (Cr, Al, Ni)-oxide. Occasionally, fine precipitates of refractory-element oxides were detected in the layer. EDS analysis also indicated a Cr concentration gradient along the scale, the interior being richer. The thin and continuous alumina that developed along the external Cr-oxide constituted the second layer of the duplex scale.

The reaction zone that developed after wet exposures had different characteristics in comparison to the one formed in dry air. As mentioned earlier, the kinetic data of the system showed that the weight gains during early oxidation were larger for exposures in air/H₂O mixtures. The examination of sample cross-sections gave results in agreement with the kinetic

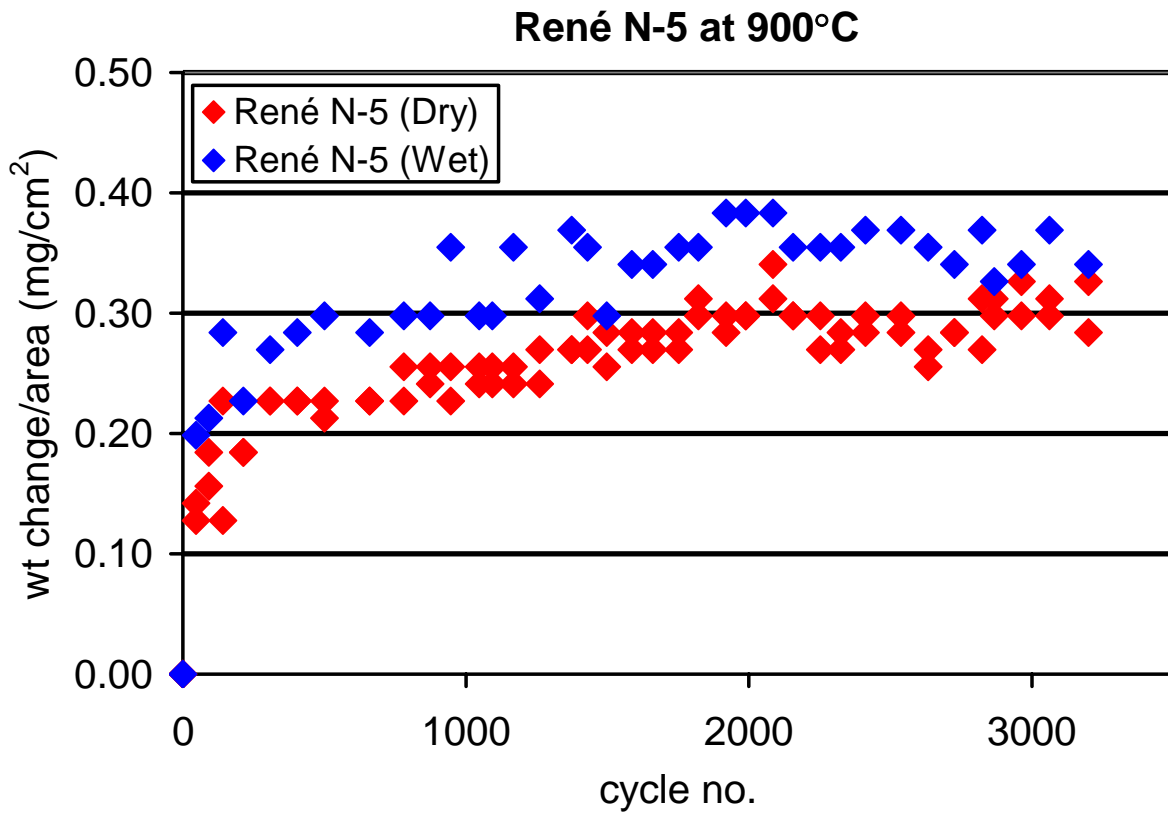


Figure 5.12: Kinetic plot of the alloy René N5 showing the weight change of the specimens in dry air and in air/H₂O mixtures at 900°C as a function of cycle number.

data. The back scattered electron image of the specimen exposed to wet air is shown in Figure 5.14. This micrograph shows that the scale consisted of a continuous alumina layer at the oxide/substrate interface, a layer of mixed oxides³ (marked as intermixed zone), and equiaxed NiO at the gas/oxide interface. Profuse amounts of transient oxides formed on the specimen surface until the establishment of continuity along the alumina layer. This layer provided a barrier to the outward transport of cations and inward transport of anions. Upon the development of continuity the system entered the steady state stage. The rate of reaction decreased significantly. The system became virtually resistant to degradation by attack of oxidizing species.

The test results of PWA 1484 showed that the striking difference between wet and dry exposures observed at 700°C did not occur at 900°C. The kinetic data indicated that the weight change trends in dry and wet air were similar, Figure 5.15. However, the weight gains for the latter case were still larger. The origin of the difference was again the early (or transient) oxidation. Comparison of cross-sectional SEM images in wet and dry air also showed more substantial transient oxide formation in the former case. The oxide scale that formed after 3200 one-hour cycles in wet air was relatively uniform, Figure 5.16. Its features were similar to the one formed on René N5 after exposures in wet air. Alumina was present as a continuous layer at the scale/alloy interface. This phase provided protection to the system. NiO developed at the oxide/gas interface. Complex oxides of Al, Ni, Cr and refractory metals formed an interlayer between alumina and NiO.

The features of the reaction zone of the dry exposed alloy were similar to the wet exposed one, Figure 5.17. However, the thickness of the scale was smaller for the former case.

³ a mixture of complex oxides of Cr, Al, and Ni, and possibly their spinels

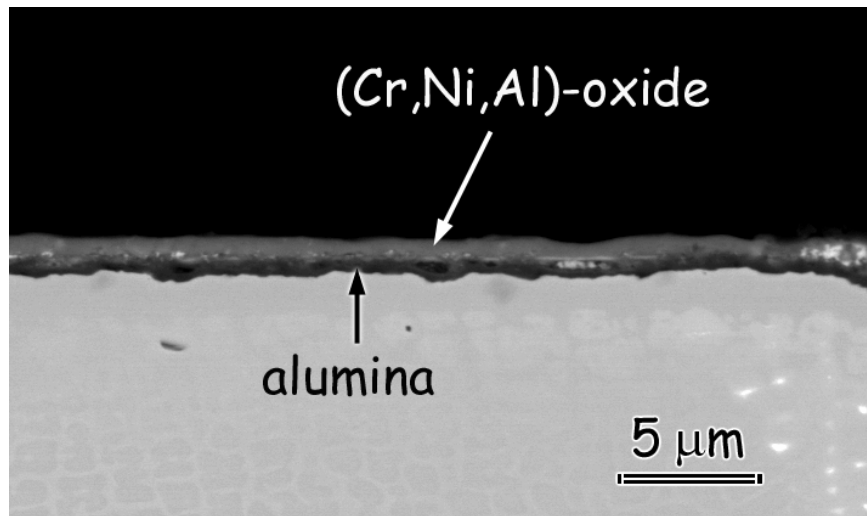


Figure 5.13: René N5 at 900°C exposed to dry air for 3200 cycles. A duplex scale developed on the specimen surface that consisted of a complex oxide of Cr, Ni and Al at the scale/gas interface, and the slow growing alumina at the matrix/scale interface.

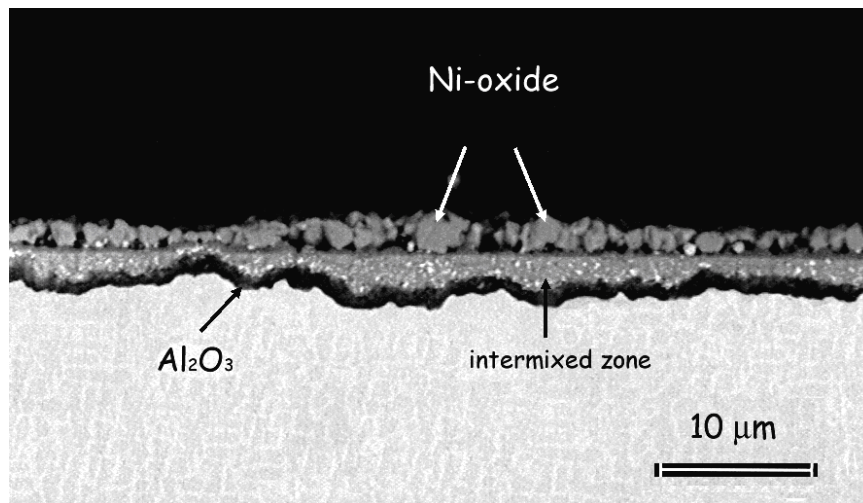


Figure 5.14: SEM image of René N5 showing the scale that formed at 900°C after exposing the alloy to air/H₂O mixtures for 3200 cycles.

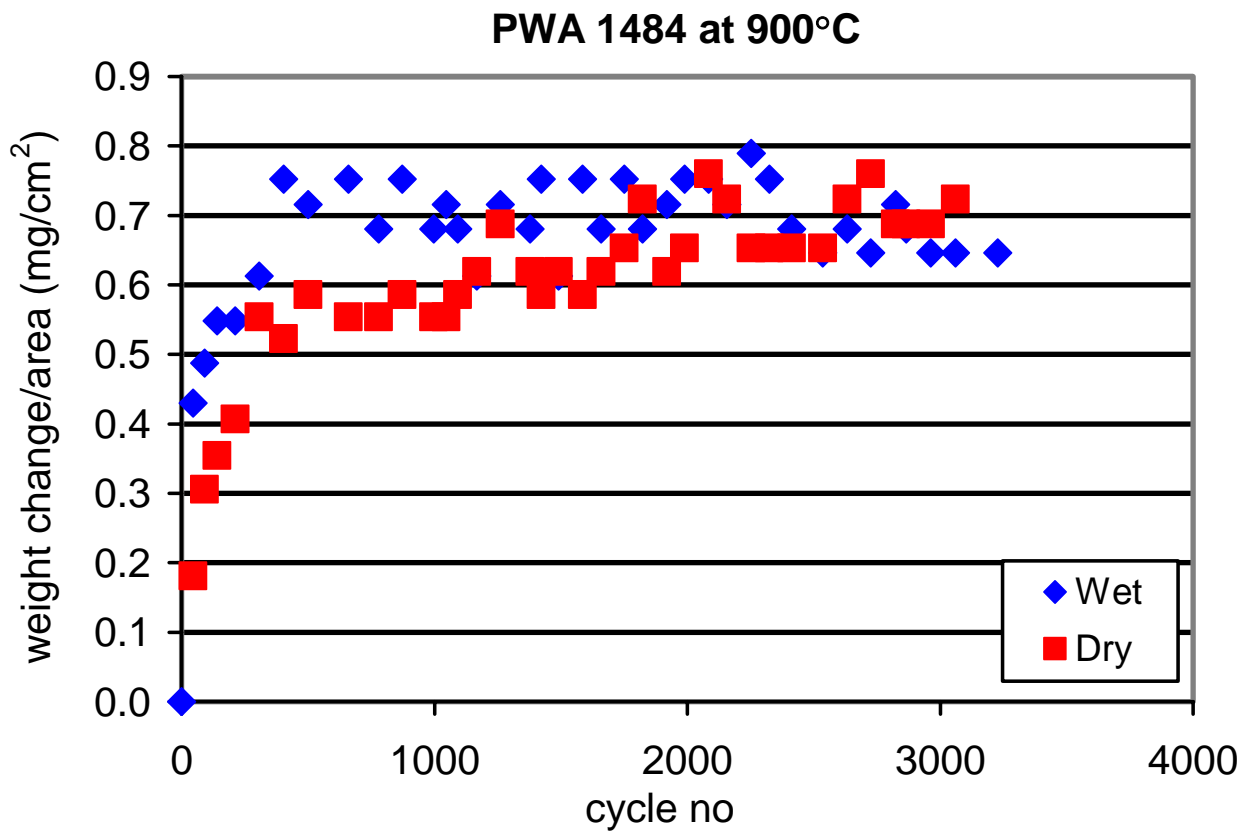


Figure 5.15: Kinetic plot of the alloy PWA 1484 showing the weight change of the specimens in dry air and in air/H₂O mixtures at 900°C as a function of cycle number.

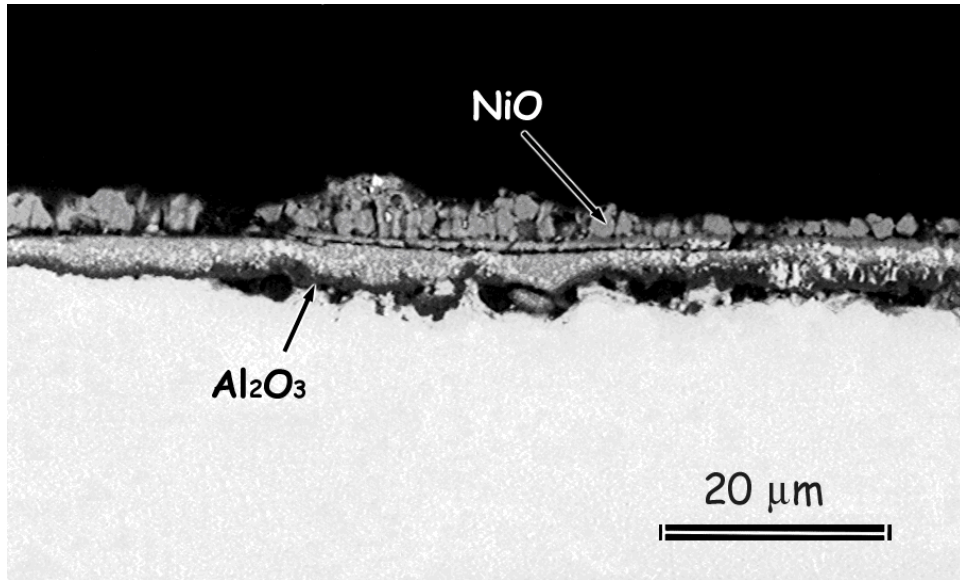


Figure 5.16: Image shows PWA 1484 at 900°C after tests in wet air for 3200 hours of cyclic exposures.

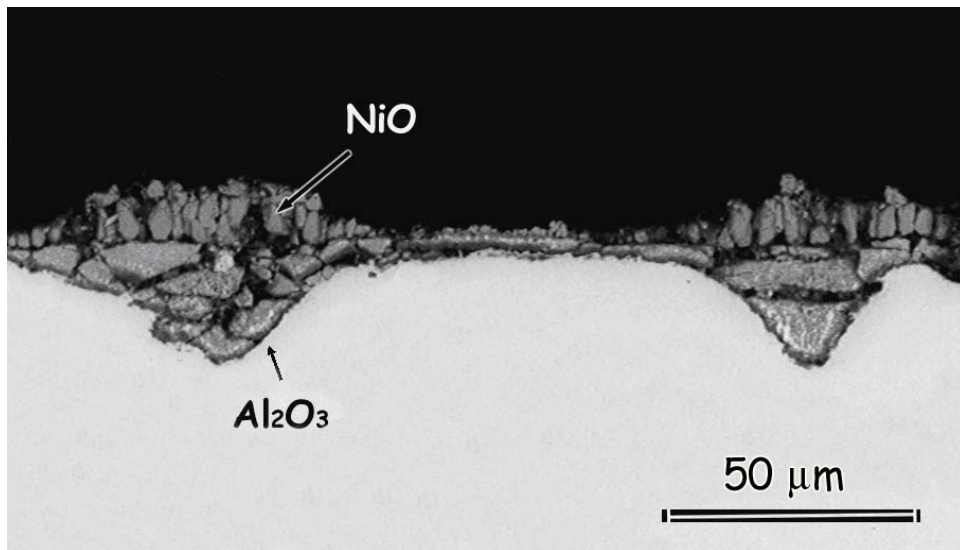


Figure 5.17: Back scattered electron image of the alloy PWA 1484 showing the oxide layer that formed at 900°C in dry air after 3200 hours of cyclic testing.

Additionally, the oxide protrusions that are shown in Figure 5.17 were present on the dry exposed sample only. These protrusions repeated themselves almost periodically every 50-200 μm . Their formation in dry air was not understood, but the regions between them were consistent with the weight change data.

Although the features of wet exposed samples exhibited by PWA 1484 were similar to René N5, the former was less oxidation resistant than René N5. Additionally, on René N5 no transient oxides and no oxide protrusions were seen in dry air. The system developed a thin dual oxide layer with relatively good protective properties. On PWA 1484 the transient oxides were present both over oxide protrusions and over the thinner parts of the scale after dry exposures.

The comparison of the kinetic plots of CM 186 at 700°C and 900°C also showed that the differences in behavior between wet and dry exposures were less significant at the higher temperature, Figures 5.8 versus 5.18. At 900°C, the weight changes in both environments were comparable. The transient stage was followed by the steady state. Similar to the other systems, the weight gain in wet air was larger than in dry. However, as mentioned, the difference was small.

During steady state, the ability of the alloy to resist attack was good. The examination of cross-sections showed that the scale that formed in wet air had characteristics similar to the oxides formed on the previously discussed systems. Transient oxides developed above the alumina layer, Figure 5.19. These oxides formed as a multilayered scale that consisted of an external equiaxed NiO layer, a continuous W-oxide layer, and finally the intermixed zone. The intermixed zone was a phase mixture of complex Ni-, Cr-, and Al-oxides. Additionally, small quantities of Ti-oxide were detected over the NiO layer as randomly distributed small blisters along the sample surface. Alumina sealed the specimen with a continuous layer. Upon the

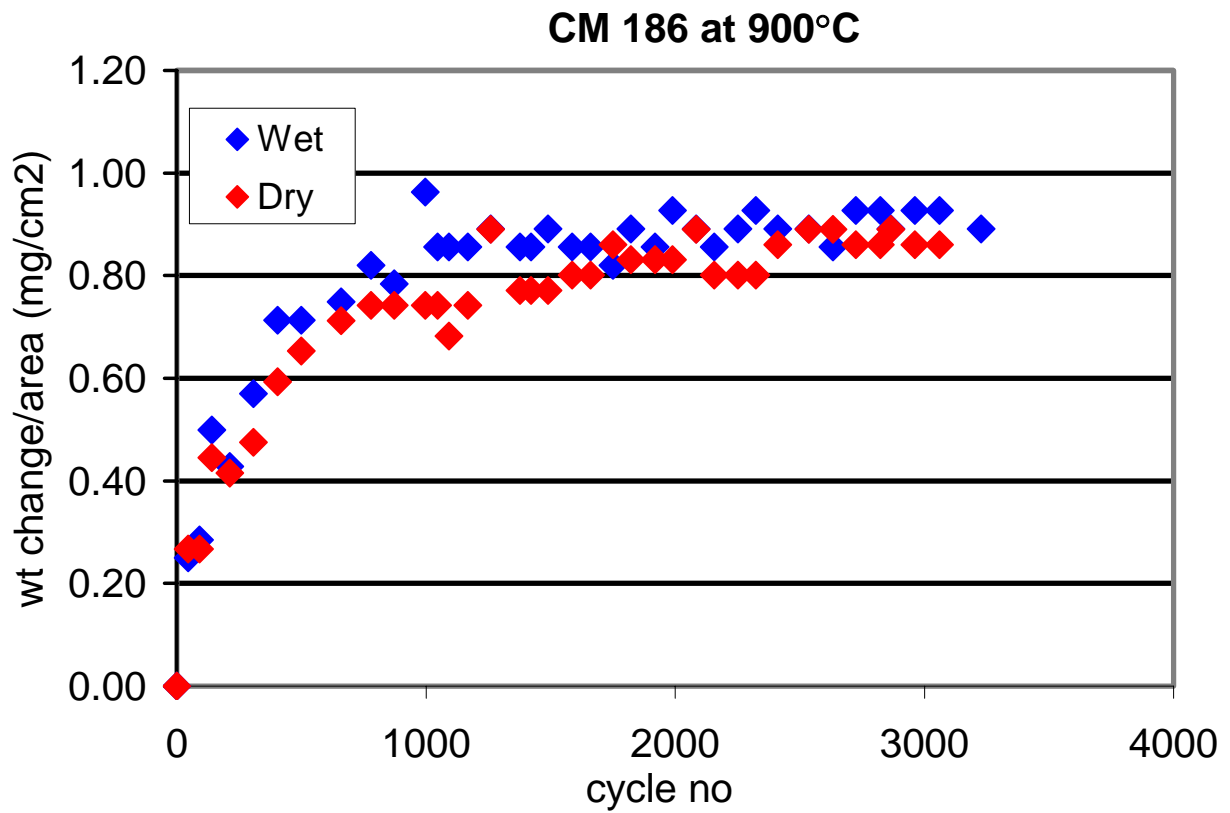


Figure 5.18: Kinetic plot of the alloy CM 186 showing the weight changes of the specimens in dry air and in air/H₂O mixtures at 900°C as a function of cycle number.

establishment of continuity, the rate of transient oxidation decreased. This also decreased the overall rate of oxidation. The system became more resistant to attack by oxidizing species.

The scale that formed in dry air was essentially a duplex oxide. The phase at the gas interface was found to be a complex oxide of the elements Cr, Ni, and Al. The inner phase was identified as alumina. Although this duplex layer was a fairly continuous scale, locations were evident where the continuity of the layer was disrupted by locally grown oxide intrusions, Figure 5.20. These intrusions (or protrusions) had the same characteristics as the scale that formed in wet air. This situation was encountered also with PWA 1484, as discussed previously. Another observation was the formation of Hf oxides. These oxides were either embedded into the continuous alumina scale, or they formed in the depleted zone. In the latter case, alumina built a rim around the Hf oxide. This structure was present both in wet and dry exposed samples, yet more profuse after wet air exposures. The size of these precipitates was very small. Their occurrence was also infrequent. The behavior of CM 186 in terms of resistance to attack was intermediate between René N5 and PWA 1484.

MarM 247 seemed to be substantially affected by water vapor at 900°C. As the cross-sectional images taken by SEM also indicate, the attack in wet air was more profuse, Figures 5.21-5.22. The scale that developed in dry air was more protective in nature and adherent to the substrate. EDS analysis showed that this phase was an (Al, Ni, Cr)-oxide which was Al-rich over the major fraction of the surface area, and Cr-rich over some parts. It formed as the primary oxide that covered most of the surface of the specimen. In limited locations, the continuity of the scale was disturbed by some oxide protrusions. Figure 5.21 shows one such case. These protrusions represent the areas where the system could not develop the primary oxide phase. Instead, alumina formed as an internal oxide. A phase with a Cr-rich composition formed at the

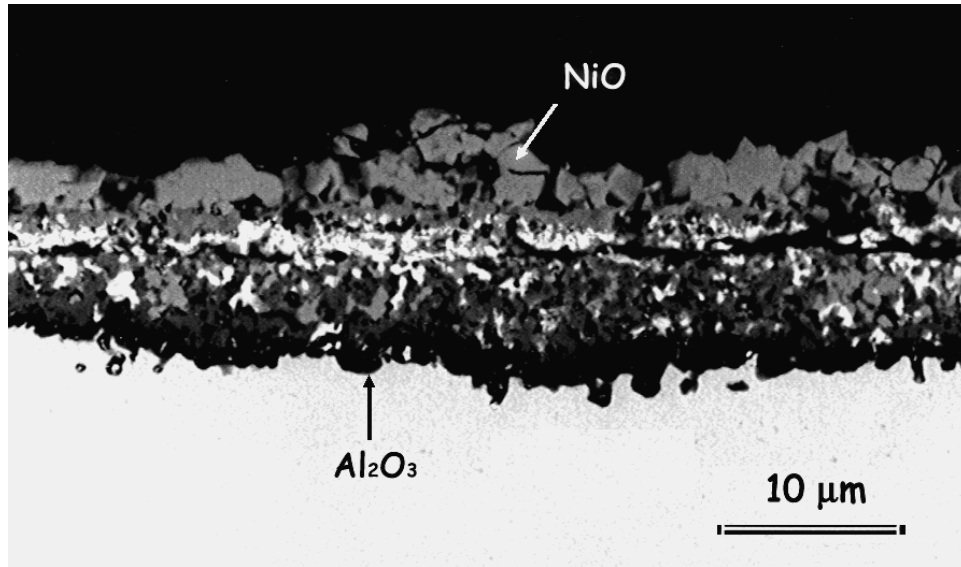


Figure 5.19: Image of CM 186 showing the alloy after testing at 900°C in air/H₂O mixtures for 3200 hours cyclically.

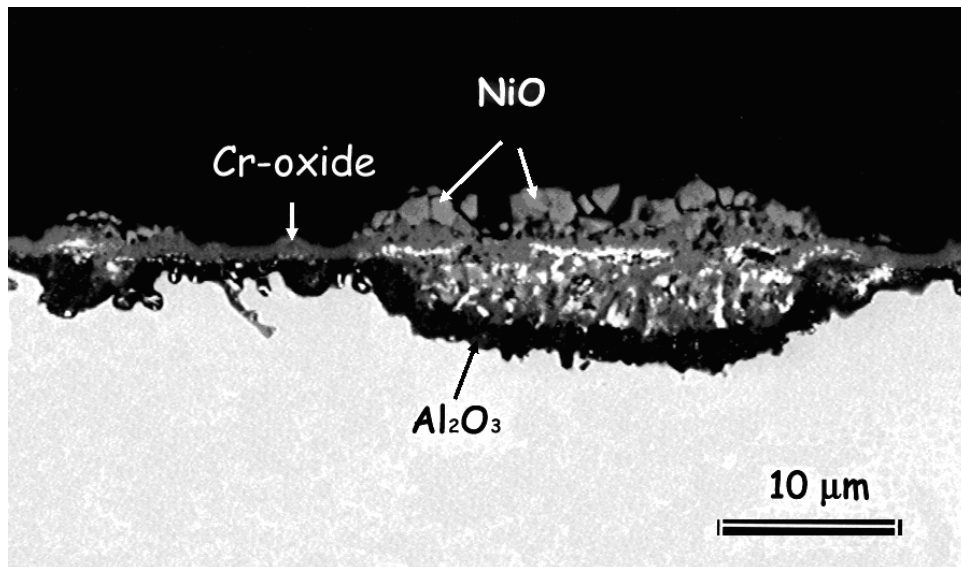


Figure 5.20: Back scattered electron image shows the reaction zone that formed on the surface of the alloy CM 186 after experiments at 900°C in dry air. The specimen was subjected to thermal cycling for 3200 hours.

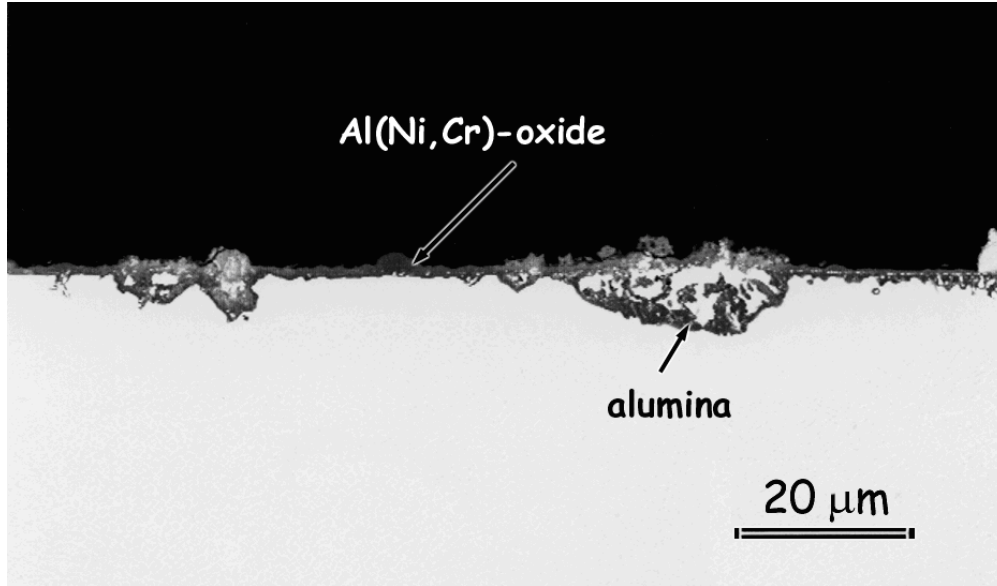
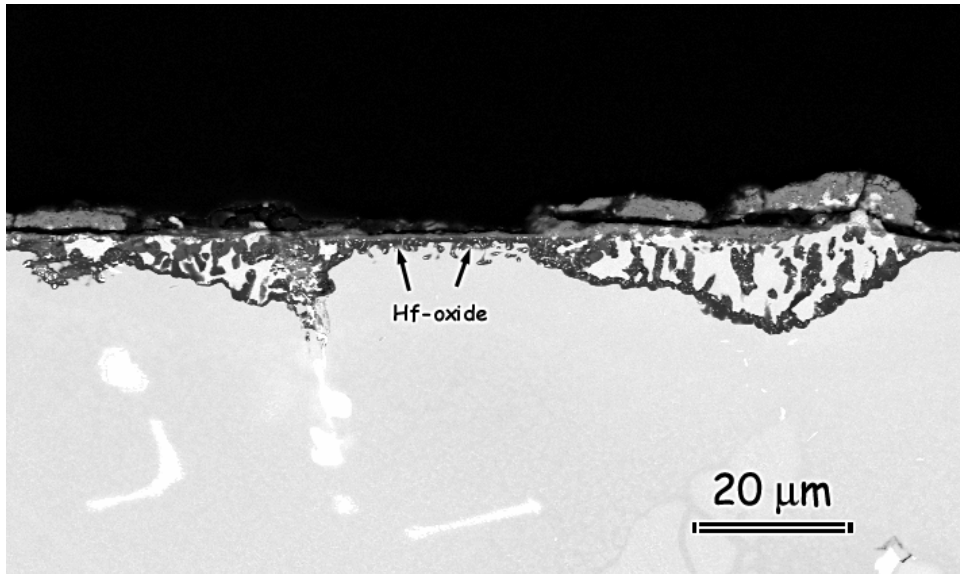
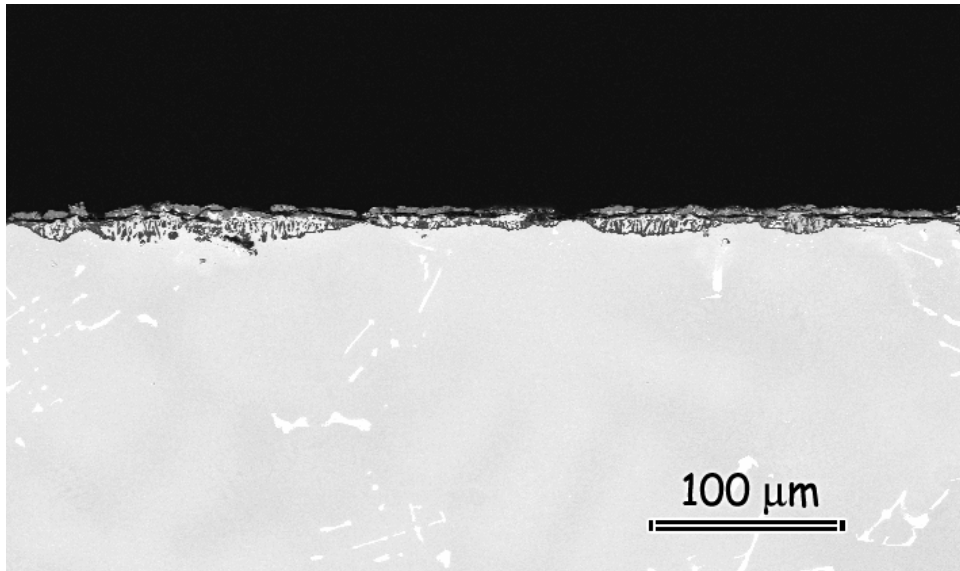


Figure 5.21: MarM 247 at 900°C in dry air after 3200 cycles. A thin scale developed on the specimen surface. Oxide protrusions were spotted in some parts along the scale.



(a)



(b)

Figure 5.22: MarM 247 at 900°C in wet air after 3200 hours of cyclic exposures. The SEM image shows the cross-section of the scale formed on the specimen. An Al-rich scale developed under the testing conditions. Some oxide protrusions with internal alumina were also evident.

gas/oxide interface above alumina. The formation of the protrusions was more profuse on the surface of the alloy exposed to air/water vapor mixtures. Figure 5.22 provides the back scattered

electron images of the alloy. Also, the thinner scale that formed in-between the protrusions was a dual oxide layer rather than the single-layered scale that formed in dry air. The dual scale consisted of a Cr-rich external phase, and alumina that formed adjacent to it. HfO_2 , which was observed on CM186, was also present on MarM 247 with the same features, and after both wet and dry exposures. NiO, which was observed to form on all other alumina forming systems tested (with the exception of dry exposed René N5) was not detected on cyclically exposed MarM 247 specimens. The weight change plot of the alloy is given in Figure 5.23.

In general, the resistance of the alloys to attack was improved at 900°C relative to 700°C in both testing environments. In dry air the specimens developed continuous scales with better protective properties. However, the continuity of these scales was interrupted by oxide protrusions, which were associated with more profuse formation of transient oxides. The microstructure of the protrusions was the same as the scale that developed in air/ H_2O mixtures. Evidently, water vapor accelerated the mechanism(s) that lead(s) to transient oxide formation. However, it was not the only responsible agent for this effect. Water vapor also suppressed selective oxidation of Al and Cr. Another common characteristic observed in the presence of water vapor was the refractory oxides that lined up at the center of the mixed oxide layer.

The composition dependency of the behavior first observed at 700°C persisted also at 900°C. Systems with higher Al and Cr additions experienced shorter transient oxidation periods, and developed the slower growing scales easier. The frequency of protrusions in dry air was inversely proportional to the Al and Cr content of the substrate, and the thickness of the transient oxide layer in wet air was smaller for these alloys.

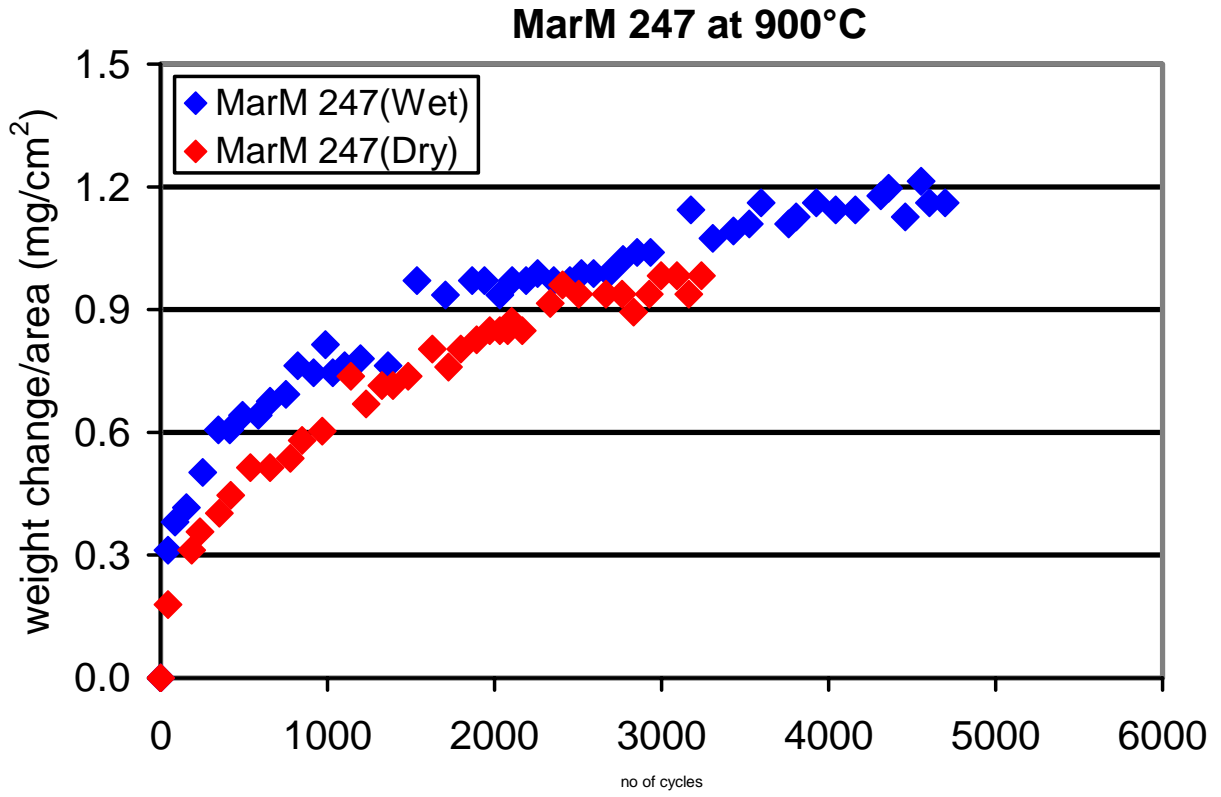


Figure 5.23: Kinetic plot of the alloy MarM 247 showing the weight changes of the specimens in dry air and in air/H₂O mixtures at 900°C as a function of cycle number.

5.1.1.3 Alumina Formers at 1000°C: The evaluation of the results for PWA 1484 and René N5 showed that the behavior of the alloys at 1000°C was comparable. The kinetics plot of each system displayed similar trends in dry and wet air, Figures 5.24 and 5.25. These alloys were more prone to spallation when water vapor was present. In this environment, the weight losses due to scale spallation started much earlier and progressed more aggressively following the initial fast oxidation. The electron microscope images of spalled surfaces are shown in Figures 5.26 and 5.27. Here, it is evident that the presence of water vapor affected scale adherence adversely. Larger areas of bare metal were exposed to hot gases in wet air after the same number of cyclic exposures. The topographic images provide a closer look at different levels of spallation, Figures 5.28.

The SEM examination of the cross-section of the oxide that developed on René N5 showed that in dry air, a double-layered and initially continuous scale formed on the surface, Figure 5.29. This scale was an Al-rich oxide with Ni and Cr at the gas/scale interface and alumina at the substrate/oxide interface. The continuity of the scale was disrupted by spallation between cycles. Some intrusions of oxides were detected along the sample surface. These intrusions had a porous morphology, and were separated from the matrix by a continuous alumina layer. EDS analysis identified this porous structure as a phase mixture, which consisted of oxides of Al, Ni and Cr. AlN precipitated in the depleted zone, preferentially –but not necessarily– below the intrusions.

Some of the micrographs showing the scale that developed after attack in wet air are given in Figure 5.30. The duplex Al-oxide scale, which was observed in dry air, was found to develop in this environment as well. However, its extent was limited to a smaller area. The major fraction of the surface was covered with a less protective complex scale. Mixed oxides of Al, Ni

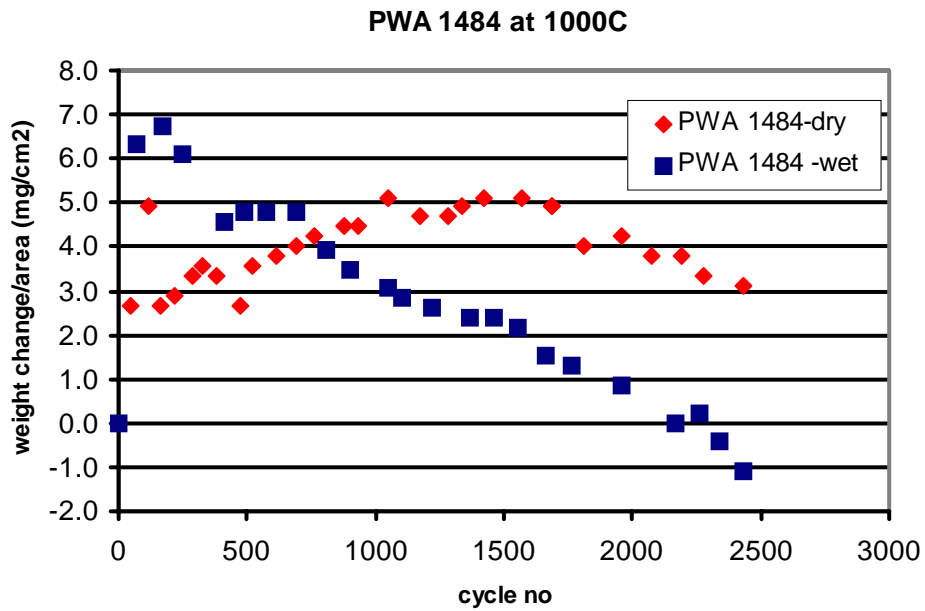


Figure 5.24: Kinetic plot of the alloy PWA 1484 showing the weight change of the specimens in dry air and in air/H₂O mixtures at 1000°C as a function of cycle number.

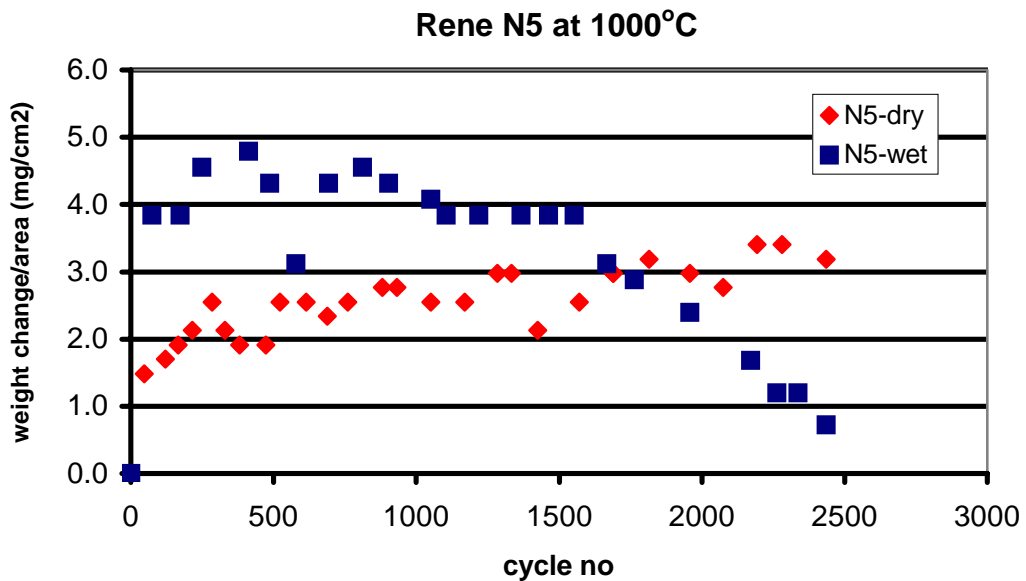
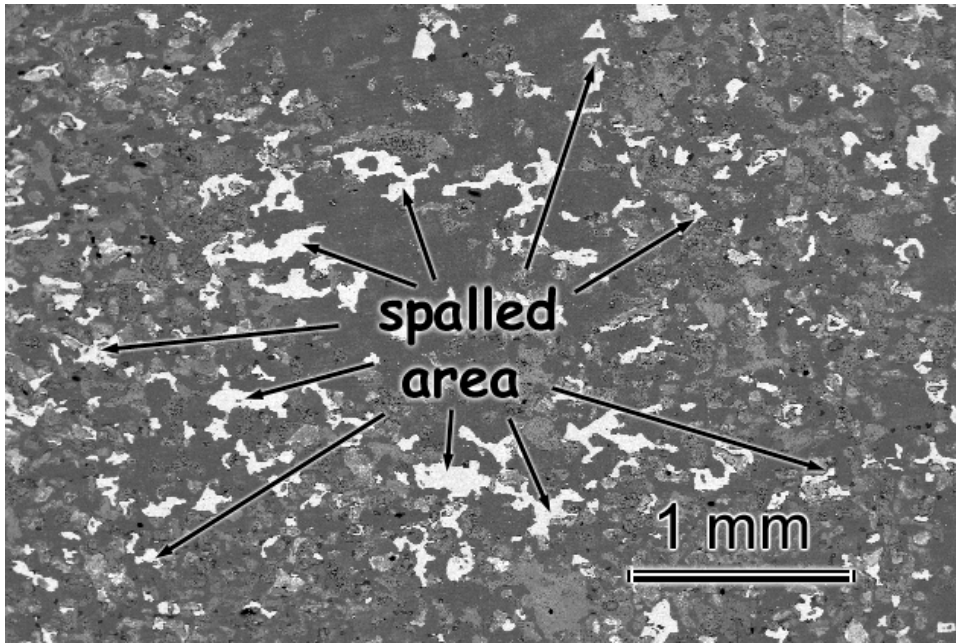
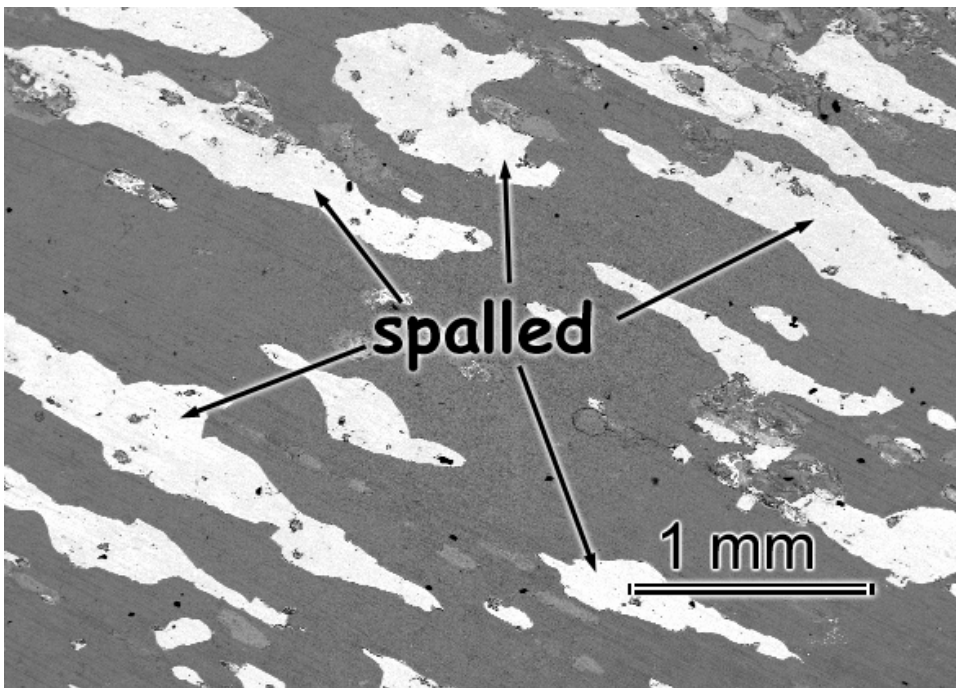


Figure 5.25: Kinetic plot of the alloy René N5 showing the weight change of the specimens in dry air and in air/H₂O mixtures at 1000°C as a function of cycle number.

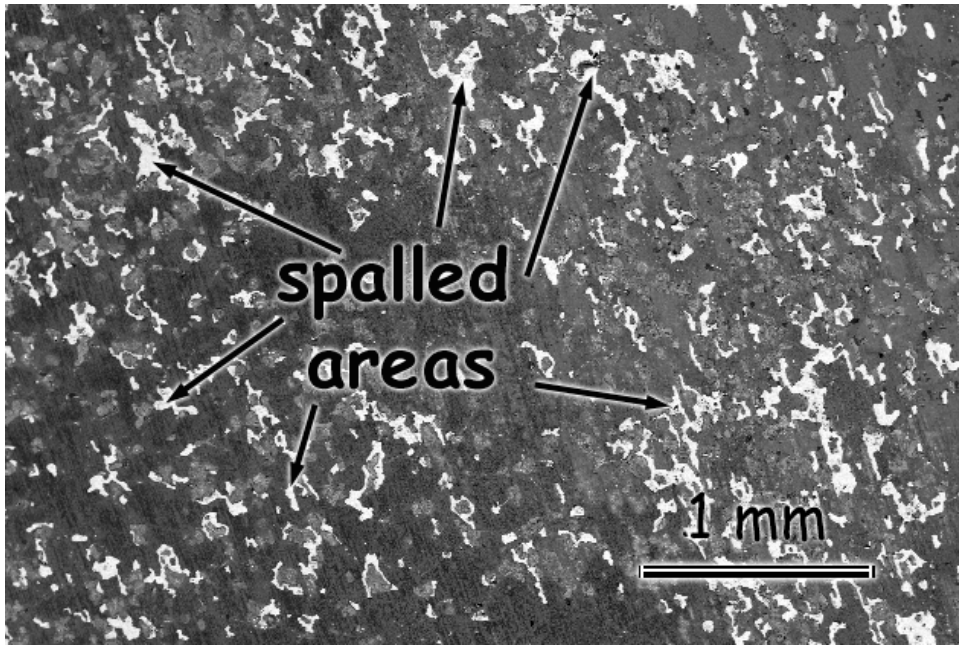


(a)

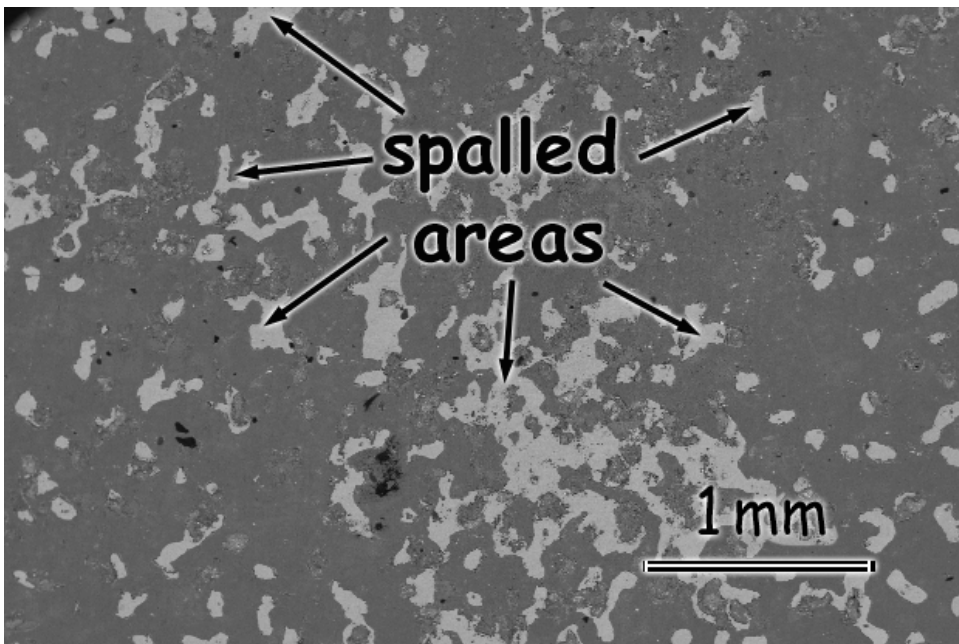


(b)

Figure 5.26: PWA 1484 at 1000°C after cyclic exposures for 2435 hours (a) in dry, and (b) in air/H₂O mixtures. The back scattered electron images show the spalled areas on specimen surfaces at low magnification. More spalling of oxides occurred after wet tests.

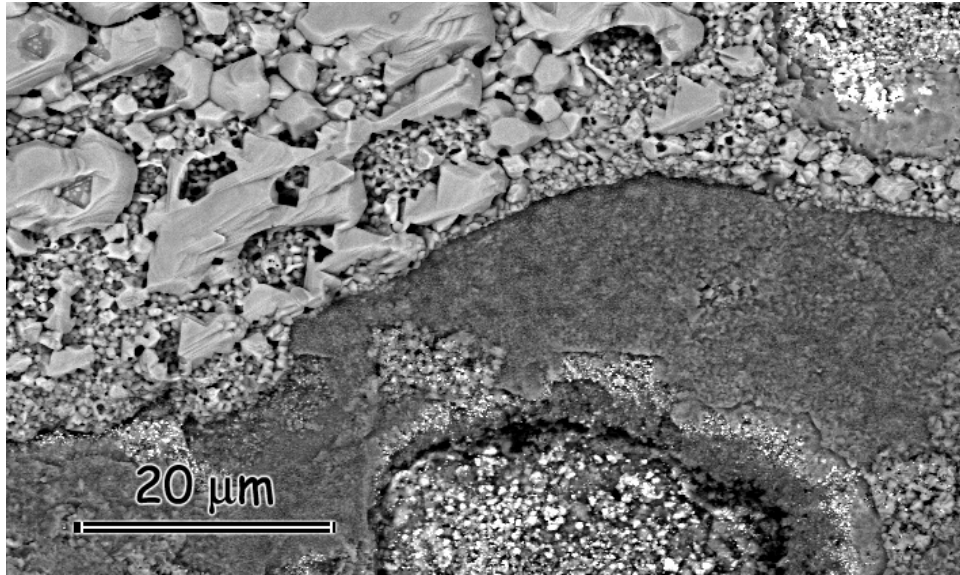


(a)

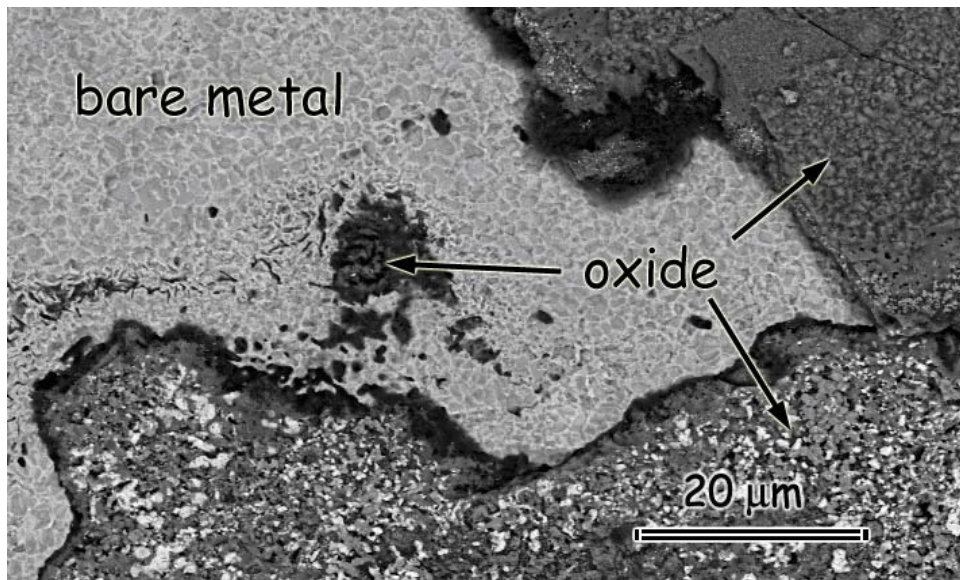


(b)

Figure 5.27: René N5 at 1000°C after cyclic exposures for 2435 hours (a) in dry air, and (b) in air/H₂O mixtures. Images show the spalled areas on specimen surfaces at low magnification.

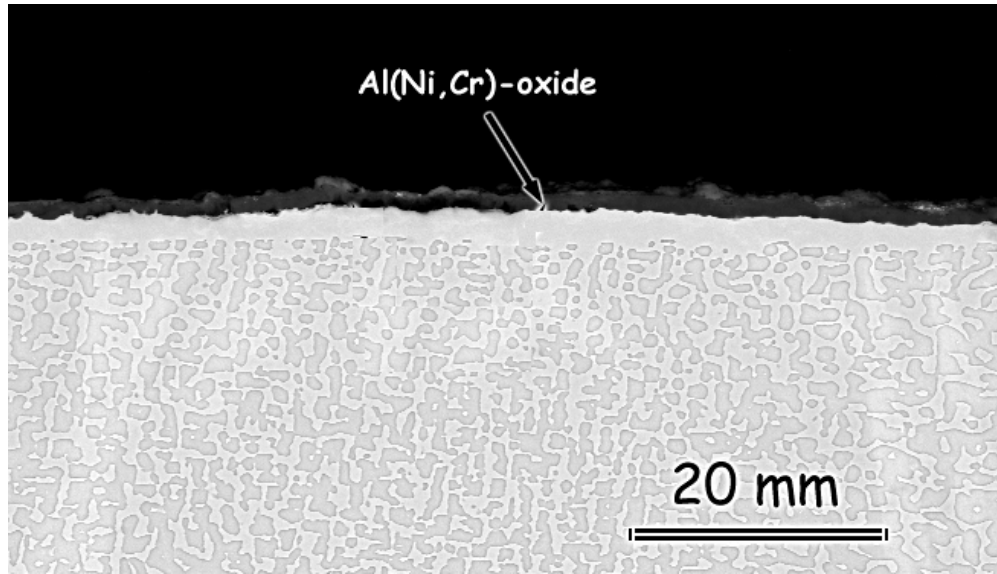


(a)

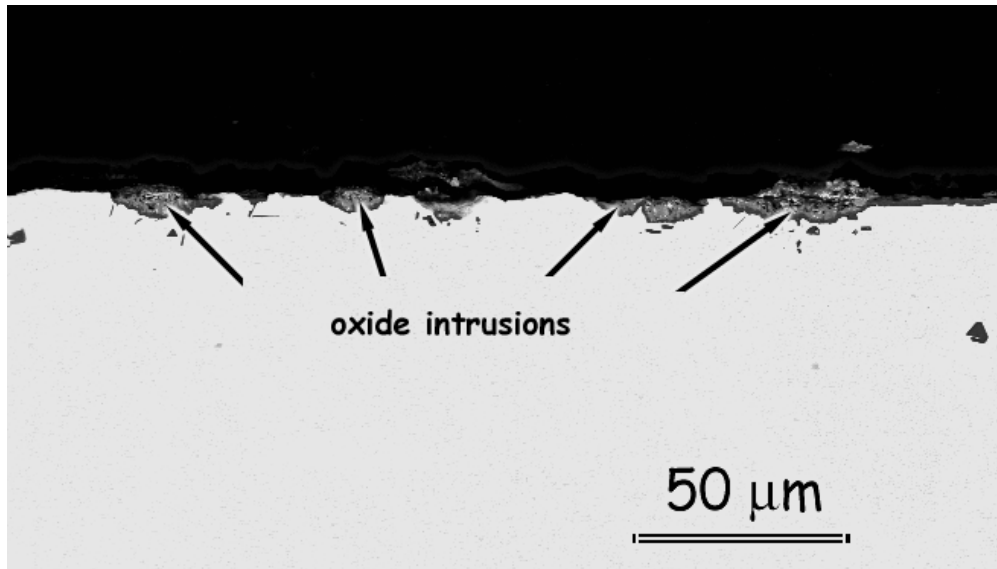


(b)

Figure 5.28: (a) PWA 1484 at 1000°C in dry air after 2435 cycles, and (b) René N5 at 1000°C in dry air after 2435 cycles. The surface images of the samples show parts of the scale where spallation occurred.

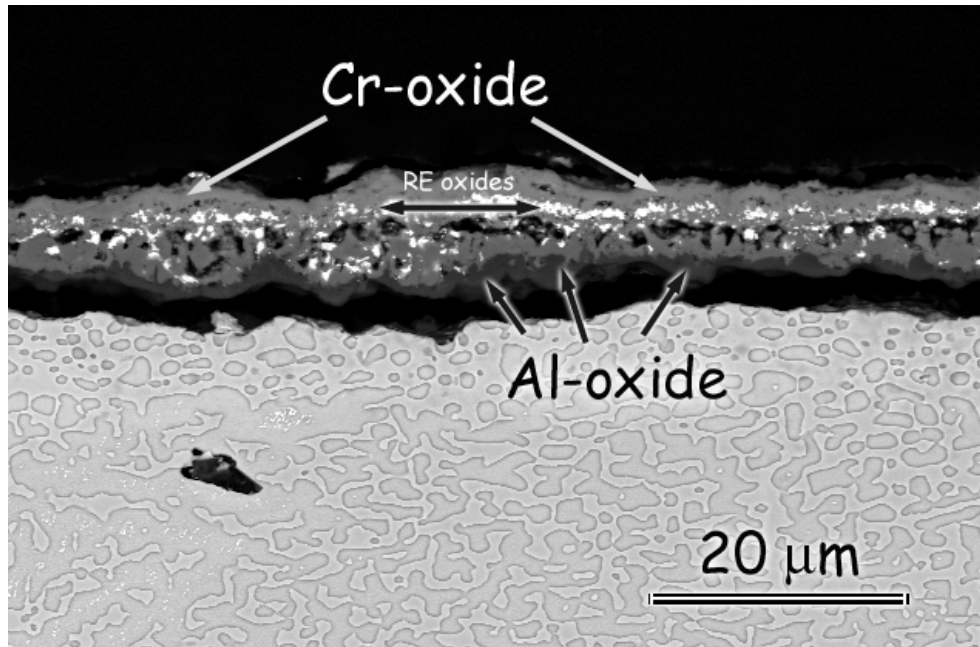


(a)

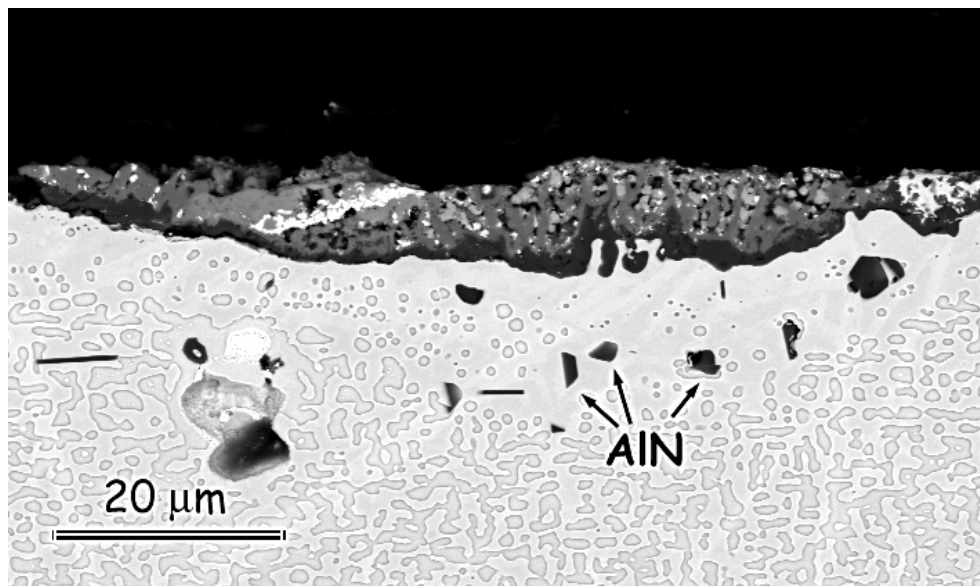


(b)

Figure 5.29: Cross-sectional SEM images of René N5 at 1000°C in dry air after 2435 cycles showing (a) the continuous dual scale that developed along the surface of the sample, and (b) the oxide protrusions.



(a)



(b)

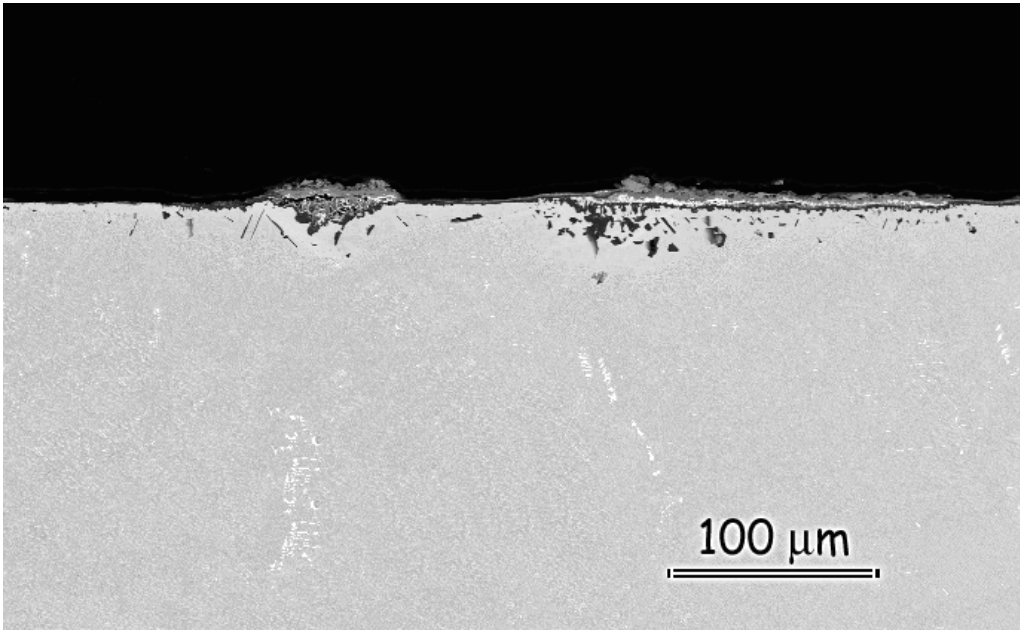
Figure 5.30: Cross-sectional SEM images of René N5 at 1000°C in wet air after 2435 cycles. (a) The micrograph shows part of the scale where complex transient oxides developed above the alumina. (b) The image shows formation of the nitride phase (AlN) in the depleted zone. This phase preferentially precipitated below oxide intrusion. However, it is present in other parts of the depleted zone too.

and Cr developed in various compositional combinations. Different sizes of reactive-element oxide precipitates were also present in these mixed oxides. Severe spallations, variations in the depths of spalled areas due to repeated spallation-reoxidation processes and the depletion of certain elements in the substrate made the evaluation of the scale more complicated.

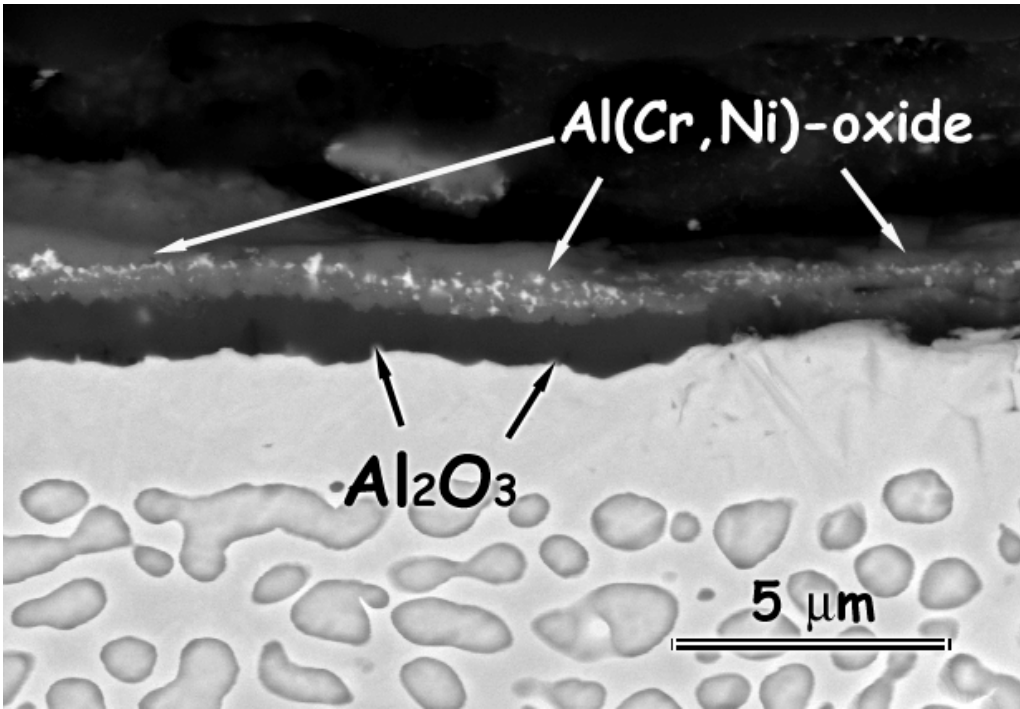
It is believed that water vapor enhanced the transient oxidation of the alloy. This statement is based on the kinetic data which showed larger weight gains in wet air during initial periods of oxidation. Unfortunately, the cross-sectional micrographs do not provide evidence for transient oxide formation. The lack of these oxides on the alloy surface is attributed to the heavy spallations between cycles, which wiped out the major fraction of the external scale.

As on René N5, the presence of water vapor caused more substantial oxide spallation on PWA 1484. However, it is important to note that the extent of spallation was not negligible in dry air. The scanning electron microscope images of the oxide surfaces in Figure 5.26 show the severity of the damage in each environment. The cross-sections of the specimens show the details of the scales that formed in dry air and in wet air, Figures 5.31 and 5.32, respectively. It is observed that the characteristics of these scales were almost the same as the ones that developed on René N5 in each testing environment. Transient NiO formed at the scale/gas interface. The nitride phase, AlN, was formed more profusely in the dry exposed sample. It precipitated preferentially, but not necessarily, below the oxide intrusions.

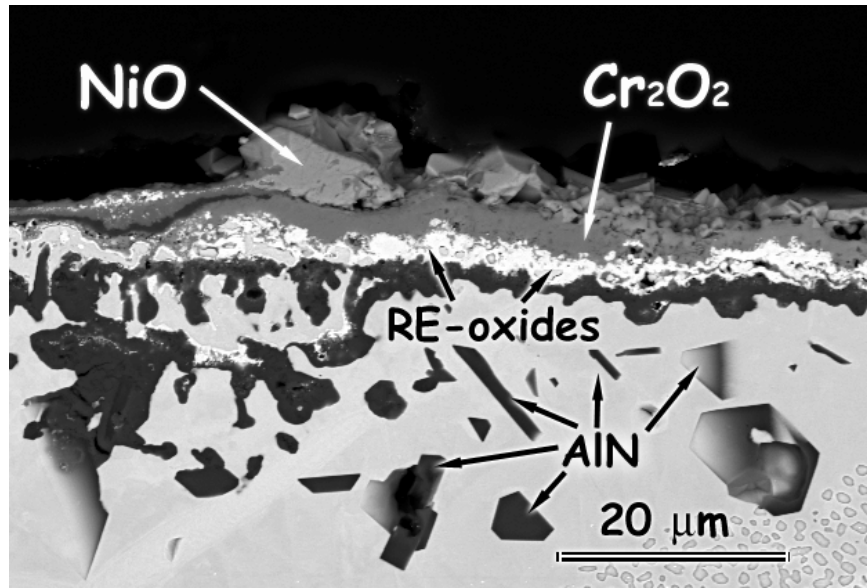
The alloy system CM 186 displayed higher weight gains in wet air in comparison to dry air during the earlier stages of oxidation, Figure 5.33. However, this statement does not hold for MarM 247. No significant differences were observed with this system in terms of specimen weight changes. The kinetic plot is shown in Figure 5.34.



(a)

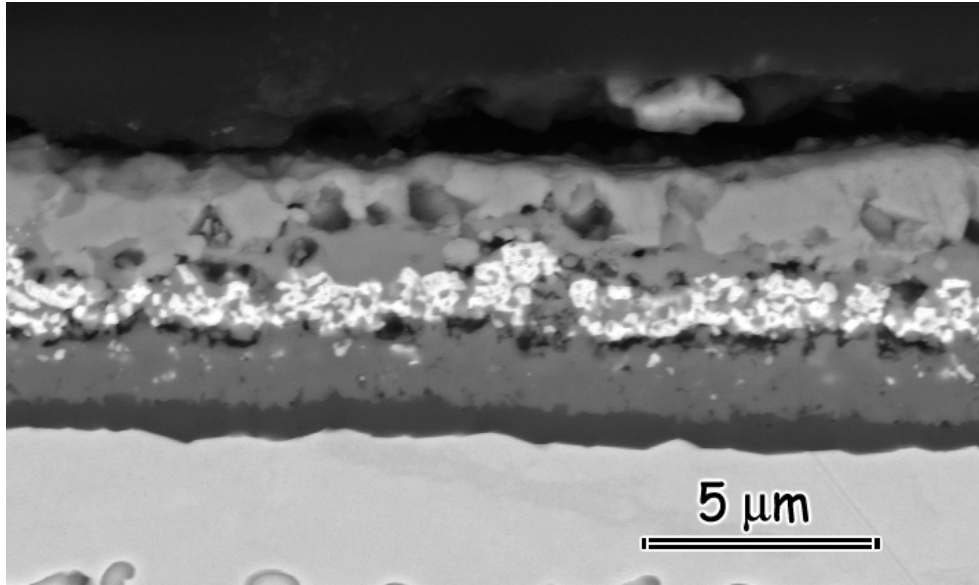


(b)

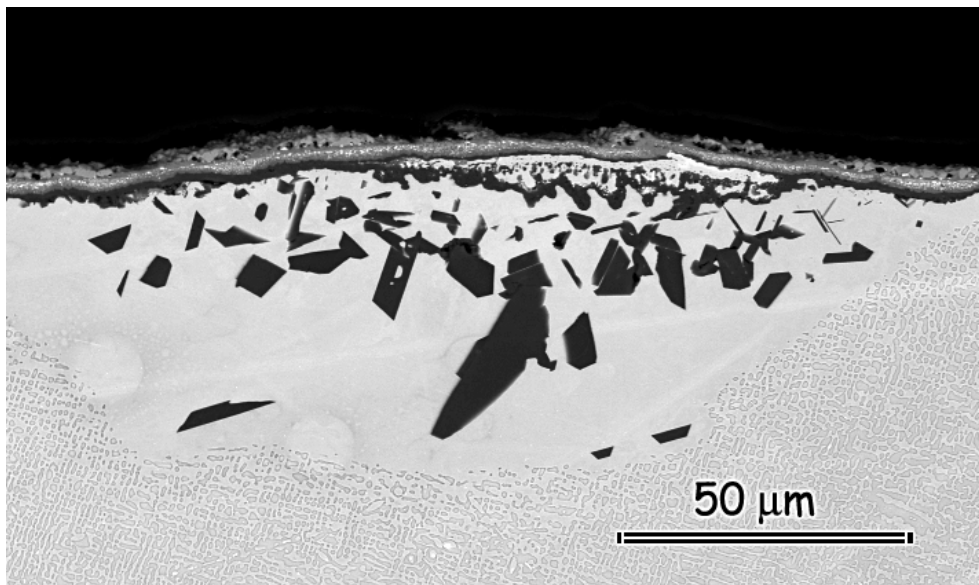


(c)

Figure 5.31: SEM images of PWA 1484 at 1000°C in dry air after 2435 cycles. (a) A thin layer of oxide developed along the sample surface. Formation of oxide protrusions interrupted the continuity of this thin layer with better protective properties. (b) The micrograph shows the thin protective scale at higher magnification. (c) AlN was also observed to form, preferentially below the oxide protrusions. The image shows such an area at high magnification.



(a)



(b)

Figure 5.32: SEM images of PWA 1484 at 1000°C after exposures in wet air. (a) A scale with substantial amounts of transient oxides covered the surface of the alloy. The transient oxide layer consisted of NiO at the scale/gas interface, a layer of reactive-element oxides, and complex (Ni,Cr,Al,Co)-oxides. Protective alumina scale formed at the substrate/oxide interface. The continuity of the scale was disrupted by scale spallations, which gave rise to formation of oxide protrusions. (b) SEM image shows the nitride phases that developed in the depleted zone at high magnification.

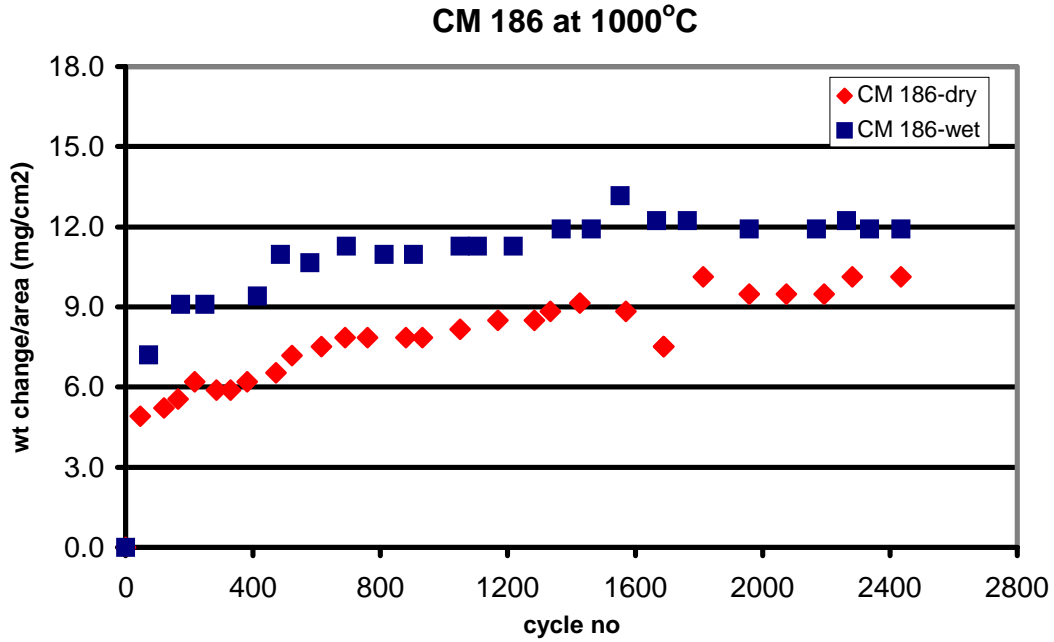


Figure 5.33: Kinetic plot of the alloy CM 186 showing the weight changes of the specimens in dry air and in air/H₂O mixtures at 1000°C as a function of cycle number.

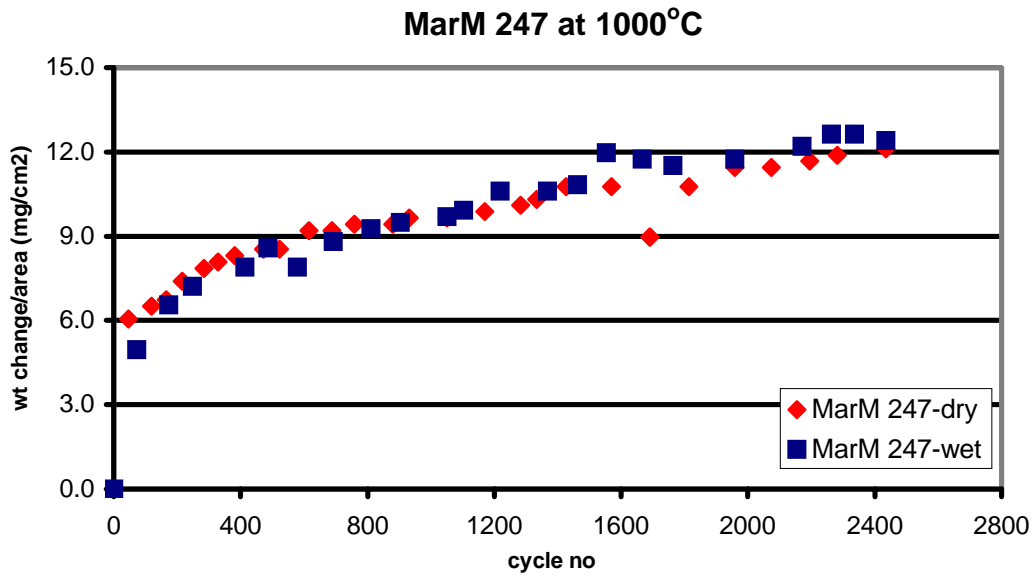
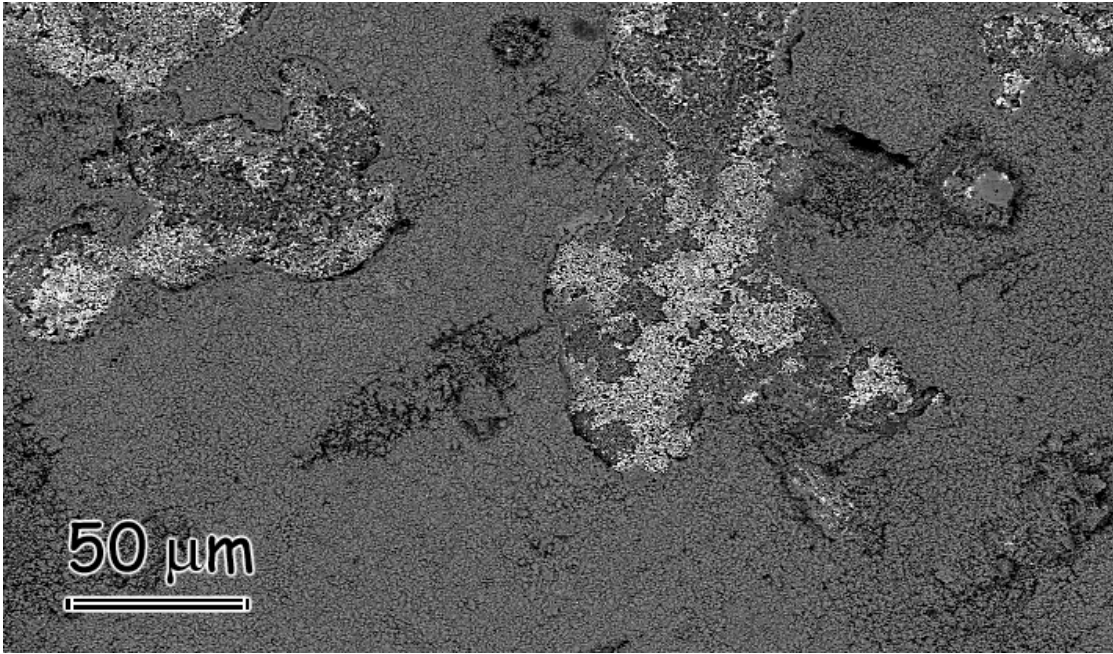


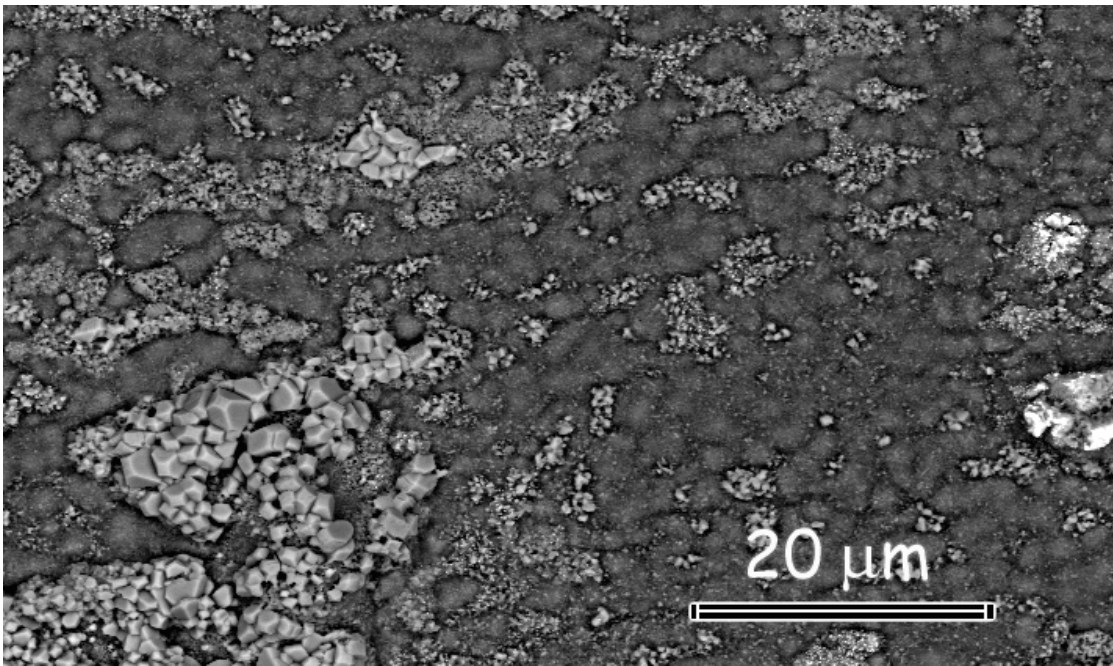
Figure 5.34: Kinetic plot of the alloy MarM 247 showing the weight changes of the specimens in dry air and in air/H₂O mixtures at 1000°C as a function of cycle number.

The EDS analysis of CM 186 specimens indicated that NiO and TiO₂, as well as oxides of Al, Cr, Co and refractory metals were present in the scale. The features of the oxide scales developed on MarM 247 were not significantly different from CM 186. Similar phases were detected on each sample. Figures 5.35 and 5.36 show the top views of sample surfaces. The micrographs display parts of the scale with oxide spallation-and-reformation. Images of specimen cross-sections are given in Figures 5.37-5.38. These micrographs also clearly show that similar scales developed on both alloy systems. Additionally, the features of the oxide layer were the same in dry air and in wet air. A deep and undesirable zone of internally formed oxides was detected on all specimens. This zone consisted of islands of HfO₂ with Al in solution embedded into an alumina matrix. A thinner phase was present at the oxide/gas interface. This phase was identified as an Al-rich complex Al(Cr,Ni)-oxide.

The kinetic data of all alumina formers, with the exception of MarM 247, indicated that the initial reactions were more aggressive in wet air, which was reflected as larger weight gains in this environment. René N5 and PWA 1484 suffered from weight losses after exposures to hot gases in each environment. However, this behavior was not observed with CM 186 or MarM 247. At first glance, the kinetic data suggested that these alloys were more resistant to spalling of oxides. However, the features of the scale surfaces, which clearly showed that scale spallation was happening, were not in agreement with the kinetic data. The examination of the cross-sections revealed a zone of internal oxides that extended undesirably deep into the alloy. This indicated that the continuous increase in specimen weights was the consequence of the excessive internal oxidation, which was associated with HfO₂ formation. The same phenomenon was not observed with René N5 or with PWA 1484 owing to their chemical composition. René N5 and

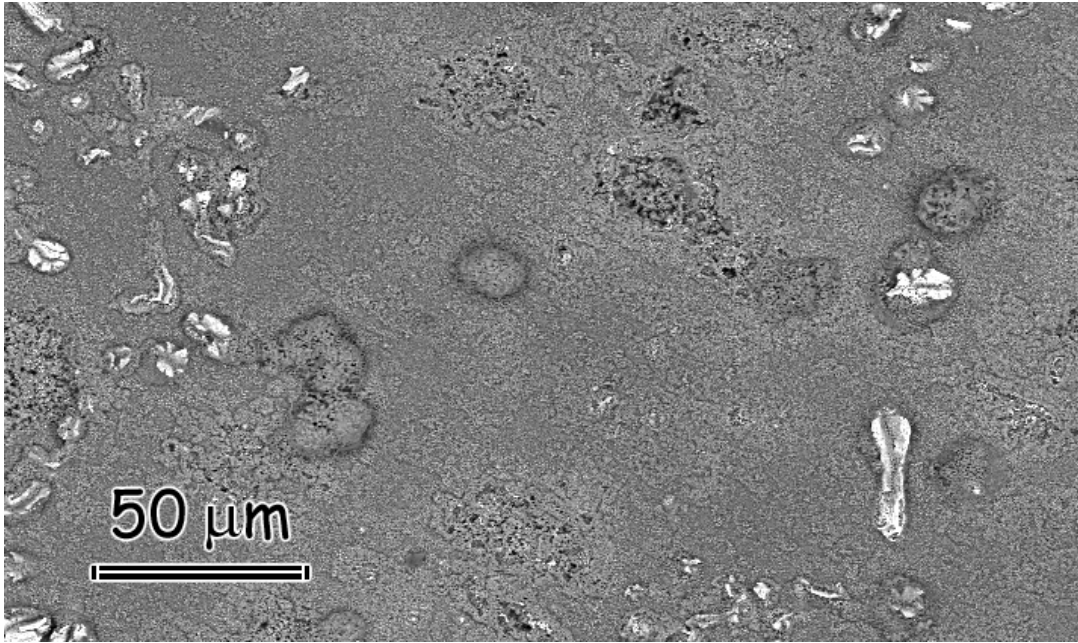


(a)

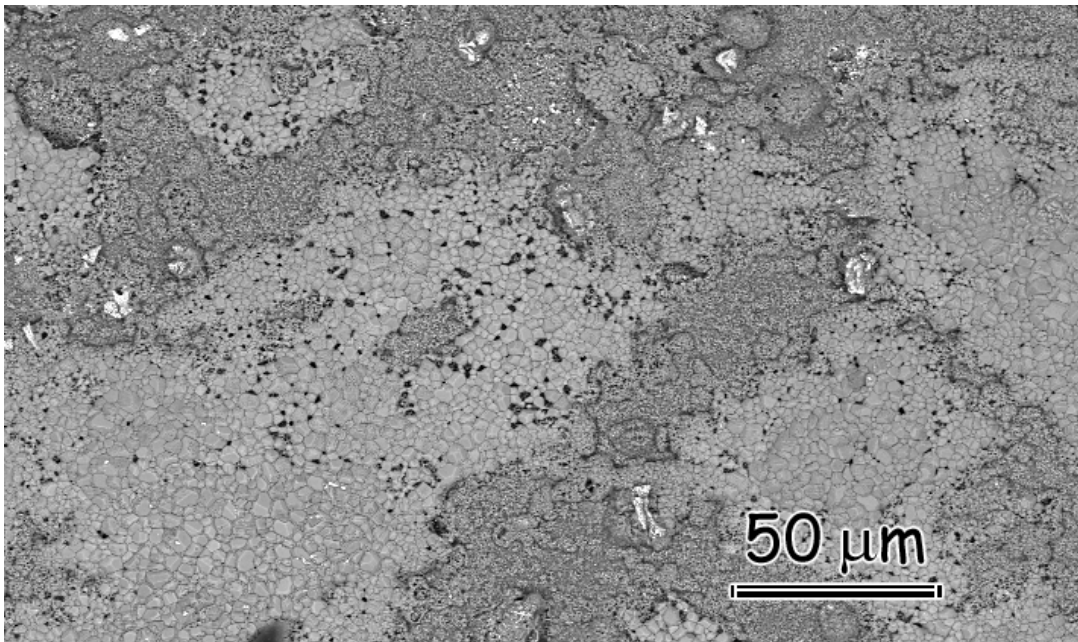


(b)

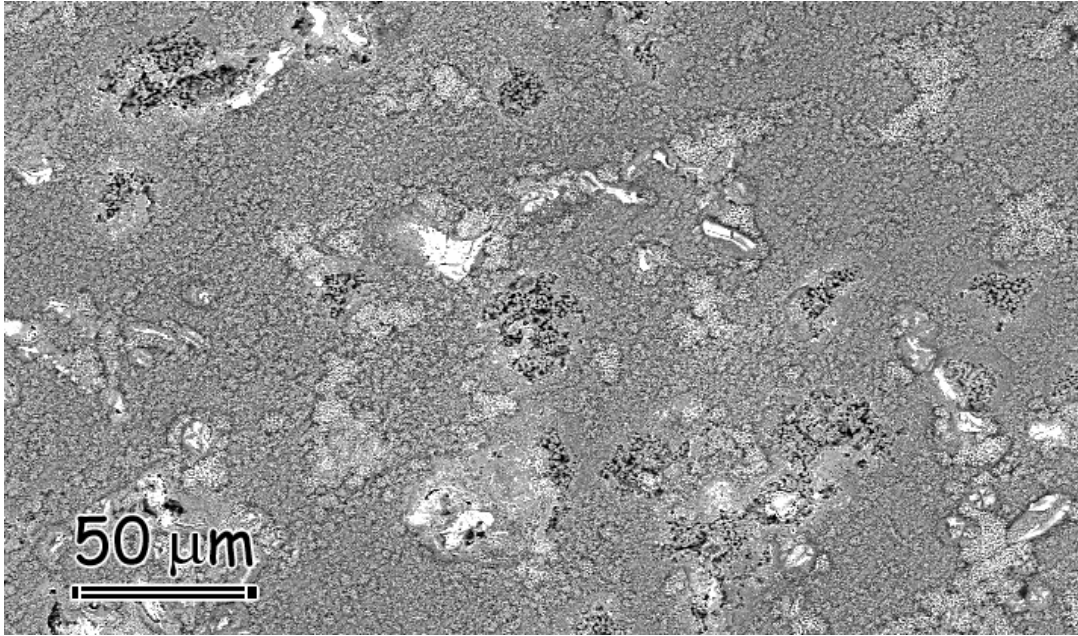
Figure 5.35: Surface micrographs of CM 186 showing the oxide scale at 1000°C (a) in wet air, and (b) in dry air after 2435 cycles.



(a)

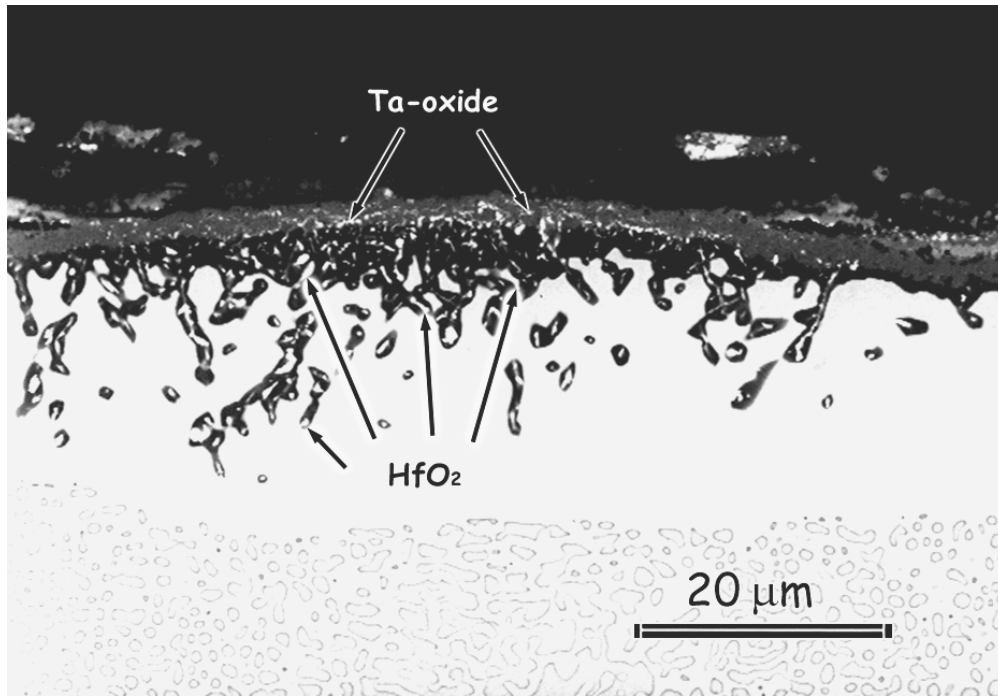


(b)

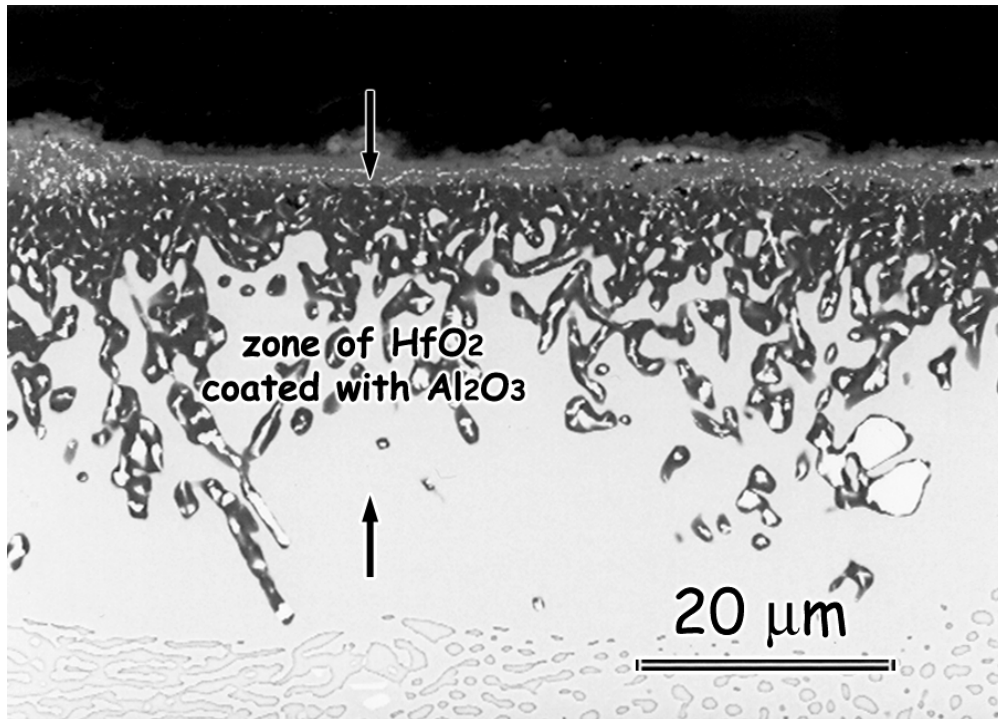


(c)

Figure 5.36: SEM images showing the surface of samples prepared from the alloy MarM 247 after 2435 hours of cyclic exposures at 1000°C (a) in dry air, (b-c) in wet air.

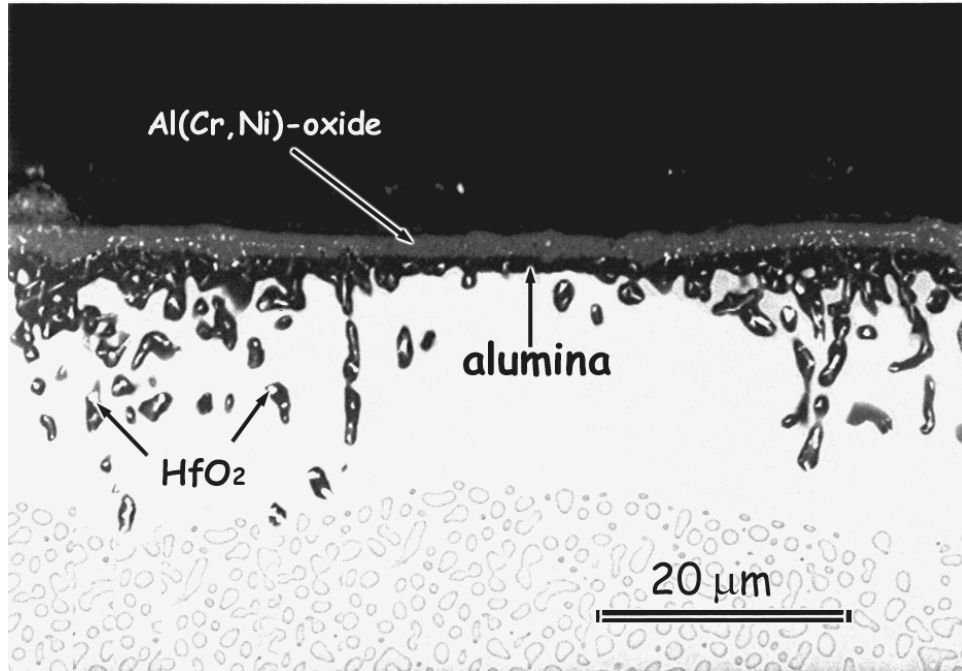


(a)

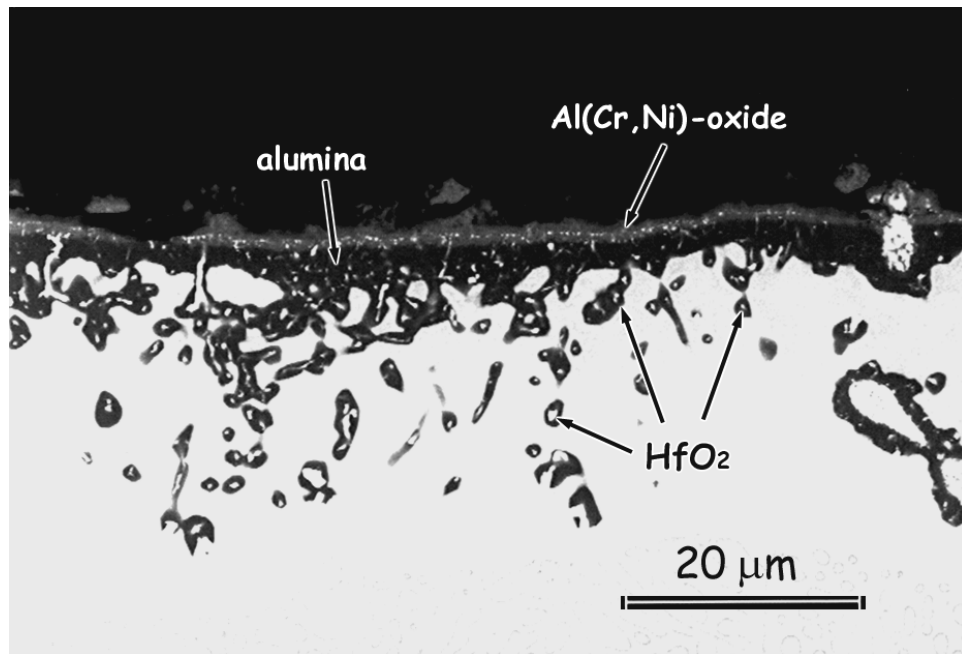


(b)

Figure 5.37: Cross-section of CM 186 at 1000°C after 2435 cycles. (a) Image shows the scale that formed in dry air. (b) SEM micrograph of CM 186 in wet air.



(a)



(b)

Figure 5.38: SEM image showing MarM 247 at 1000°C after 2435 cycles. A zone of internal oxides developed after exposures. (a) Cross-section of the scale that developed in dry air. (b) MarM 247 in wet air. Image shows the zone of HfO₂ coated with alumina.

PWA 1484 had only 0.1wt% Hf, while CM 186 and MarM 247 had 1.4 and 1.3 wt% Hf, respectively (Table 4.1).

The mechanism leading to the formation of the described phase mixture is explained according to the following model. Hf diffuses outwards and reacts with oxygen to form HfO_2 , which is a more stable oxide than alumina. Oxygen transport in hafnium dioxide is known to be substantially greater compared to alumina. It is also believed that some of the rapid oxygen diffusion occurs along the HfO_2 /alloy interface. After Hf is oxidized, oxygen reacts with Al to form alumina. HfO_2 particles incorporate into the scale through the inward growth of alumina [16].

These results suggest that for applications at temperatures of 1000°C and higher where oxidation resistance is a requirement, Hf additions into the alloy should be controlled more closely. Accelerated internal alumina formation would lead to rapid deterioration of the components. The alloys René N5 and PWA 1484 do not suffer from this problem due to their low Hf contents. However, it would be inaccurate to conclude that their performance is superior to CM 186 or MarM 247.

Experimental data indicated that, the main problem at higher temperatures was poor adherence of oxide scales to the substrate material rather than selective oxidation of Al. System deterioration by scale spallation became a major concern. This was more severe in air/water vapor mixtures.

5.1.2 Isothermal Exposures of Alumina Formers

The comparative cyclic tests in dry air and in wet air at ambient pressure showed that water vapor had adverse effects on the oxidation behavior of alumina forming systems. One of these

effects was on selective oxidation of Al. It was observed that water vapor mixtures did not favor the formation of protective alumina scales. Additionally, the presence of H₂O resulted in increased oxide spallation. This became especially significant at higher temperatures. Scale spallations are typically caused by growth stresses and thermal stresses. The former one is the major source of oxide spallation for isothermal exposures, while the latter one becomes more important for thermally cycled components. In general, thermal stresses are much larger than growth stresses, [26]. For most systems, the thermal expansion coefficient of the oxide is smaller than that of the metal/alloy. Some of the values are listed in Table 5.1 as they appear in the literature, [3]. The differences between the thermal expansion coefficients usually result in residual compressive stresses in the scale upon cooling, which often times leads to spallations.

In this study, some isothermal tests were designed in order to understand the contribution of cyclic exposures to scale spallation, as well as to the selective oxidation of Al in an indirect way. Since spalling of oxides also depletes the metal in terms of the element, formation of alumina scales becomes more and more difficult. These experiments were done at 900°C in air/H₂O mixtures. The conditions of testing were kept identical to the cyclic exposures, i.e. $P_{\text{total}} = 1$ atm and $P_{\text{H}_2\text{O}} = 0.3$ atm.

Another set of isothermal exposure tests were done in 100% steam environment at high pressure. This time, the purpose was to see the influence of water-vapor-only environments, and the effect of high pressures on the oxidation reactions. Specimens were put into autoclaves at 250 psi (~17 atm). Each alloy was tested at 700°C and 900°C. The partial pressure of oxygen under the specified conditions was 4.5×10^{-7} atm, and 1.5×10^{-5} atm at 700°C and 900°C, respectively. The results at 700°C were compared only to cyclic tests at $P_{\text{total}} = 1$ atm, where

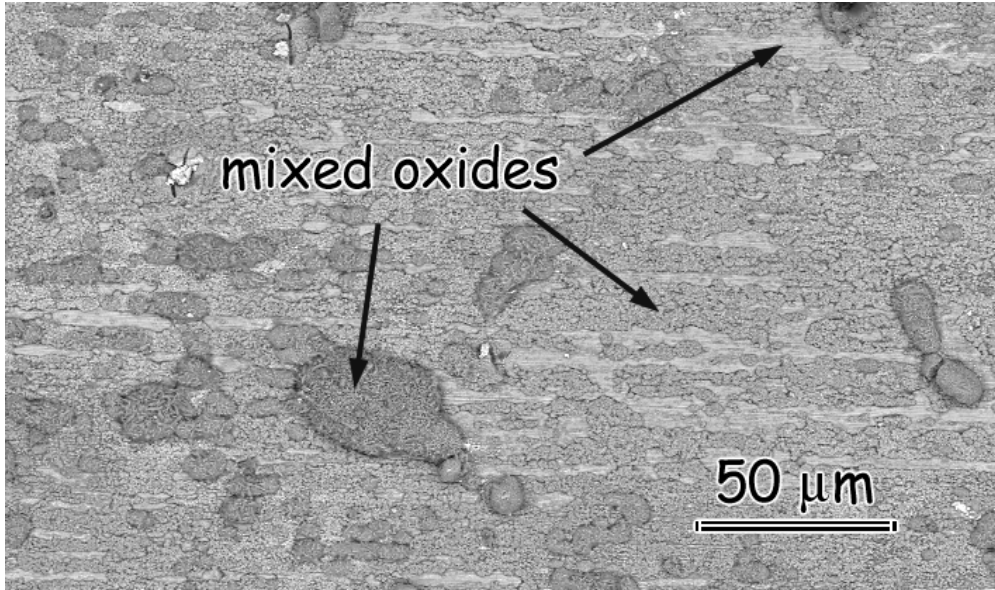
Table 5.1: Linear thermal expansion coefficients of select metals and their oxides, [3].

<i>System</i>	<i>Thermal Expansion coefficient</i>	
	<i>Oxide</i>	<i>Metal</i>
Co/CoO	15.0×10^{-6}	14.0×10^{-6}
Cr/Cr ₂ O ₃	7.3×10^{-6}	9.5×10^{-6}
Cu/CuO	9.3×10^{-6}	18.6×10^{-6}
Cu/Cu ₂ O	4.3×10^{-6}	18.6×10^{-6}
Fe/FeO	12.2×10^{-6}	15.3×10^{-6}
Fe/Fe ₂ O ₃	14.9×10^{-6}	15.3×10^{-6}
Ni/NiO	17.1×10^{-6}	17.6×10^{-6}

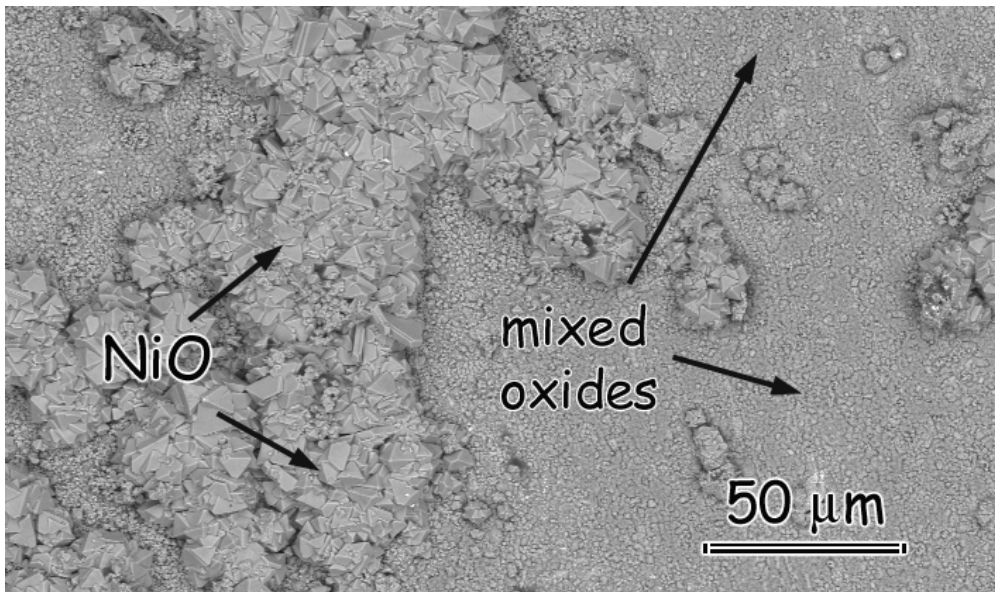
$\text{PH}_2\text{O} = 0.3 \text{ atm}$. At 900°C , the results of the high pressure tests were compared to isothermal and cyclic tests at ambient pressure (i.e. low PO_2 vs. high PO_2).

5.1.2.1 Isothermal Exposures at 700°C : Comparison of specimens prepared from CM 186 showed that the transient oxidation behavior of the system was affected by the oxidizing environment and/or by the mode of testing very significantly. Surface images of the exposed alloys are given in Figure 5.39. These micrographs clearly show that NiO formation was substantially reduced in high pressure steam. After cyclic exposures at ambient pressure large islands of NiO developed at the alloy/gas interface. However, the oxide blisters that formed on the isothermally exposed specimens were identified as mixed oxides. The images showing the cross-sections of the samples are given in Figure 5.40. These micrographs also confirm that NiO formation was suppressed after isothermal exposures in high pressure steam. Under these conditions, the system developed a thin and continuous scale. This scale was identified as a phase mixture of complex oxides of the elements Ni, Al, Cr, and Co. Although some internal oxidation was evident, the extent of it was not as significant as it was for the cyclically tested specimens at ambient pressure in wet or in dry air. The internally developed phase was identified as alumina. The formation of large transient oxide protrusions observed on specimens exposed cyclically to wet air at ambient pressure was suppressed in the low PO_2 environment. These protrusions consisted mainly of NiO, and some refractory element oxides.

Tests done with PWA 1484 gave similar results. The extremely thick layer of transient oxides which developed during cyclic exposures in wet air at ambient pressure was not observed on the specimens subjected to isothermal steam tests, Figure 5.41. The topographic images of the alloy in each environment are shown in Figure 5.42. The external scale that developed over

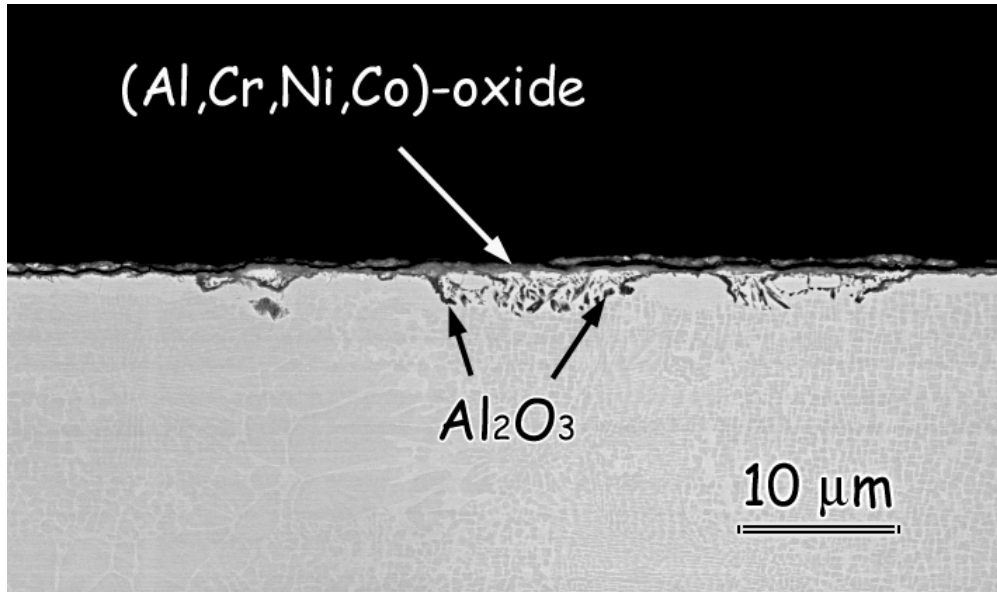


(a)

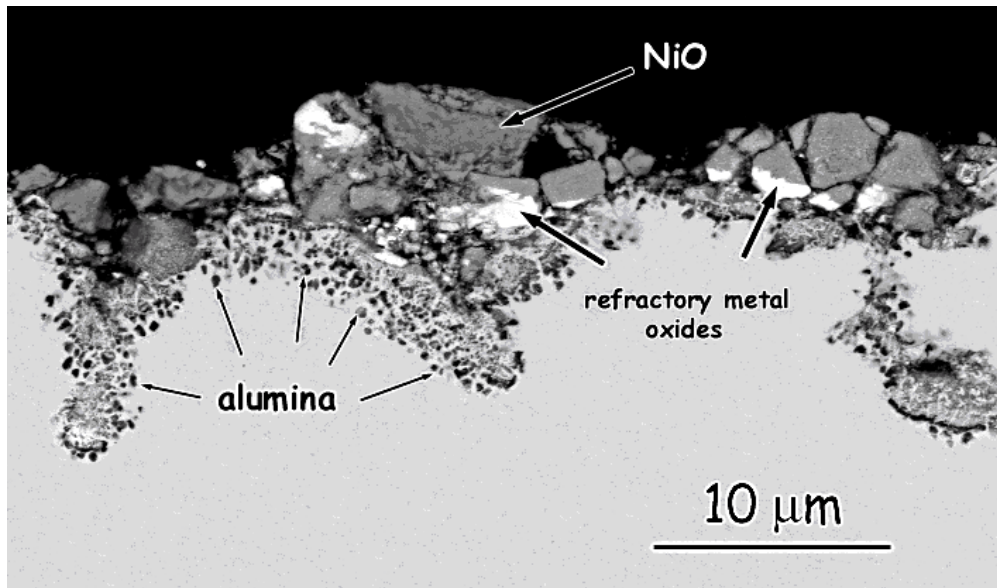


(b)

Figure 5.39: Surface images of CM 186 at 700°C. (a) EDX analysis showed that mixed oxides formed on the alloy after exposing the system to high pressure steam after 4320 hours. (b) Cyclic exposures to air/water vapor mixtures at ambient caused formation of large NiO islands over mixed oxides (3200 cycles).

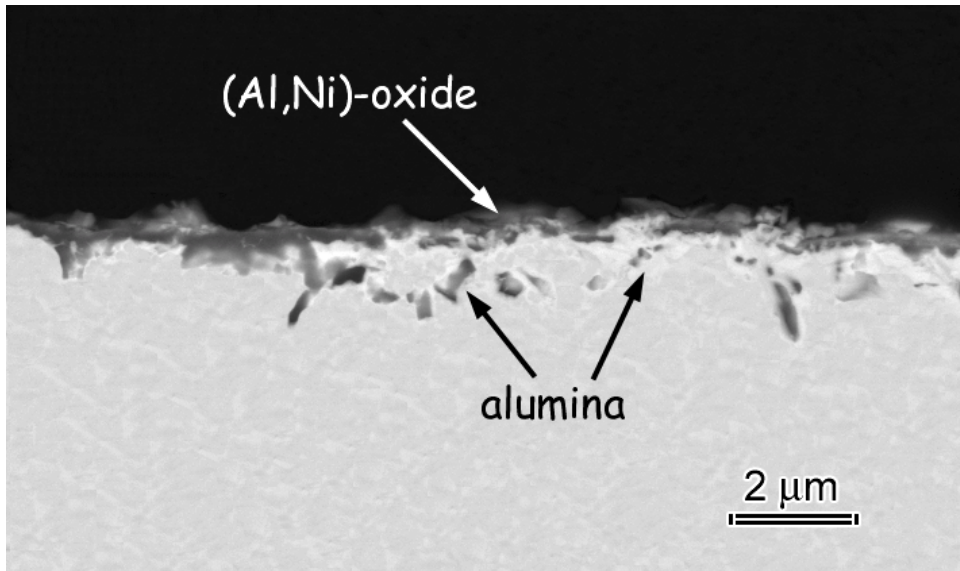


(a)

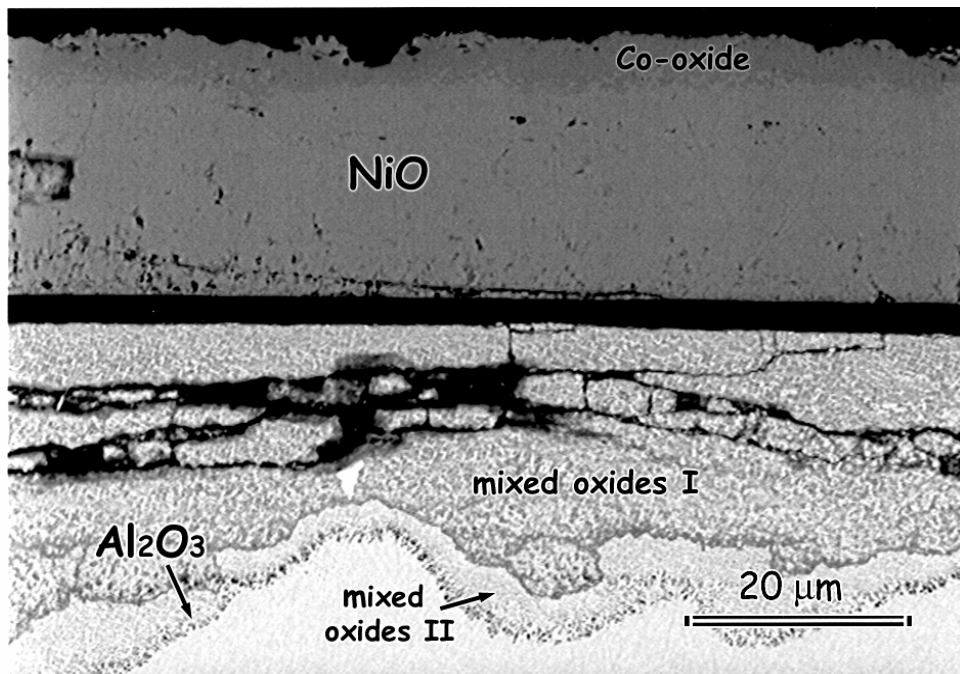


(b)

Figure 5.40: SEM micrographs showing the cross-section of CM 186 at 700°C. (a) Specimen isothermally exposed to high pressure steam in an autoclave for 4320 hours. (b) The scale that developed after cyclic exposures in wet air at ambient pressure after 3200 cycles.

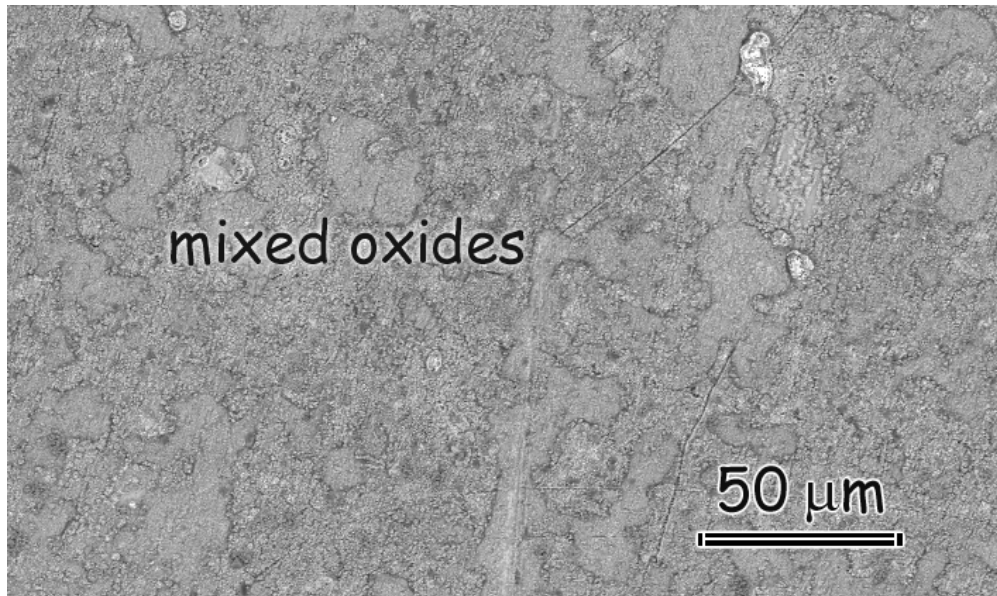


(a)

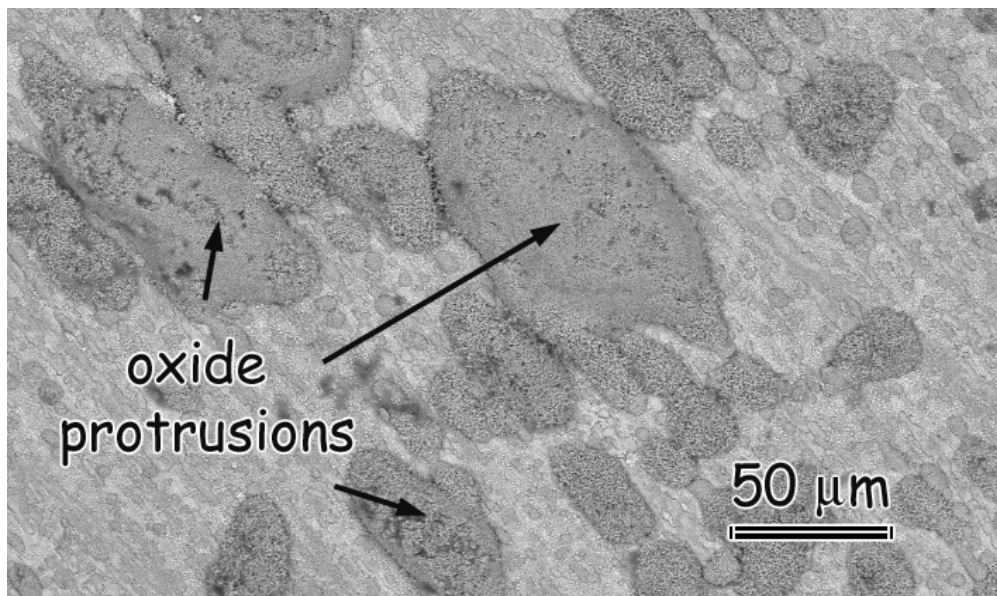


(b)

Figure 5.41: PWA 1484 at 700°C. Micrographs show the cross-section of the scale the system developed at this temperature. (a) Isothermal tests in steam at high pressure for 4320 hours resulted in the formation of a thin scale on the surface of the specimen. (b) A thick multi-layered scale of transient oxides formed after cyclic tests in wet air for 3200 hours.



(a)



(b)

Figure 5.42: PWA 1484 at 700°C. (a) Isothermal tests in high pressure steam for 4320 hours caused formation of a thin layer of mixed oxides that covered the whole surface area of the specimen. (b) The micrograph shows the scale that formed after cyclic tests in wet air at 1 atm total pressure with $P(\text{H}_2\text{O}) = 0.3$ atm after 3200 cycles. The major part of the scale was covered by a continuous and thick layer of (Ni,Co)-oxide. In very limited parts of the scale, non-continuous islands of NiO were detected.

the specimen subjected to isothermal steam was identified by EDX analysis as a phase mixture, which consisted of mainly (Al,Ni)-oxide with Cr in solution. This layer covered the total surface area of the specimen. Cross-sectional examination indicated that the scale was very thin and continuous. Some internal alumina formation was also evident, Figure 5.41(a). The morphology of this scale was similar to the reaction zone that developed after cyclic tests in dry air, Figure 5.8(b), rather than in wet air.

MarM 247, which was not as vulnerable to transient oxidation as PWA 1484 or CM 186 in wet air at ambient pressure, developed oxides with similar microstructures in each environment, Figures 5.10 versus 5.43. The depths of internal oxides were slightly larger on the isothermally exposed sample. Other than this, there were no major differences between cyclic and isothermal test results.

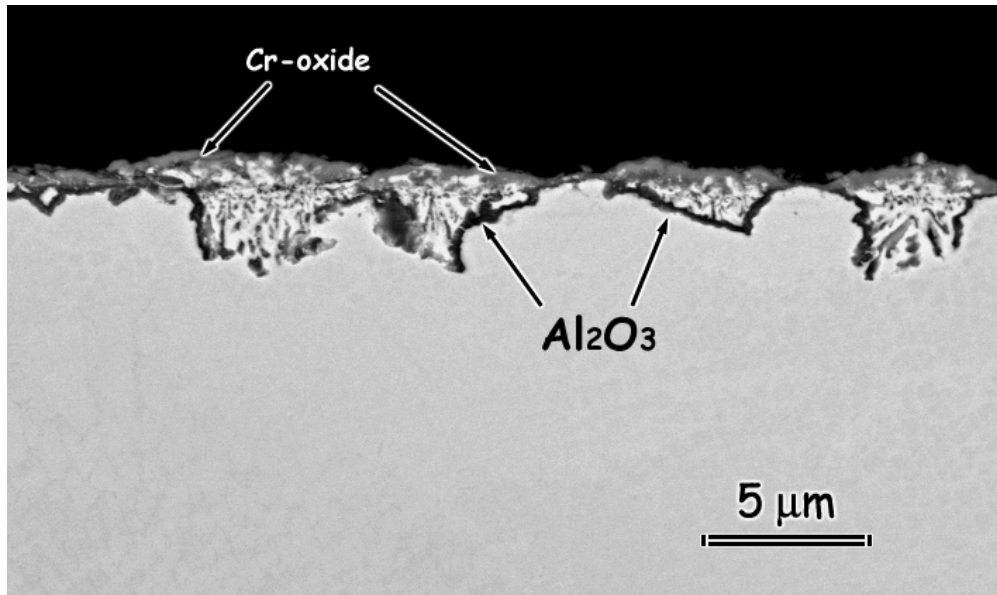
The cyclic tests at ambient pressures showed that transient oxidation was accelerated in water vapor/air mixtures. The data obtained from 100% steam tests, on the other hand, revealed that isothermal tests in low PO_2 suppressed extensive formation of transient oxides, especially NiO, for systems which were more vulnerable to this type of degradation at atmospheric pressure. As a consequence, the reaction rates were slowed down remarkably on these alloys. At this temperature, no apparent effects of scale spallation were observed.

5.1.2.2 Isothermal Exposures at 900°C: The surface images of CM 186 specimens tested at 900°C in high pressure steam and in air/H₂O mixtures at atmospheric pressures are given in Figure 5.44. These micrographs show that, formation of NiO was significantly suppressed in the low PO_2 environment. This result is consistent with the observations at 700°C. After cyclic tests almost the total surface area was covered with NiO, Figure 5.44(a). On the other hand, this

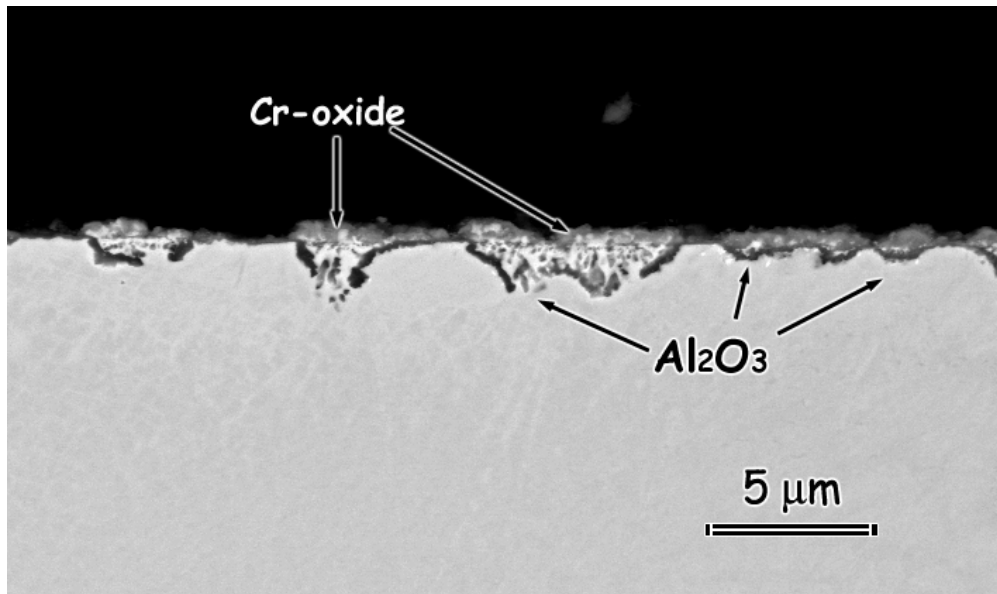
oxide was detected only in small amounts on the specimen tested isothermally in steam. Comparison of isothermal tests in high pressure gases to the isothermal atmospheric pressure experiments showed that oxidation reactions were accelerated profusely in 100% steam environment, although NiO formation was suppressed significantly, Figure 5.45. The micrograph of the sample cross-section shows the thick scale that formed on the surface, Figure 5.45(a). This scale is a complex oxide mixture of the elements Al, Cr, Ni, and Co. The scales that formed after exposures at ambient pressure -cyclic or isothermal- displayed features which were closer to each other, Figures 5.18 and 5.45(b). The main difference was the deceleration of transient oxide formation during isothermal tests in air/H₂O mixtures compared to cyclic tests in wet air. However, still less transient oxidation took place during cyclic tests in dry air.

Figure 5.46 shows the top view of the oxide scale that developed on MarM 247 at 900°C in pure steam at high pressure. The alloy developed a layer of mixed oxides that covered the sample surface evenly after exposures. This scale was found to be Cr-rich overall. Islands of NiO with underlying Co-oxide particles were observed to develop in some locations. Cross-section of the sample showed that the Cr-rich oxide formed a thin layer, Figure 5.47. Al oxidized internally underneath this scale without being able to develop continuity. The scale morphology was uniform along the whole sample cross-section.

After exposing the alloy to air/H₂O mixtures isothermally at 1 atm total pressure, a non-uniform layer with the frequent appearance of oxide protrusions developed. The microstructure of the scale is shown in Figure 5.48. The features of the layer were similar to the ones that developed after cyclic exposures at 1 atm pressure, Figure 5.49. Hf-oxide was observed to develop more profusely during isothermal tests at ambient pressure.

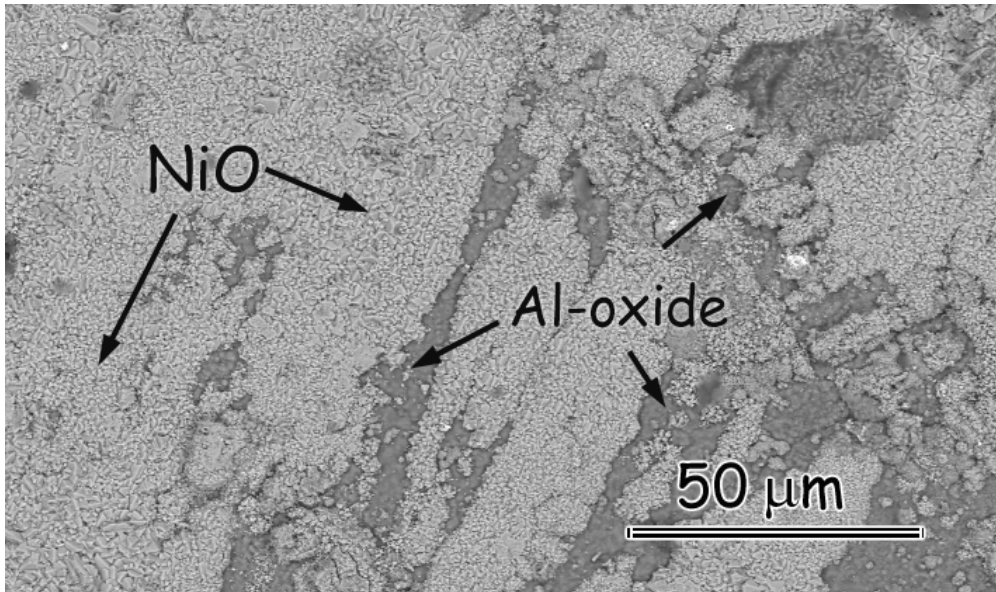


(a)

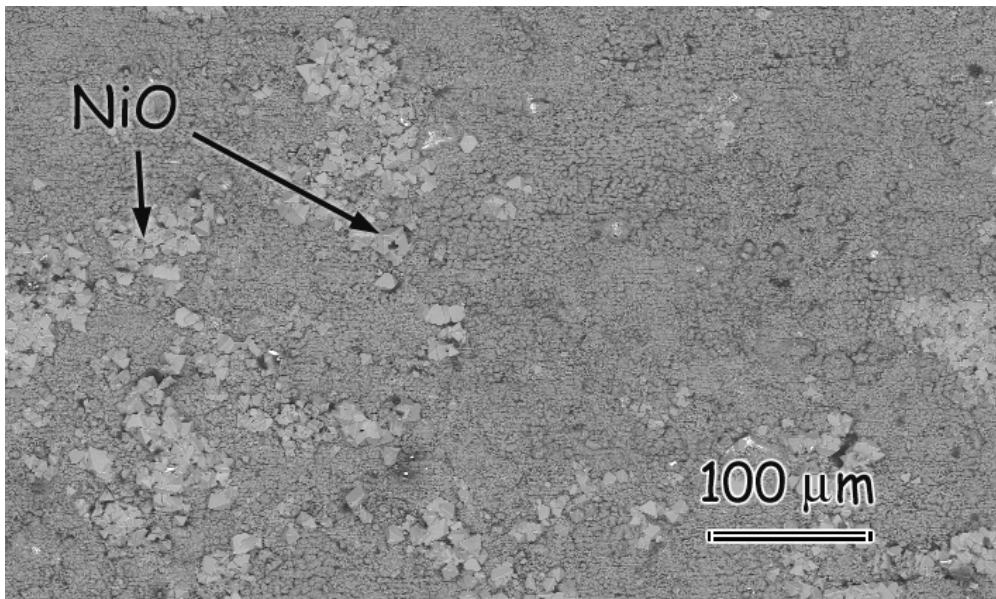


(b)

Figure 5.43: MarM 247 at 700°C. (a) The image shows the cross-section of the scale that formed on the specimen after exposure to high pressure steam isothermally for 4320 hours. (b) Same alloy after cyclic exposures in air/H₂O mixtures at a total pressure of 1 atm, where P(H₂O) = 0.3 atm.

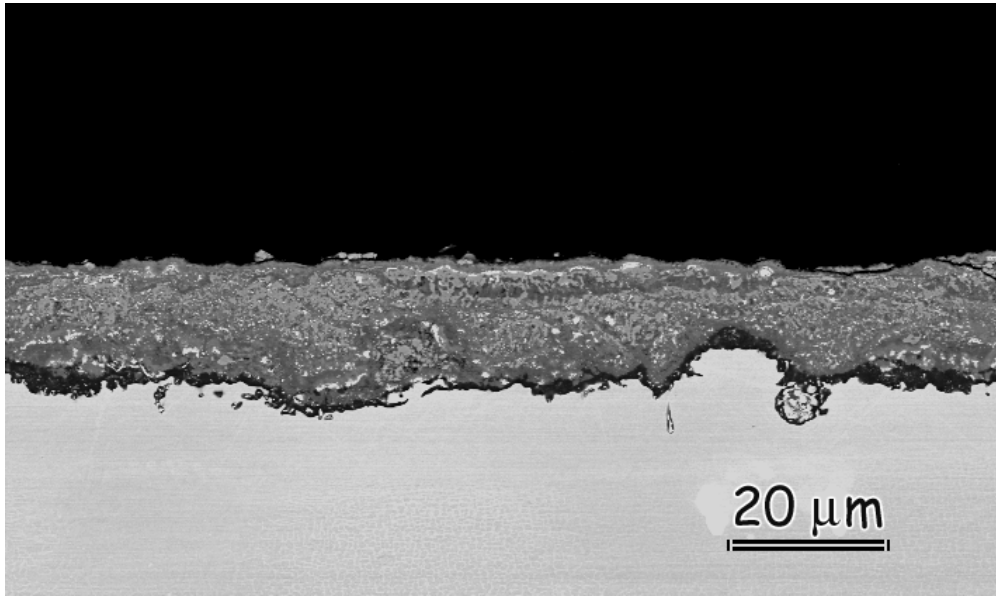


(a)

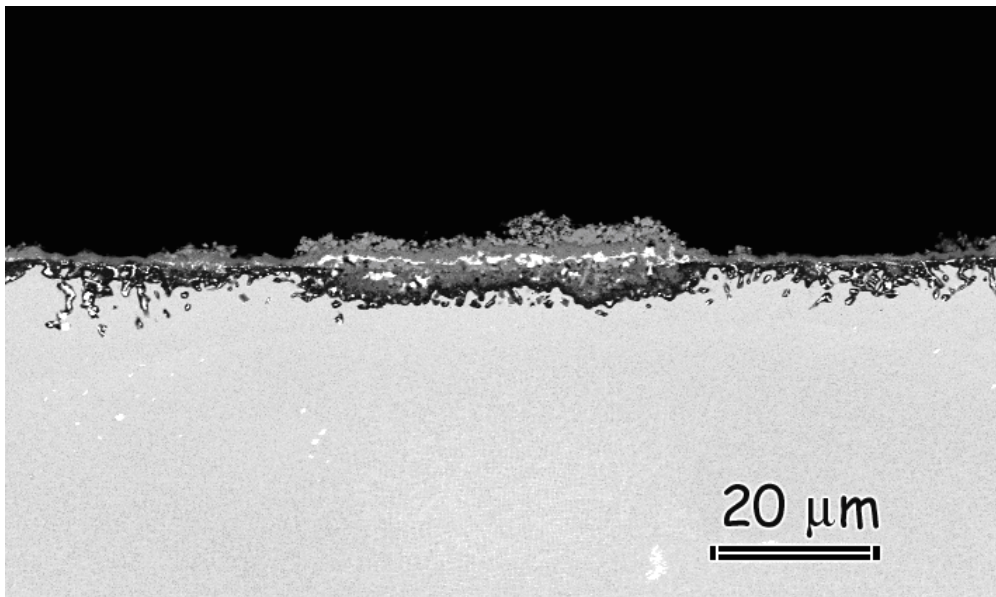


(b)

Figure 5.44: Surface images of CM 186 at 900°C after isothermal tests (a) in air/H₂O for 2400 hours at 1 atm total pressure [$P(\text{H}_2\text{O}) = 0.3 \text{ atm.}$], and (b) in high pressure steam for 4320 hours.



(a)



(b)

Figure 5.45: CM 186 at 900°C. (a) Cross-sectional image showing the scale that formed after isothermal steam tests for 4320 hours. (b) Scale that formed on the specimen surface after isothermal tests in wet air where $P_{total} = 1$ atm for 2400 hours.

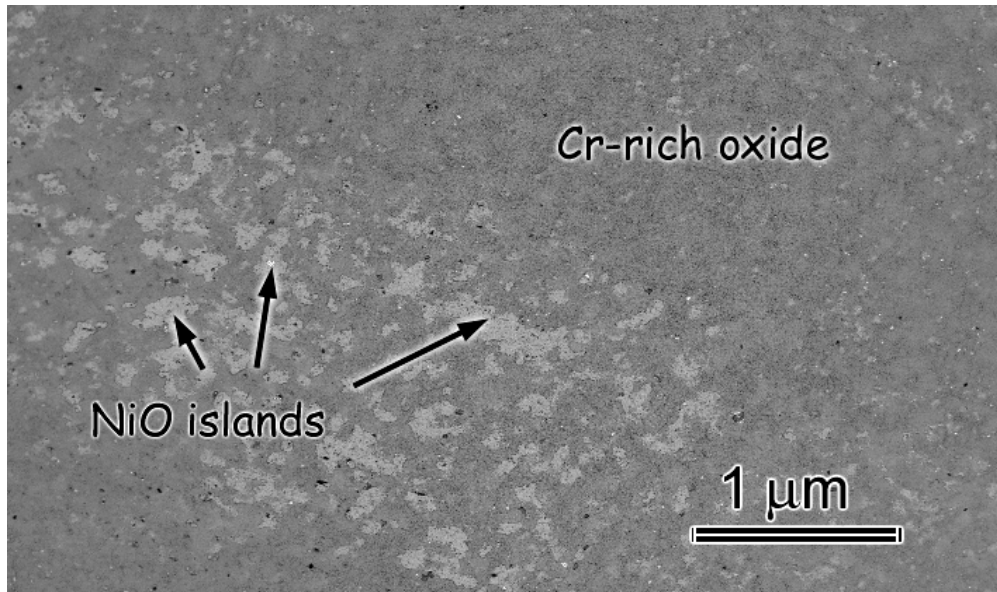


Figure 5.46: MarM 247 at 900°C after isothermal tests at high pressure in 100% steam. A Cr-rich scale covered the surface of the specimen. Some NiO islands with underlying Co-oxide were spotted along the surface on some limited locations.

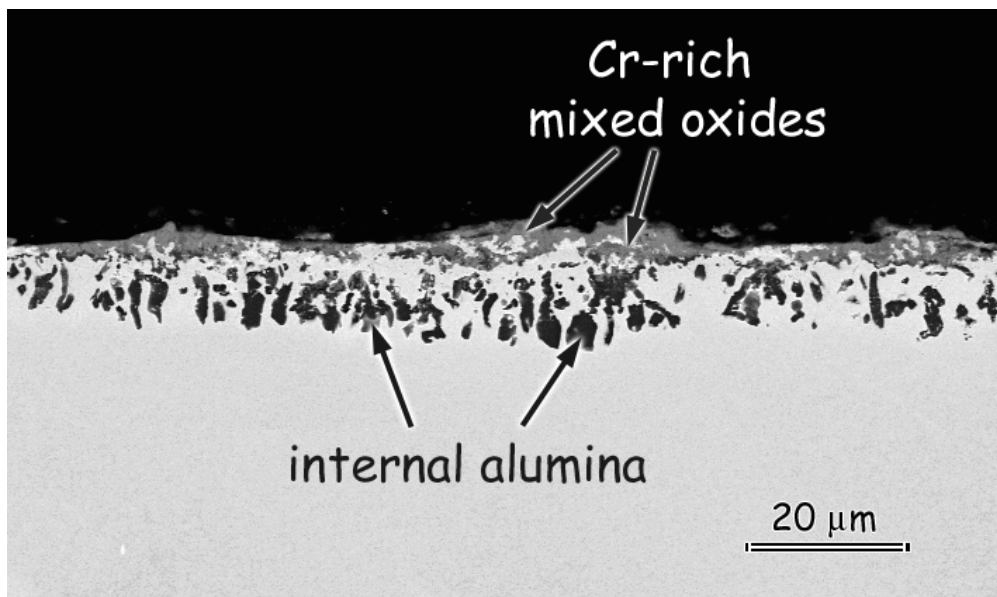
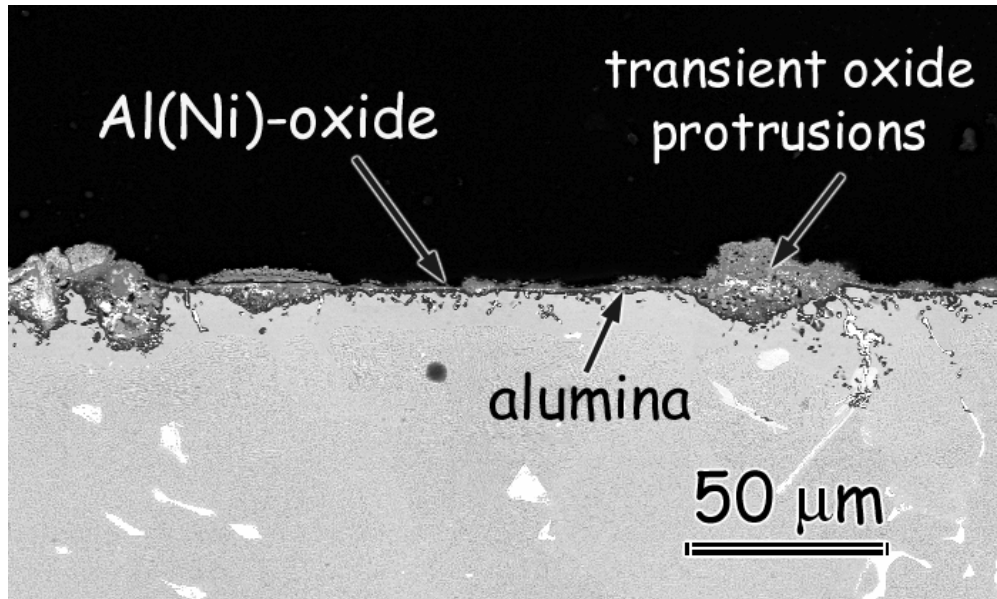
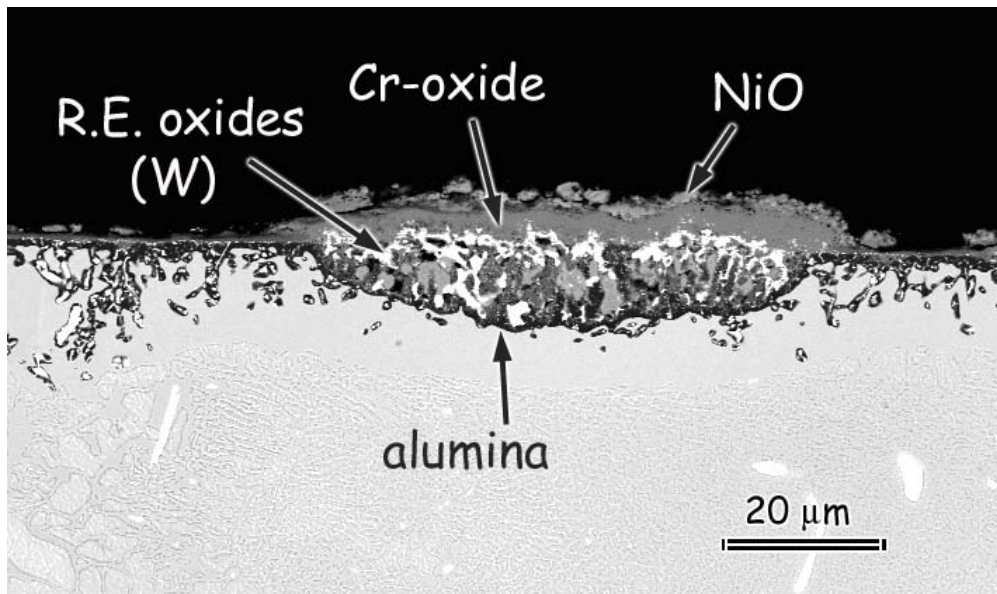


Figure 5.47: MarM 247 at 900°C after isothermal tests at high pressure in 100% steam. The image shows the cross-section of the reaction zone. Internally formed alumina was detected below the external scale.

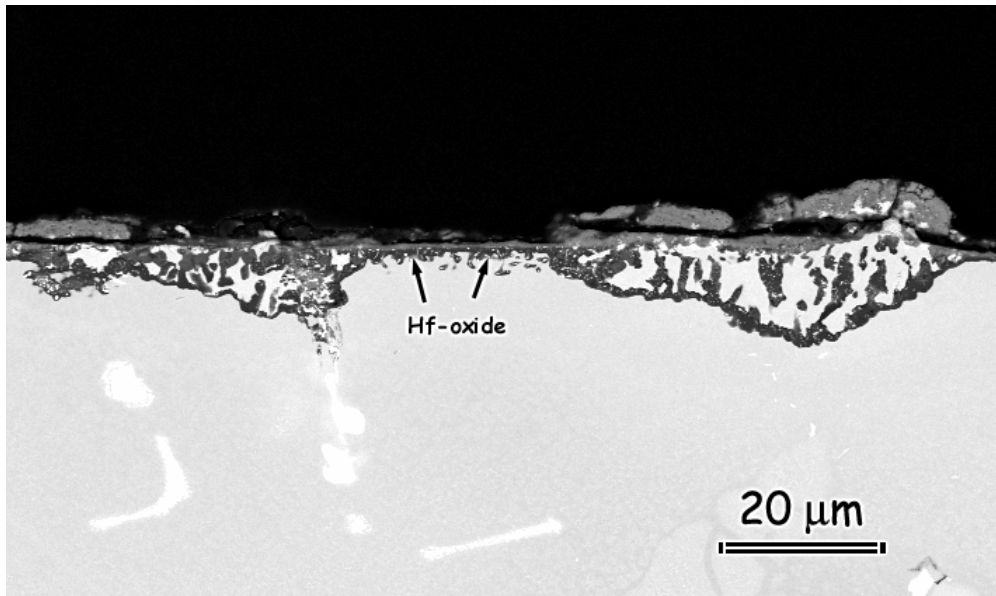


(a)

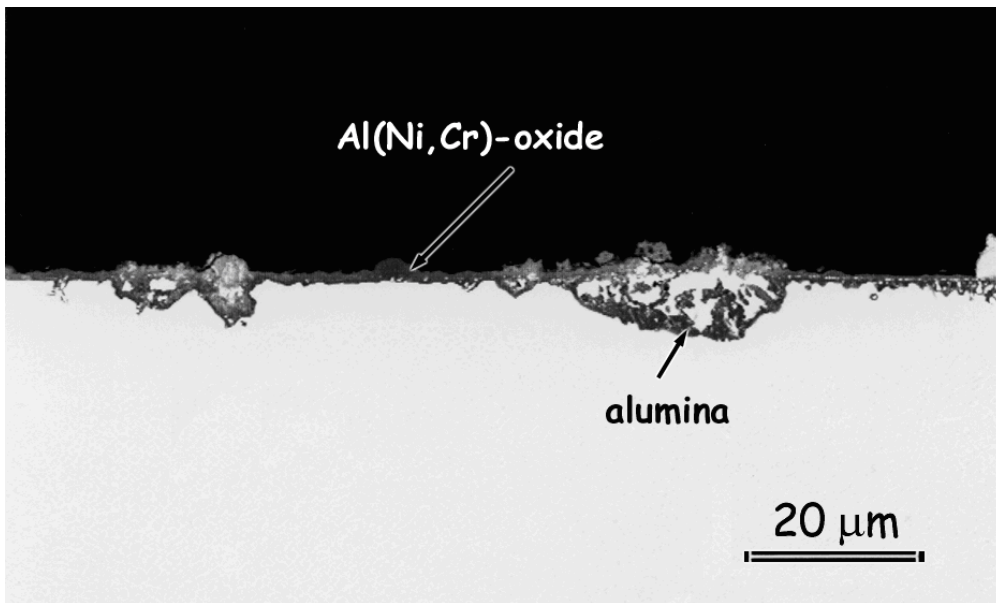


(b)

Figure 5.48: MarM 247 at 900°C isothermally exposed to air/H₂O mixtures at $P_{\text{total}} = 1$ atm ($P_{\text{H}_2\text{O}} = 0.3$ atm). Micrographs show the cross-section of the scale. The alloy developed an Al-rich thin dual layer along the surface with a slow growth rate. However, many locations with oxide protrusions were present on the surface too. These locations were the areas where the system could not form the oxide with better protective properties. Instead, faster growing phases developed.



(a)



(b)

Figure 5.49: MarM 247 at 900°C cyclically exposed to hot gases at atmospheric pressure (a) in wet air, and (b) in dry air. The back scattered electron images show the cross-section of the oxide scale.

Overall, less transient oxidation occurred in 100% steam environment. However, selective oxidation of Al was adversely affected by this environment. More profuse internal oxidation of Al was observed for this case compared to ambient exposures regardless of the environment or mode of testing (i.e. dry/wet, or cyclic/isothermal).

The scale that developed on PWA 1484 during ambient isothermal tests was very similar to the one that formed after cyclic tests under the same conditions. The main difference was the formation of a thinner layer after isothermal exposure. The compositions and the morphologies of the phases were essentially the same for each case. An external scale of transient oxides formed until alumina developed continuity. This scale consisted of NiO at the gas/oxide interface, and a mixed oxide zone between NiO and alumina. Figure 5.50 shows the cross-section of the specimen tested in air/water vapor at atmospheric pressure. Figure 5.51 provides a comparison of the scales that developed at high pressure after isothermal tests, and at ambient pressure after isothermal and cyclic tests. At first glance, it seems like similar oxides formed under each condition. However, a closer examination shows that formation of the transient NiO was completely avoided during high-pressure steam –or low PO_2 - tests. Figure 5.52 shows the surface images of the alloy for each condition. As the micrograph also indicates, only the mixed oxides formed in the pure-steam environment. This external scale was essentially the same as the one formed at 700°C, only thicker. The results indicated that, the main effect of low PO_2 , or pure water vapor at high pressure was to eliminate the formation of NiO. Isothermal conditions seem to be not as effective in terms of suppressing NiO formation, although a thinner layer of the oxide formed after isothermal tests at ambient pressure. The adverse effect on selective Al oxidation that was seen with MarM 247 was not observed on this alloy. Alumina developed a continuous protective layer as Figure 5.51 shows.

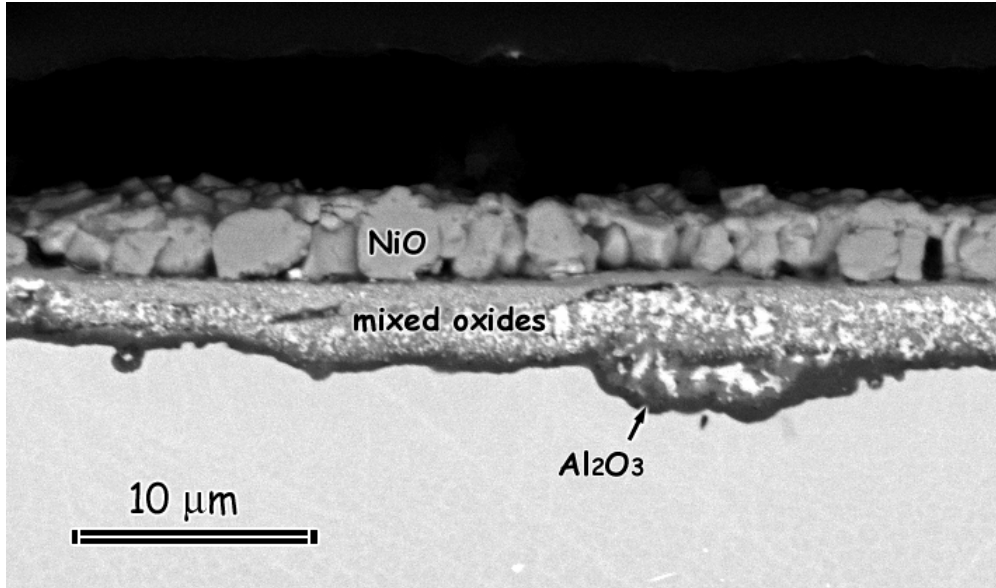
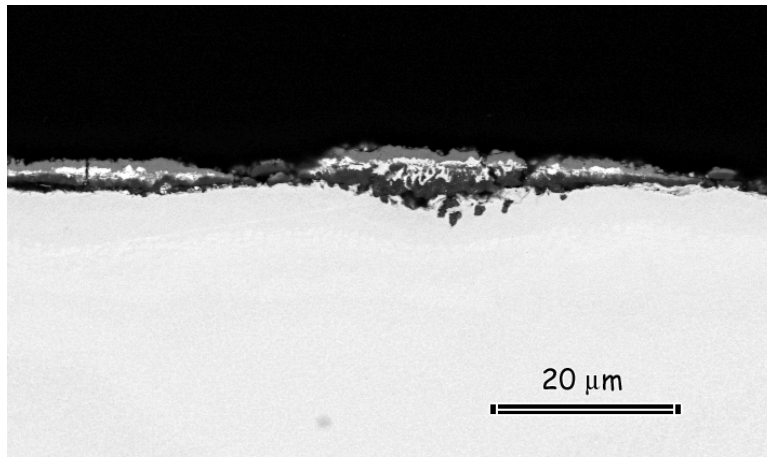
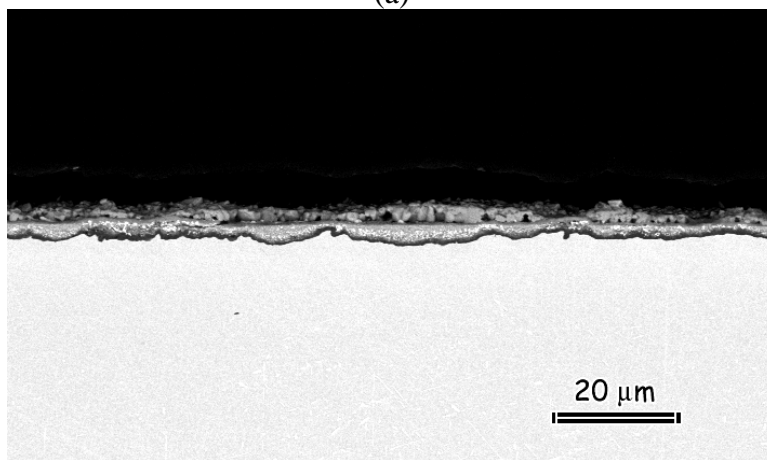


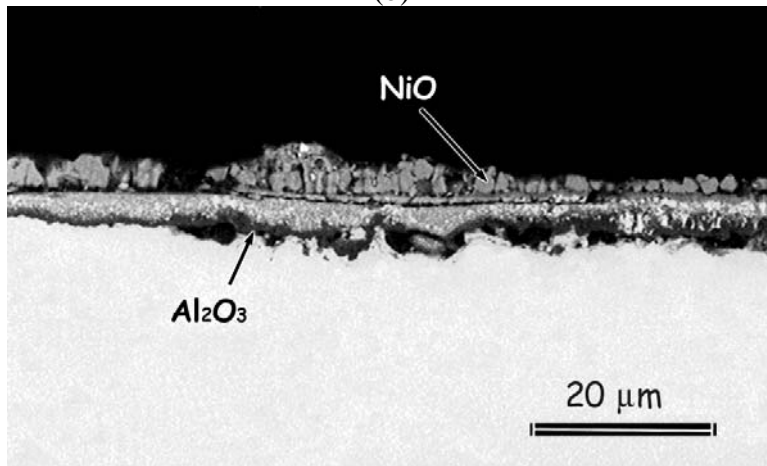
Figure 5.50: Cross-section of PWA 1484 isothermally exposed to wet air at 900°C, $P_{total}=1$ atm.



(a)

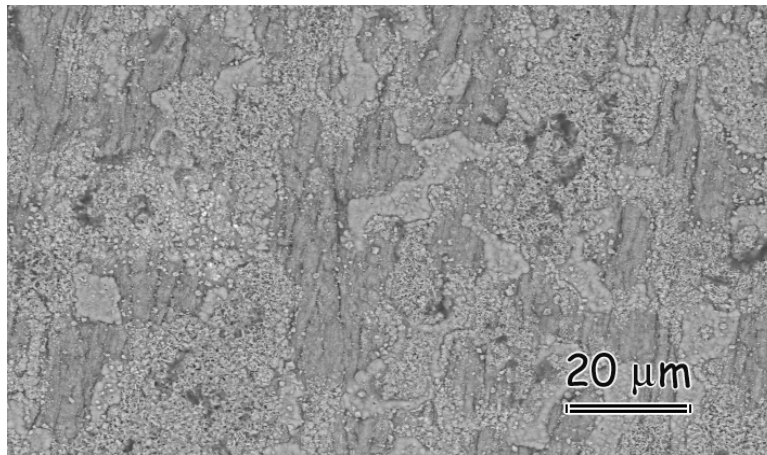


(b)

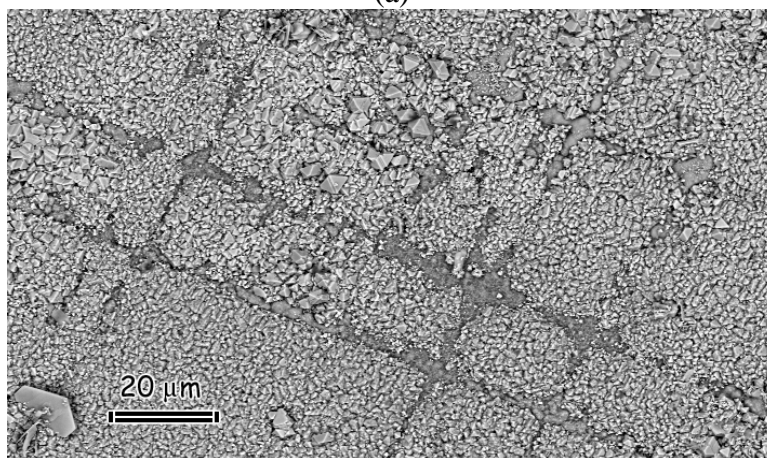


(c)

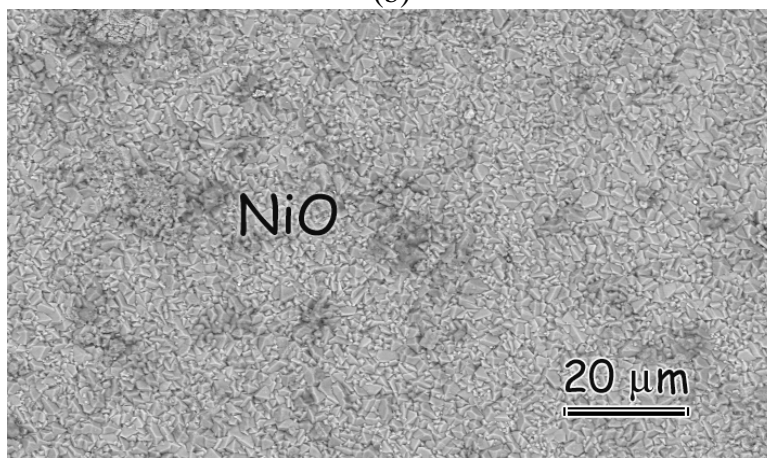
Figure 5.51: SEM images of PWA 1484 showing the specimen cross-sections after tests at 900°C. The testing conditions for each sample were (a) isothermal in 100% steam at high pressure for 4320 hours, (b) isothermal in wet air at ambient pressure for 2400 hours (equivalent to 3200 cyclic hours), and (c) cyclic in wet air at ambient pressure for 3200 cycles.



(a)



(b)



(c)

Figure 5.52: Surface images of PWA 1484 at 900°C showing the external oxide scale that formed after (a) and (b) isothermal exposures in high pressure steam and in wet air at ambient pressure respectively, (c) cyclic exposures at atmospheric pressure in air/H₂O mixtures.

All the results obtained so far lead to the conclusion that the isothermal steam tests did not favor NiO formation. Similar observations were evident at 700°C as well. This effect appeared to be stronger at 900°C. The major reason for the suppressed NiO formation is believed to be the low PO₂ during the steam tests. This is consistent with the literature. It is well known that NiO growth is a strong function of PO₂, [95]. It was also observed that the cyclic tests made the system more vulnerable to NiO formation due to the heavier scale spallations.

5.1.3 Effect of Surface Finish

Tests with two different surface finishes were performed to see whether the condition of the pre-exposed surface had an impact on the oxidation behavior of the systems under investigation. Coupons of PWA 1484 were ground down to 600 grade by abrasive paper on one side, and polished with 0.05 μm alumina on the other. Samples were exposed to dry and wet air at 700°C for 1, 2, and 4 hours isothermally. Microscopic evaluation of alloy cross-sections showed that the diffusion properties of the system were influenced by the surface condition. Thicker NiO formation and deeper internal oxidation were the characteristics of the samples with finer finishes. The depth of the reaction zone also increased for longer exposures. Another observation was the impact of water vapor on the reaction rate. The presence of H₂O in the oxidizing gases accelerated transport of the oxidizing species and caused more pronounced transient oxidation, Figures 5.53 through 5.56.

Similar tests were also done with René N5 at 900°C and 700°C. This time the samples were exposed only for 4 hours. The results were in the same direction as with PWA 1484. At 700°C, almost no scale developed in dry air on the surface with the 600-grit finish. The polished surface of the same sample, on the other hand, was affected from attack slightly more. Similar results

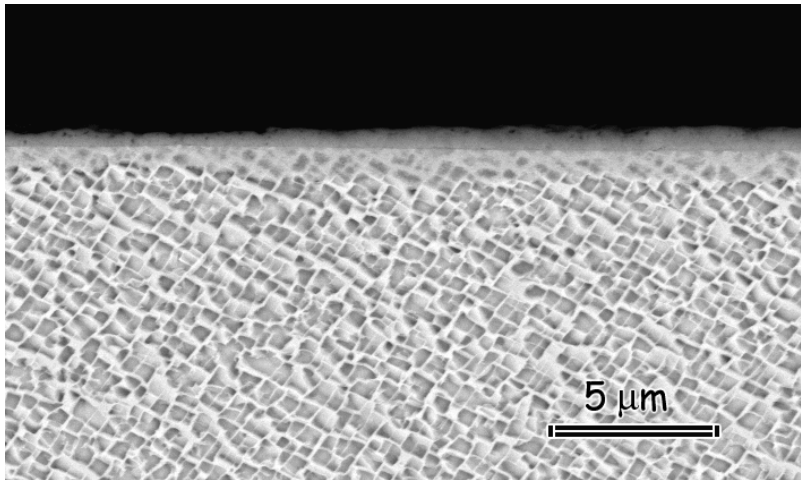
were observed with the samples exposed to wet air. The attack was more pronounced on the polished surface. Comparison of wet exposures to dry ones showed that oxygen ingress was faster in wet air. The features of the scale that formed after wet exposures were similar to PWA 1484. The effect was more pronounced at 900°C. The corresponding micrographs are given in Figures 5.57-5.60.

These tests showed that, for the alumina formers the pre-exposed surface condition was an important parameter that should be taken into account while evaluating the behavior of the alloys. Water vapor combined with smoother surface finish accelerated the rate of reaction remarkably. Similar observations were reported by several authors for different systems, [13-15, 71]. Typically, heavy deformation at the substrate surface results in the easier formation of the protective oxide. The higher defect density in the more worked system accelerates the outward diffusion of the metal in the substrate by providing easy diffusion paths. Therefore, protective scales can be formed more readily on such surfaces.

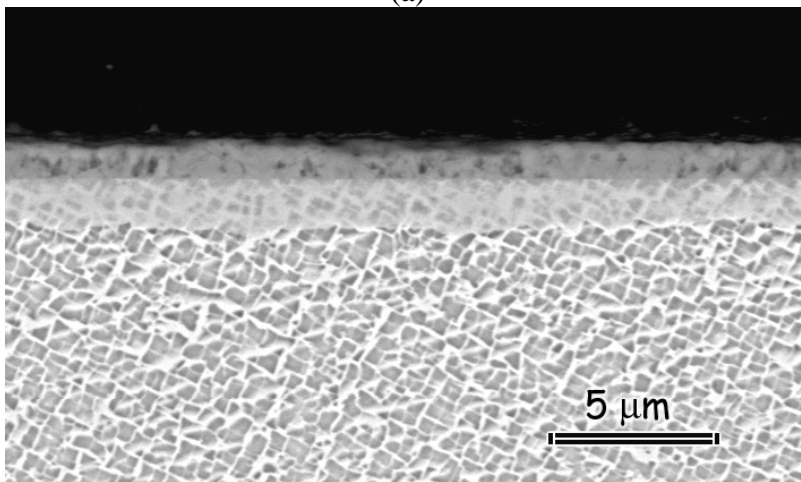
5.2 SUPERALLOYS THAT ARE CLASSIFIED AS CHROMIA FORMERS

5.2.1 Chromia Formers Cyclically Exposed in Dry Air and in Air/Water Vapor Mixtures with $P_{H_2O} = 0.3$ atm, at a total pressure of 1 atm

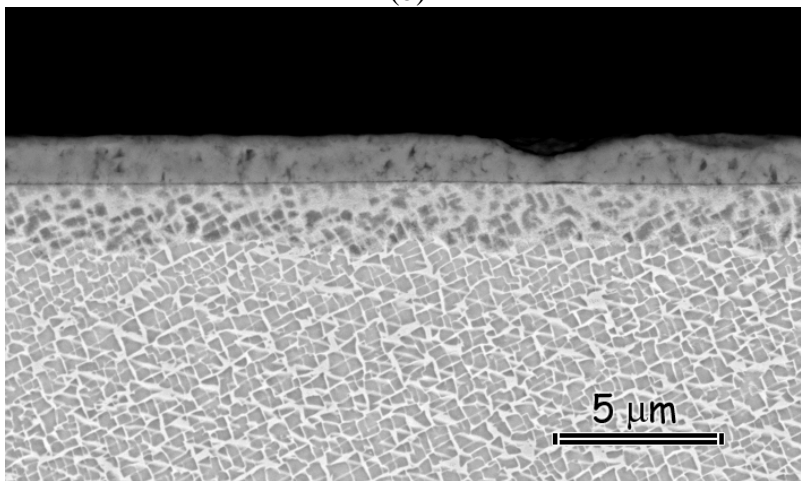
In the previous sections, the test results of the alloy systems which are classified primarily as alumina-formers were discussed. Tests were also done to understand the effect of water vapor on the oxidation of alloys that develop chromia scales for protection. For this work, the



(a)

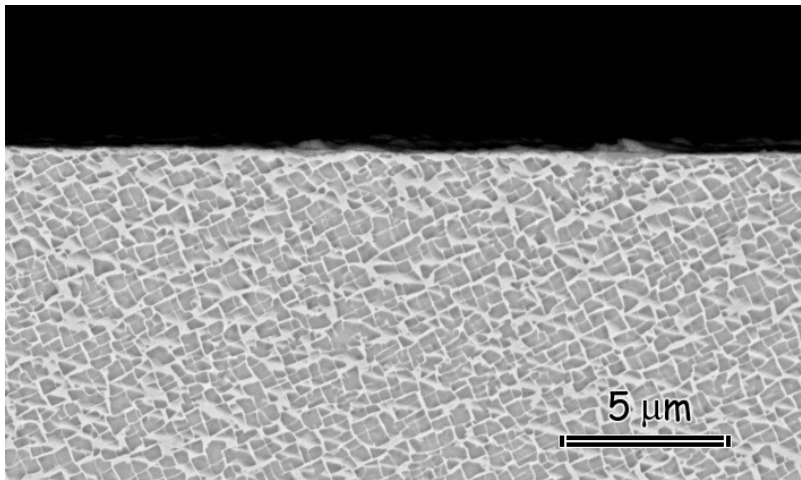


(b)

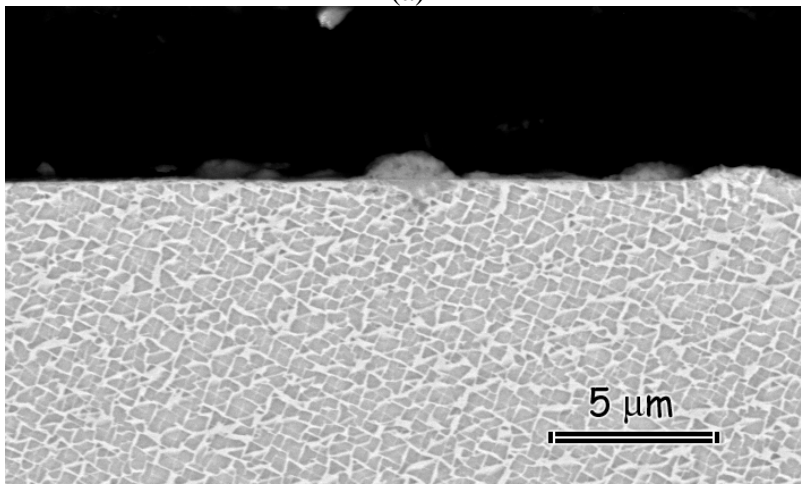


(c)

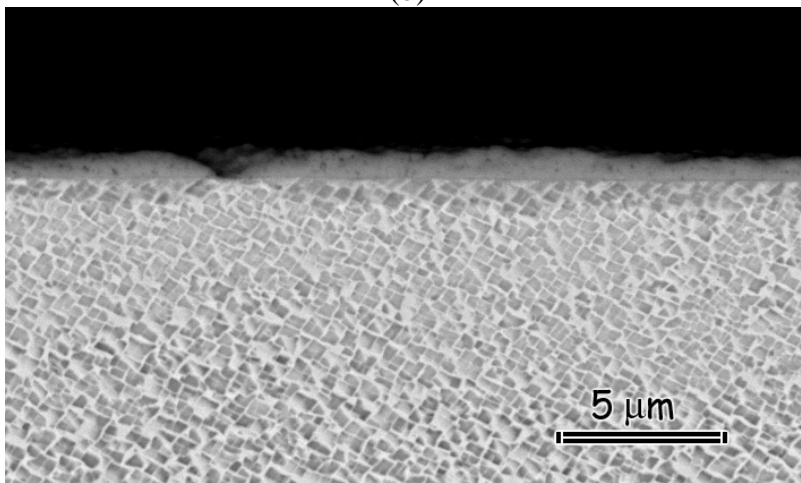
Figure 5.53: SEM micrographs of PWA 1484 at 700°C after exposures in wet air (a) for 1 hr, (b) for 2 hours, and (c) for 4 hour. The sample surfaces were polished down to 0.05 micron alumina.



(a)

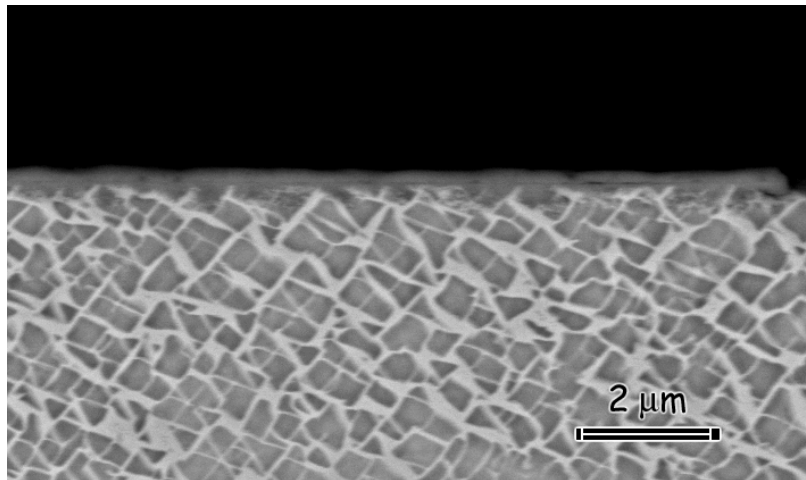


(b)

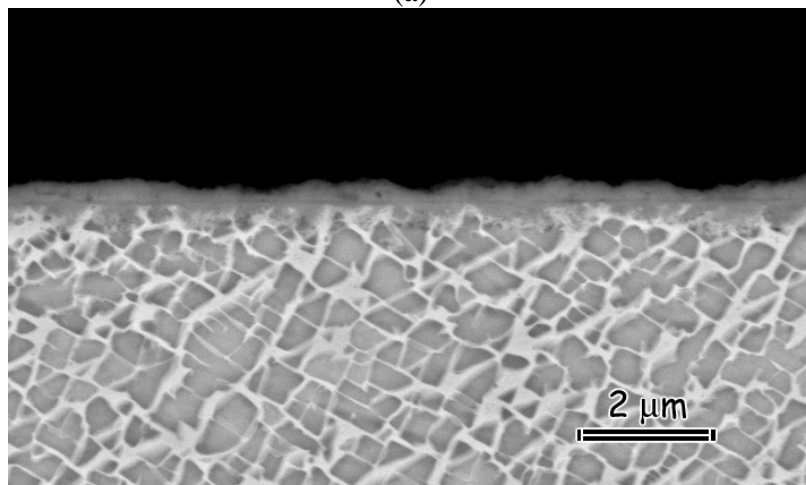


(c)

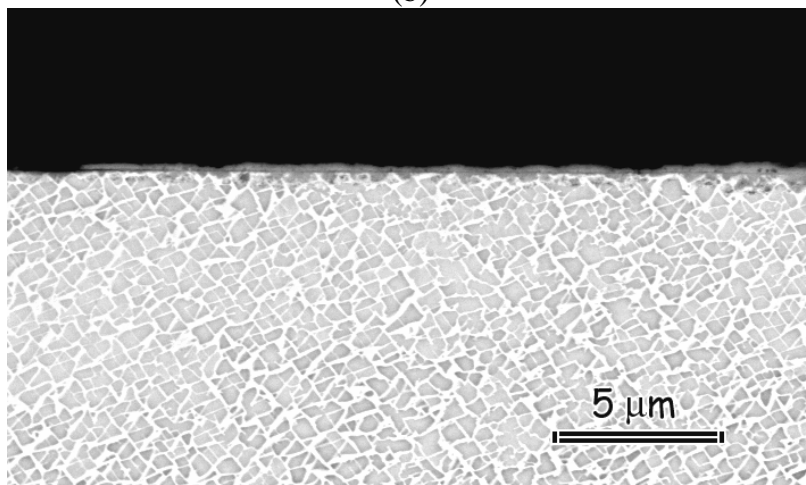
Figure 5.54: SEM images of PWA 1484 at 700°C after exposing the alloy to wet air, (a) for 1 hr, (b) for 2 hours, and (c) for 4 hours. The surfaces were ground down to 600-grit with abrasive paper.



(a)

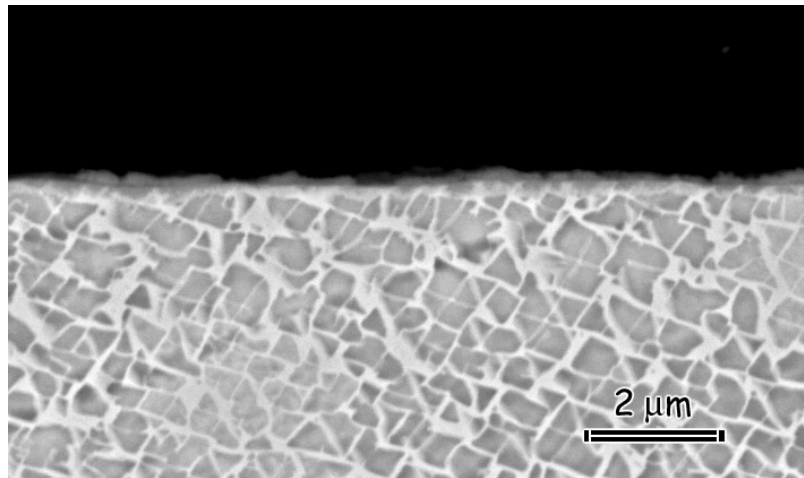


(b)

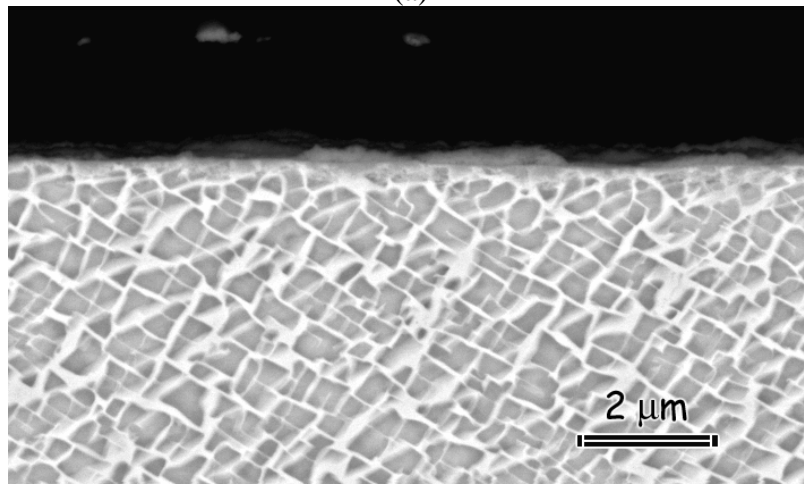


(c)

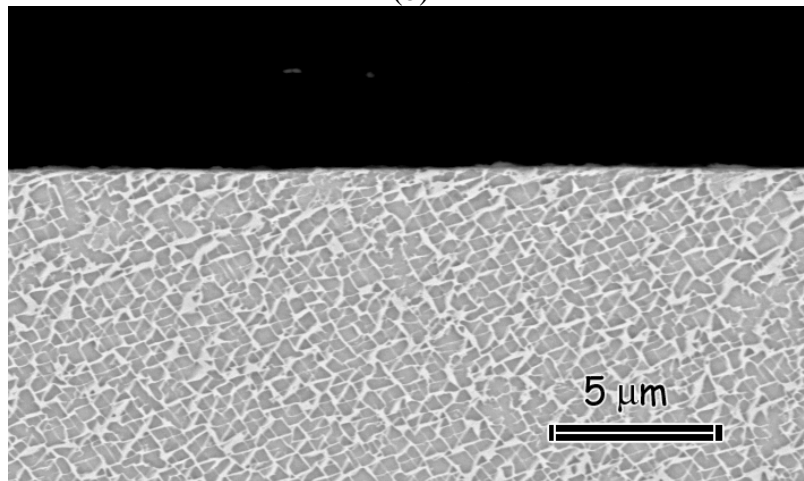
Figure 5.55: SEM micrographs of PWA 1484 showing the cross-section of the oxidation zone at 700°C in dry air (a) after 1 hr, (b) after 2 hours, (c) after 4 hours. The surfaces of the alloy were polished down to 0.05 micron alumina.



(a)

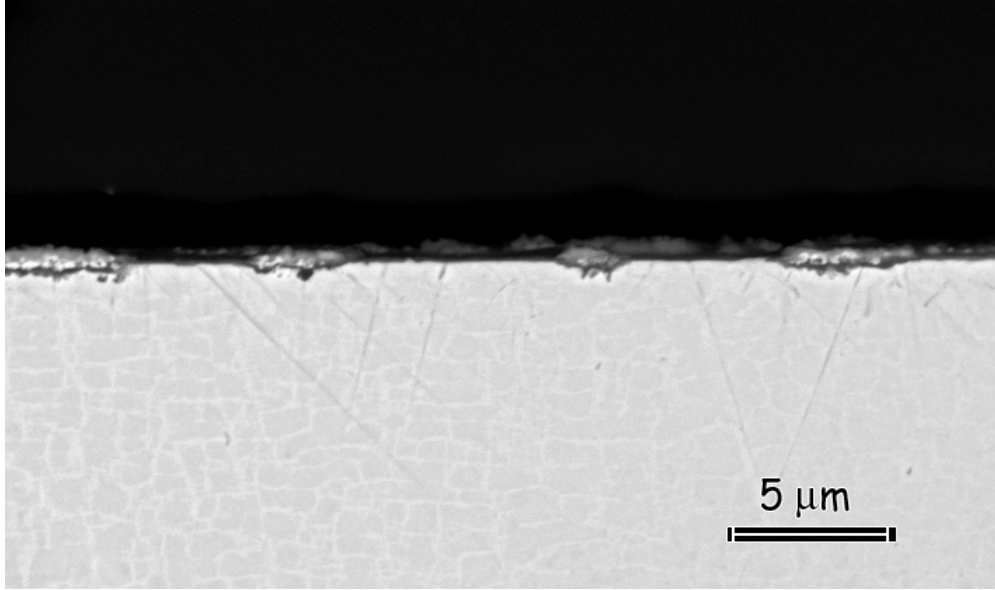


(b)

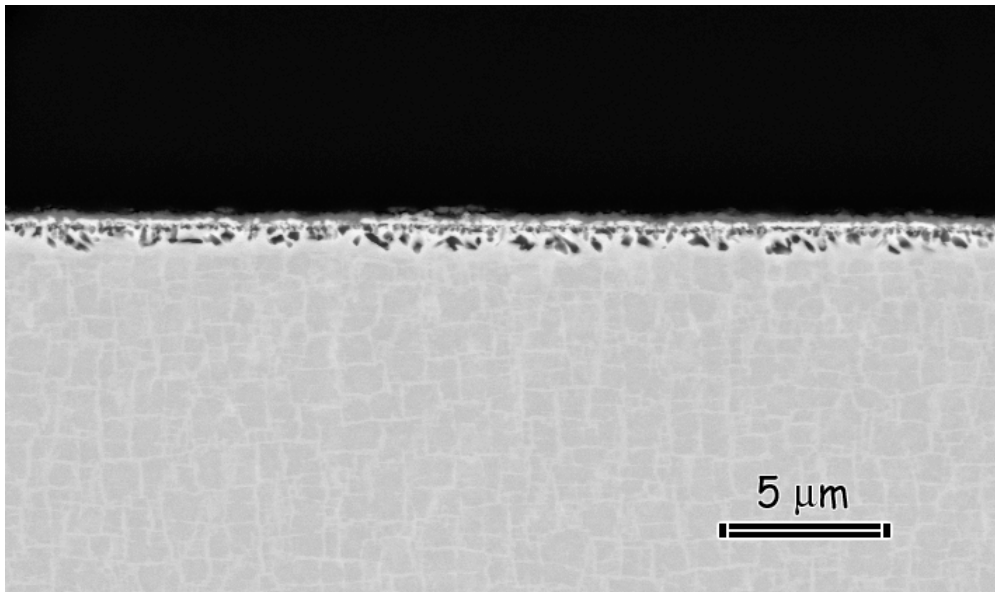


(c)

Figure 5.56: SEM images of PWA 1484 showing the scale that formed at 700°C in dry air after (a) 1 hr, (b) 2 hours, and (c) 4 hours. Sample surfaces were ground down to 600 grade abrasive paper prior to testing exposure.

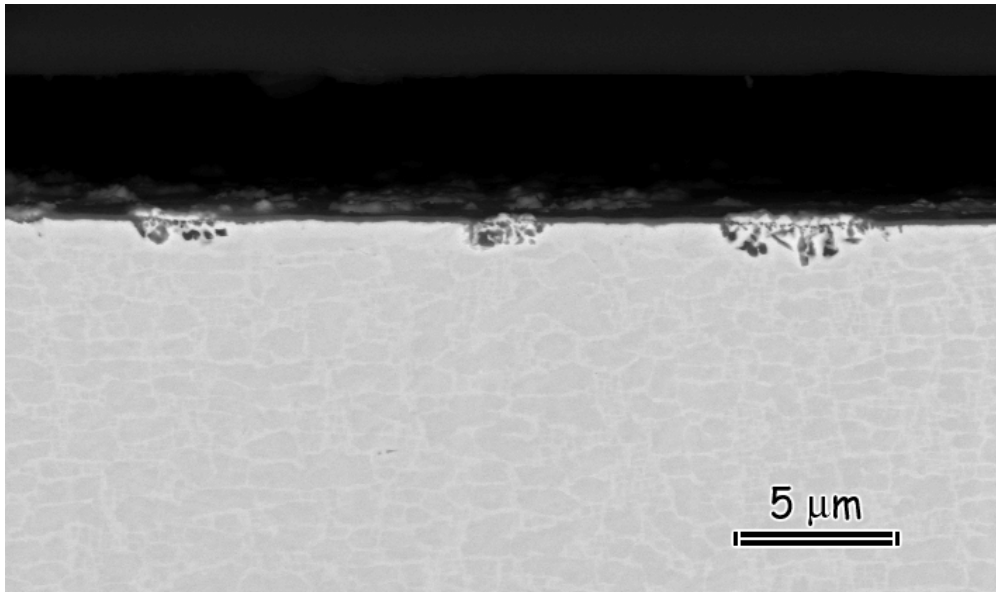


(a)

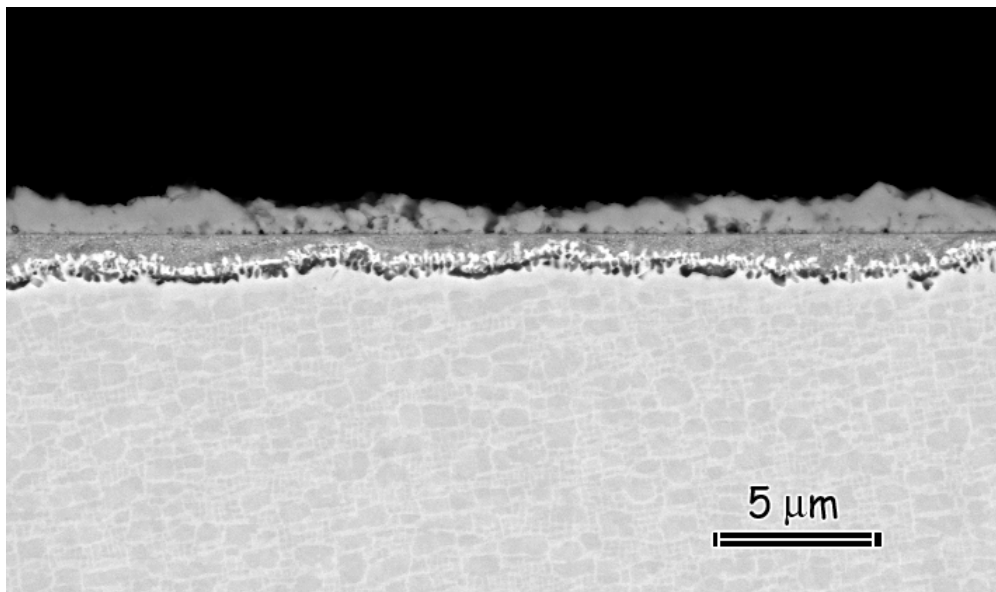


(b)

Figure 5.57: SEM image of René N5 that shows the cross-section of the scale at 900°C after 4 hours of isothermal exposures in dry air. (a) The surface of the sample was ground down to 600-grade SiC abrasive paper. (b) Pre-exposed surface was polished with 0.05 micron alumina.

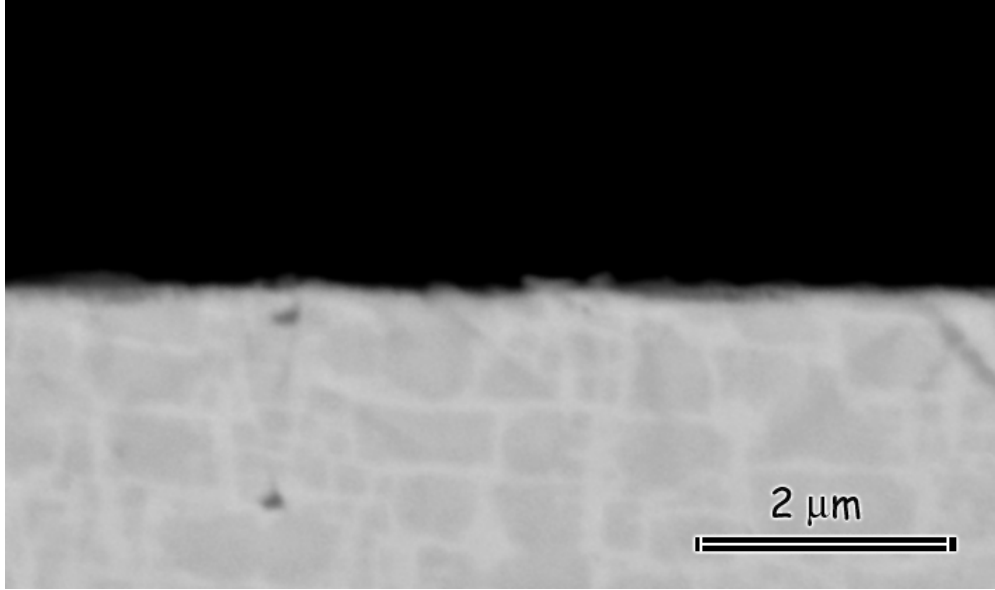


(a)

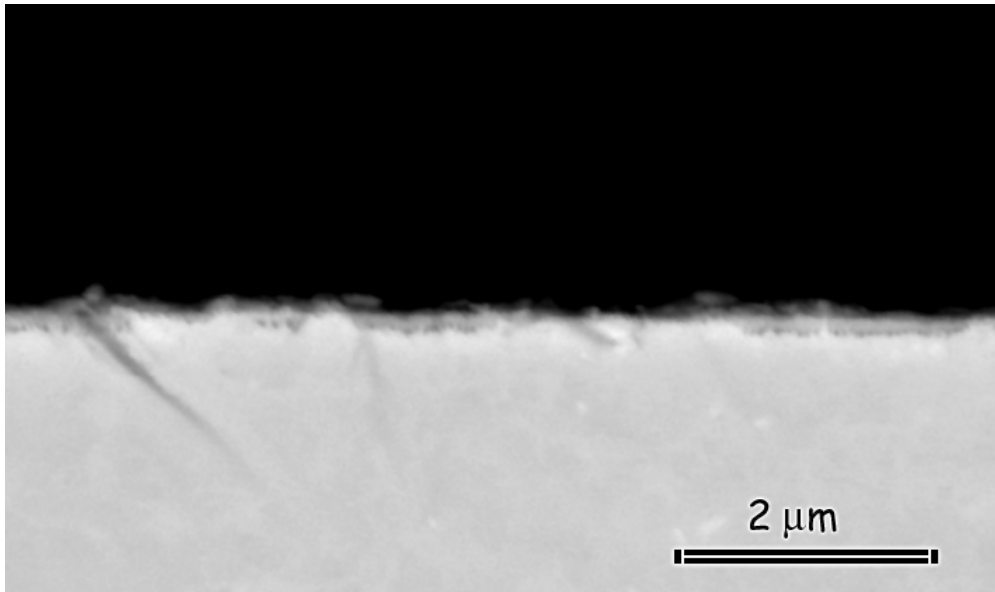


(b)

Figure 5.58: SEM images of René N5 at 900°C in wet air after 4 hours. Micrographs show the cross-section of the scale. (a) Sample surface was ground with abrasive paper down to 600 grade before exposure. (b) Sample surface was polished with 0.05 micron alumina prior to exposure.

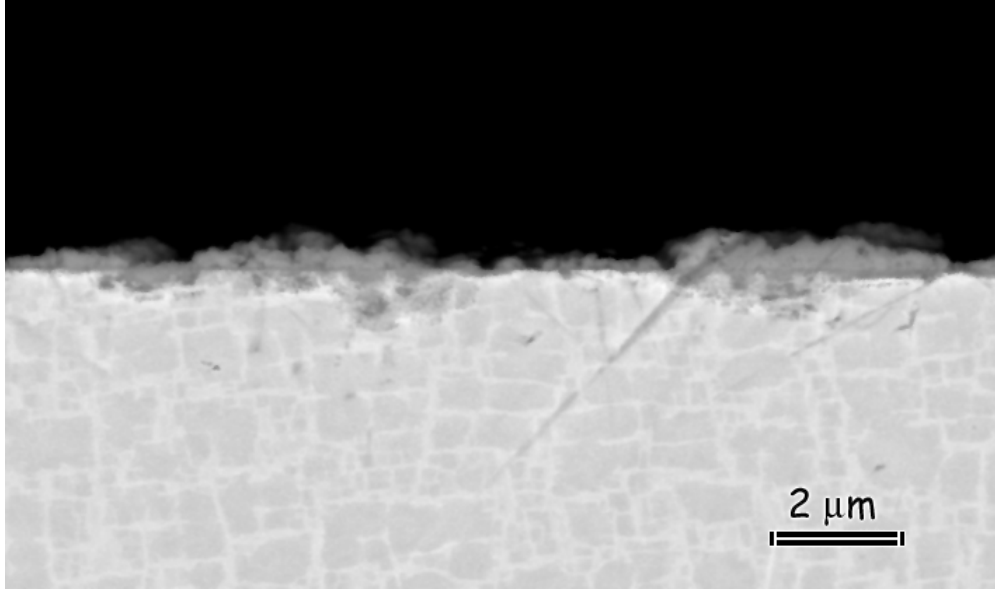


(a)

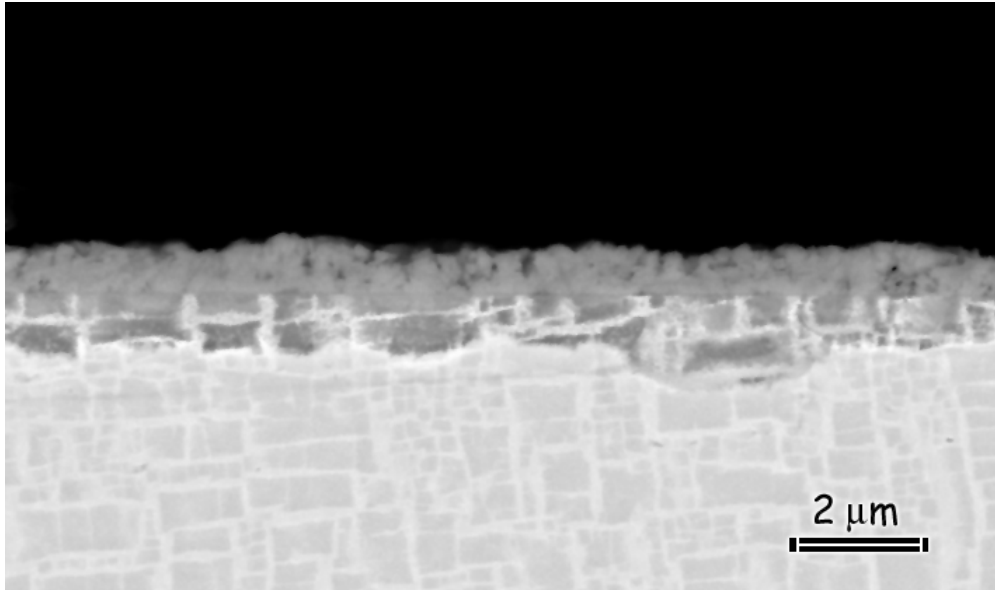


(b)

Figure 5.59: René N5 at 700°C in dry air after 4 hours of isothermal testing. SEM images show the scale in cross-section. (a) Surface finish of the unexposed sample was 600-grade abrasive paper. (b) The surface of the alloy was polished with 0.05 micron alumina prior to testing.



(a)



(b)

Figure 5.60: SEM micrographs showing René N5 at 700°C in wet air after 4 hours of isothermal exposure. (a) Surface finish was 600-grade SiC abrasive paper. (b) Polishing the surface with 0.05 micron alumina increased the oxygen diffusion rate remarkably.

superalloy systems IN 738 and X-40 were utilized. The results obtained with these systems will be discussed in the following sections.

5.2.1.1 Chromia Formers at 700°C: The test results at 700°C indicated that the degree of attack on chromia forming superalloys, i.e. IN 738 and X-40, in dry air as well as in wet air was not very severe. The polycrystalline Ni-based alloy IN 738 developed an outer chromia scale with some internal stringers of alumina that formed below the external layer. A thin layer of TiO₂ was observed to develop over the chromia in wet as well as in dry air. Comparison of dry and wet exposed specimens showed that the thickness of the chromia was larger, and the zone of internal oxidation was deeper after tests in wet air. The cross-sections of the specimens showing the scales are given in Figure 5.61. These results were in agreement with the data showing the weight changes of specimens as a function of exposure times. Figure 5.62 indicates that the weight gains were larger in air/H₂O mixtures compared to dry air.

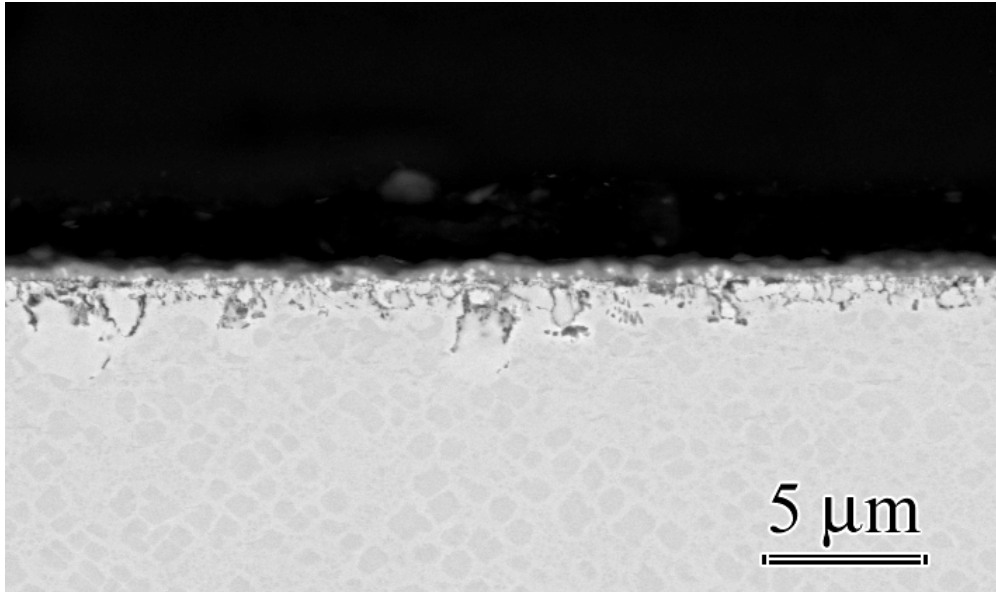
The Co-based alloy X-40 displayed the best oxidation resistance at this temperature among all the alloys in test including the alumina formers. The kinetic plots showed that the weight changes were significantly smaller compared to the rest of the alloys after dry and wet exposures, Figure 5.63. The cross-sectional examination of the specimens by SEM revealed the formation of a thin chromia scale on the surface, Figure 5.64. Although not very significant, the reaction rate was higher in air saturated with water vapor. The scale thickness was slightly larger, and the chromia/substrate interface was less smooth as Figure 5.64 (b) indicates.

The observations suggested that, the diffusion rate of cations and/or anions through the oxide layer was affected by the presence of water vapor. Thicker scales developed after exposing the

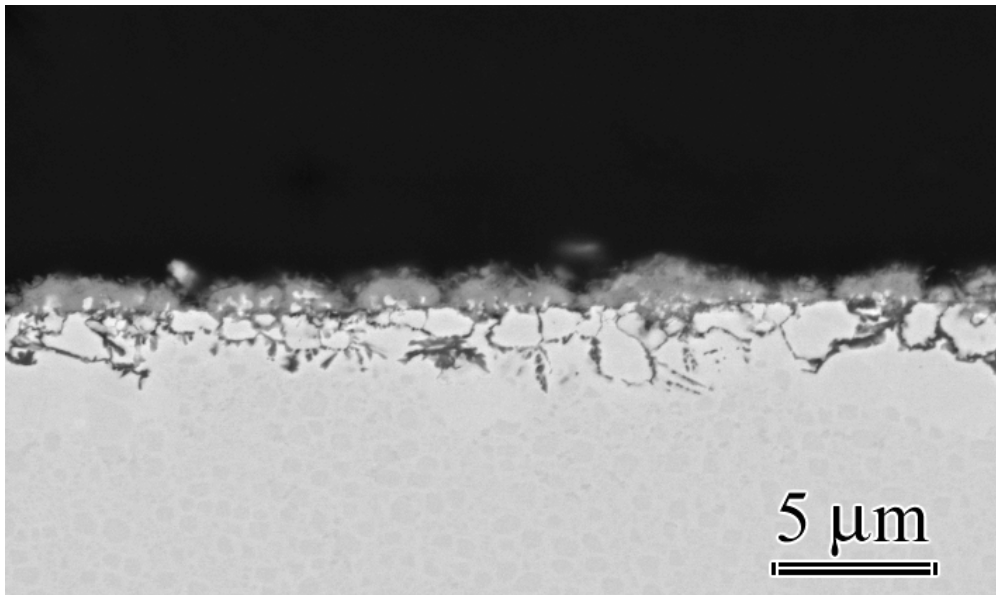
alloys to air/H₂O mixtures. The reaction rate of oxygen with aluminum, as well as chromium increased under this condition. The effect was less pronounced on X-40.

5.2.1.2 Chromia Formers at 900°C: Increasing the exposure temperature from 700°C to 900°C caused a drastic change in terms of the resistance of these systems against attack by oxidizing species. Water vapor effects also became more intense at this temperature. Overall, the alloys were not very resistant. The attack was more aggressive in the wet environment compared to dry air.

For IN 738 the weight gains were larger during early oxidation in air/H₂O mixtures than in dry air, Figure 5.65. With extended exposures the system entered the breakaway stage. This trend began after 1000 hours in both environments. It showed itself as drastic weight losses in the wet environment. In dry air, on the other hand, the alloy continued to gain weight rapidly up to 2200 cycles. These rapid weight gains followed the linear rate law more closely instead of the parabolic law, which means that although no weight losses were observed, the system was already in the breakaway stage. After 2200 hours, weight losses started to dominate in the dry environment as well. Examination of specimen cross-sections showed that substantial scale spallation occurred during dry exposures, Figure 5.66 (a). The outer chromia scale was highly porous rather than dense and protective. The alumina stringers that formed as internal oxides at the matrix/chromia interface extended deep into the alloy. In wet air, the extent of scale spallation was less compared to dry air. The fraction of the areas without drastic spallation was larger. Figure 5.66 (b) shows part of the scale where the oxide was still in contact and had a uniform thickness. The chromia layer had a porous structure. Pores were evident in the mid-section of the scale. A thin layer of TiO₂ was detected at the oxide/gas interface. The same



(a)



(b)

Figure 5.61: IN 738 at 700°C (a) in dry air, and (b) in wet air after 2520 hours of cyclic testing.

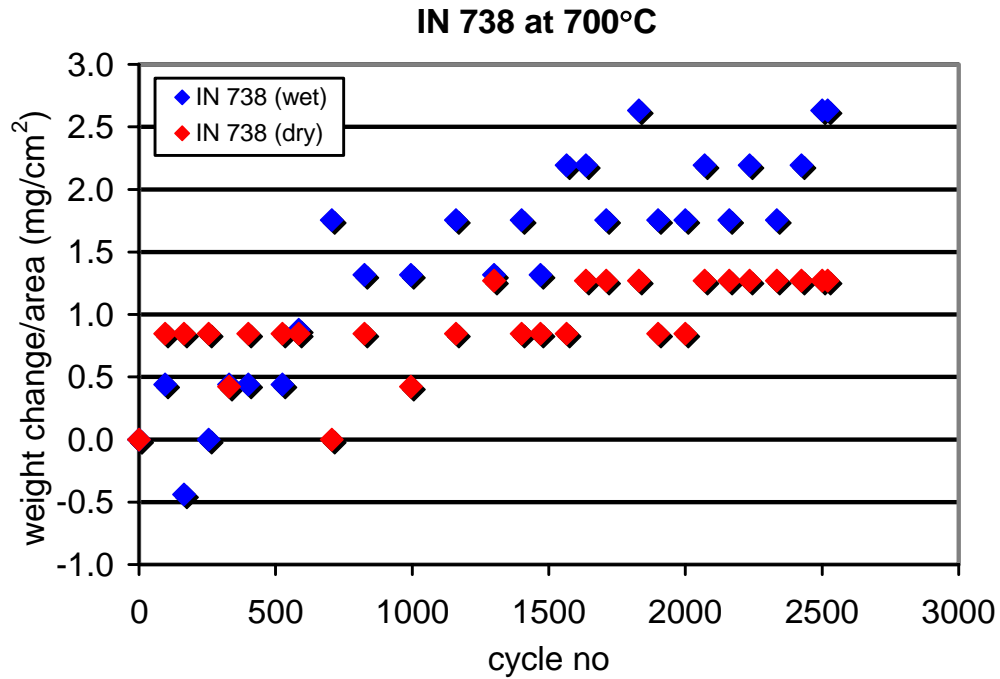


Figure 5.62: Kinetic plot of the alloy IN 738 showing the weight changes of the specimens in dry air and in air/H₂O mixtures at 700°C as a function of cycle number.

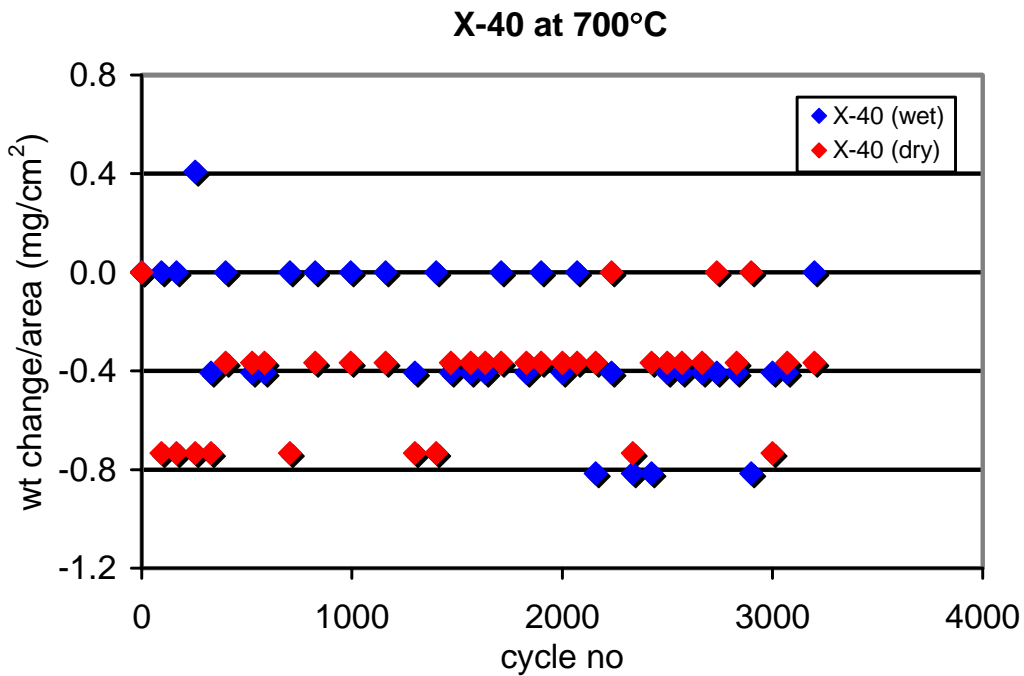
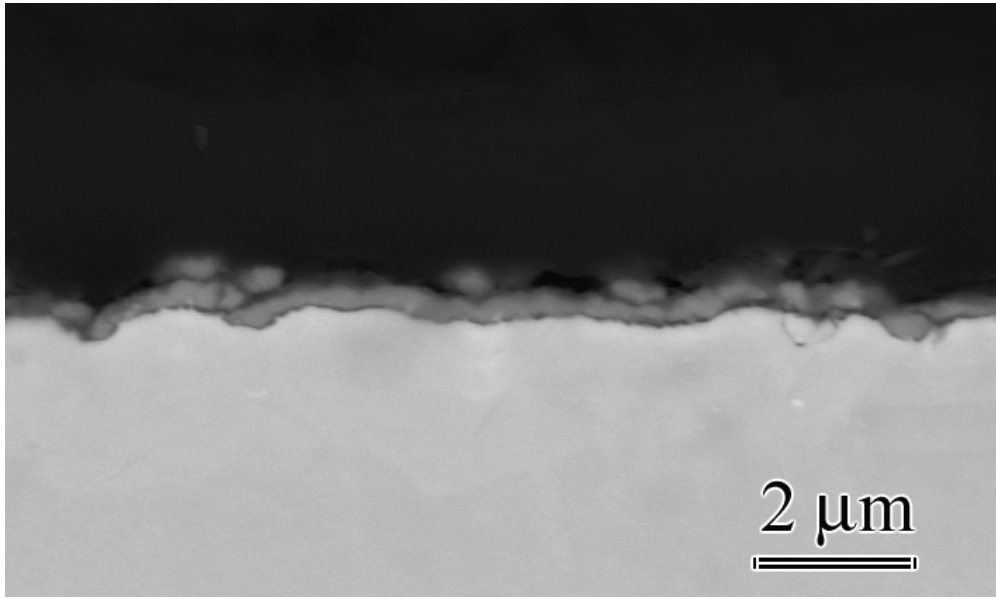
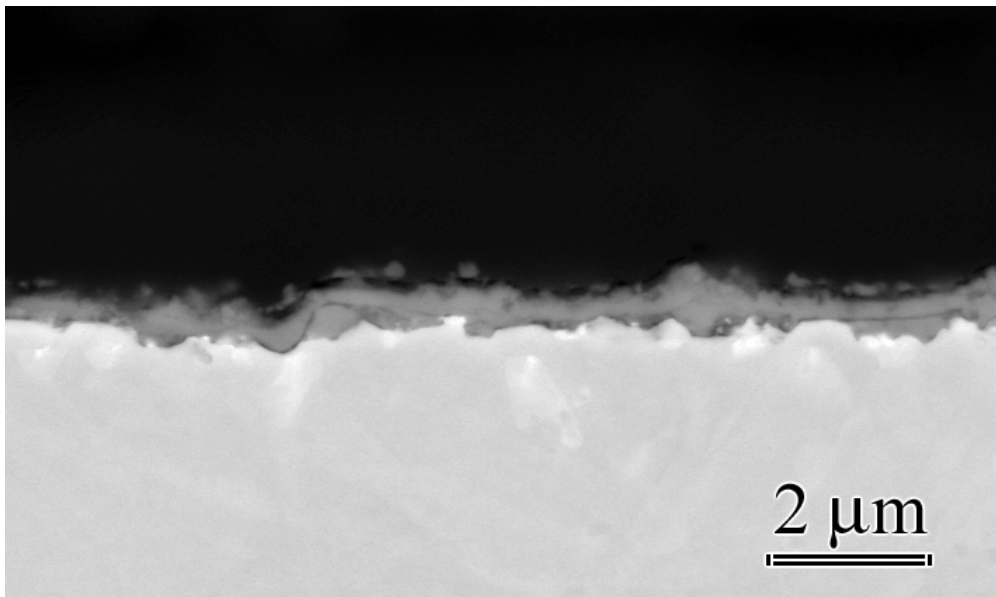


Figure 5.63: Kinetic plot of the alloy X-40 showing the weight changes of the specimens in dry air and in air/H₂O mixtures at 700°C as a function of cycle number.



(a)



(b)

Figure 5.64: X-40 at 700°C (a) in dry air, and (b) in wet air. Similar scales formed in both environments. The oxide layer was identified as chromia.

phase was present also on the dry exposed specimen in areas where the scale did not spall off very profusely. In both environments, TiN precipitates were detected below the alumina stringers. This condition developed as a consequence of the depletion of the substrate material in Cr, and therefore losing its ability to heal itself by forming the protective chromia scale. The number of these precipitates was greater in dry air. One of the areas where the nitride phase was detected is shown in Figure 5.66 (c).

X-40, which was a better alloy than IN 738 at 700°C, was much less protective at 900°C. The weight gains during transient oxidation were slightly higher in wet air than in dry, Figure 5.67. The recession of metal due to scale loss started around the same time in both atmospheres (i.e. approximately after 900-1000 cycles). The back scattered electron images of sample cross-sections after 2050 hours of exposure are shown in Figure 5.68. Severe damage by spalling of oxides was evident, which was more substantial in dry air. In both environments, the oxide scale was a mixture of Cr₂O₃ and faster growing mixed oxides of Co, Cr and W. Void formation was detected at the oxide/gas interface. The carbide network that was present in the as-processed condition of the alloy gave rise to internal oxidation by providing easy diffusion path to anions, and caused formation of a porous phase in the subscale. The pores are possibly caused by the vaporization of W-oxide(s), which would also affect the weight losses as W is a heavy metal.

Continued exposure showed that the alloy became more prone to attack in wet air compared to dry air. Kinetic data indicated that the weight loss rate in wet air exceeded that in dry air. Even more prolonged exposures resulted in a secondary increase in weight gain. The cross sections of the specimens exposed in dry and wet air for 4250 hours are shown in Figures 5.69(a-d). As these micrographs clearly show, thicker scales formed after wet exposures. The scale consists of highly non-protective oxides. The secondary increase in weight was a consequence of

the formation of these rapidly growing oxides. EDX analysis identified this phase as a Co-rich oxide with some Cr in it. Extensive scale loss depleted the substrate in terms of Cr. The system could not continue to form the slower growing chromia scale because of the lack of sufficient and continuous Cr supply. As a result, Co-oxide formation became more favorable. The degree of damage was much less in dry air than in air/H₂O mixtures.

The mechanism(s) leading to weight losses on chromia formers are complicated. The thermal cycling of the specimens, which introduces thermal stresses to the system combined with the growth stresses due to oxide formation result in the detachment of the scale from the substrate which eventually leads to spallation, and hence to weight losses. Chromia vaporization by volatile oxide formation is another complication that confronts these alloys. At high temperatures, oxygen and oxygen bearing species react with Cr₂O₃ and form the more stable vapor oxides. Thus, there is the interplay between vapor species formation and scale spallation that leads to alloy degradation. The data obtained from the tests presented so far would not allow one to differentiate between these two factors. Therefore, additional tests using model alloys were done to understand the predominant mechanisms in each environment better. These experiments will be discussed in a later chapter.

5.2.1.3 Chromia Formers at 1000°C: At this temperature, the oxidation resistance of the alloys IN 738 and X40 was so poor that they should not be considered as candidate materials for use in service. Regardless of the environment, the attack was very extensive. The weight change versus time of exposure plots showed that, X-40 was very prone to attack by oxidizing species in either atmosphere at 1000°C, Figure 5.70. Kinetic data of the alloy indicated a very rapid initial oxidation period followed by a sharp turn into the breakaway stage. The rate of degradation was

faster in wet air than in dry. The secondary weight increase, which occurred at 900°C, was also observed at this temperature in both environments.

Other than the fact that the reaction rates were accelerated at the higher temperature, the general features of the oxide morphologies were very similar to the microstructures observed at 900°C. The SEM images of sample cross-sections are given in Figures 5.71-5.72. The adherence of the scale was disrupted by detachments and voids at the Cr-oxide/substrate interface. The oxidation along the carbide network, which was first observed at 900°C, was evident also at this temperature. The phases that formed along this network were identified as chromia and W-oxide. The depth of this zone was around 60 μm . Below this layer, a secondary oxygen-affected zone developed. This is the region where the reactions between the carbide network and oxygen started, but did not result in formation of chromia or W-oxide. This zone started at the interface closer to the gas, and progressed towards the center with a concentration gradient in terms of oxygen. The depth of the zone was larger in wet air.

IN 738 degraded extremely rapidly at 1000°C. The spallation rate of the alloy in both environments was tremendously high as is evident in the kinetic plot, Figure 5.73. The weight loss per area of the alloy was approximately 50 times higher than that of X-40 after 400 cycles in the wet environment. The SEM photomicrographs of the sample cross-section showed that the alloy developed a non-uniform scale with substantial oxidation in wet air, Figure 5.74(a). Repeated rapid oxide formation combined with heavy spallation resulted in excessive metal recession. The source of the large voids found in the center of the sample was not clearly identified. It is believed that they were mostly casting defects. However, there is also the possibility that they developed during exposures. Another, and a more likely, possibility is that they were present in the pre-exposed specimen, but became larger during exposure by

accelerated outward cation diffusion. This porous structure of the substrate also enhanced oxygen diffusion down into the center of the substrate and increased the extent of internal oxidation. The peripheries of the central voids were surrounded with oxides, an alumina rim and a complex Al-Cr-Ti oxide, Figure 5.74(c). The features of the specimen exposed in dry air were similar to the wet exposed one, Figure 5.74(b). Examination of the sample cross-section showed that the scale that formed on the surface was non-uniform in thickness and in composition. Large voids were present also on this sample. However, the number and size of these features were smaller for the dry case. According to the kinetic data, weight losses started slightly later in dry air in comparison to wet air. However, regardless of the oxidizing environment, the degradation of the alloy was very aggressive. The depletion of the elements Cr and Al in the substrate contributed to the drastic failure of the alloy.

The presence of non-negligibly large amounts of voids on specimens of the alloy IN 738 complicate the evaluation of results, as the source of these defects could not be identified with certainty. It is not clear how much of the deterioration was related to the accelerated anion and cation transport through these pores, which were sites of easy diffusion. It is also not meaningful to compare the two alloys. However, it would not be wrong to say that the degradation of chromia formers was accelerated at 1000°C.

5.2.2 Comparison of Isothermal Tests to Cyclic Tests

Similar to the alumina formers, isothermal tests were done also with the chromia forming systems. For this work, the conditions of testing were kept the same as those for the alumina formers. High pressure steam experiments were done at 700°C and 900°C in the autoclave under a pressure of 250 psi (~17 atm). The results at 700°C were compared to cyclic tests at $P_{\text{total}} = 1$

atm. Additional isothermal tests were also done at 900°C at atmospheric pressures in air/H₂O mixtures with P_{H₂O} = 0.3 atm. At this temperature, the results for isothermal tests at high and low pressures were compared to each other as well as to cyclic tests at ambient pressure.

5.2.2.1 Tests at 700°C: IN 738 developed a continuous and perfectly adherent chromia scale with internally formed alumina after isothermal tests in 100% steam.

Comparison of cross-sectional back scattered electron images showed that the chromia layer that formed after isothermal exposures was thicker, more compact, and uniform than the one that formed after cyclic tests, Figures 5.75. However, it should be considered that the exposure times for each case were different. Isothermal steam tests were done for 4320 hours. This is equivalent to 5760 cycles. On the other hand, the results for cyclic tests were obtained after 2520 cycles. The TiO₂ which was present on the cyclically exposed sample as very fine fibers was also detected on the specimen tested in high pressure steam.

Similar results were obtained with X-40. The chromia scale that formed during isothermal exposures was thick and adherent, Figure 5.76. Another feature that was observed on the steam exposed sample is that pores developed at the oxide/substrate interface by vacancy condensation. This is typical for oxides which grow by predominant outward cation transport. The surface of this oxide was also smoother than the scale that formed during cyclic exposures at higher oxygen pressures. The latter surface was a rather wavy one.

As mentioned, both alloys developed thicker oxide layers with good adherence properties during isothermal exposures in 100% steam. The large difference between exposure times, i.e. 3200 and 2520 cycles for X-40 and IN 738, respectively, versus 4320 hours (corresponding to 5760 cycles), made the direct comparison of the results more difficult. However, thicker oxide

formation in spite of very low PO_2 levels was an important result. Further discussion will be done in later chapters with references to the results presented in this section.

5.2.2.2 Tests at 900°C: At this temperature, isothermal tests in high pressure steam promoted the formation of a compact and adherent chromia layer with no pores on IN 738, Figure 5.77 (a). The general compositional characteristics of the scale were the same as the ones that developed at atmospheric pressures, i.e. an external chromia, and internally developed alumina. The thin TiO_2 that formed on the sample surface after cyclic tests in ambient pressure was also present on this specimen. Another observation is that high pressure steam (or low PO_2) decreased the reaction rate significantly. The scale thickness under this condition was remarkably smaller than isothermal or cyclic exposures in air/ H_2O mixtures at ambient pressure in spite of the fact that the total exposure time was longer for the former case.

The chromia scale that developed after isothermal exposures at $\text{PH}_2\text{O} = 0.3$ atm was adherent yet porous, Figure 5.77 (b). The thin layer of TiO_2 that was observed to form on the cyclically exposed samples was also present on this specimen. Aluminum oxidized internally, forming the stringers under chromia. It was expected that thicker scales would form on this sample compared to the specimen exposed to the same environment cyclically, as spalling of oxides would be avoided due to the elimination of thermal cycling. Comparison of backscattered electron images proved that this was the case, Figures 5.77 (b-c). Thicker scales formed on the isothermally tested sample. The time of exposure to hot gases was the same for both cases.

Isothermal exposures of X-40 to steam and to air-30% water vapor resulted in the formation of scales with different features. For the high pressure case, the oxide that formed was a monolayered chromia, Figure 5.78(a). This scale was thin, and had some porosity at the oxide/gas

interface. No significant internal oxidation was evident. Isothermal wet tests at atmospheric pressures resulted in the formation of thicker and non-uniform scales. Images showing the cross-section of the sample tested in this environment are given in Figure 5.78 (b-c). The system developed thick layers of chromia in some parts, Figure 5.78 (b). The concentration of vacancies at the chromia/substrate interface was higher in comparison to the chromia that formed in high pressure steam. Internal oxidation via the carbide network was also more pronounced. It was observed that islands of Co-rich oxides with underlying porous and non-protective phases formed along the reaction zone. One such area is shown in Figure 5.78 (c). These results suggested that the reaction rate was affected by oxygen partial pressure. Thinner scale formation in the high pressure steam environment suggested that the reaction leading to chromia formation proceeded slower in the low PO_2 environment. Less vacancy condensation at the chromia/substrate interface observed in this atmosphere also pointed to the same possibility. This happened, because the concentration of cations diffusing to the gas interface was smaller.

Comparison of isothermal and cyclic tests at ambient pressure showed that the faster growing, non-protective oxides that were observed after testing the specimens cyclically did not form as extensively during isothermal exposures. The degree of degradation was substantially higher after cyclic exposures. This occurred most likely due to the spalling of chromia scales between cycles, which depleted the system in Cr. Layers of protective oxides could not be maintained. Instead, the less stable, faster growing CoO formed. The images given in Figure 5.67-68 show the details of the scale.

5.2.3 Effect of Surface Finish

Short term exposure tests with IN 738 and X-40 at 700°C were performed to observe the effect of different surface conditions on the development of chromia scales. The specimens were prepared using the same procedure as for PWA 1484 and René N5, i.e. 0.05 μm alumina finish on one side, 600 grade abrasive paper finish on the other side. The examination of the oxide scales indicated that the oxidation process was not affected by the pre-exposed surface condition.

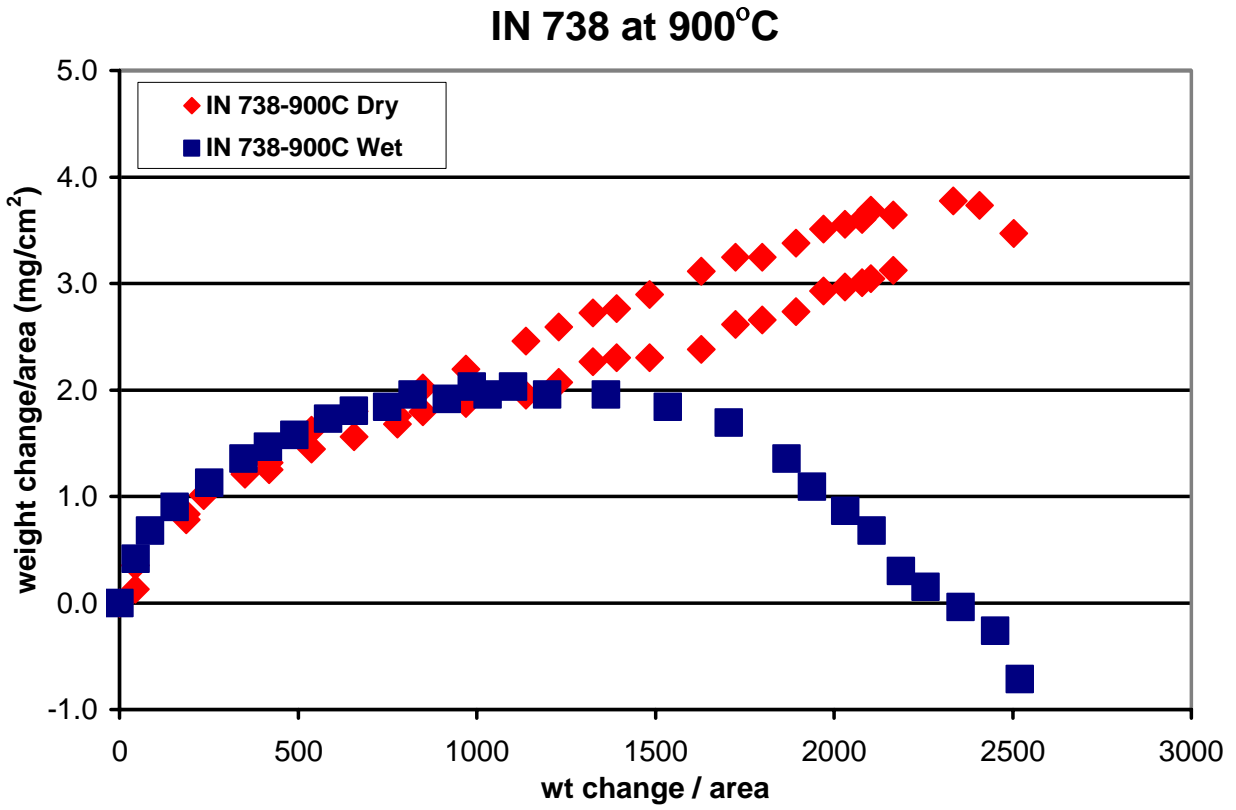
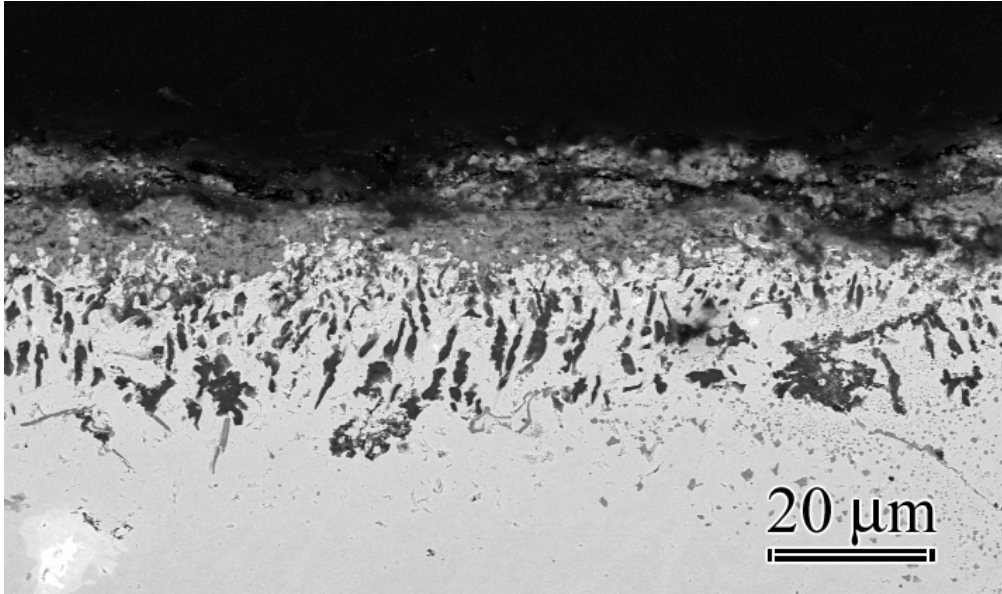
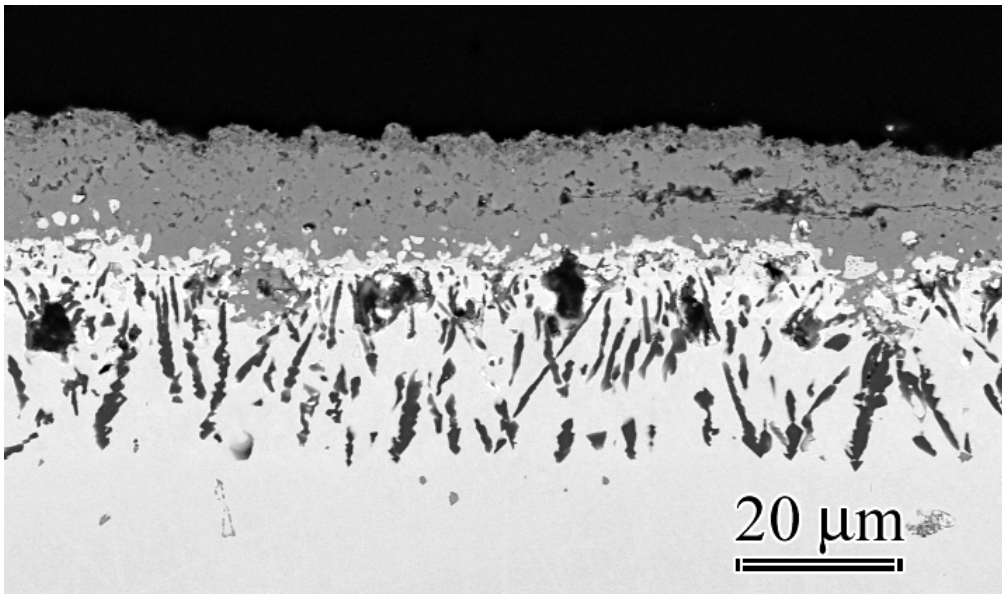


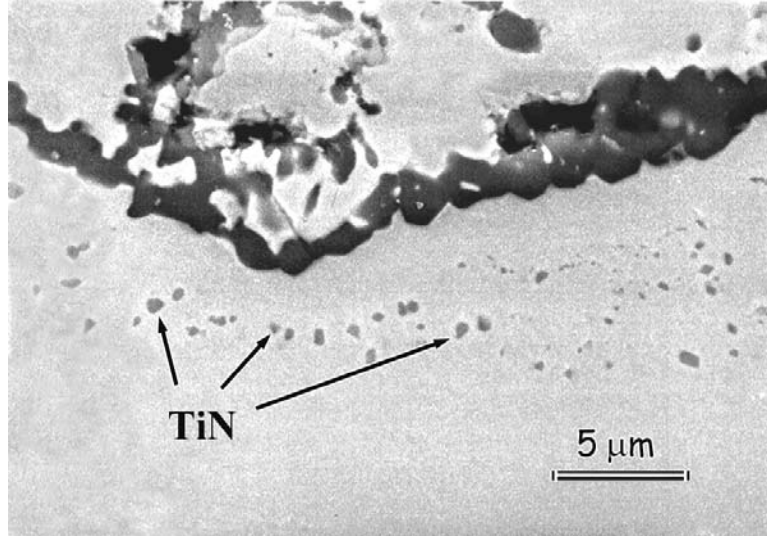
Figure 5.65: Kinetic plot of the alloy IN 738 showing the weight changes of the specimens in dry air and in air/H₂O mixtures at 900°C as a function of cycle number.



(a)



(b)



(c)

Figure 5.66: IN 738 at 900°C after cyclic exposures for 2520 hours (a) in dry air, and (b) in wet air, (c) TiN formed in the depleted zone in dry as well as in wet air. The micrograph shown displays the formation of the phase for the dry-exposed specimen.

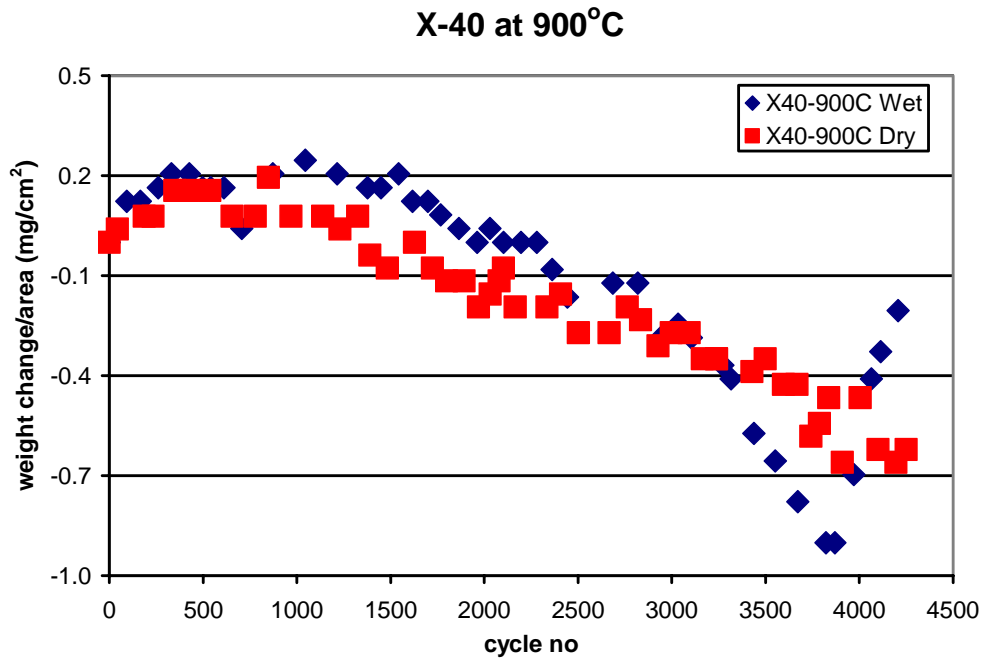
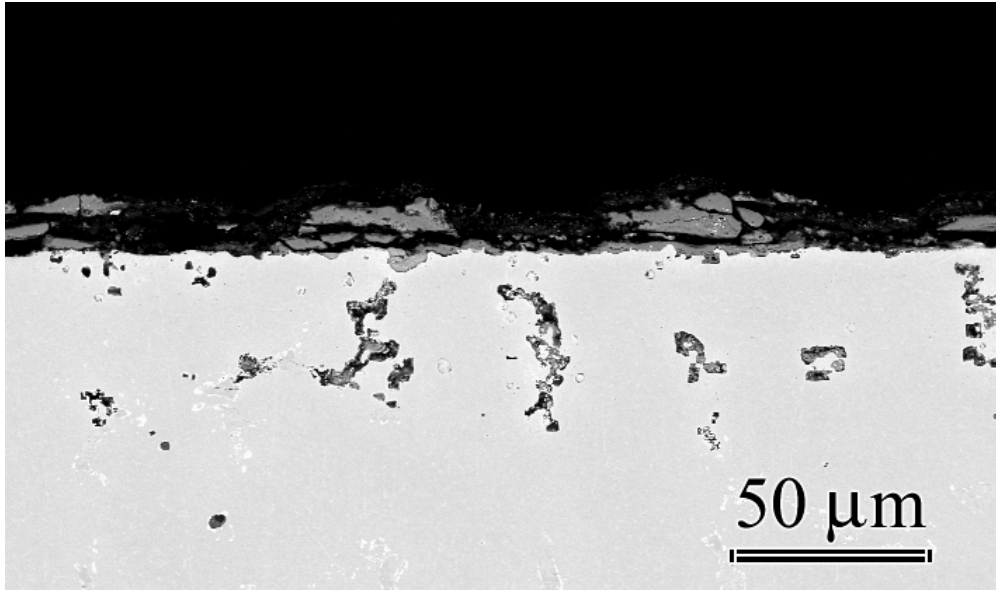
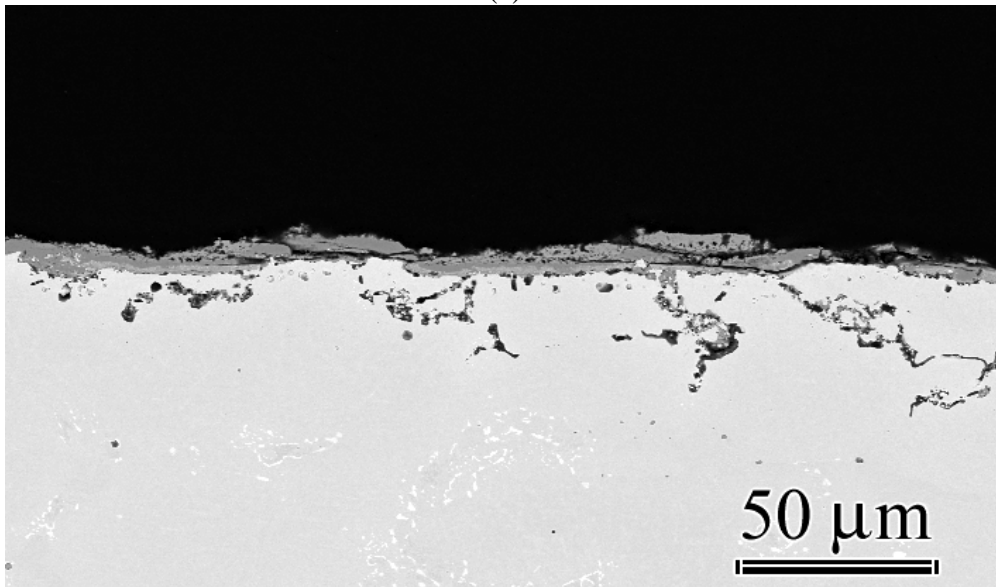


Figure 5.67: Kinetic plot of the alloy X-40 showing the weight changes of the specimens in dry air and in air/H₂O mixtures at 900°C as a function of cycle number.

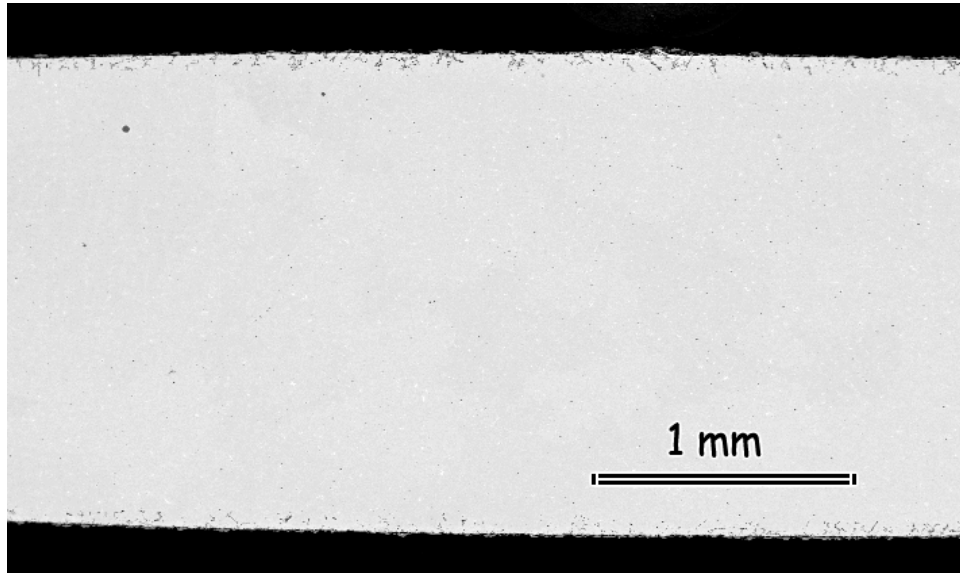


(a)

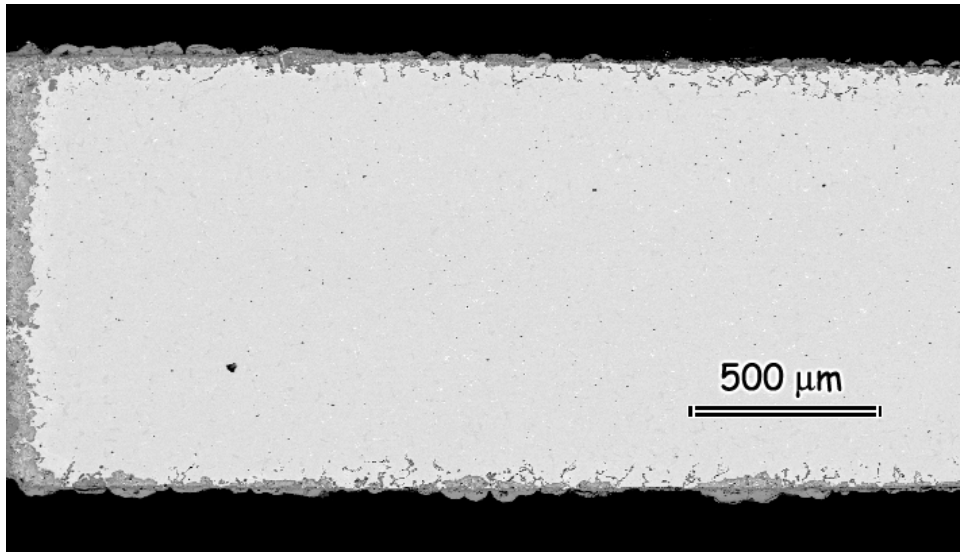


(b)

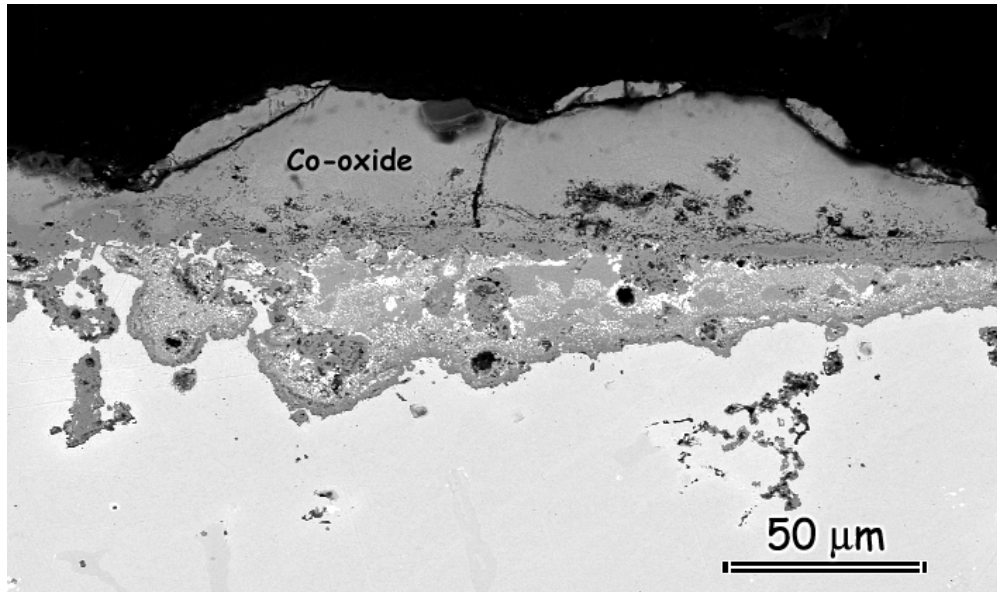
Figure 5.68: SEM images of X-40 at 900°C after exposures to hot gases for 2050 hours. (a) Substantial scale spallation occurred in dry air. (b) Micrograph shows the oxide layer that formed in air/water vapor mixtures at atmospheric pressure.



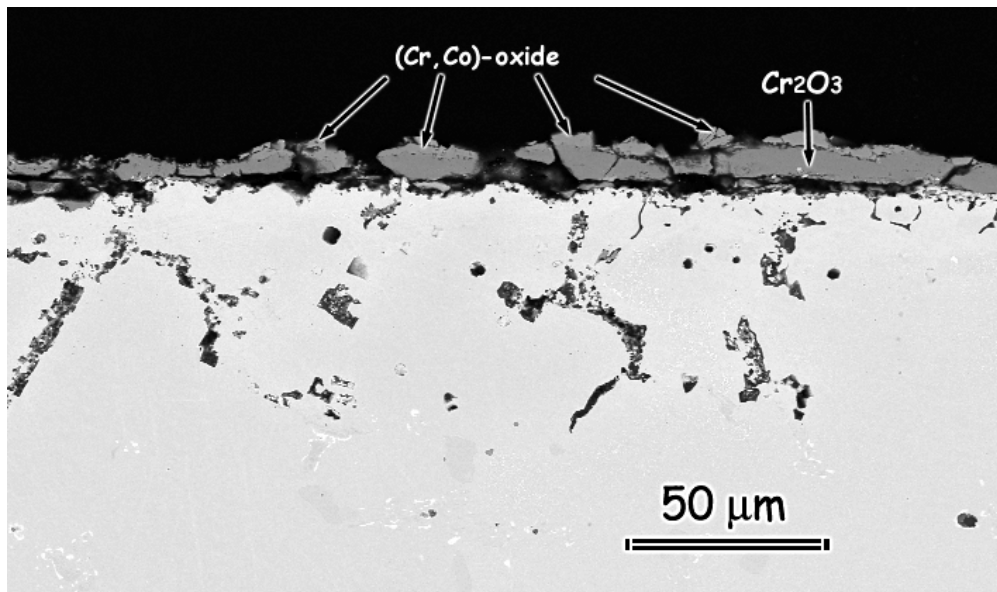
(a)



(b)



(c)



(d)

Figure 5.69: X-40 at 900°C after 4250 hours of cyclic testing. (a) Image shows the cross-section of the specimen exposed to dry air at low magnification. (b) Same alloy after tests in wet air. (c) Cross-section of X-40 at 900°C in wet air after 4250 cycles shown at higher magnification. Alloy lost its protectiveness. Co-oxide developed at the top of the scale. (d) Cross-section of X-40 at 900°C in dry air after 4250 cycles shown at higher magnification.

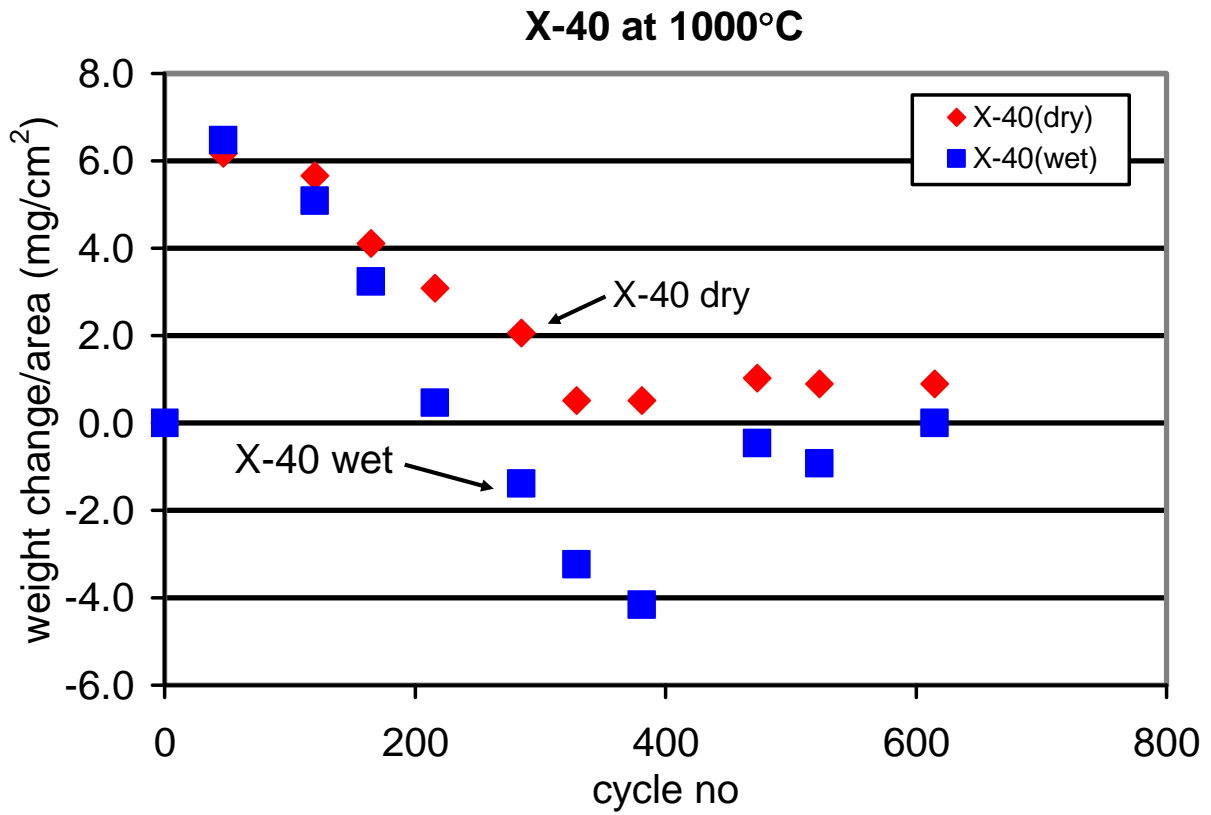
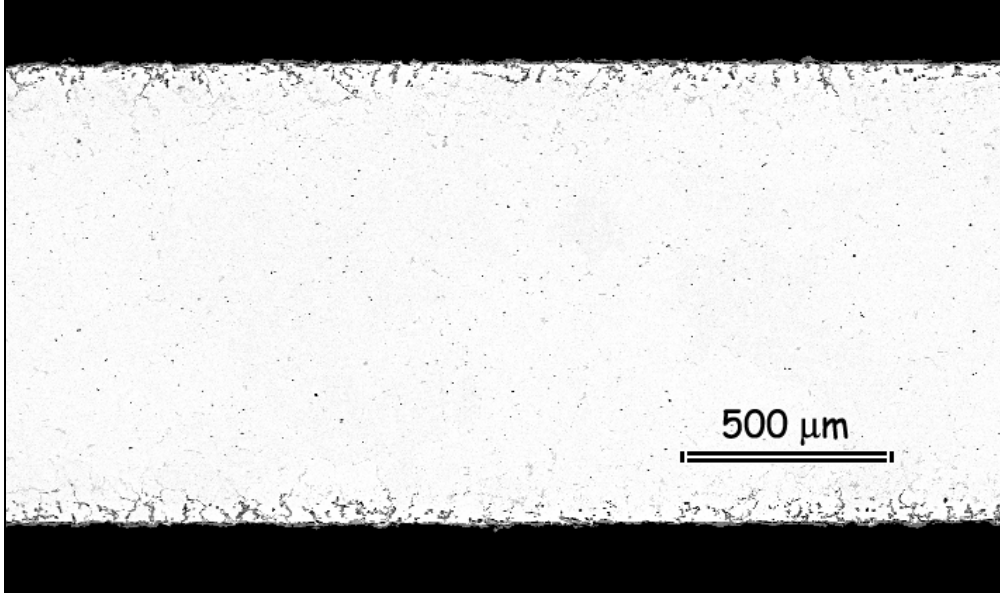
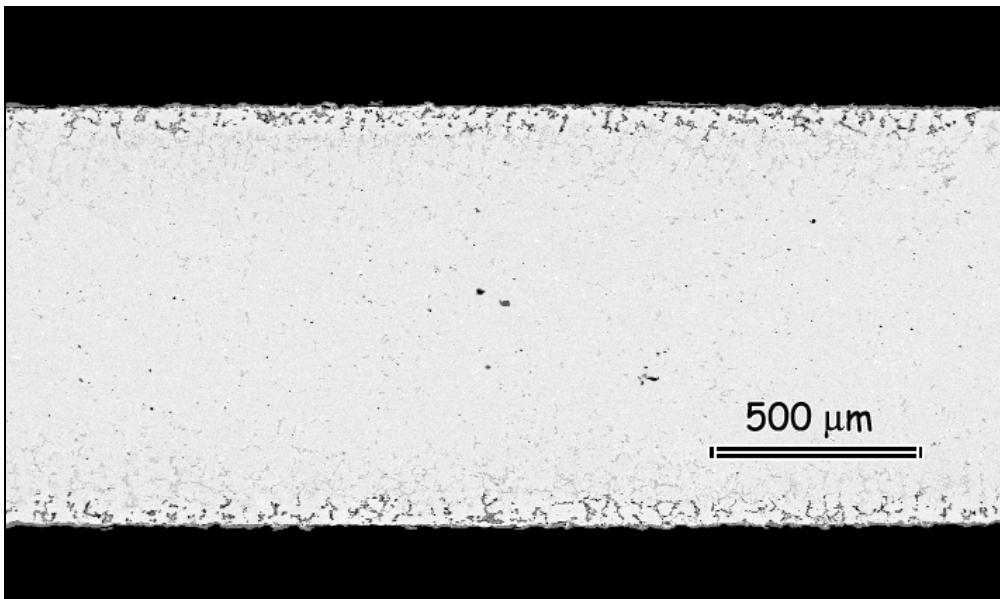


Figure 5.70: Kinetic plot of the alloy X-40 showing the weight changes of the specimens in dry air and in air/H₂O mixtures at 1000°C as a function of cycle number.

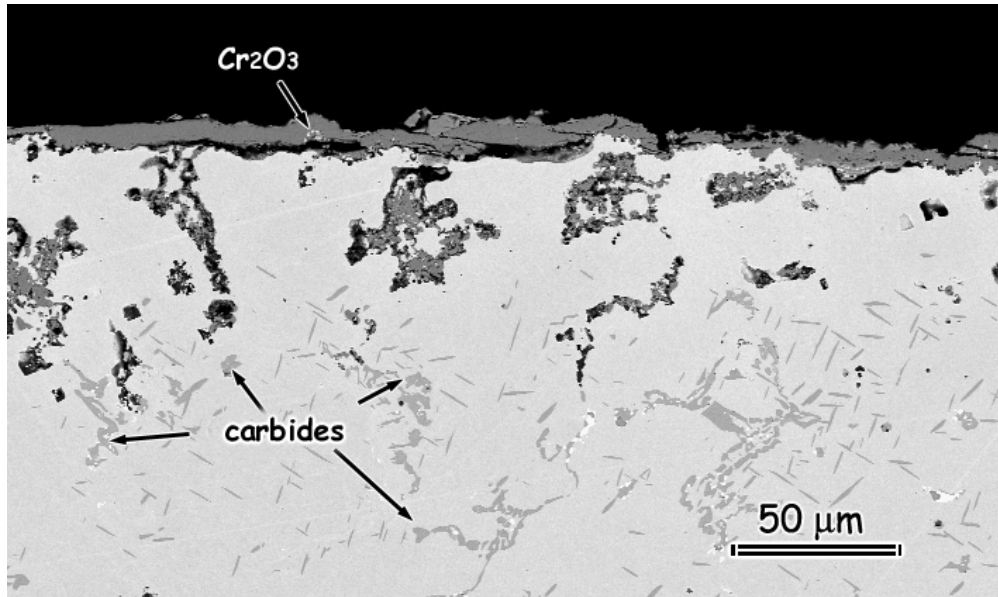


(a)

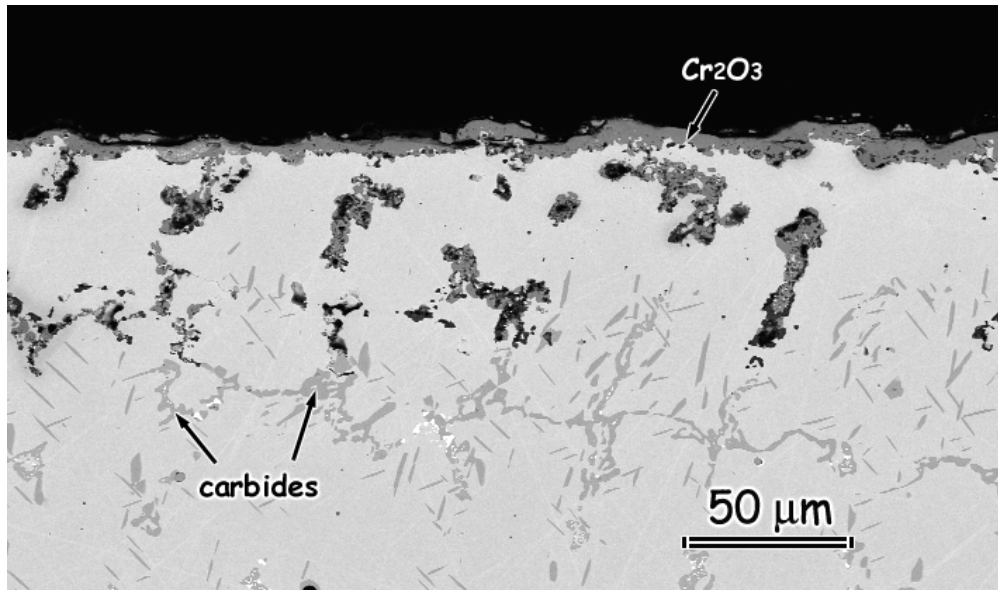


(b)

Figure 5.71: X-40 at 1000°C in wet air after 615 cycles. (a) The micrograph shows the scale that formed on the specimen surface in dry air at a low magnification. (b) The image shows the reaction zone that developed after tests in air/H₂O mixtures.



(a)



(b)

Figure 5.72: X-40 at 1000°C after cyclic exposures in hot gases for 615 hours. (a) The SEM image shows the cross-section of the specimen exposed to dry air. (b) Micrograph showing the scale that formed after tests in wet.

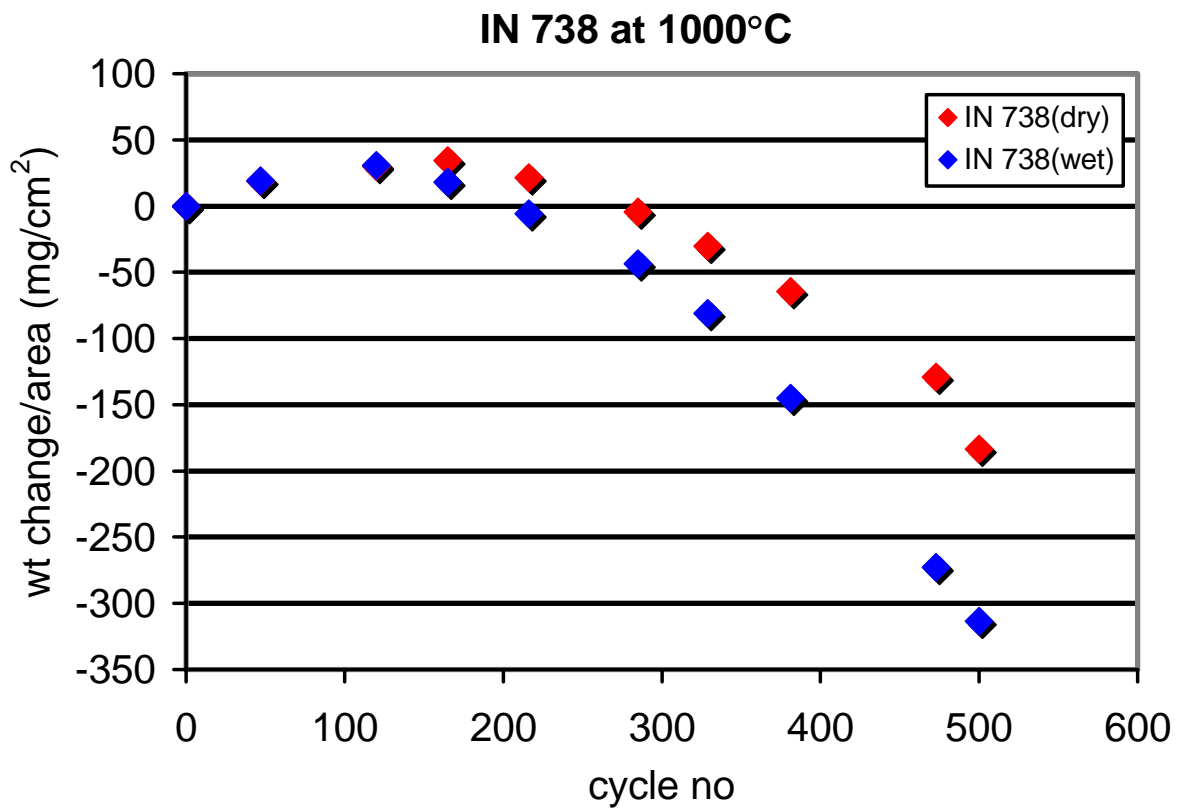
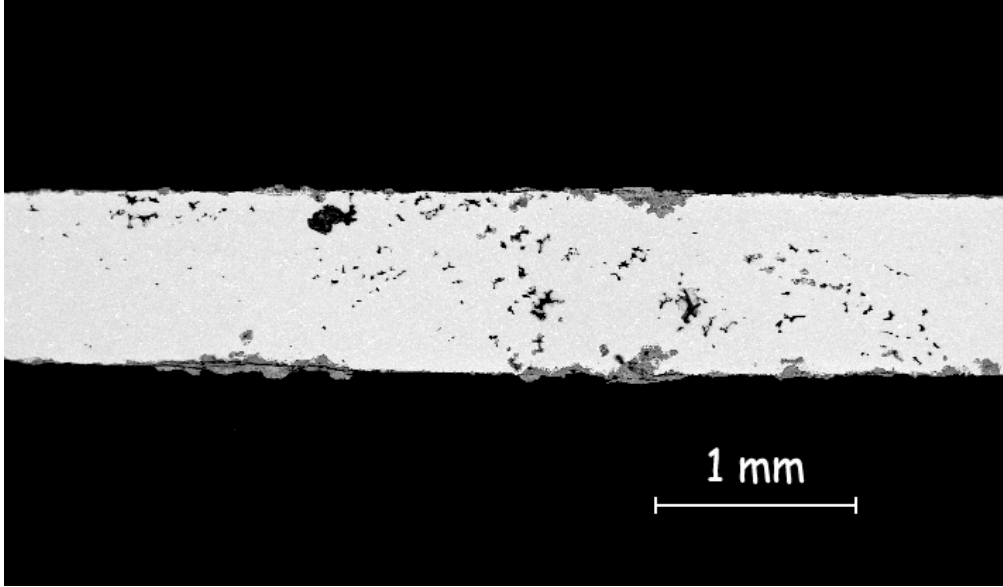
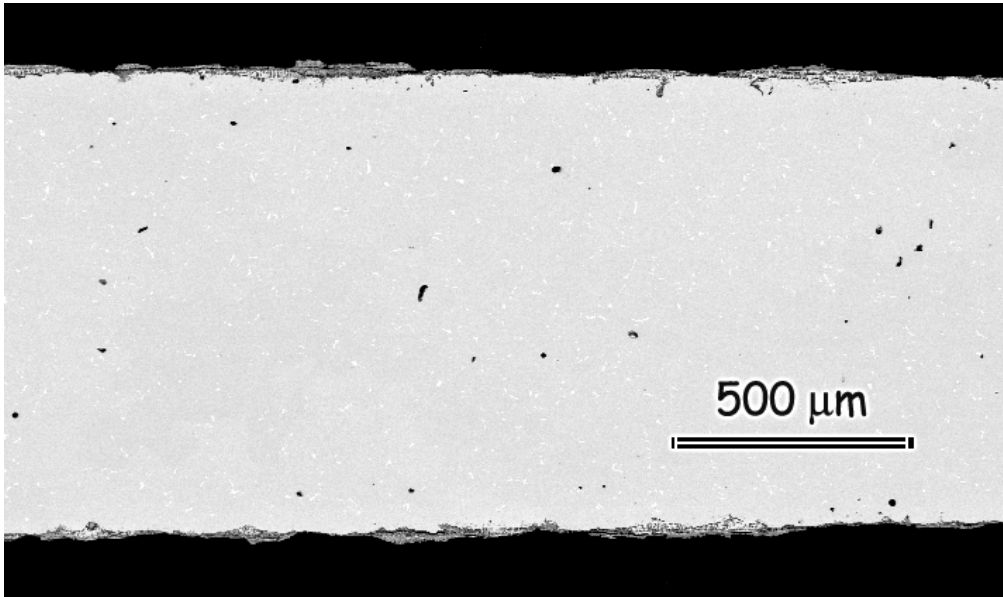


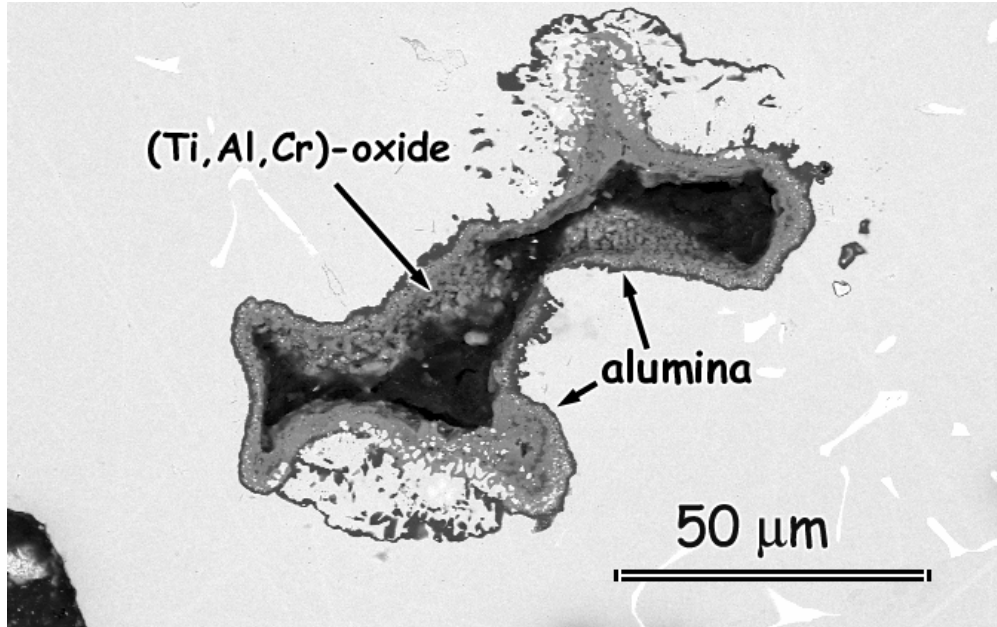
Figure 5.73: Kinetic plot of the alloy IN 738 showing the weight changes of the specimens in dry air and in air/H₂O mixtures at 1000°C as a function of cycle number.



(a)

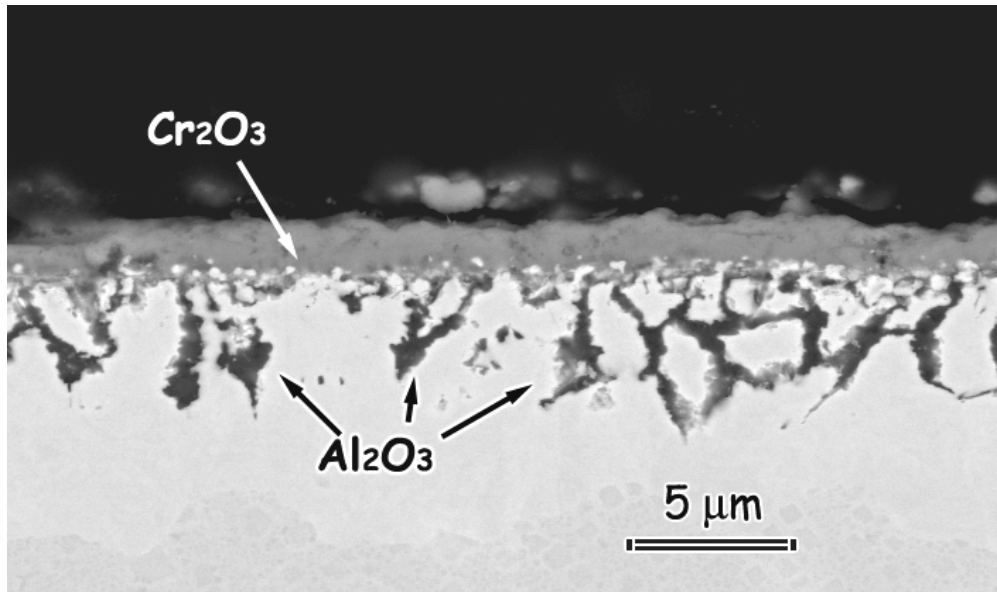


(b)

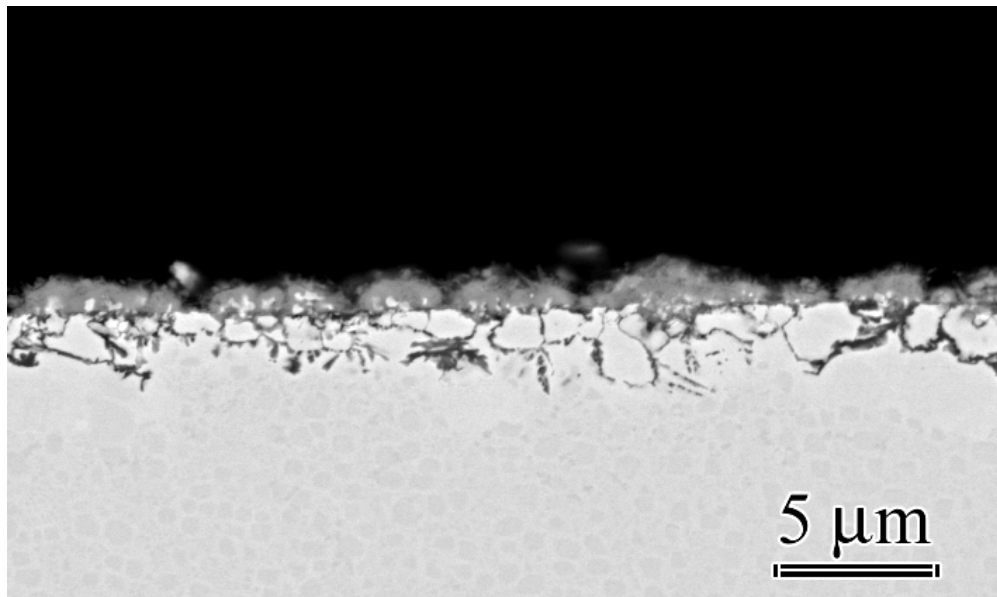


(c)

Figure 5.74: IN 738 at 1000°C after 500 cycles. (a) SEM image shows the cross-section of the sample exposed to wet air at low magnification. (b) Specimen cross-section after tests in dry air. (c) Micrograph shows a pore with internally formed oxide around its periphery in wet air.

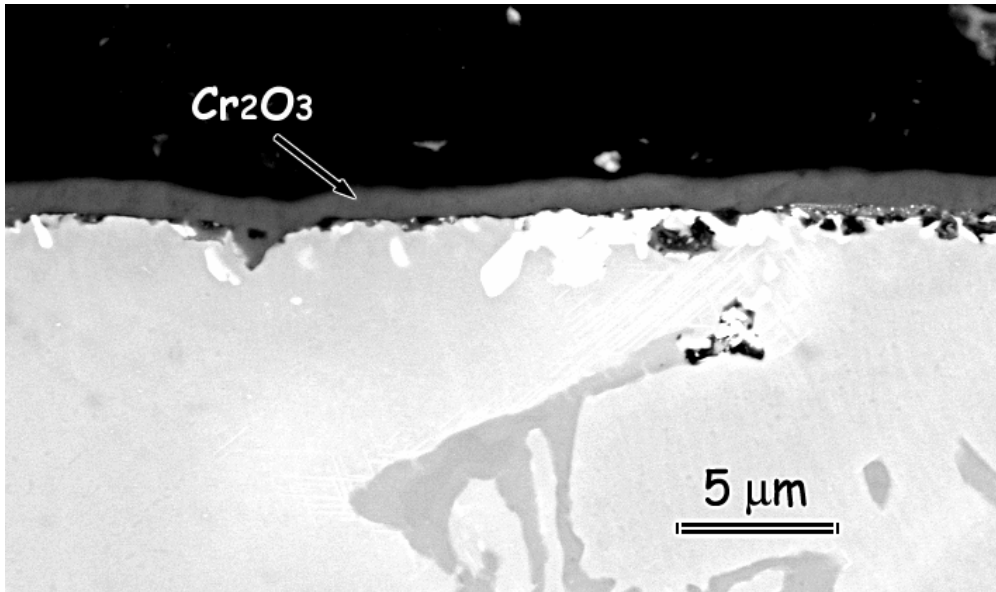


(a)

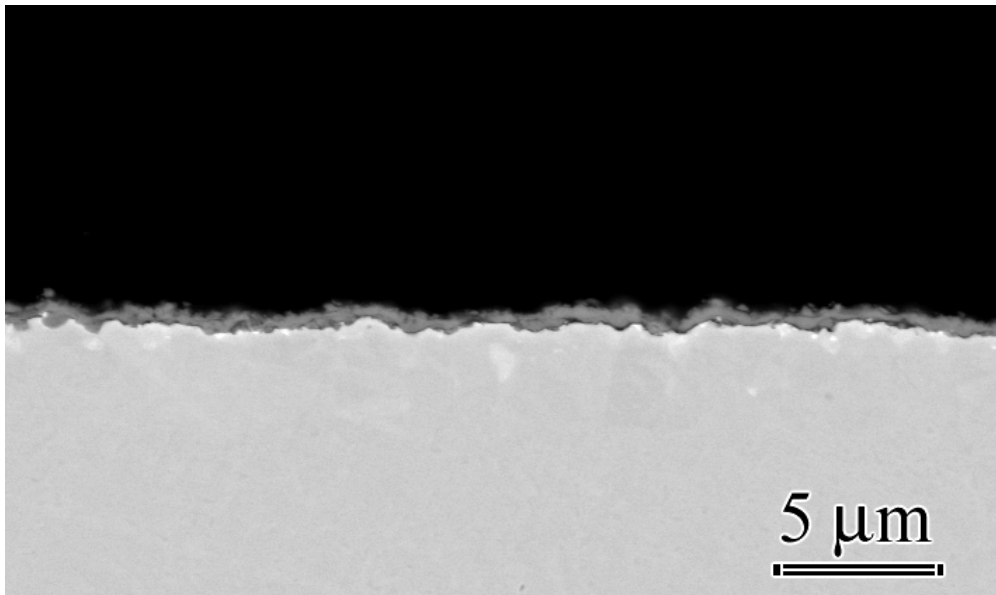


(b)

Figure 5.75: SEM images showing the oxide scales that formed on IN 738 at 700°C. (a) Image shows the reaction zone after exposing the alloy to high pressure steam isothermally for 4320 hours. (b) The oxide layer that formed in air/H₂O mixtures atmospheric pressure after cyclic tests for 2520 hours.



(a)



(b)

Figure 5.76: Back scattered electron image shows X-40 at 700°C. (a) Alloy was subjected to isothermal tests in high pressure steam for 4320 hours. (b) Same system after cyclic tests in wet air for 3200 hours.

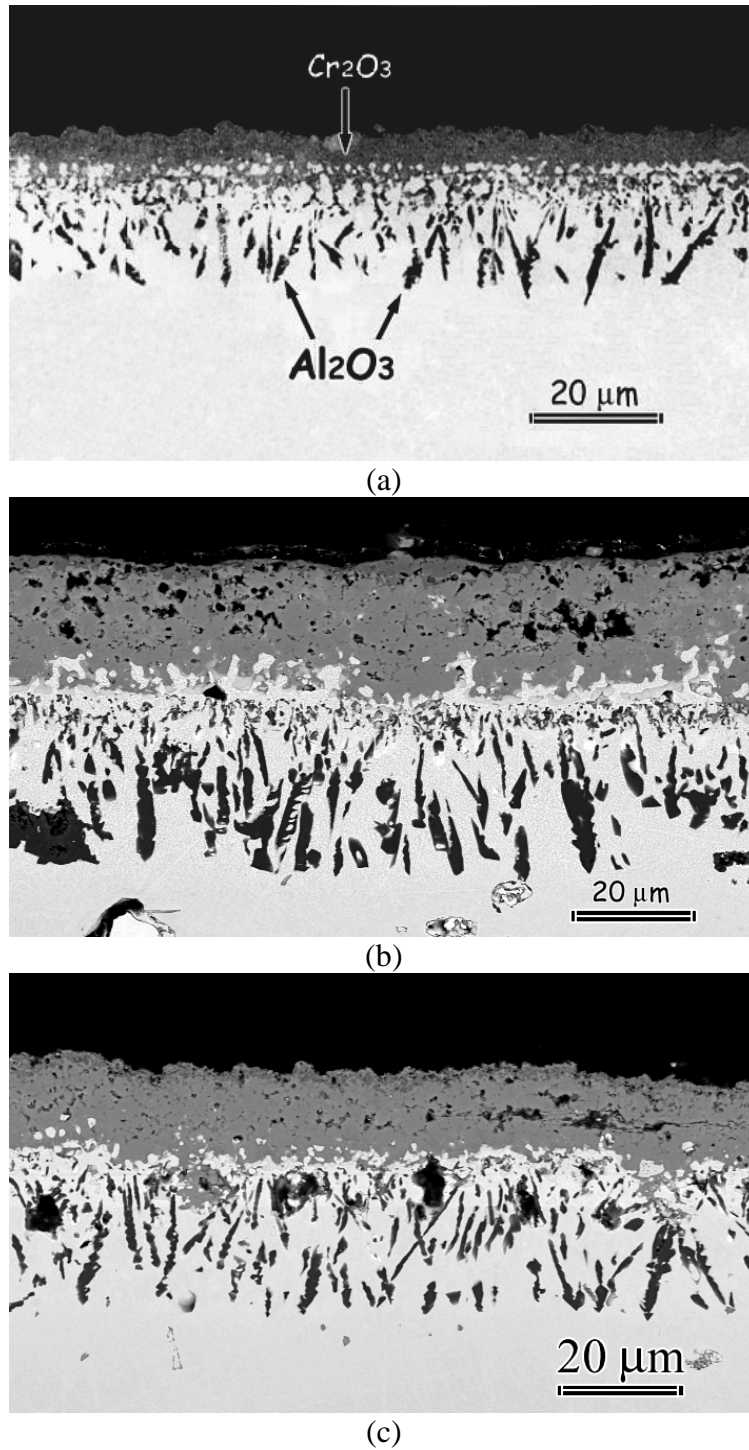
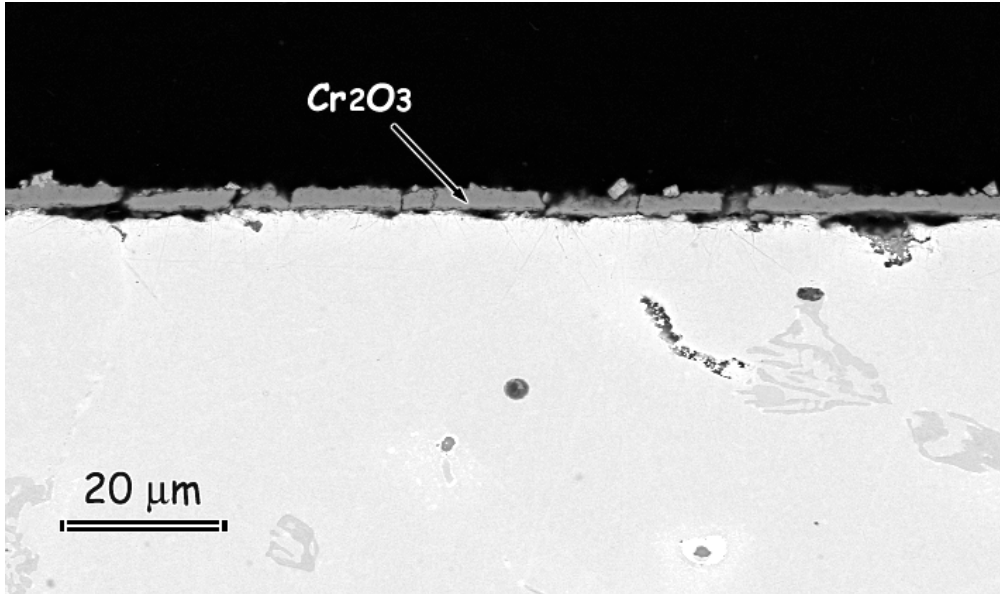
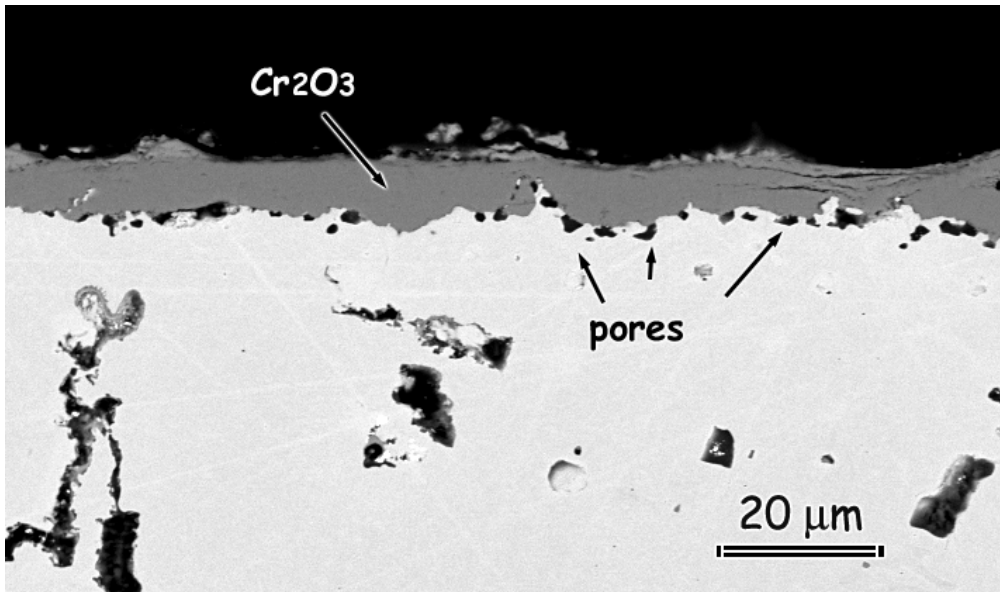


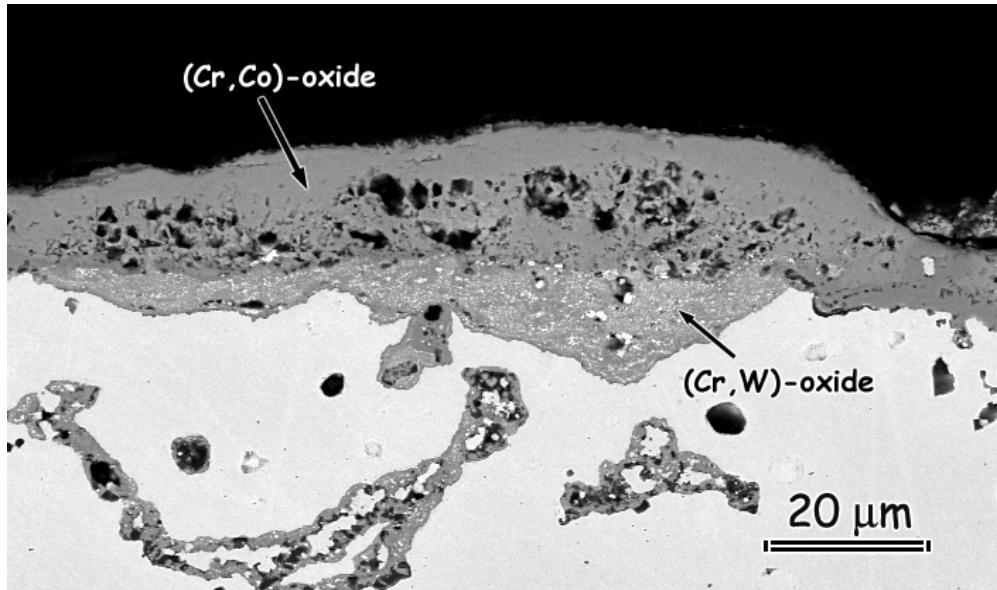
Figure 5.77: SEM images of IN 738 at 900°C. (a) Specimen tested isothermally in high pressure steam for 4320 hours. A dense chromia scale developed on the surface. TiO_2 formed a thin external layer. (b) Same alloy tested isothermally in air/ H_2O mixtures at atmospheric pressure for 4320 hours. (c) Image shows the scale that formed after cyclic tests in wet air at ambient pressure after 2520 cycles.



(a)



(b)



(c)

Figure 5.78: Back scattered electron images of X-40 at 900°C after isothermal tests. (a) Cross-section of the scale that formed in pure steam environment at high pressure. (b-c) Scale that developed in wet air at ambient pressure. All specimens were tested for 4320 hours.

6.0 RESULTS PART II

6.1 TESTS WITH MODEL ALLOYS

The test results with the complex superalloys provided some understanding regarding the behavior of these systems in environments with and without water vapor. The information obtained was important, yet insufficient to develop a more in-depth understanding of the mechanisms leading to this type of alloy degradation. The main difficulty faced with these systems was their compositional complexity. Each alloy contained numerous elements, and each one of them had interactions with one another to some degree. Under the current testing conditions it was not possible to isolate these effects. Therefore, it was decided to do more testing with simpler systems as models. This way, a better control over the experimental parameters was established. Although work was needed on both alumina and chromia formers, it was decided to focus on chromia scales. The model system was chosen as the Ni-Cr binary system.

In this part of the study, two modes of testing were utilized; cyclic and isothermal. For these tests the partial pressure of H₂O was set to 0.1 atm instead of 0.3 atm. The total pressure of gases was atmospheric pressure. Cyclic tests were done in the same horizontal tube furnaces used for the experiments on superalloys. Isothermal tests were done in a vertical furnace

utilizing TGA techniques. In the following sections, the results for the cyclic experiments will be presented first; the isothermal TGA test results will be discussed later.

6.1.1 Cyclic Tests with Ni-Cr Model Alloys

Cyclic experiments with Ni-Cr systems were designed to understand the effect(s) of water vapor on the selective oxidation of Cr and on the spalling of chromia scales. The alloy compositions were chosen as Ni-15Cr, Ni-20Cr, and Ni-30Cr. Ni-15Cr is known to develop internal Cr₂O₃ in air and in oxygen. Ni-20Cr is a borderline composition for transition from internal oxidation to continuous Cr₂O₃ formation in dry air. Ni-30Cr develops continuous Cr₂O₃ scales in oxygen and in air [96]. This selection of compositions made it possible to make observations at each critical stage of oxidation. Tests were done in dry air and in wet air so that comparative studies could be performed. The differences in the behavior of Ni-15Cr and Ni-20Cr in dry air and in air/H₂O mixtures yielded information on the effect(s) of water vapor on selective Cr oxidation. Tests with Ni-30Cr helped to understand the effects of water vapor on the spalling of chromia scales.

In addition to these alloys, Ni-15Cr-0.1Ce and Ni-30Cr-0.1Ce were tested. It is well known that reactive element additions improve scale adherence significantly in air and in oxygen. These experiments were included in the planning of the tests to see how effective these elements would be in environments containing water vapor. The comparison of the Ce-doped and the Ce-free alloys was expected to give information on the spallation of the chromia scales in wet gases.

In the following, the results obtained will be presented starting with the experiments at 700°C, followed by the exposures at 900°C.

6.1.1.1 Cyclic Tests at 700°C: The weight change data obtained from cyclic tests in dry air and in air/H₂O mixtures ($P(\text{H}_2\text{O})=0.1$ atm, $P_{\text{total}}=1$ atm) are given in Figures 6.1 and 6.2, respectively. These plots showed that in both environments Ni-15Cr was the system that displayed the largest weight gains.

Examination of alloy surfaces revealed that in dry air two types of oxides developed on different parts of the specimen. Some areas consisted predominantly of NiO, while the others were chromia-rich. These regions are marked on Figure 6.3. In the predominant-chromia region smaller sized islands of NiO were also detected, Figure 6.4. Cross-sectional examination showed that in areas with profuse transient oxidation, chromia formed as an internal oxide. Otherwise, it developed as a thin mono-layered external scale, Figure 6.5. The transient oxide protrusions consisted of NiO at the oxide/gas interface, and (Ni,Cr)-oxides between the NiO and the chromia. Examination of the scale suggested that equal amounts of transient oxides and chromia developed at the oxide/gas interface.

The surface of the specimen tested in wet air also appeared to have different colors over different grains, Figure 6.6(a). However, this time there were no noticeable compositional differences between each area. The surface of the specimen was covered by a thin chromia layer. Another observed feature was the individual Cr₂O₃ grains with a flake-like morphology that formed all over the specimen, Figure 6.6(b). These crystals were present on the wet exposed sample only. It also appeared that no significant transient oxidation took place in this environment. Neither surface examination, nor cross-sectional investigation showed signs of noticeable transient oxide formation. The image of the specimen cross-section is given in Figure 6.7.

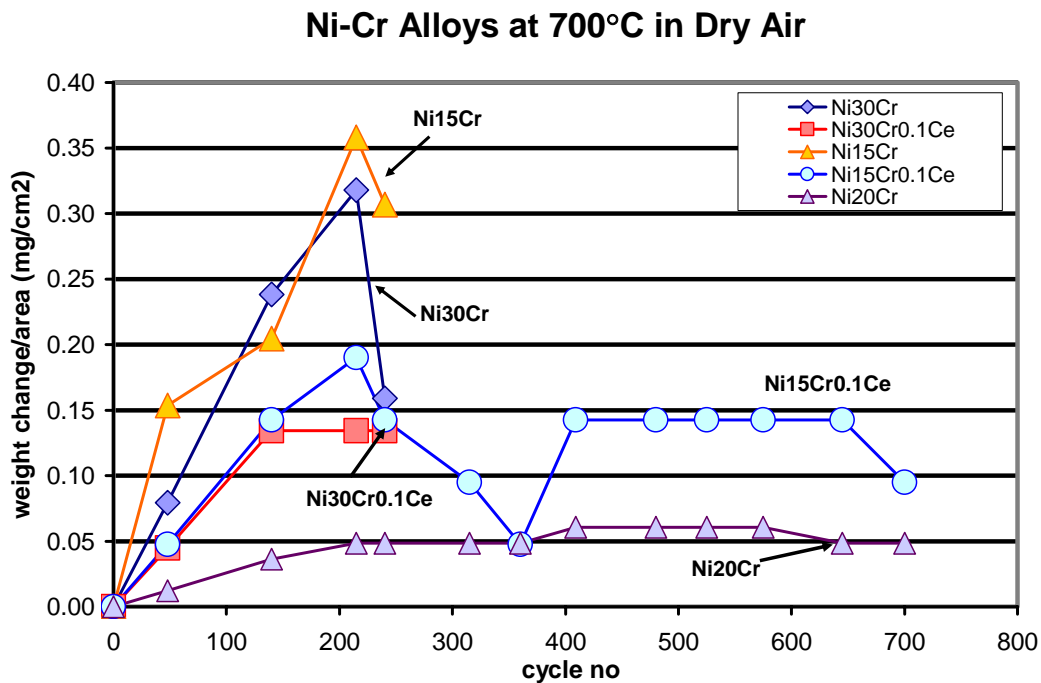


Figure 6.1: Kinetic plot of Ni-Cr alloys cyclically exposed to dry air at 700°C at a total pressure of 1 atm. The diagram shows differences in weight gains for different alloy compositions.

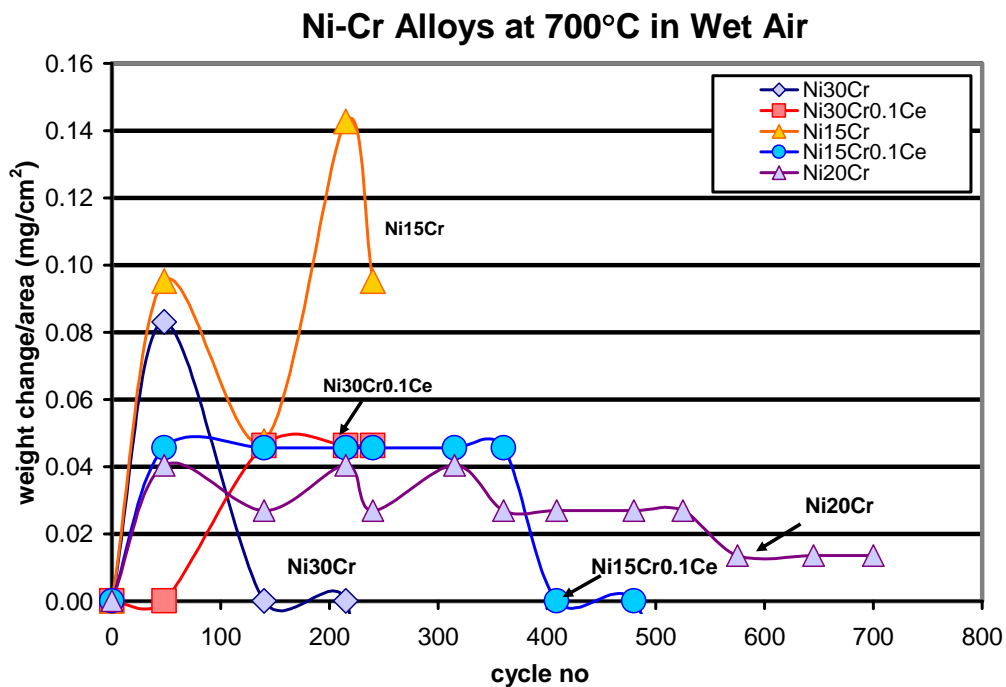


Figure 6.2: Kinetic plot of Ni-Cr alloys cyclically exposed to wet air at 700°C, where $P(\text{H}_2\text{O}) = 0.1 \text{ atm}$ and $P_{\text{total}} = 1 \text{ atm}$. The diagram shows differences in weight gains for different alloy compositions.

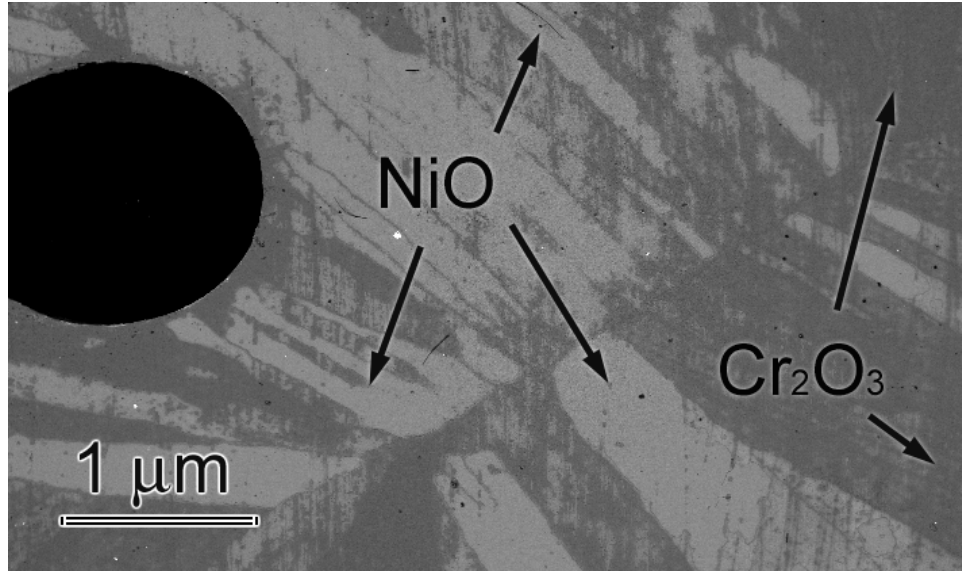


Figure 6.3: SEM image shows surface of Ni-15Cr at 700°C after tests in dry air. Lighter-colored grains were the areas where NiO formed as an external scale. The darker colored grains were where chromia developed.

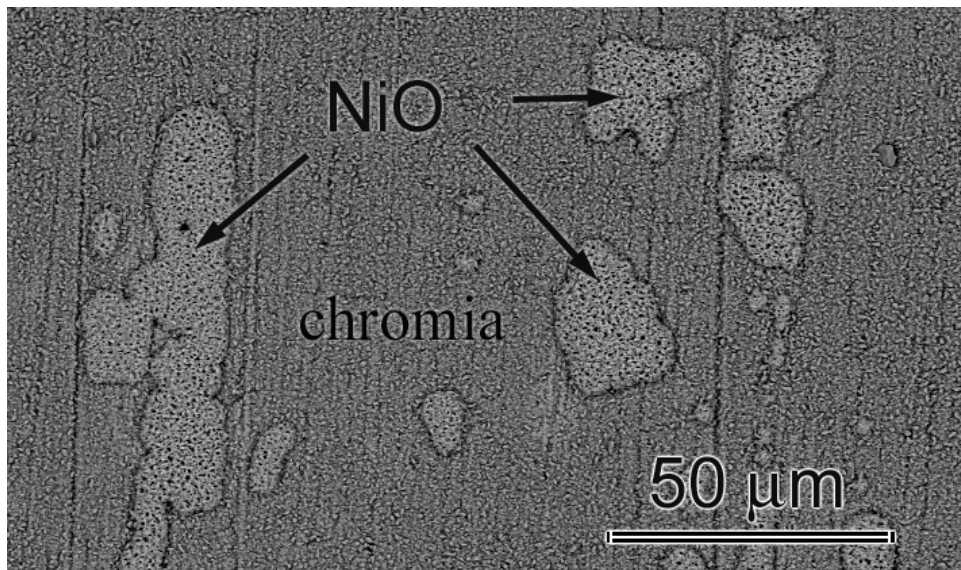
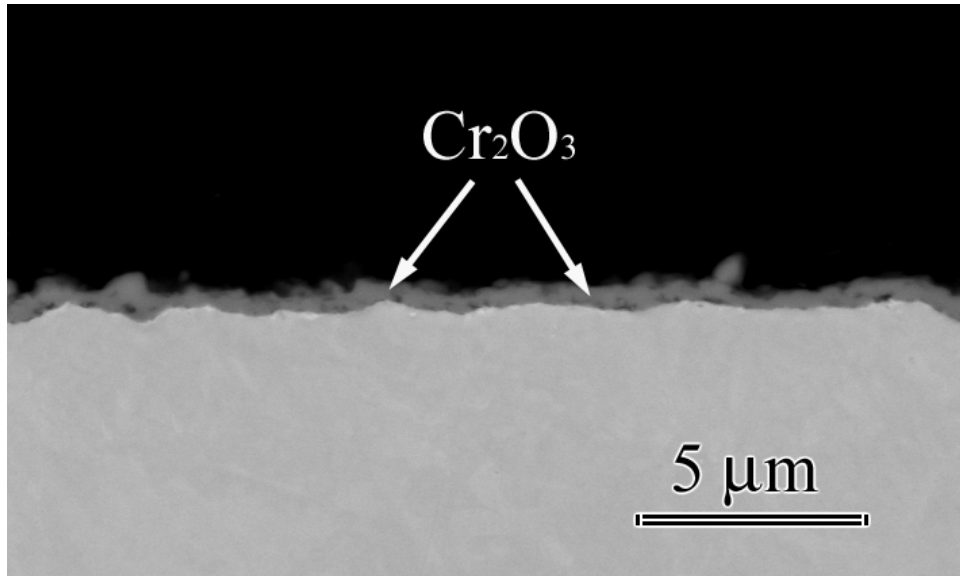
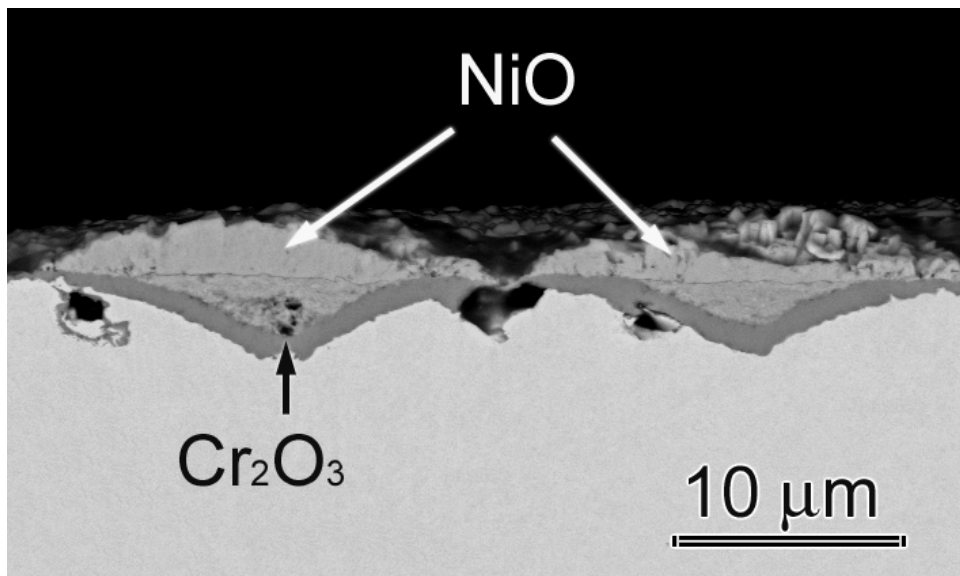


Figure 6.4: Image shows the formation of NiO islands on Ni-15Cr at 700°C in dry air where chromia formed as the primary oxide. These areas were defined as the darker colored grains in Figure 6.3,

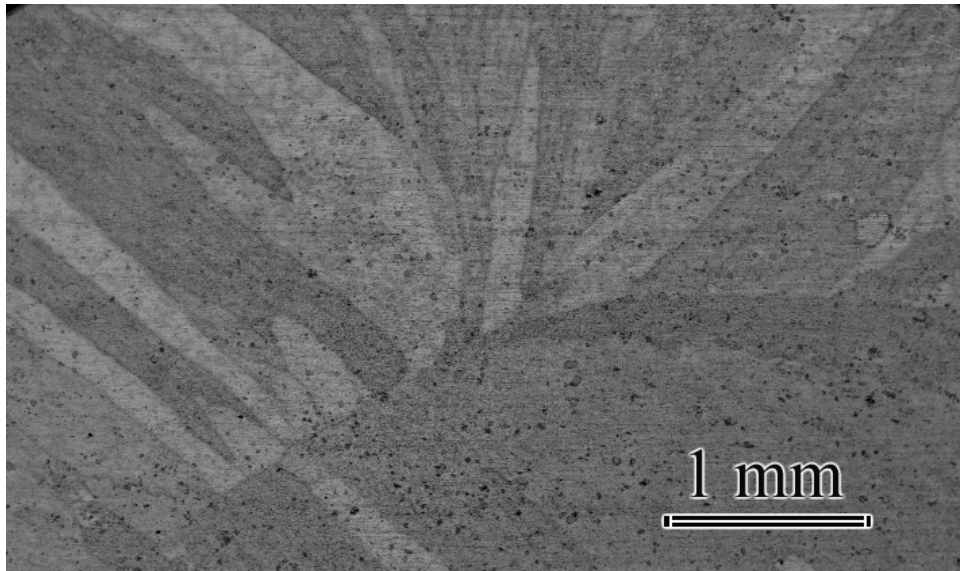


(a)

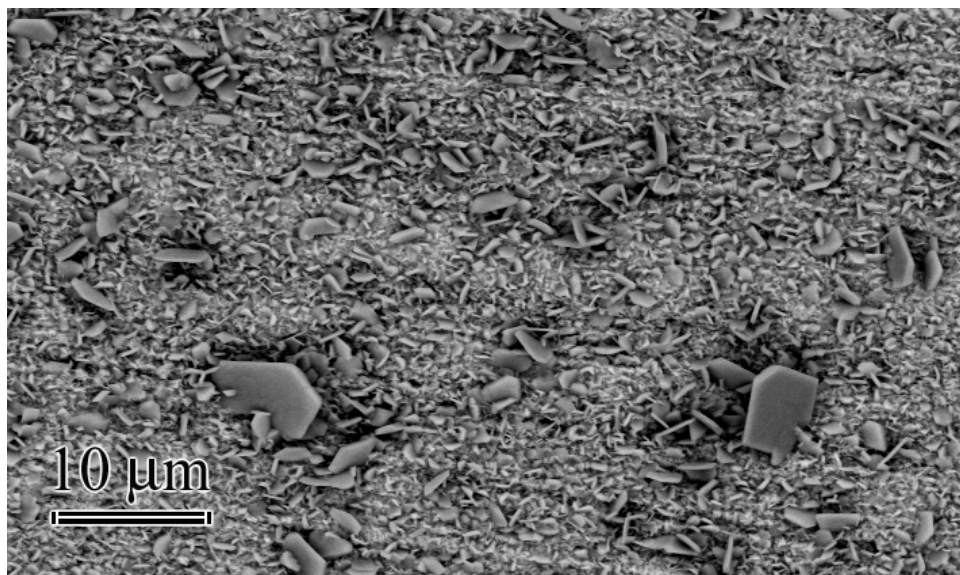


(b)

Figure 6.5: SEM image showing the cross-section of the scale that developed over Ni-15Cr in dry air at 700°C after 240 cycles. (a) Chromia scale (b) Transient oxidation.



(a)



(b)

Figure 6.6: Ni-15Cr at 700°C after cyclic tests in wet air. The specimen was subjected to thermal cycling for 240 hours.

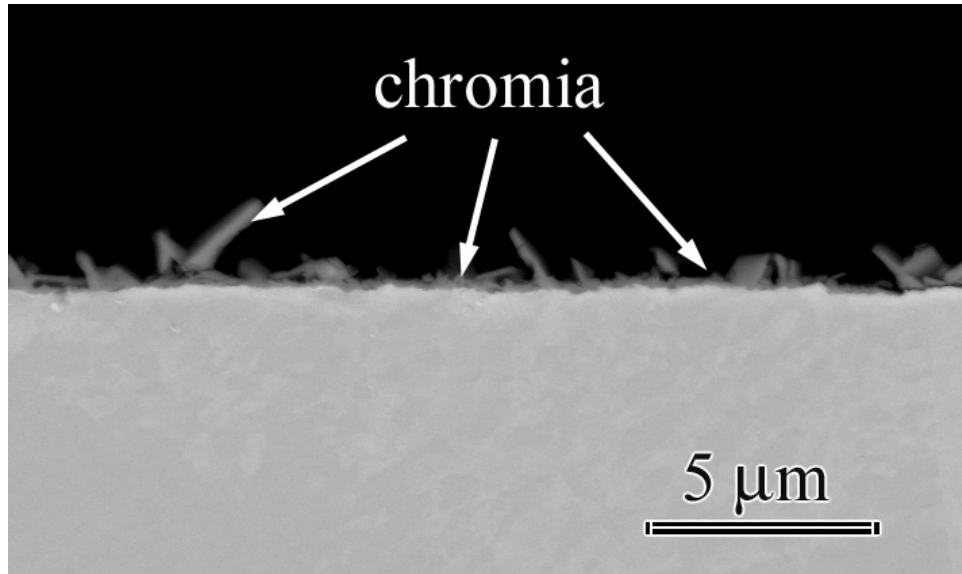
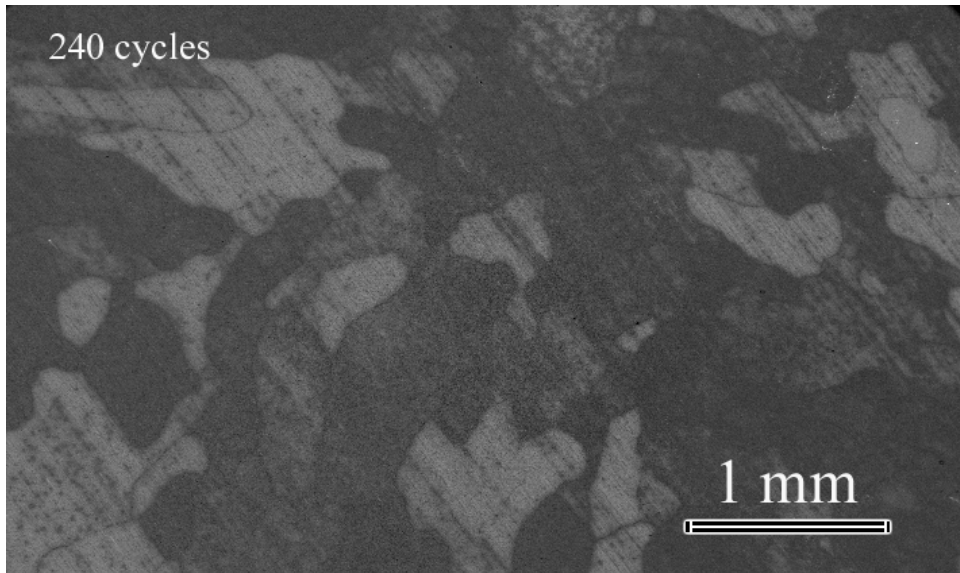


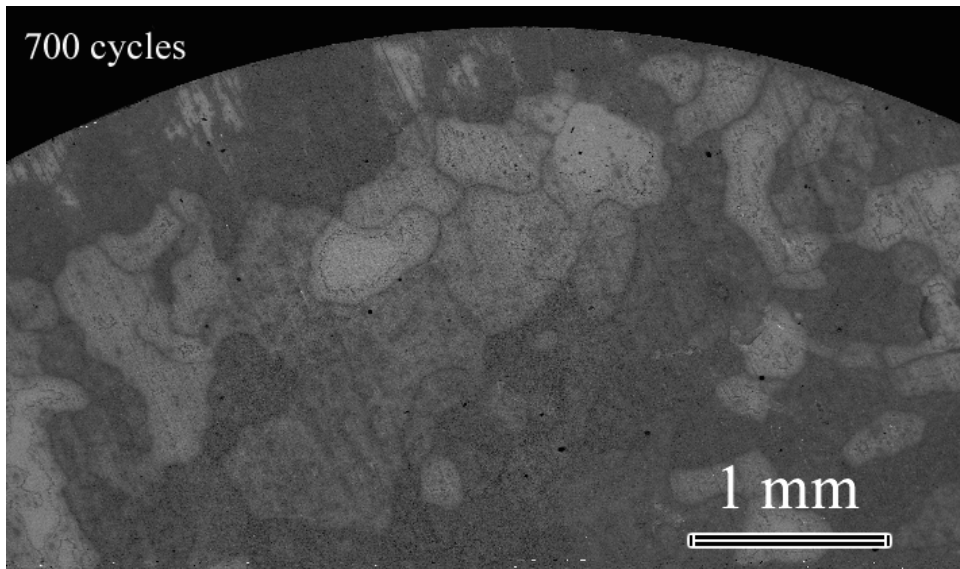
Figure 6.7: SEM image of Ni-15Cr showing the scale in cross-section that developed at 700°C after cyclic tests in wet air for 240 cyclic hours.

Comparison of scale thicknesses after wet and dry exposures showed that the chromia layer which formed in wet air was much thinner compared to the one in dry air. Here, the scale thickness was considered to be the thickness of the continuous base-oxide. The height of the flaky chromia -which looks like blades in cross-section- was ignored. Another difference between wet and dry tests was the tendency for transient oxidation. In wet air practically no transient oxidation was evident, while it was very substantial after dry tests.

The analysis of the oxide scales that developed on Ni-15Cr-0.1Ce showed that the general oxidation behavior of this system was very similar to Ni-15Cr from a compositional stand point. However, the weight changes for each alloy were substantially different. In dry air, the Ce-added system displayed significantly smaller weight gains. In wet air, the total weight change of this system was at negative values, while that for the Ce-free alloy was still positive. After tests in dry air, regions with two different colorations developed over the specimen surface. The lighter colored areas were where NiO formed as an external phase. The darker colored regions were where chromia formed as the primary oxide. A back scattered SEM image of the specimen surface is given in Figure 6.8. Increasing exposure time did not seem to cause noticeable changes on the grain size of Cr_2O_3 . However, the grain size of NiO increased remarkably. Figure 6.9 shows the progression with time. The cross-section of the sample showed that in some parts of the specimen, chromia formed as a single-layered protective external oxide. However, in regions where the NiO islands developed, it formed as an internal scale, Figure 6.10. Still, the continuity was established. Comparison of dry exposed Ni-15Cr to Ni-15Cr-0.1Ce showed that the thickness of the transient oxide protrusions were larger for the former case. Also, the chromia scale was thicker for the Ce-free alloy, even though the difference was not very substantial.



(a)



(b)

Figure 6.8: Low-magnification SEM image of Ni-15Cr-0.1Ce showing the NiO (light-colored) and chromia formation over the surface at 700°C after exposing the alloy to dry (a) for 240 cycles, and (b) for 700 cycles.

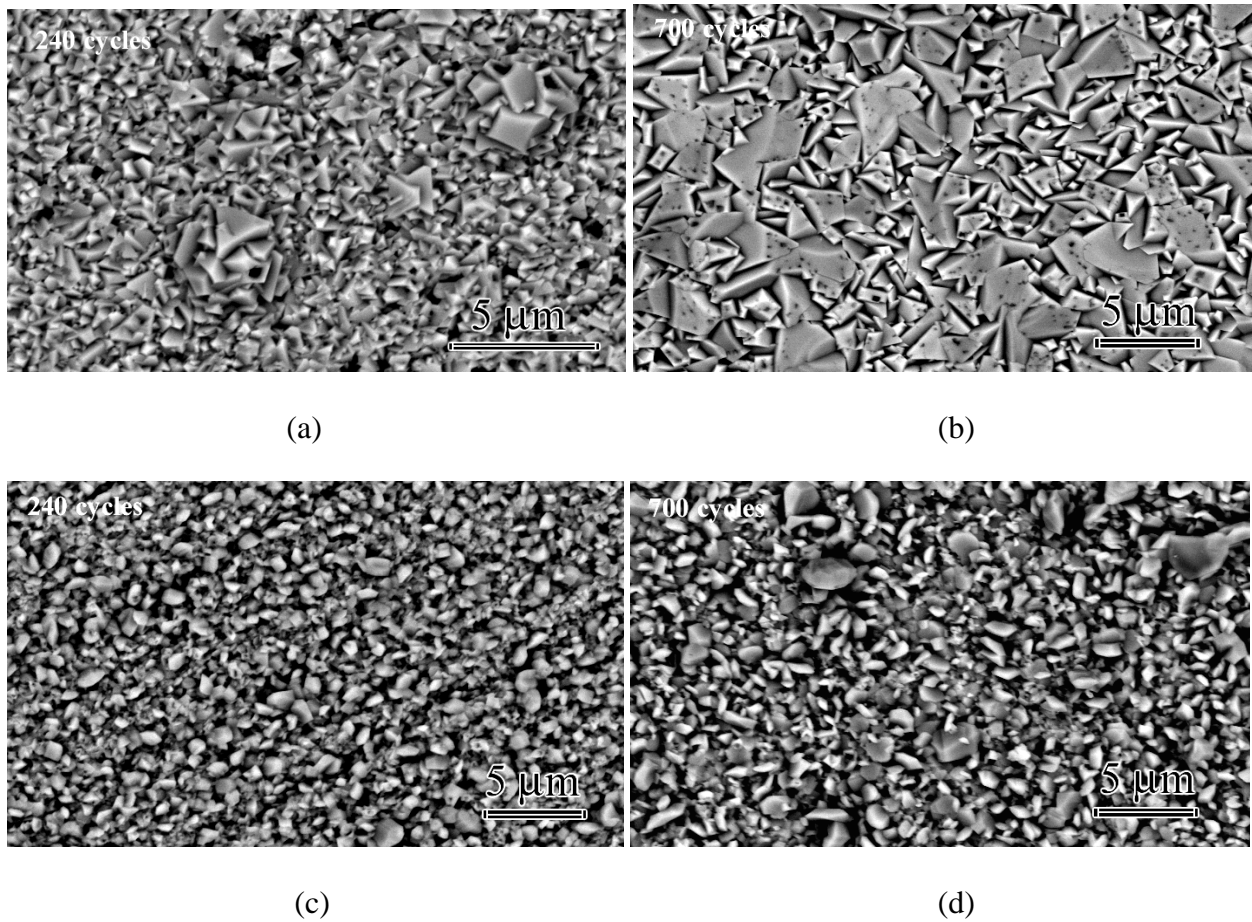
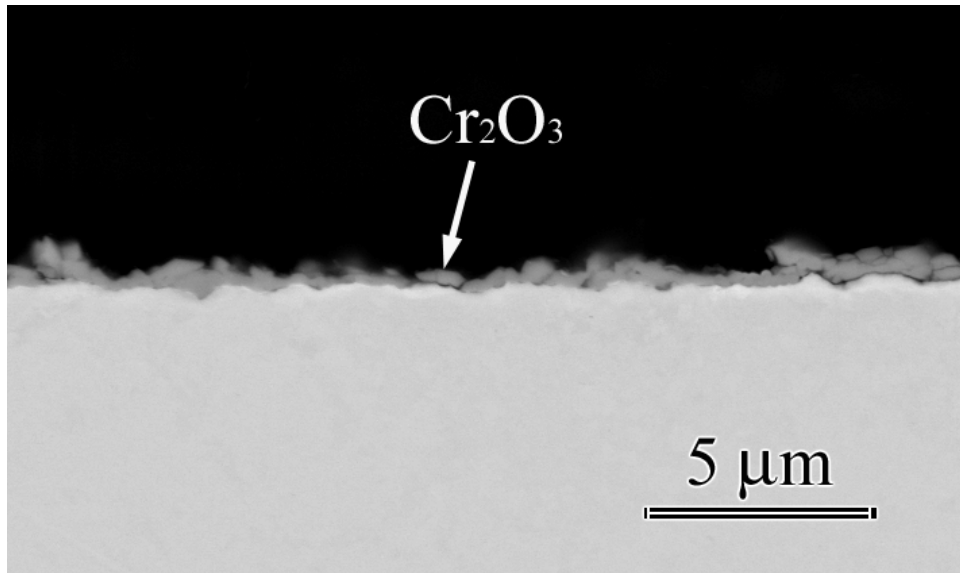
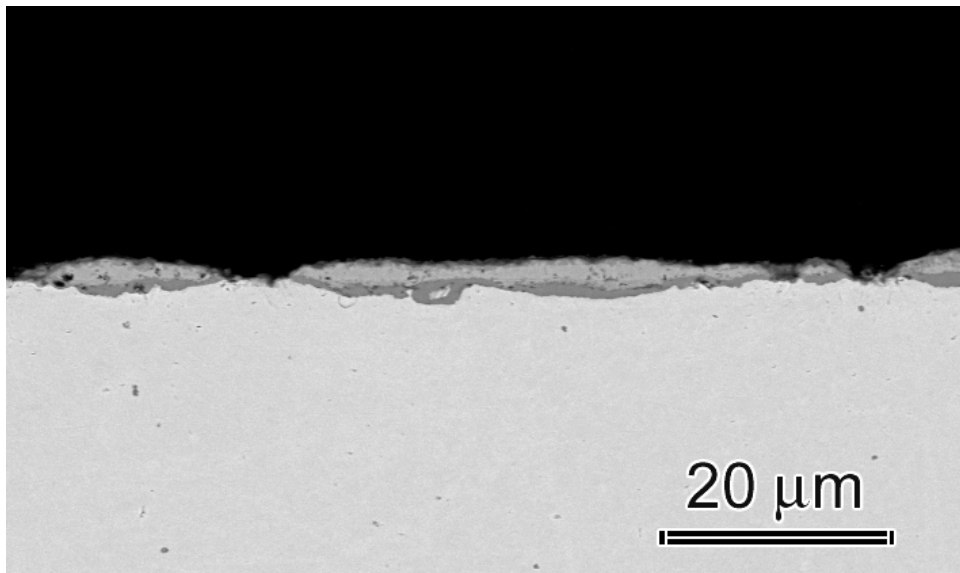


Figure 6.9: Ni-15Cr0.1Ce at 700°C in dry air (a-c) after 240 hours of cyclic testing, and (b-d) after 700 hours of cyclic testing. (a-b) NiO, (c-d) Chromia.

Exposures in air/water-vapor mixtures resulted in the development of continuous chromia scales over the specimen surface. The Cr_2O_3 crystals with the flake-like morphology which were first observed on Ni-15Cr after wet tests were present on this sample as well, Figure 6.11. Comparisons revealed that they formed even more substantially over the Ce-added system. Similarly, no transient oxidation was detectable on the sample. Figure 6.12 shows the scale in cross-section. As the image illustrates, a thin layer of chromia separated the gas environment



(a)



(b)

Figure 6.10: Back-scattered electron image of Ni15Cr0.1Ce showing the cross-section of the scale that formed at 700°C in dry air after 700 cycles. (a) Continuous chromia, (b) Transient oxides.

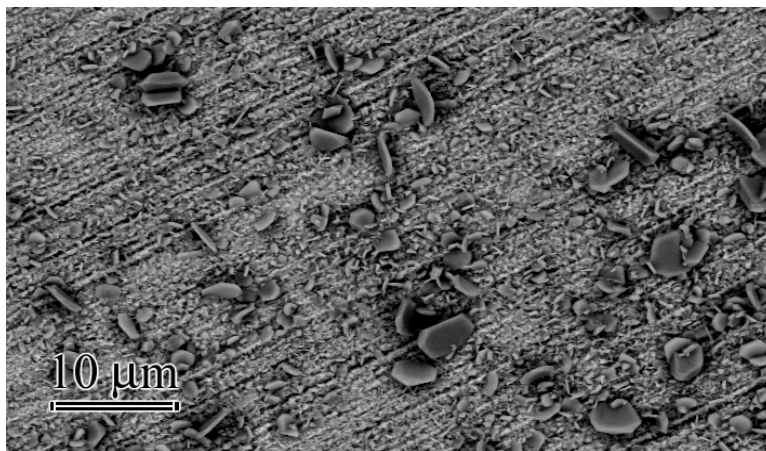
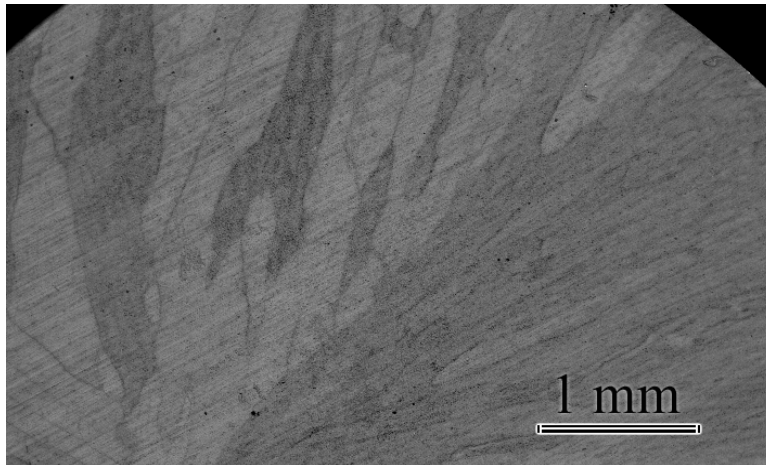


Figure 6.11: Back-scattered SEM image of Ni-15Cr-0.1Ce at 700°C after 240 cycles in wet air. Micrographs show the surface of the oxide scale that developed.

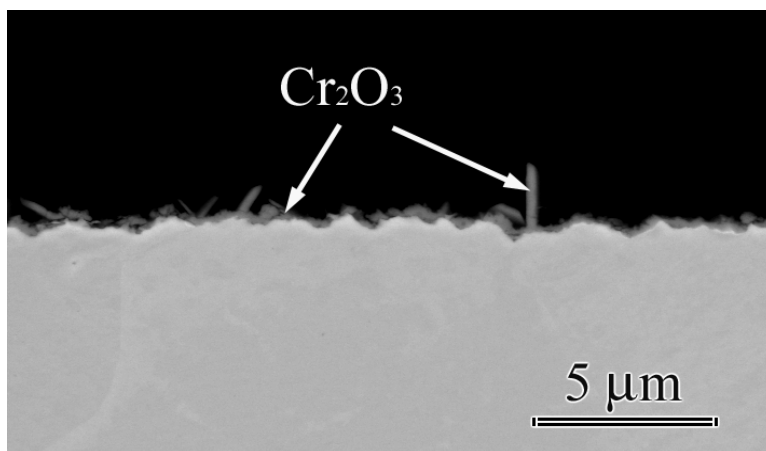
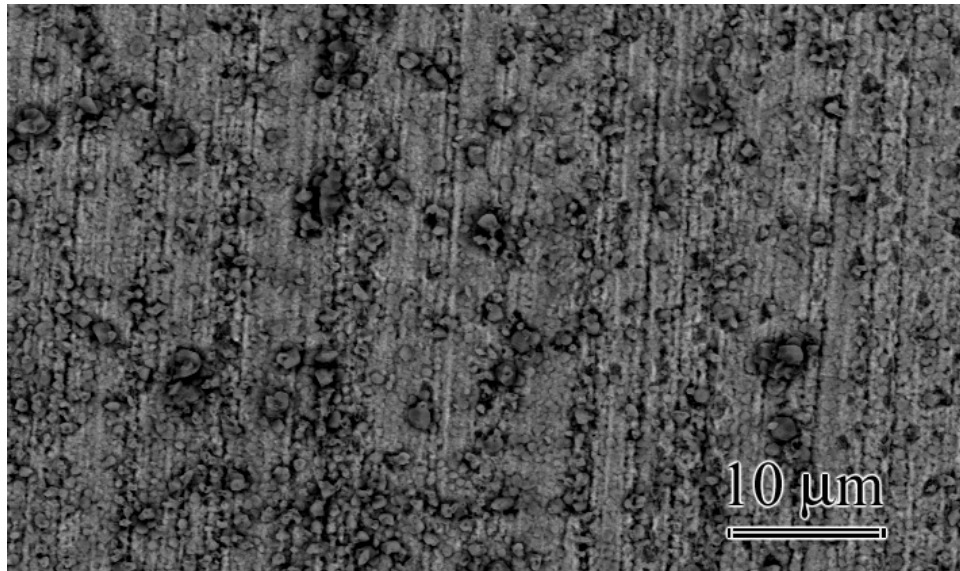


Figure 6.12: SEM image of Ni-15Cr-0.1Ce showing the oxide layer that developed at 700°C in wet air after 700 cycles in cross-section.

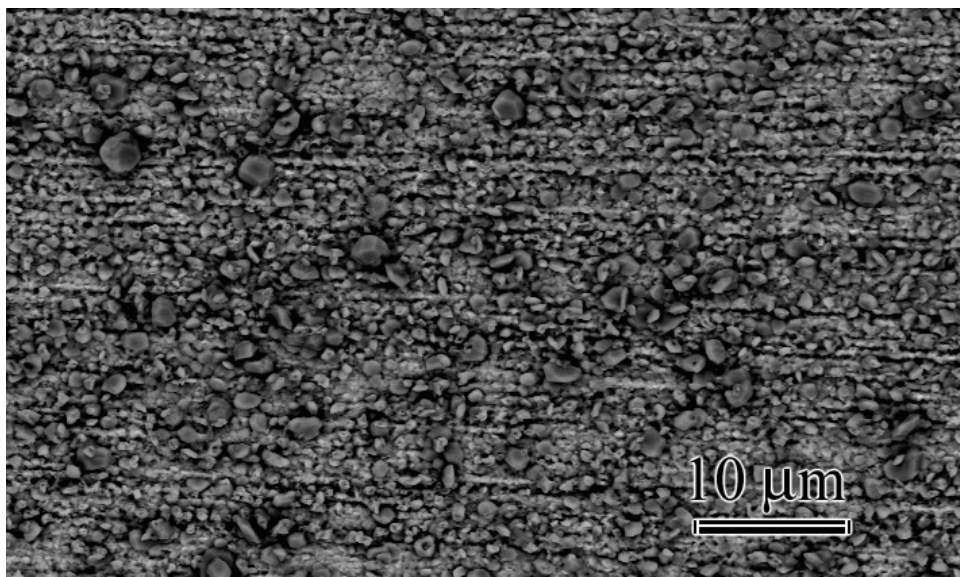
from the substrate. The thickness of this scale was observed to be smaller in comparison to the one that developed in dry air. However, no noticeable differences existed between Ni-15Cr and Ni-15Cr-0.1Ce in the wet environment.

Tests with Ni-20Cr showed that oxidation was more aggressive in dry air than in air/water-vapor mixtures. In dry air a thin chromia scale covered the surface. Granular Cr_2O_3 particles were observed to develop over this continuous scale. These particles were morphologically different from the flakey Cr_2O_3 found on Ni-15Cr and Ni-15Cr-0.1Ce after wet tests. Over time, the continuous chromia became thicker. However, its composition did not change. The grain size of the Cr_2O_3 crystals was also observed to remain the same. However, the thickening base-oxide started to overgrow it. Figures 6.13(a) and 6.13(b) show the surface images of the alloy after exposures for 240, and for 700 cycles, respectively. Cross-sectional examination showed that while the major part of the specimen surface was covered by a thin chromia scale. Areas with profuse transient oxidation were also present. Figure 6.14 shows the chromia layer, as well as the transient oxides.

Similar to dry air, a Cr-rich oxide developed on the surface of the specimen subjected to testing in air/ H_2O mixtures. The granular Cr_2O_3 crystals which were present on the dry exposed specimen formed also after wet tests alongside the flakey chromia that was observed in wet air with the previously mentioned Ni-Cr alloys. The granular crystals were much smaller in size ($<0.5 \mu\text{m}$ in diameter), and constituted a small fraction of the total chromia crystals. The oxide with the flakey morphology formed more widely and in a range of sizes (between ~ 1 to several microns in diameter). Figures 6.15 and 6.16 show the surface and the cross-sectional images of the specimen, respectively. Comparison of chromia thicknesses in wet and dry air showed that

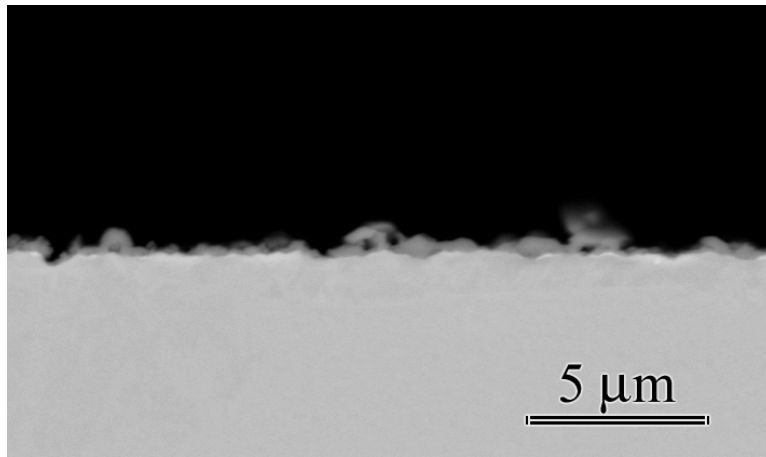


(a)

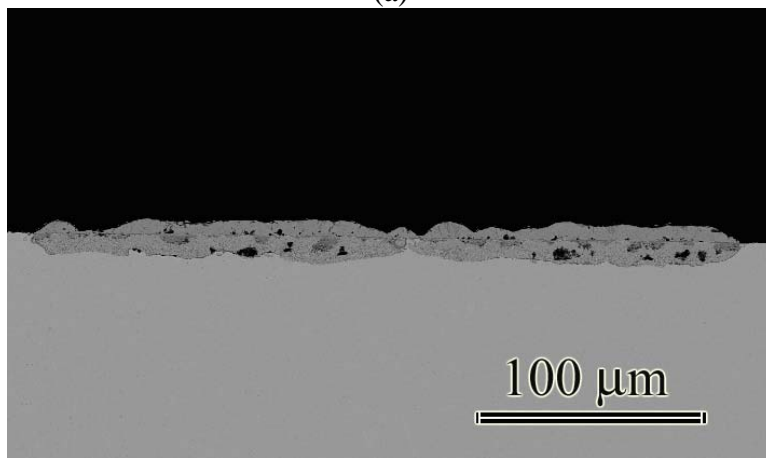


(b)

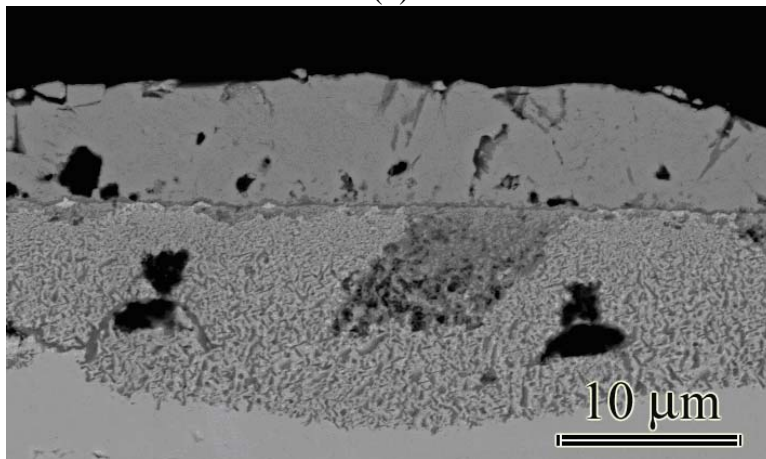
Figure 6.13: Back-scattered electron images show the surface of the Ni-20Cr specimen after cyclic tests in dry air at 700°C. (a) Ni-20Cr at 700°C after 240 cycles, and (b) Ni-20Cr at 700°C after 700 cycles in dry air.



(a)



(b)



(c)

Figure 6.14: Cross-section of Ni-20Cr at 700°C after 700 cycles in dry air (a) Chromia scale (b-c) transient oxides.

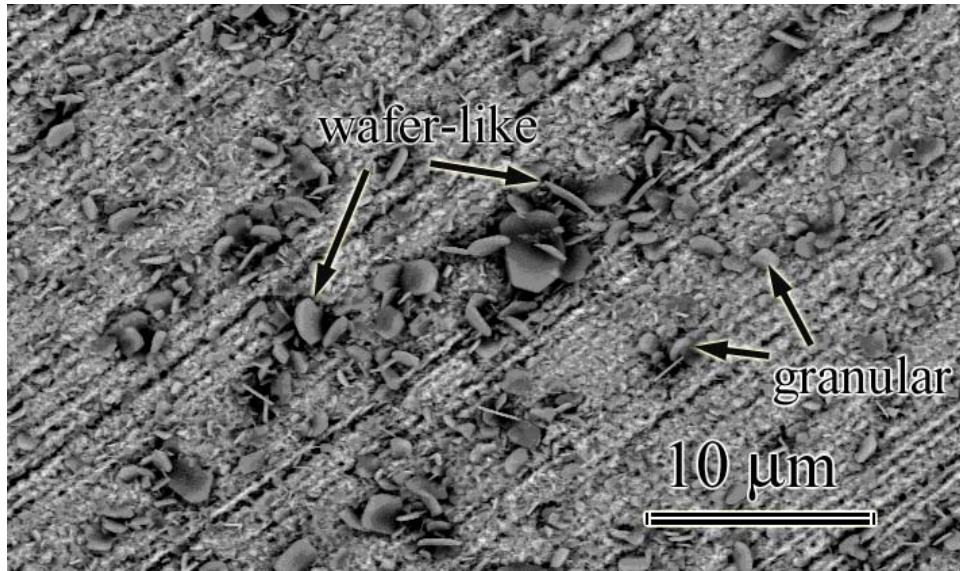


Figure 6.15: Ni-20Cr in wet air at 700°C after 240 cycles.

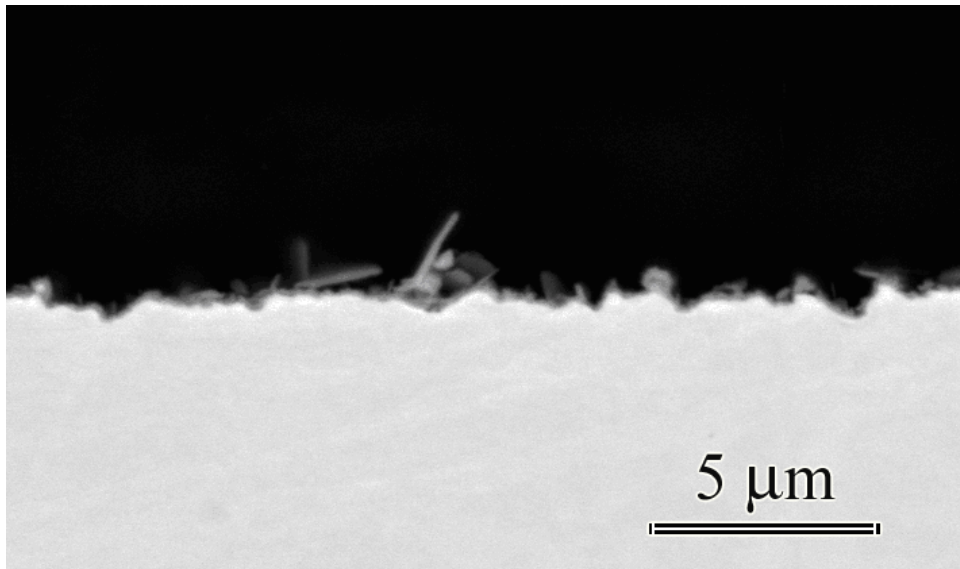


Figure 6.16: SEM image of Ni-20Cr at 700°C in wet air after 700 cycles. Micrograph shows the cross-section of the specimen.

the scale that developed in air/H₂O mixtures was thinner. Also, there was no evidence for transient oxidation in this environment.

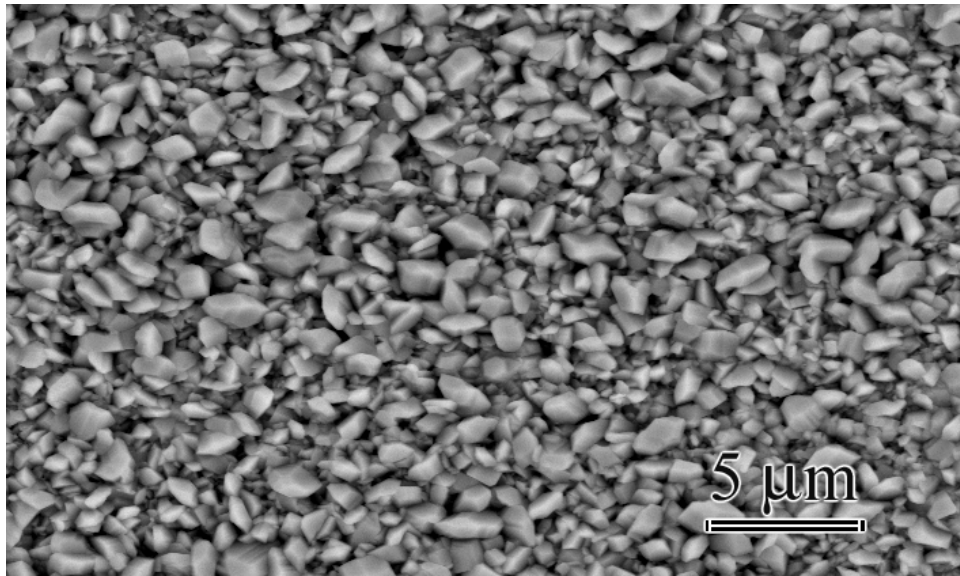
The total weight gain of the specimen in wet air after 700 hours of cyclic exposures was less compared to dry, Figures 6.1 and 6.2. Weight losses were observed in wet air, while they were not as noticeable during dry exposures.

Comparison of Ni-20Cr, Ni-15Cr and Ni-15Cr-0.1Ce showed that for these alloys transient oxidation was a problem mostly in dry air. Increasing the Cr content from 15 wt% to 20 wt% improved the resistance of the system to non-protective oxide formation substantially. In air/water-vapor mixtures, none of the alloys displayed noticeable signs of transient oxide formation. Instead, thin layers of chromia scales developed on the specimen surfaces. It was also observed that, the oxide/substrate interface was generally wavy on the samples subjected to wet air tests, while it appeared to be more flat after dry tests. Comparison of the reaction kinetics showed that Ni-20Cr was the system that displayed the slowest oxidation rate in dry air. It also suffered the least from weight losses in wet air. Overall, Ni-20Cr was the alloy that had the best resistance to attack in either environment.

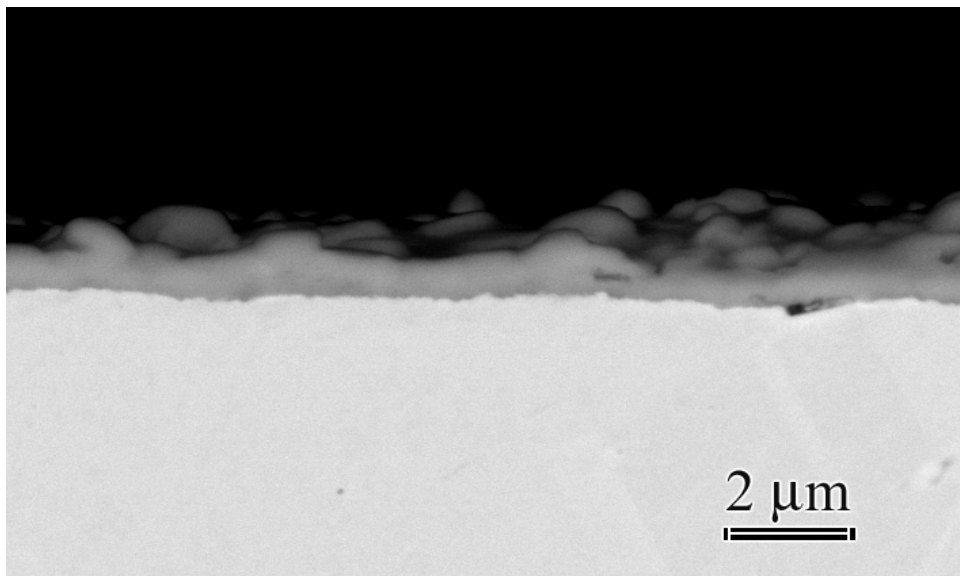
Tests with Ni-30Cr resulted in the formation of transient-oxide-free chromia scales both in dry air and in air/H₂O mixtures. The SEM images showing the surface and the cross-section of the specimen subjected to tests in dry air are given in Figure 6.17. In this environment, a thick and continuous chromia scale developed. Similar to other Ni-Cr alloys, the substrate/oxide interface was observed to be smooth. Tests in wet air also resulted in the formation of continuous layers of chromia. However, the thickness of this scale was remarkably smaller. Unlike in dry air, the oxide/matrix interface was wavy. The flakey chromia that was distinct to wet environments developed on this alloy as well. Figure 6.18 shows the back scattered electron

images of the oxide that developed over the specimen. Kinetic plots of the system showed that the reaction rate of the alloy was as fast as Ni-15Cr in dry air. However, unlike Ni-15Cr it developed protective chromia scales only, and no transient oxides. In wet air, very rapid weight losses took place. In this environment Ni-30Cr was the alloy that experienced the fastest degradation.

Examination of the specimen surfaces showed that the properties of the oxides that developed on Ni-30Cr-0.1Ce were very similar to its Ce-free version. In dry air, the reactions between the hot gases and the alloy substrate resulted in the formation of continuous chromia layers, Figure 6.19. Comparisons showed that the thickness of this scale was slightly less than the Ce-free alloy. No transient oxidation was evident either in dry air or in air/H₂O mixtures. The scale that formed in the wet environment was also not different from Ni-30Cr, Figure 6.20. The oxide/substrate interface had a wavy character. The flake-like Cr₂O₃ crystals were present over the continuous chromia scale; and even more profusely than Ni-30Cr. As discussed before, comparison of Ni-15Cr to Ni-15Cr-0.1Ce also showed that Cr₂O₃ with the flake-like morphology formed more substantially on the Ce-added alloy. For Ni-30Cr-0.1Ce, although the weight gains in dry air were more than twice larger compared to wet air, the reactions were still milder in comparison to Ni-30Cr in either environment. No extreme weight losses were observed in air/H₂O mixtures, which was a problem with Ni-30Cr. These results suggested that Ce additions improved scale adherence in wet air for Ni-30Cr. This effect was not observed very strongly on Ni-15Cr-0.1Ce. However, it should be also considered that the times of exposures were different for each system. Tests with Ni-30Cr-0.1Ce were ended at 240 cycles, while the other alloy was tested for up to 700 hours. The onset of rapid weight loss for the second system was around 370 hours. Another effect of Ce was on the reaction rates. Comparison of oxidation kinetics of Ni-

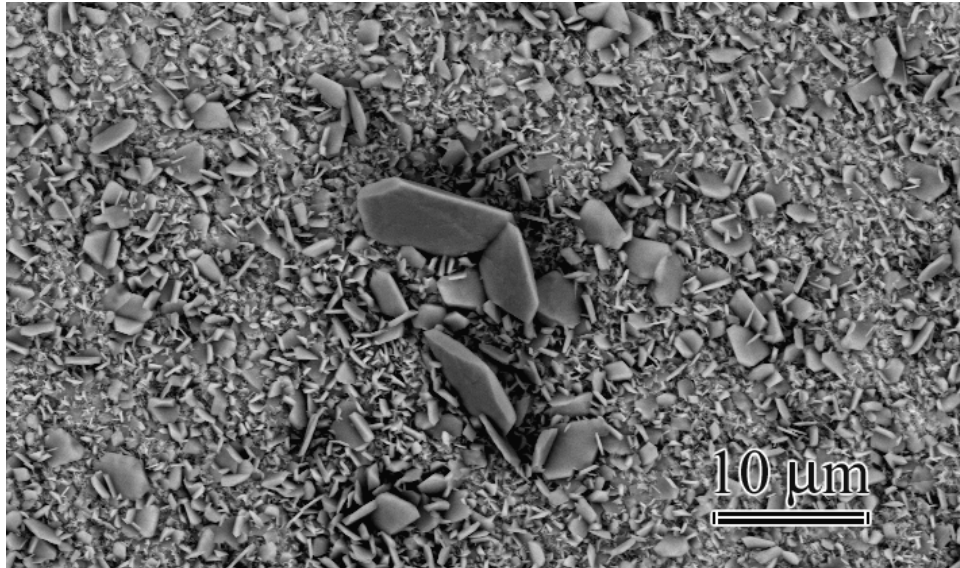


(a)

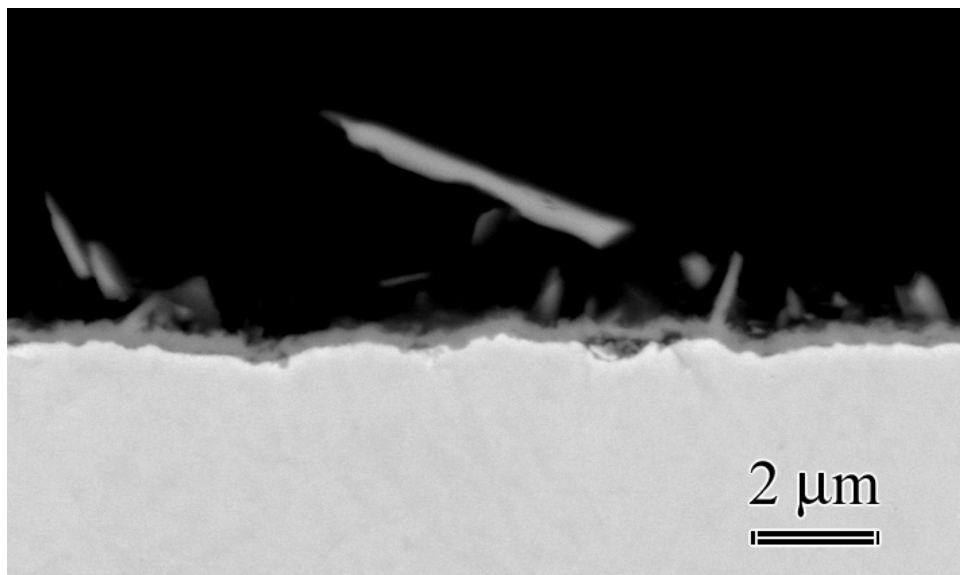


(b)

Figure 6.17: Ni-30Cr at 700°C in dry air after 240 cycles. (a) Micrograph shows the chromia that developed over the specimen surface. (b) Back scattered electron image showing the cross-section of the chromia scale. The oxide/alloy interface was observed to be flat.

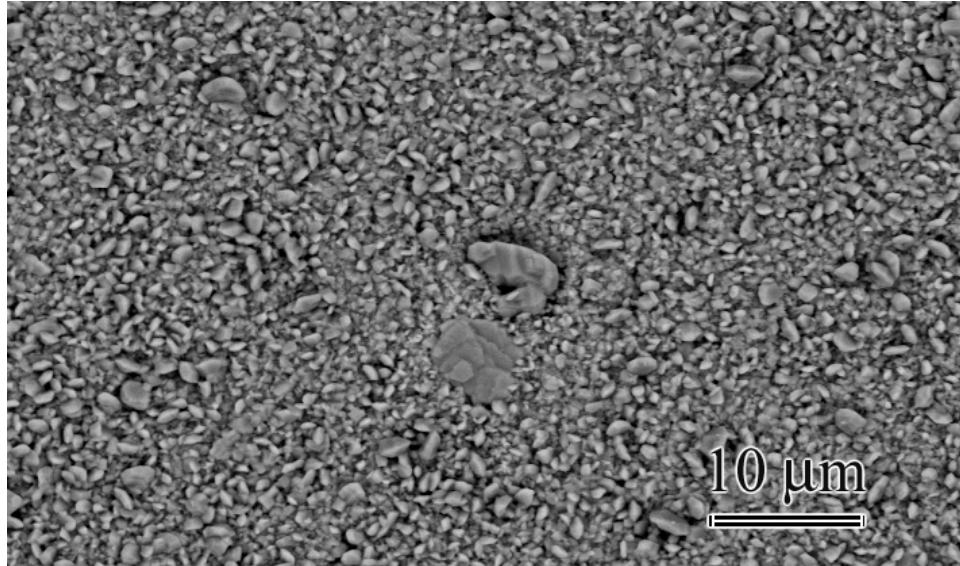


(a)

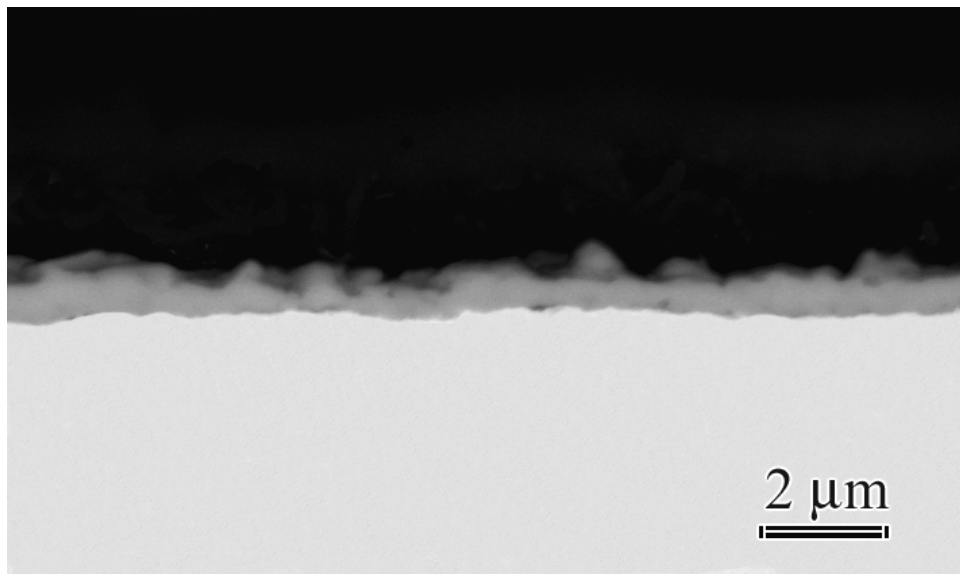


(b)

Figure 6.18: SEM image shows Ni-30Cr at 700°C in wet air after 240 cycles. (a) The surface image of the scale. Flakey Cr_2O_3 crystals developed over the continuous chromia layer. (b) Micrograph shows the oxide layer in cross-section.

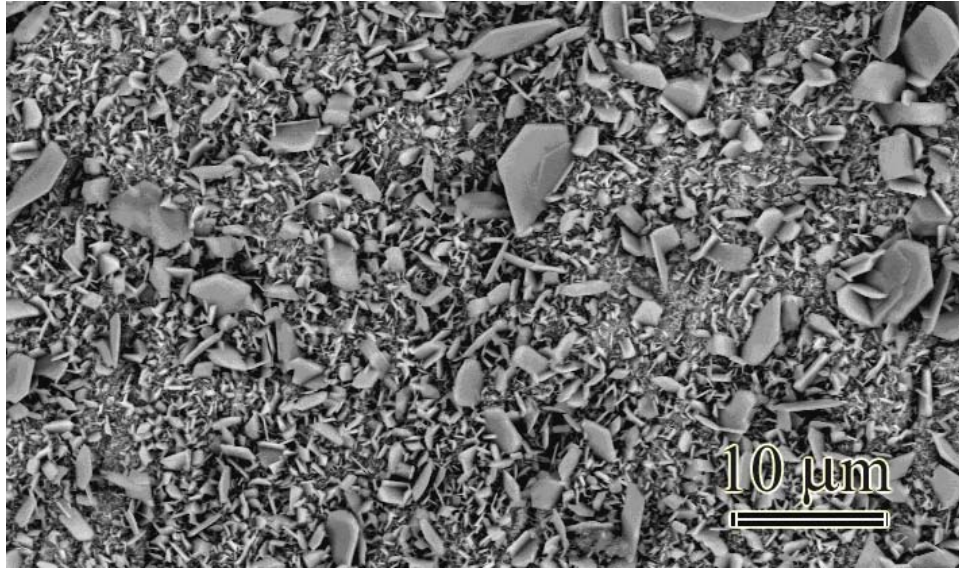


(a)

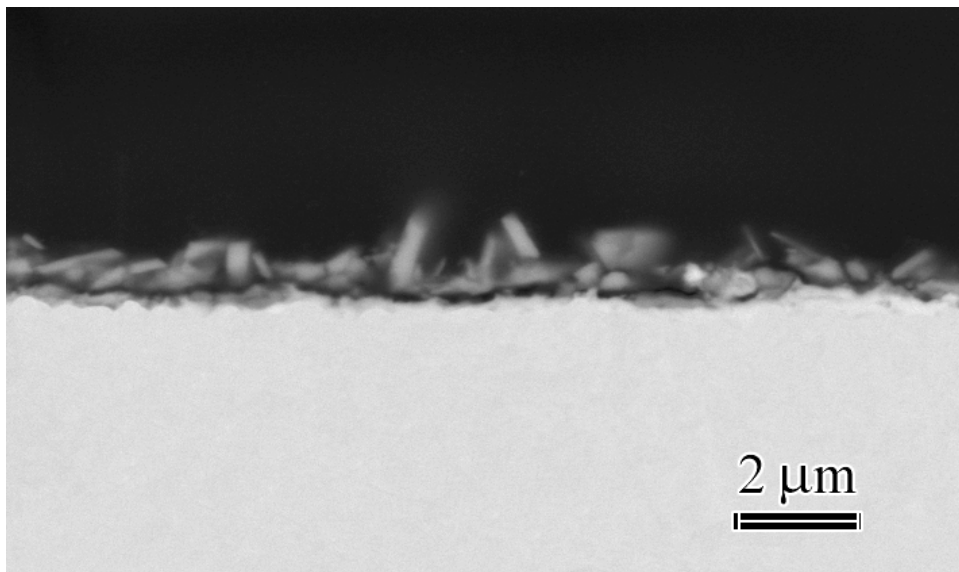


(b)

Figure 6.19: Ni₃₀Cr_{0.1}Ce in dry air at 700°C after 240 cycles. (a) Topographic image of the oxide layer. (b) Cross-section of the specimen showing the mono-layered chromia.



(a)



(b)

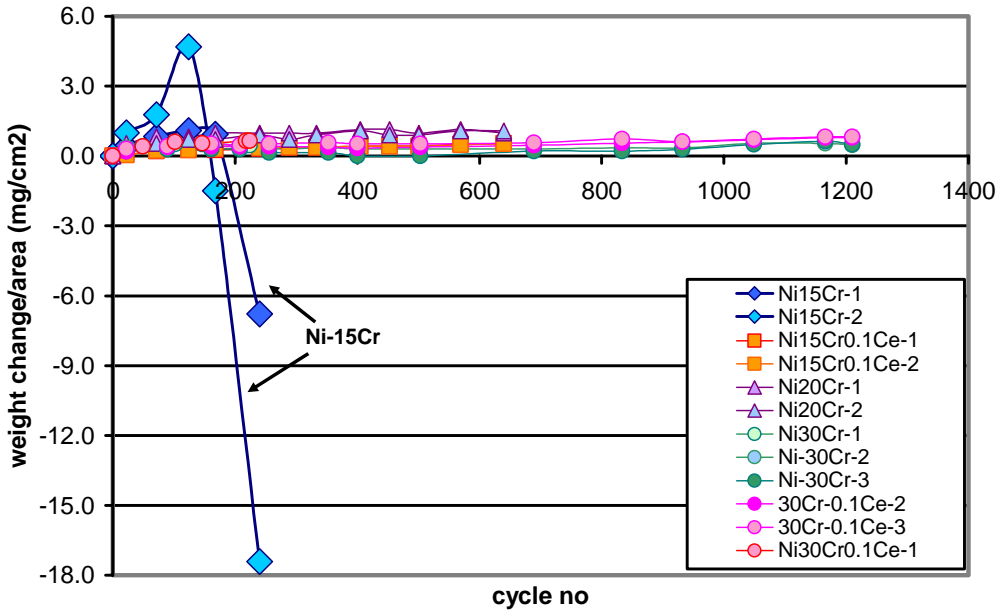
Figure 6.20: Ni-30Cr-0.1Ce at 700°C in wet air after cyclic tests for 240 hours. (a) Image shows the surface of the chromia layer that developed on the specimen. (b) Cross-sectional micrograph of the specimen.

15Cr and Ni-15Cr-0.1Ce showed that the presence of Ce in the system slowed down the reactions significantly. This effect was more subtle on Ni-30Cr-0.1Ce.

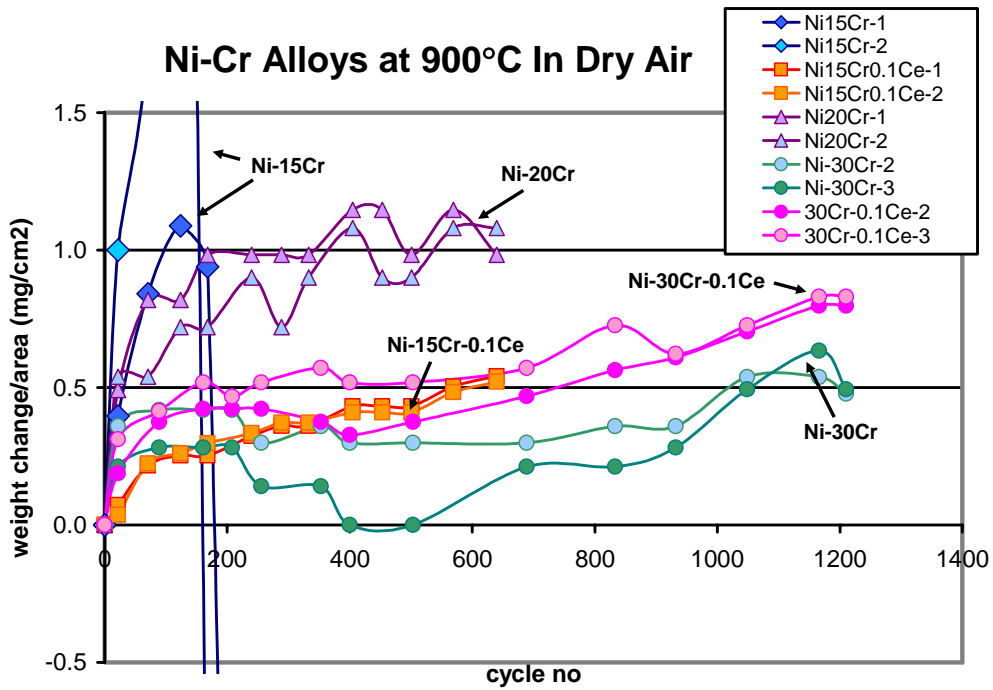
6.1.1.2 Cyclic Tests at 900°C: The exposures at 900°C resulted in very rapid reactions for the alloy Ni-15Cr. It started to form rapidly growing oxides which quickly lead to very profuse scale spallation in dry air. In the wet environment, the oxidation proceeded with high rates as well. However, no weight losses were encountered even though the tests continued for longer times (240 hours in dry air versus 650 in wet air). Instead, the system continued to gain weight steadily after the initial fast oxidation period.

The plots representing the oxidation kinetics of the alloy are given in Figures 6.21 and 6.22 for dry and wet tests, respectively. EDX analysis showed that, in dry air thick layers of NiO developed over the specimen surface. Large pieces of oxide were observed to spall off during weight measurements when the samples were taken out of the furnace, which left the oxide surface that was still in contact with a very irregular geometry. The images of the test pieces after 124, and 240 hours of cyclic exposures are shown in Figure 6.23. The SEM micrographs of the cross-sections are presented in Figure 6.24. Here, the thick and multilayered scale can be seen. Apparently, chromia could not develop continuity under the test conditions. Instead, it formed internally as fine oxide particles embedded in a Ni-rich oxide phase at the substrate/oxide interface. The layer with striations between the external NiO and the internally formed chromia/Ni-oxide phase was a laminated structure, which consisted of thin layers of NiO and chromia. This morphology indicated that the system tried to form a healing Cr_2O_3 layer, but could not maintain continuity due to the heavy depletions of the substrate in Cr.

Ni-Cr Alloys at 900°C In Dry Air



(a)



(b)

Figure 6.21: The weight changes of Ni-Cr alloys at 900°C in dry air are plotted as a function of cycle number (a) on a large scale, and (b) on a smaller scale to show the details.

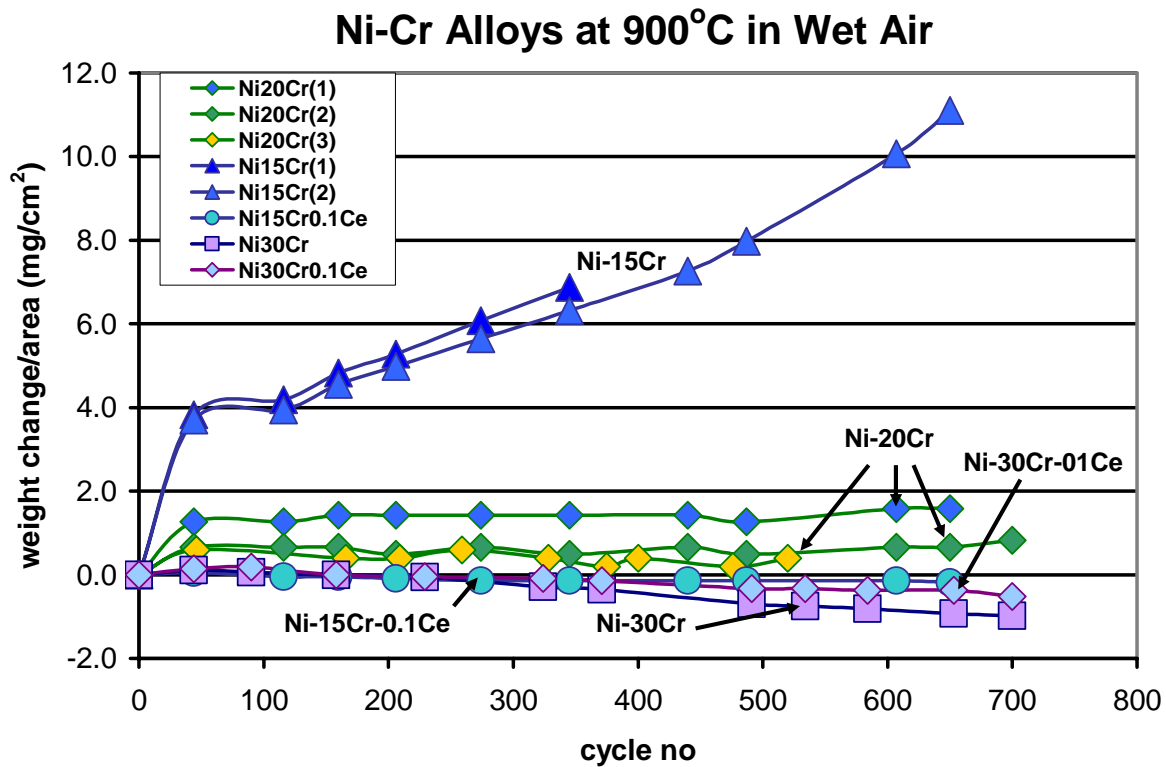


Figure 6.22: The weight changes of Ni-Cr alloys at 900°C in wet air are shown as a function of cycle number. Each cycle was a 1 hour period with 45 minutes in the hot zone and 15 minutes in the cool zone of the furnace.

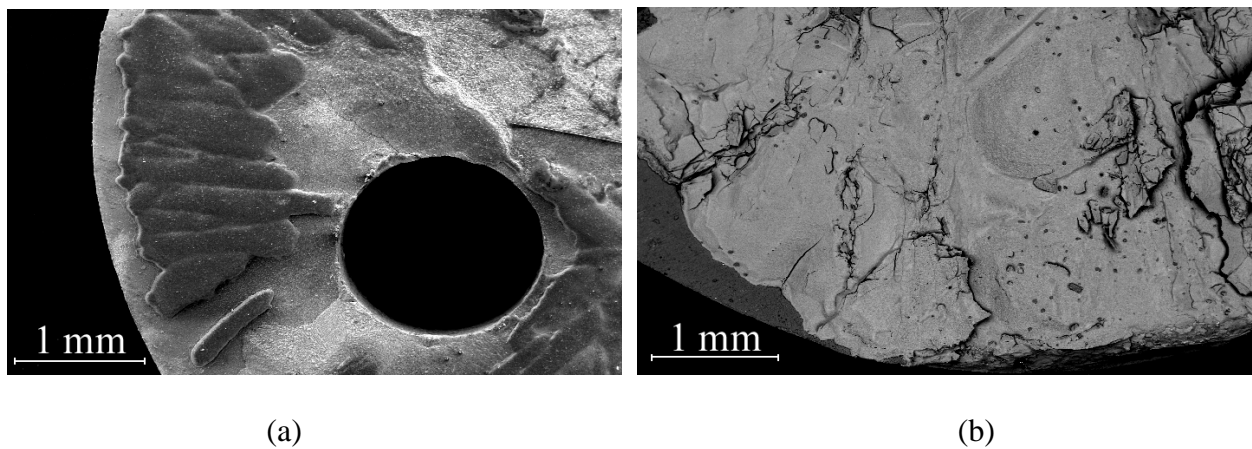
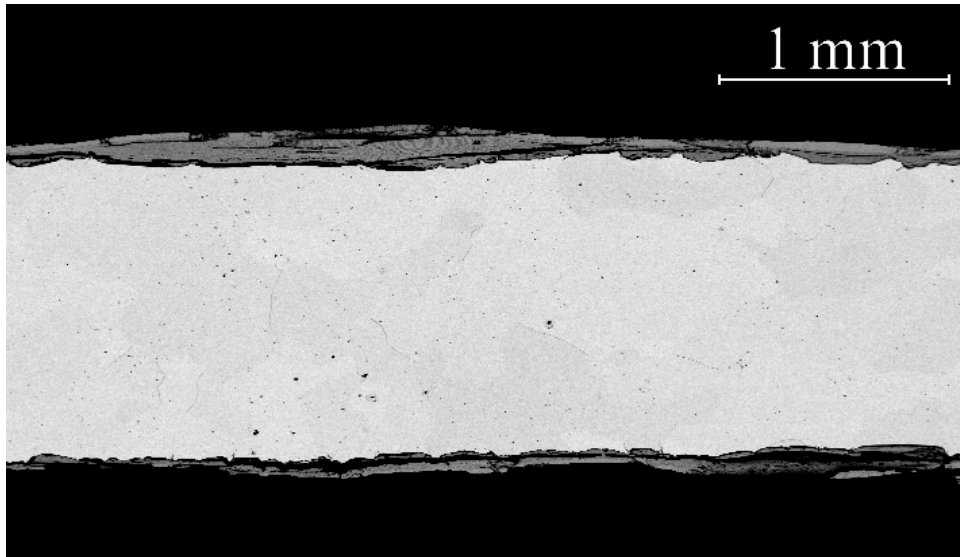
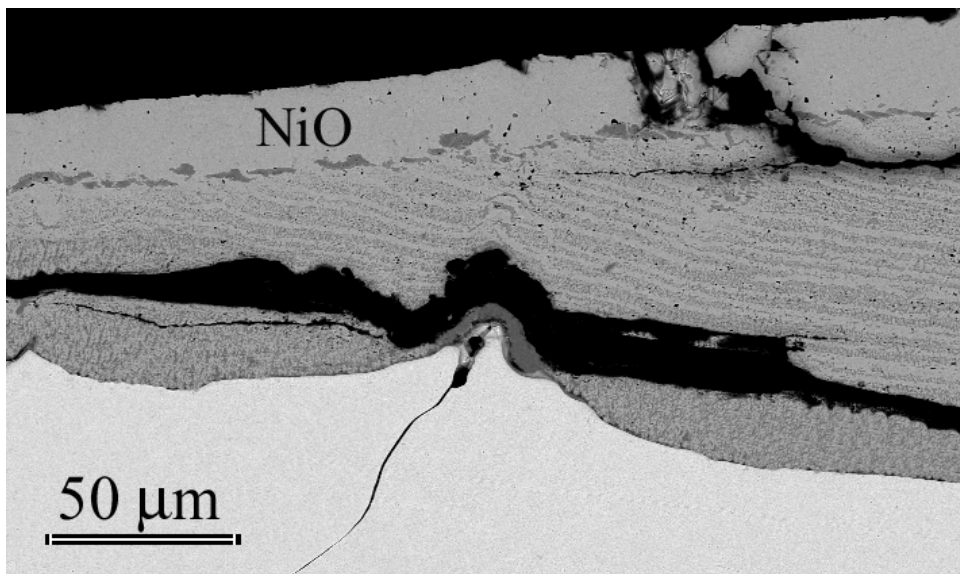


Figure 6.23: Secondary electron images show the surface of Ni-15Cr after cyclic tests in dry air at 900°C (a) for 124 hours, and (b) for 240 hours.



(a)



(b)

Figure 6.24: Back scattered electron images of the scale cross-section that developed on Ni-15Cr at 900°C in dry air after cyclic tests for 240 hours.

In wet air, the reactions leading to NiO formation proceeded slower. Initially, chromia was the primary oxide phase that developed on the specimen surface. In time, NiO formation became more aggressive, and eventually took over the chromia scale. Figure 6.25 shows the surface of the alloy at two different exposure times. These images show the transition from chromia to NiO as the dominating oxide phase. After 650 hours, the external scale consisted of NiO only. Cross-section of the specimen showed that, chromia developed as an internal oxide. It started to form in the vicinity of the grain boundaries which acted as fast diffusion paths, and eventually developed continuity by a lateral growth along the oxide/substrate interface, Figure 6.26. In dry air, although there was evidence for chromia formation at and around the grain boundaries, the alloy was not able to develop continuity the same way it did in wet air, Figure 6.24. A cartoon demonstrating schematically the oxidation in wet and dry air is given in Figure 6.27.

The kinetic data of the Ni-15Cr-0.1Ce system suggested that the addition of Ce as a reactive element improved the resistance of the alloy to transient oxidation. In dry air, although the specimen continued to gain weight steadily, the total mass gain was remarkably smaller compared to Ni-15Cr. It was even less than Ni-20Cr, which is an alloy expected to develop

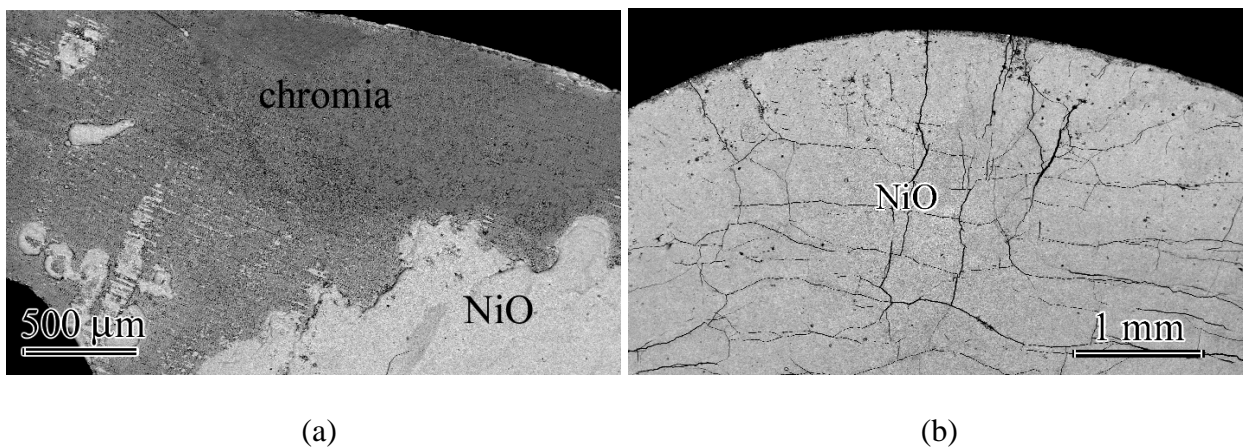
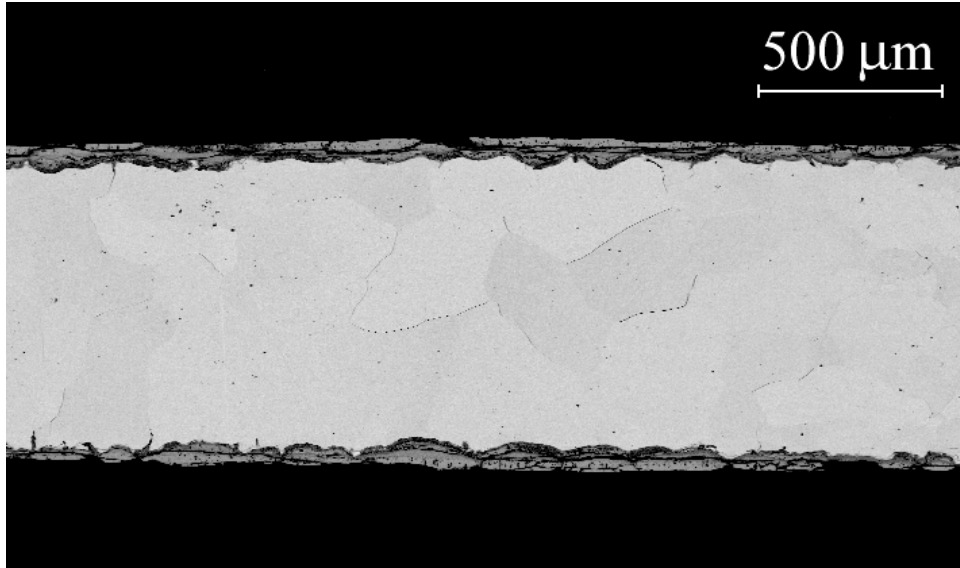
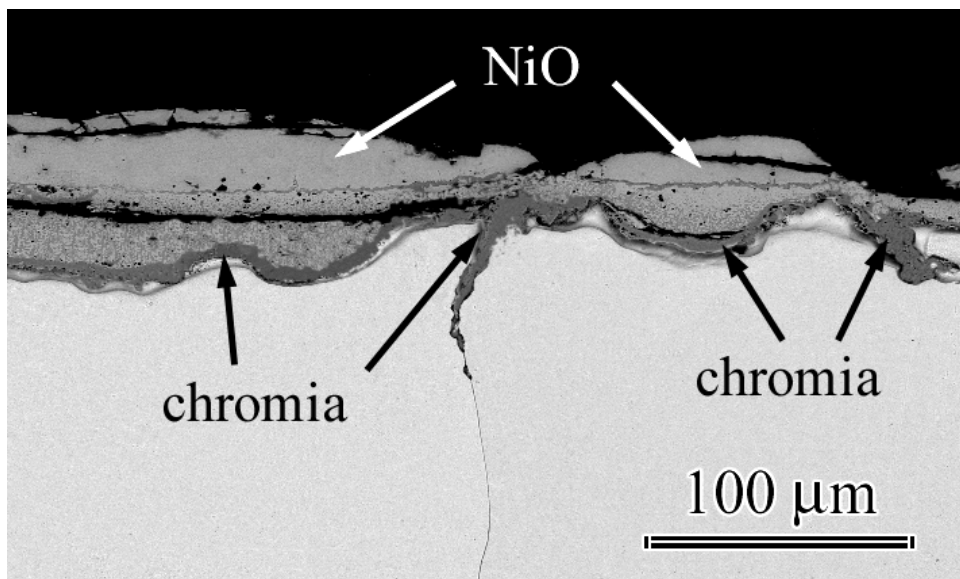


Figure 6.25: Secondary electron images show the surface of Ni-15Cr after cyclic tests in wet air at 900°C (a) for 206 hours, and (b) for 650 hours.



(a)



(b)

Figure 6.26: Back scattered electron images of the scale cross-section that developed on Ni-15Cr at 900°C in wet air after cyclic tests for 350 hours.

slower growing chromia easier due to its higher Cr concentration. In wet air, the oxidation kinetics of the alloy was comparable to the other Ce-added alloy, i.e. Ni-30Cr-0.1Ce.

Surface analysis showed that, in dry air, the scale that formed consisted mainly of chromia. Formation of NiO in some areas was also evident. In Figure 6.28 these areas are labeled. Although the region where NiO developed initially did not spread wider, small blisters of this oxide started to form on the chromia phase during later stages of oxidation. It was observed that their size and number increased over time, Figure 6.29. The cross-section of the scale after 1000 hours of cyclic exposures is shown in Figure 6.30. In this environment, a thin and porous chromia developed at the specimen surface. Void formation at the oxide/substrate interface and in the depleted zone was very pronounced. Some internal oxidation was also evident. It was observed that both the oxide/substrate and the substrate/gas interfaces were irregularly shaped.

Tests in air/H₂O mixtures resulted in the formation of scales similar to dry air. Figure 6.31 shows the low magnification image of the alloy surface after 206 cycles. The reaction zone consisted of chromia and some NiO. However, unlike in dry air, prolonged exposures did not cause formation of additional NiO blisters. After 700 hours, the scale still consisted of chromia, Figure 6.32. The cross-section of the specimen showed that this chromia was compact rather than porous. Although there was some internal oxidation, it was much less than the dry case.

Tests in dry air with the system Ni-20Cr resulted in the formation of chromia scales. The grain size of chromia was observed to increase with time, Figure 6.34. Although some NiO formation was detected, as shown in Figure 6.35, it was less significant than Ni-15Cr-0.1Ce or Ni-15Cr. Chromia was observed to develop as a continuous scale with uniform thickness over the alloy. Detachments at the scale/substrate interface were evident, Figure 6.36. However, they did not lead to oxide spallation.

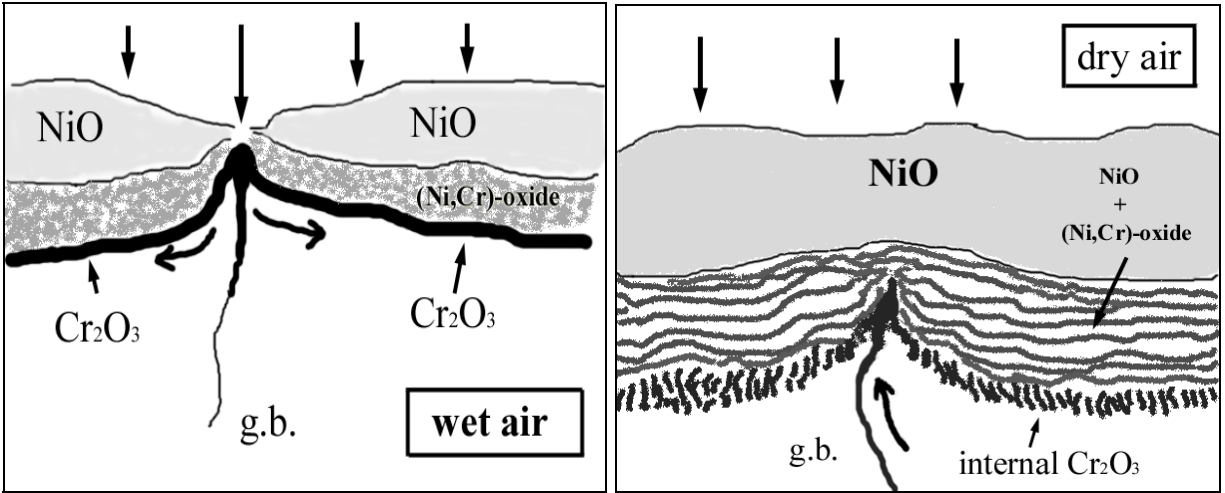


Figure 6.27: In wet air, fast diffusion of Cr through the grain boundaries results in the formation of Cr_2O_3 at and around the boundary. Chromia grows laterally and eventually develops a continuous layer at the substrate/oxide interface. In dry air, although Cr diffuses through the grain boundaries, it can not develop continuity. Instead, it forms as an internal oxide.

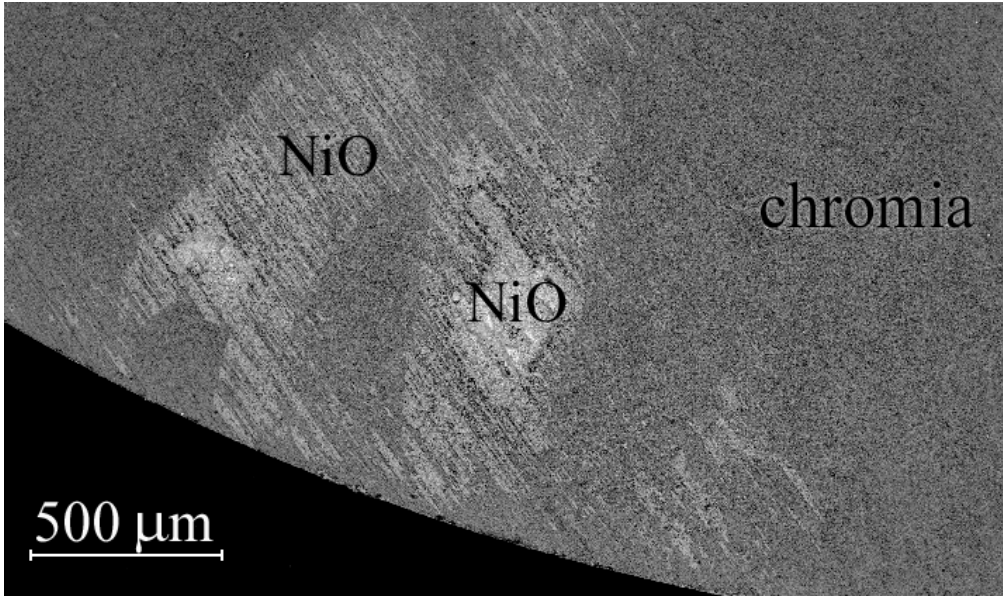
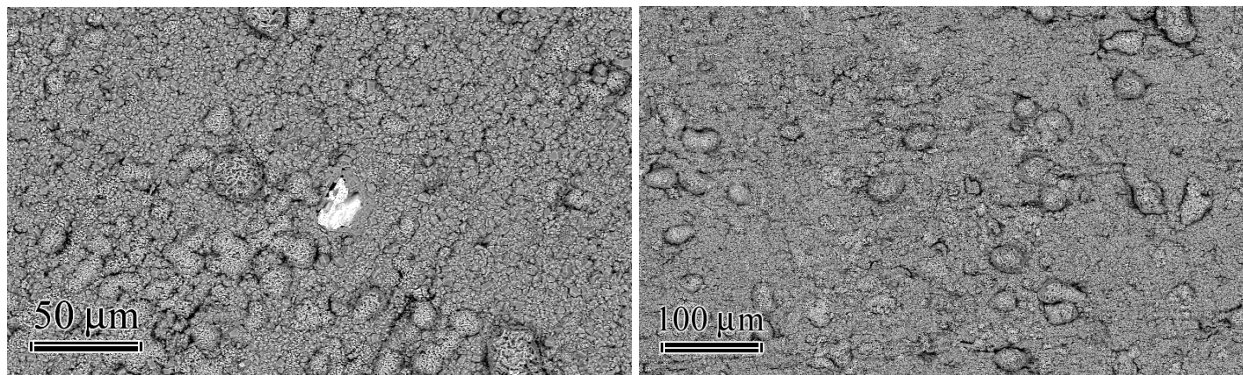


Figure 6.28: Ni-15Cr-0.1Ce at 900°C in dry air after 124 cycles. Image shows the surface of the alloy. Chromia was the main oxide phase that developed on the alloy surface. However, formation of NiO was also observed.



(a)

(b)

Figure 6.29: Ni-15Cr-0.1Ce at 900°C in dry (a) after 500 cycles, and (b) after 1000 cycles. Images show formation of NiO blisters over chromia. In time their size and number increased. Note that the scales for each micrograph are different.

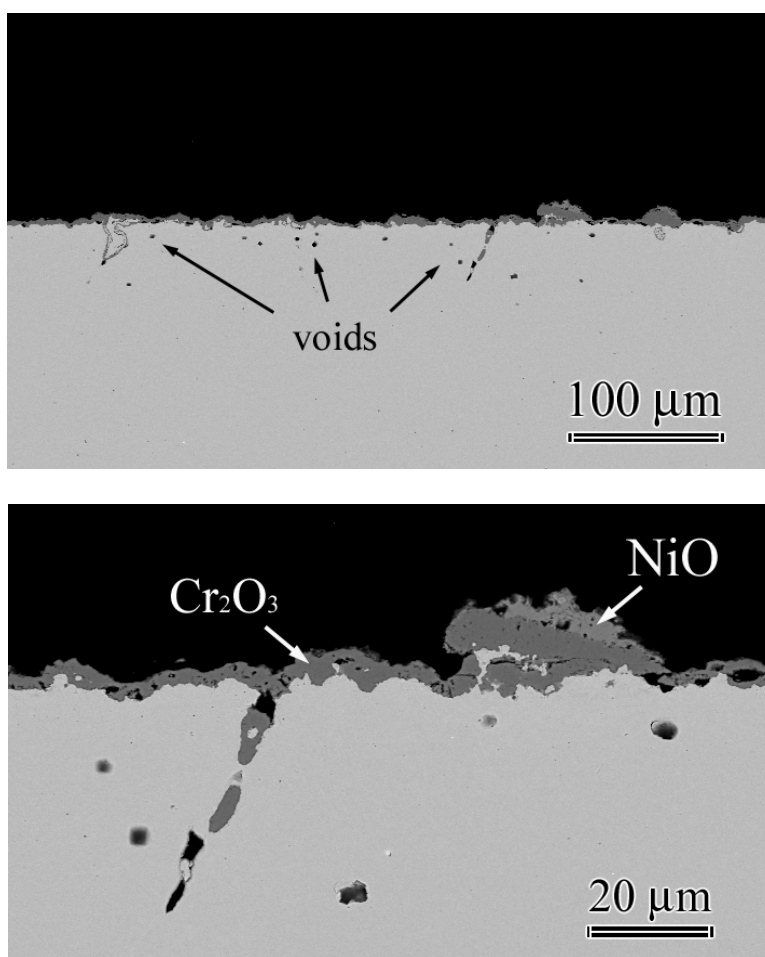


Figure 6.30: Ni-15Cr-0.1Ce at 900°C in dry air after 1000 cycles.

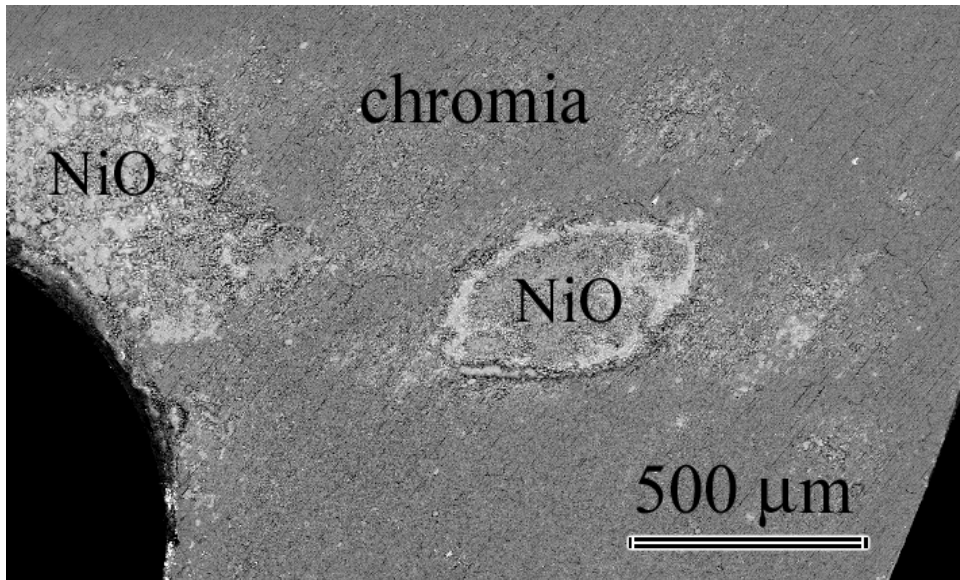


Figure 6.31: Ni-15Cr-0.1Ce in wet air after 206 cycles at 900°C.

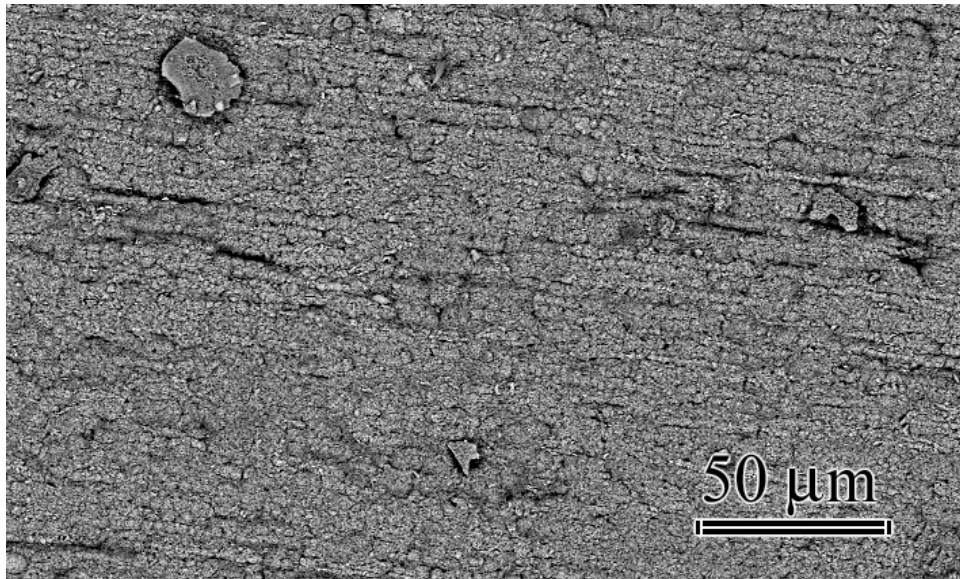


Figure 6.32: Ni-15Cr 0.1Ce at 900°C in wet air after 700 cycles.

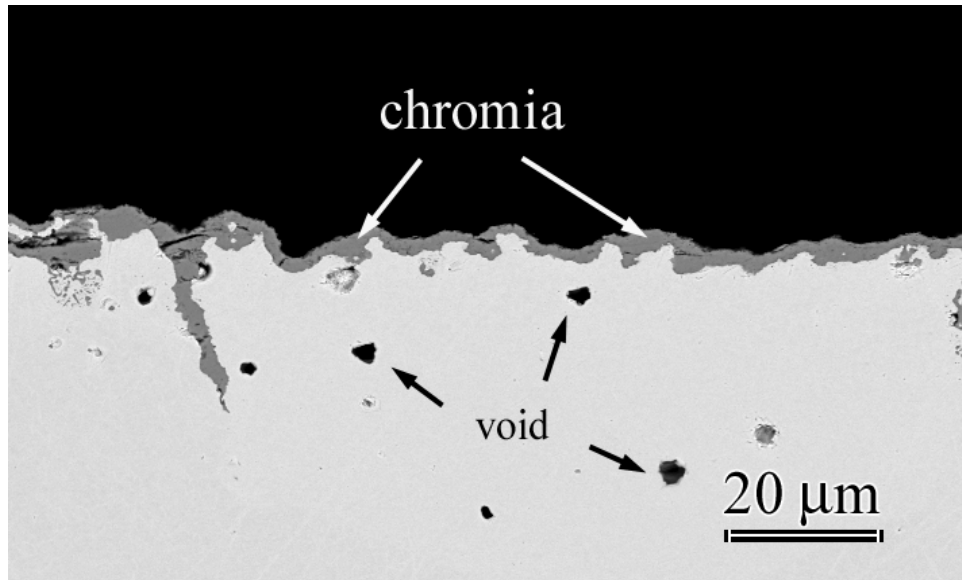


Figure 6.33: Ni-15Cr-0.1Ce in wet air at 900°C after 700 cycles.

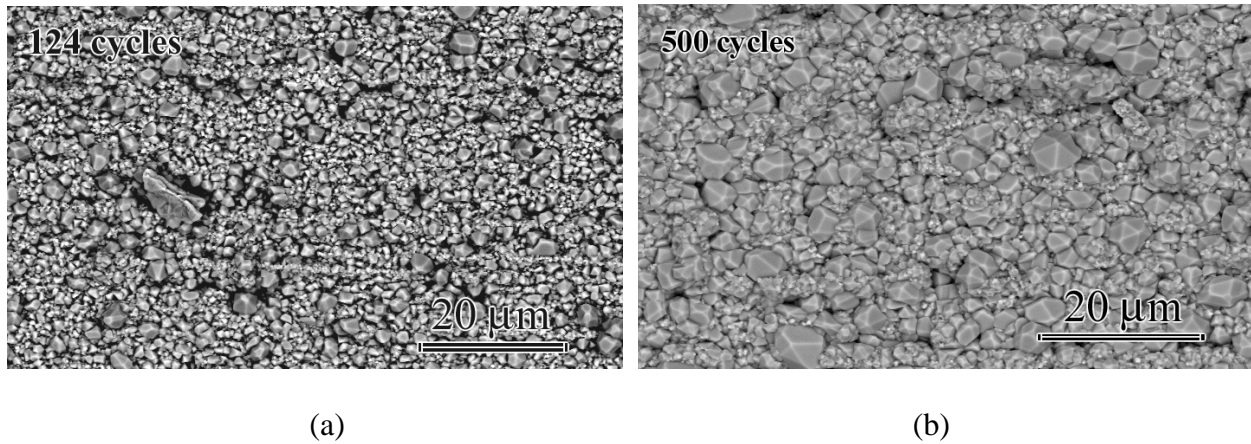


Figure 6.34: Ni-20Cr at 900°C in dry air (a) after 124 cycles, and (b) after 500 cycles.

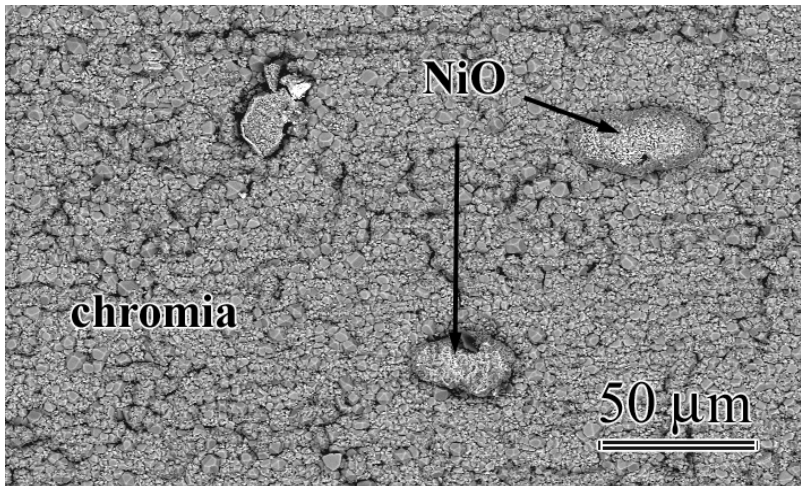


Figure 6.35: Ni-20Cr in dry air at 900°C.

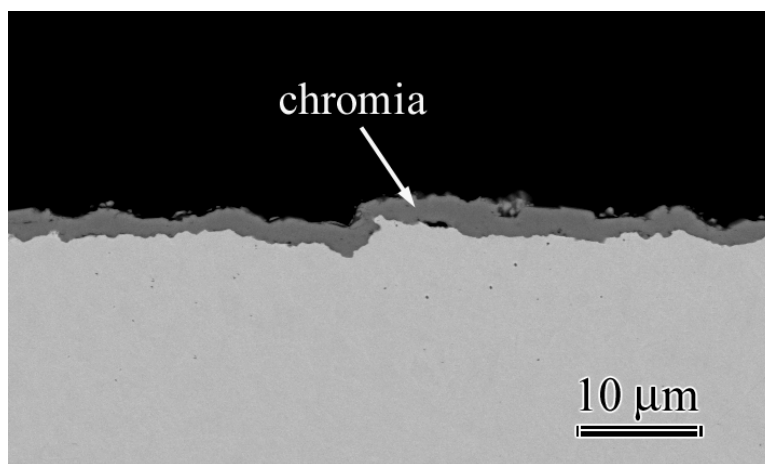
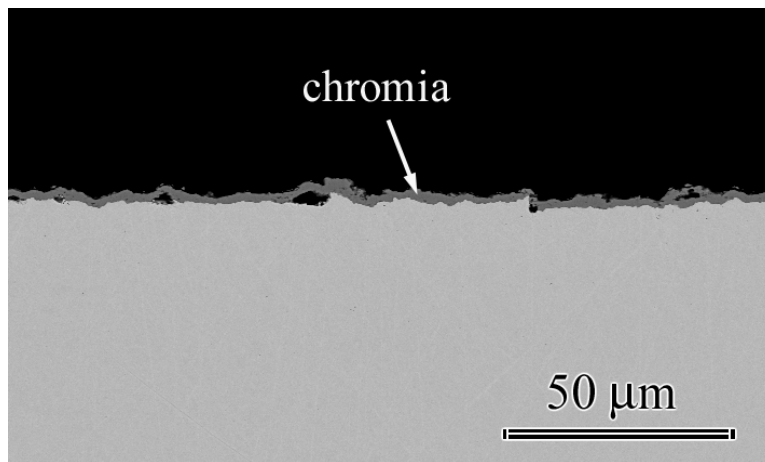


Figure 6.36: Ni-20Cr at 900°C in dry air after 1000 cycles.

The specimens subjected to cyclic tests in air/H₂O mixtures developed chromia and NiO scales. The images showing the specimen surfaces at low magnification are given in Figure 6.37. Examination of the surfaces at different stages of oxidation showed that, the size of the area where NiO had initially formed remained the same until the end of the tests. The Cr₂O₃ crystals with the flake-like morphology that were observed to be unique to air/H₂O mixtures were detected over this alloy as well, Figure 6.38. Cross-sectional examination of the sample showed that, the detachments noted after dry tests did not develop in wet air in areas where chromia developed as a mono-layered protective scale. However, void formation in the depleted zone, and occasionally in the chromia was noticed. The thickness of the scale was larger for the wet exposed samples. In areas where transient oxides developed, chromia formed at the oxide/substate interface as a continuous oxide. The images showing the scale cross-section are presented in Figure 6.39.

Analysis of oxidation kinetics for Ni-20Cr showed that the reaction rates in wet and dry air did not differ significantly. The weight changes of the samples were similar in both testing environments.

Tests in dry air with Ni-30Cr-0.1Ce resulted in the formation of chromia scales with significant scale spallation, which became more substantial as the exposure time increased, Figure 6.40. Large amounts of transient oxide islands were also evident, Figure 6.41. In time, the number and size of these oxide blisters increased, Figure 6.42. Cross-sectional examination of the reaction zone showed that after 224 hours of cyclic testing, a thick and fairly uniform chromia scale developed. Some NiO formation over the continuous chromia was also noted. After 1210 cycles, the oxide layer became very irregular. Substantial internal oxidation was

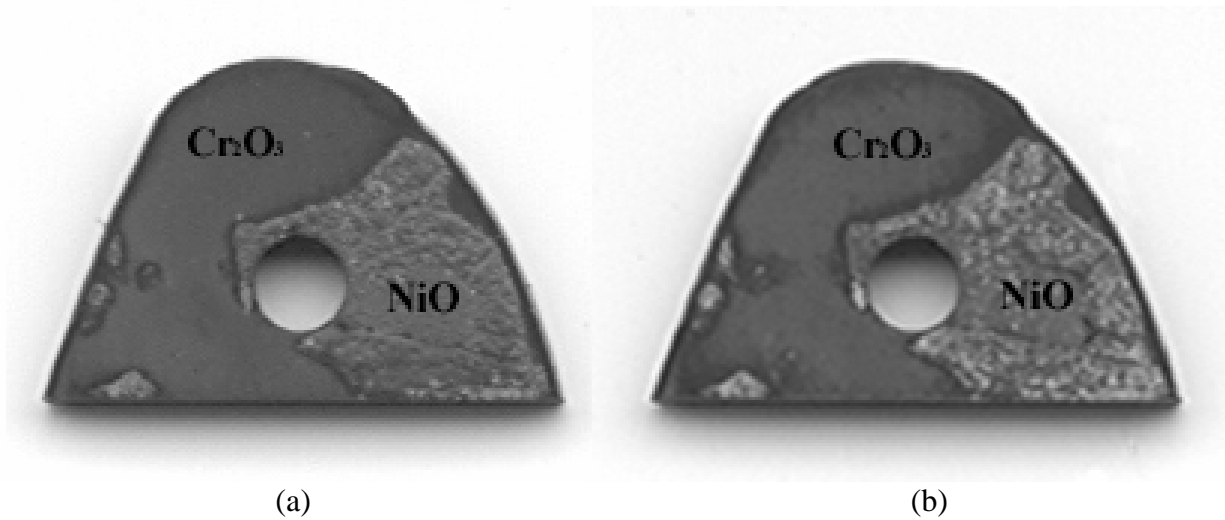


Figure 6.37: Ni-20Cr in wet air at 900°C (a) after 100 cycles, (b) after 200 cycles. Lighter colored areas are where NiO developed. Darker colored oxide was chromia. NiO did not spread over the surface with continued exposures.

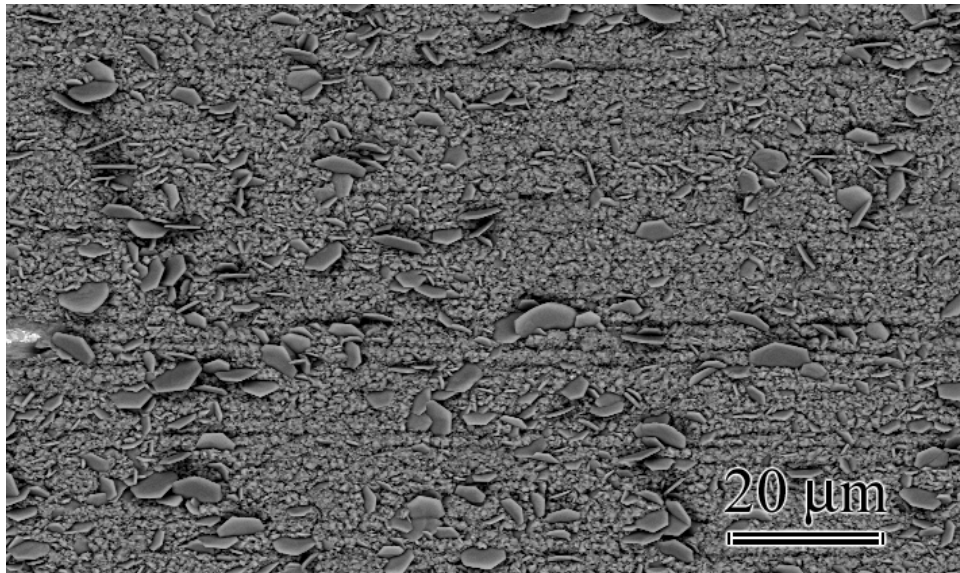


Figure 6.38: Ni-20Cr in wet air at 900°C 165 cycles.

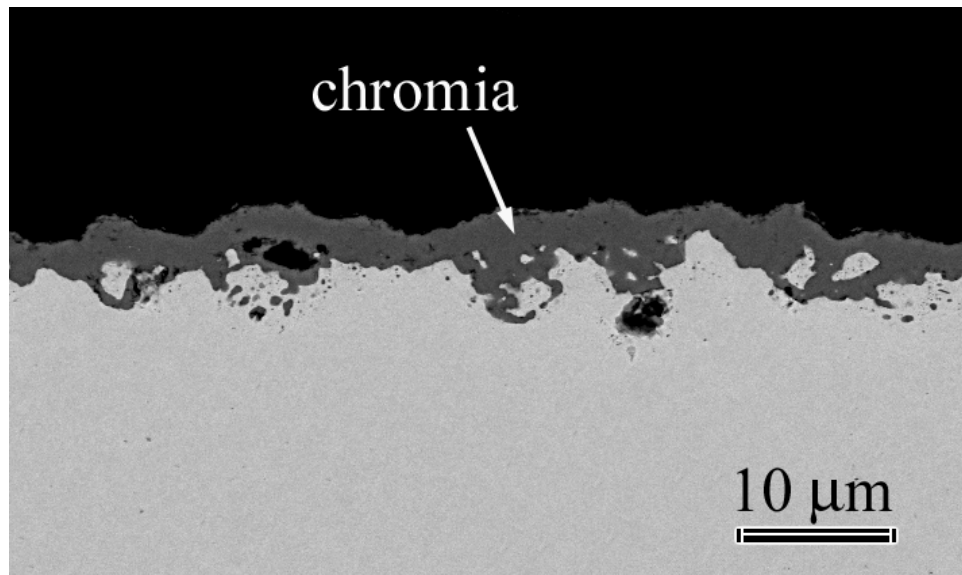
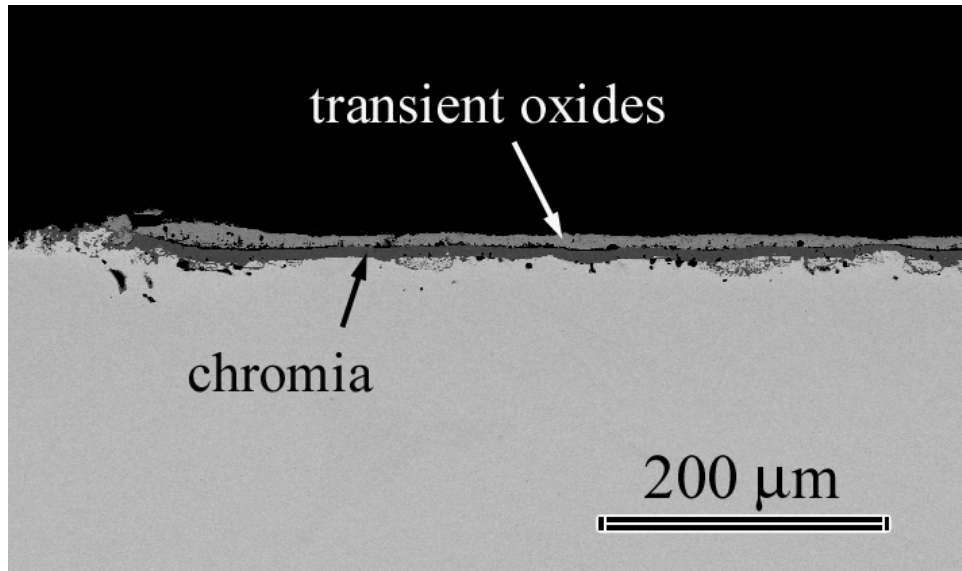


Figure 6.39: Ni-20Cr at 900°C in wet air after 700 cycles.

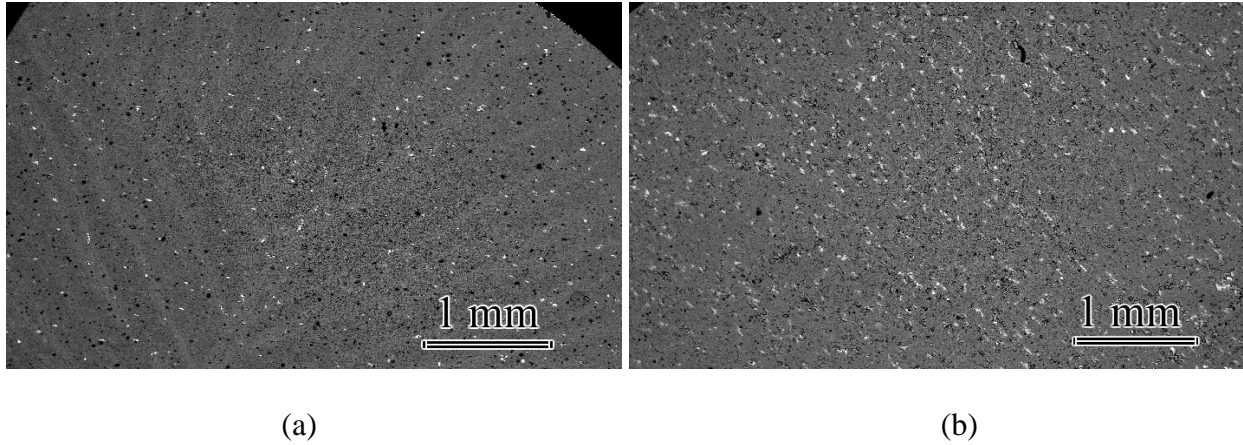


Figure 6.40: Ni-30Cr-0.1Ce at 900°C in dry air after (a) 99 cycles, and (b) 224 cycles. Scale spallation was evident, which became more pronounced with longer exposure times.

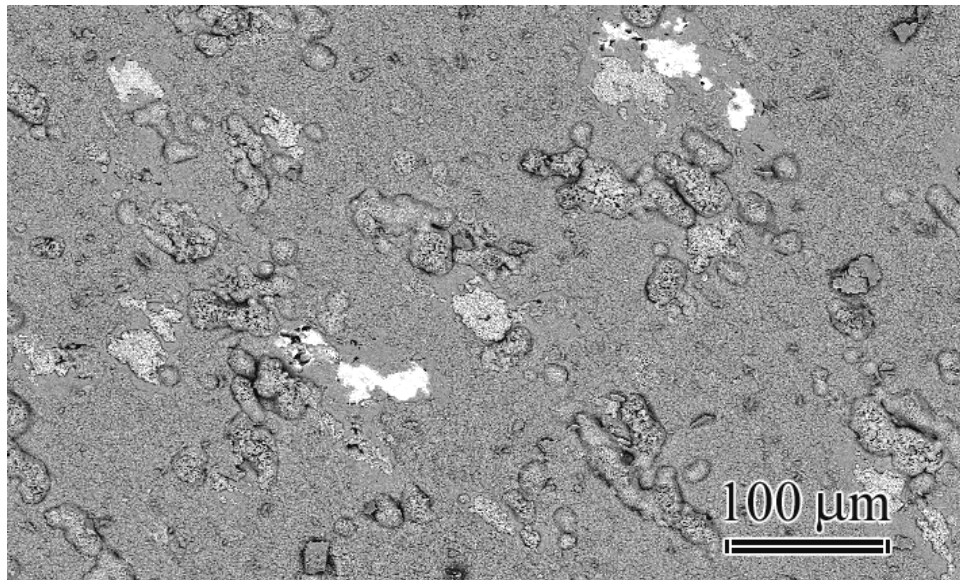


Figure 6.41: Ni-30Cr-0.1Ce at 900°C in dry air after 224 cycles. Image shows formation of NiO as small islands. Scale spallation is also evident in the micrograph.

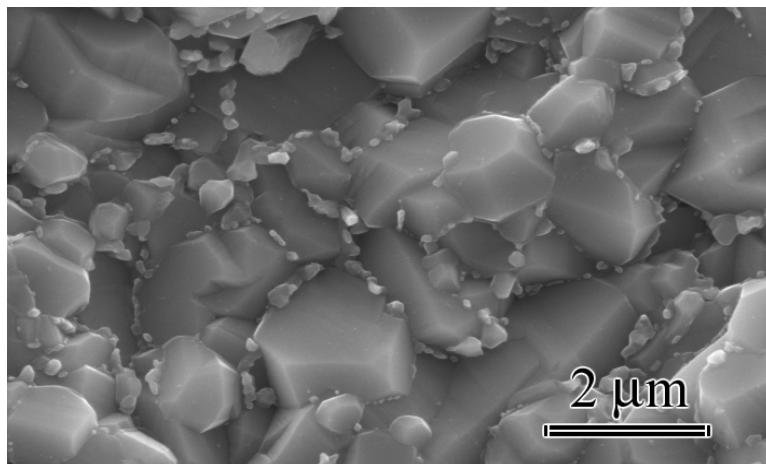
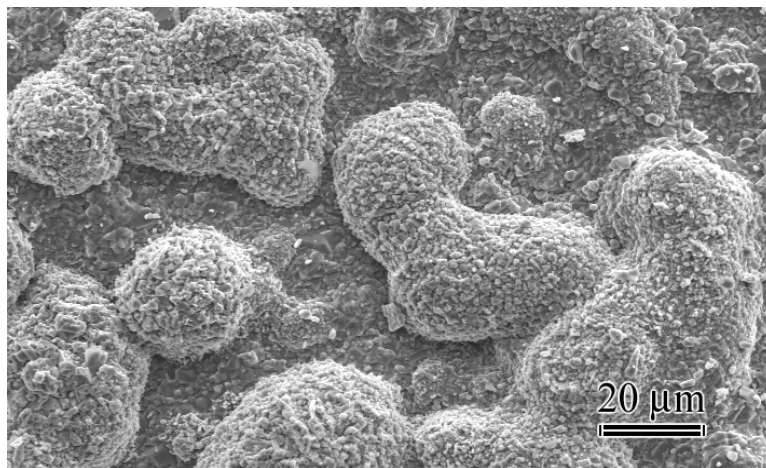
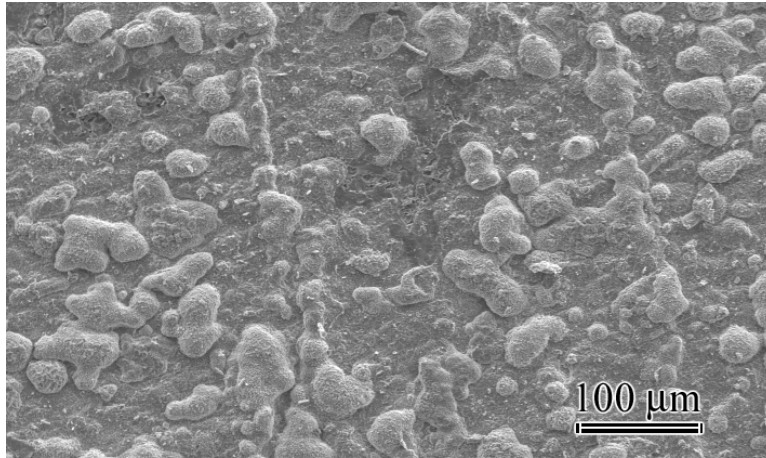
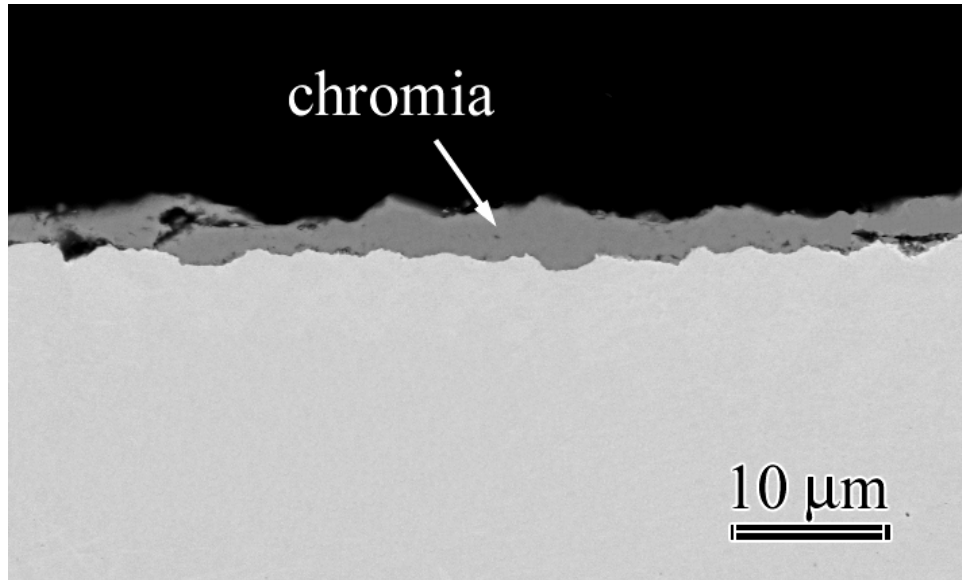


Figure 6.42: Secondary electron images of the alloy Ni-30Cr-0.1Ce at 900°C in dry air after 1210 cycles.

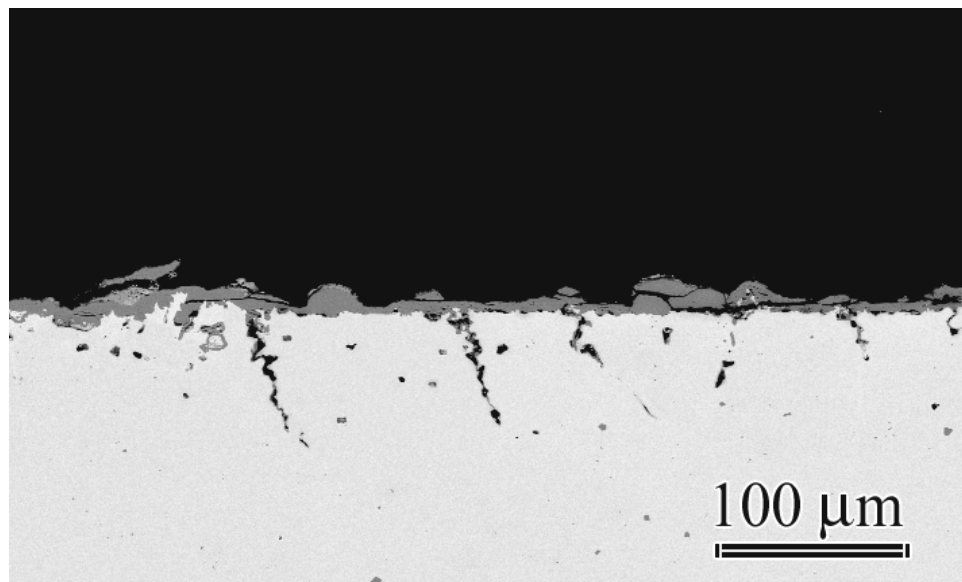
evident. Development of non-protective oxides was observed to be very profuse. Formation of voids in the depleted zone became significant, Figure 6.43. The kinetic data of the system in dry and wet air is re-plotted in Figure 6.44 together with Ni-30Cr. Evidently, the system was very vulnerable to weight losses in wet air. However, comparison of surface images for wet and dry tests showed that, scale spallation started earlier in dry air, and was also more aggressive at later stages of reactions, Figures 6.40 versus 6.45. The flake-like Cr_2O_3 crystals were present on the specimen surface even after 100 cycles. However, as the exposures continued they started to disappear as a result of spalling of initially formed chromia. These areas, where the protective scale spalled off, became sites for formation of the non-protective NiO, Figure 6.46.

Examination of the cross-section showed that the initially formed chromia was fairly smooth and uniform. Some void formation at the oxide/substrate interface was evident. Comparison to dry tests revealed that the layer which formed after wet tests was thinner, Figure 6.43(a) versus Figure 6.47(a). Continued tests resulted in substantial internal oxidation. Void formation became more pronounced at the oxide/substrate interface, as well as in the depleted zone. The scale morphology changed from a rather smooth interface to an irregular one, Figure 6.47.

Tests in dry air with Ni-30Cr resulted in the formation of scales that primarily consisted of chromia. Some NiO formation was also evident. As the tests continued more transient oxides developed on the surface, Figure 6.48. In some cases, these oxides formed over areas where re-oxidation occurred after the slow growing protective scales spalled off. Void formation at the oxide/alloy interface as well as in the substrate started before 224 cycles, and became more profuse as the reactions continued, Figures 6.49 and 6.50. The morphology of the scale was highly irregular after 1210 cycles.



(a)



(b)

Figure 6.43: Ni-30Cr-0.1Ce at 900°C in dry air (a) after 224 cycles, and (b) after 1210 cycles.

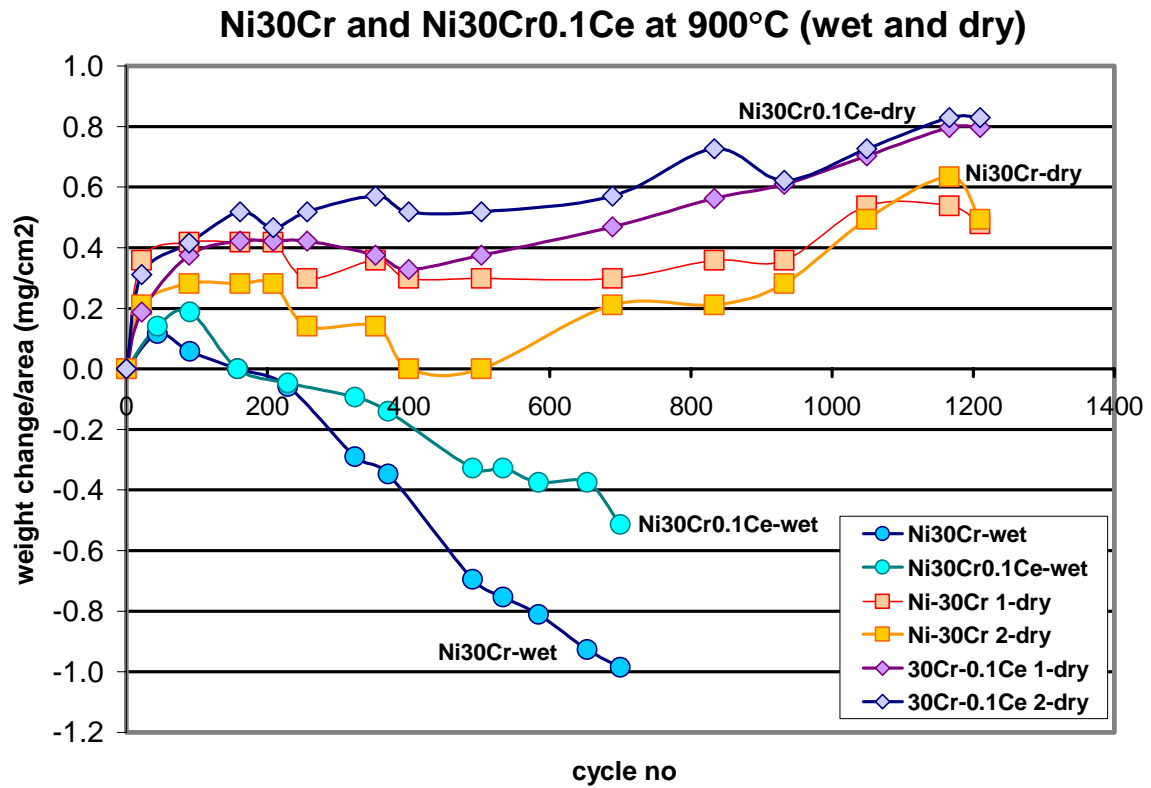
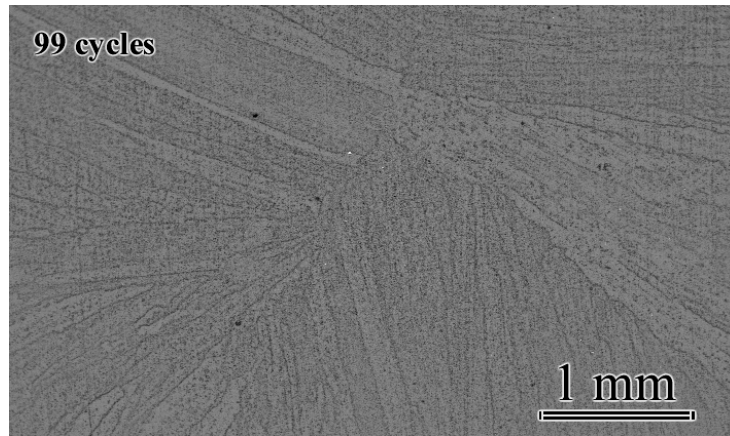
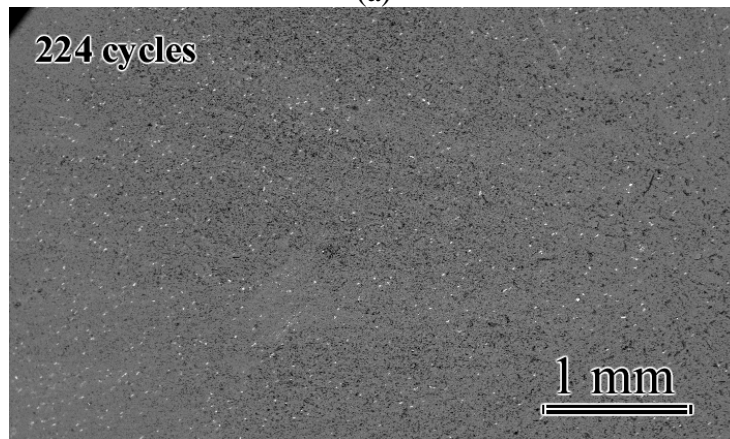


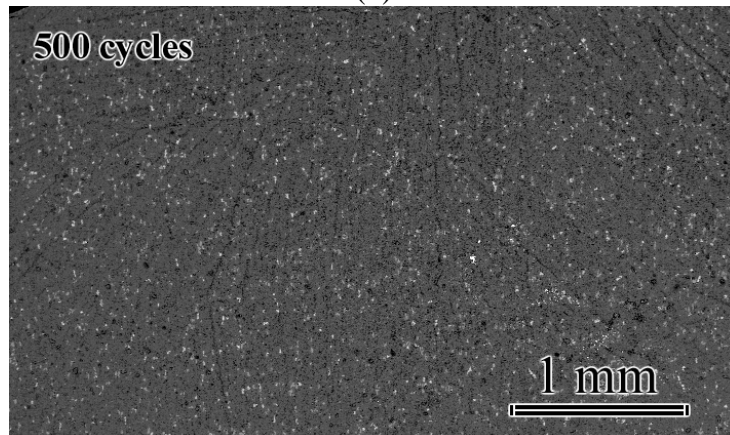
Figure 6.44: The kinetic data of the alloys Ni-30Cr and Ni-30Cr-0.1Ce at 900°C in dry and wet air.



(a)

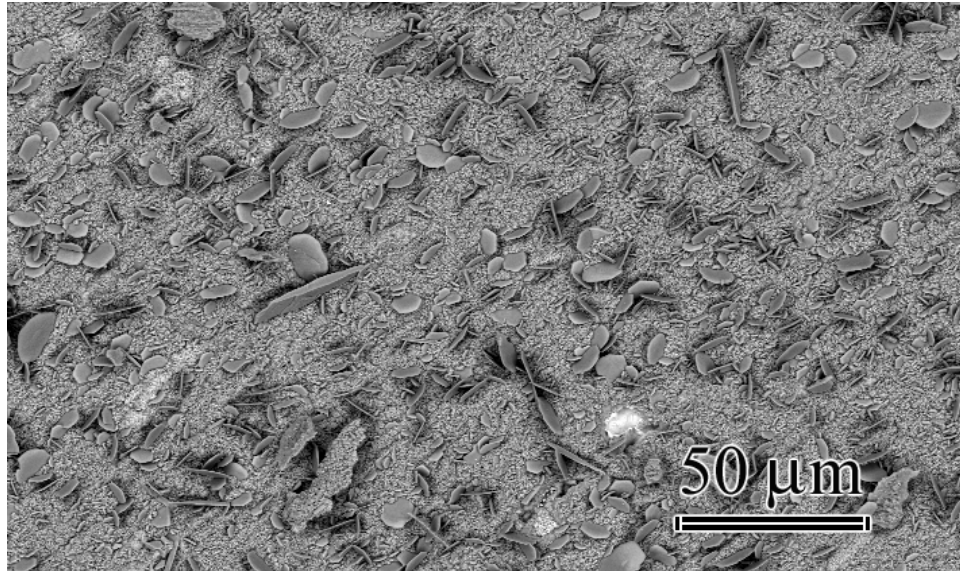


(b)

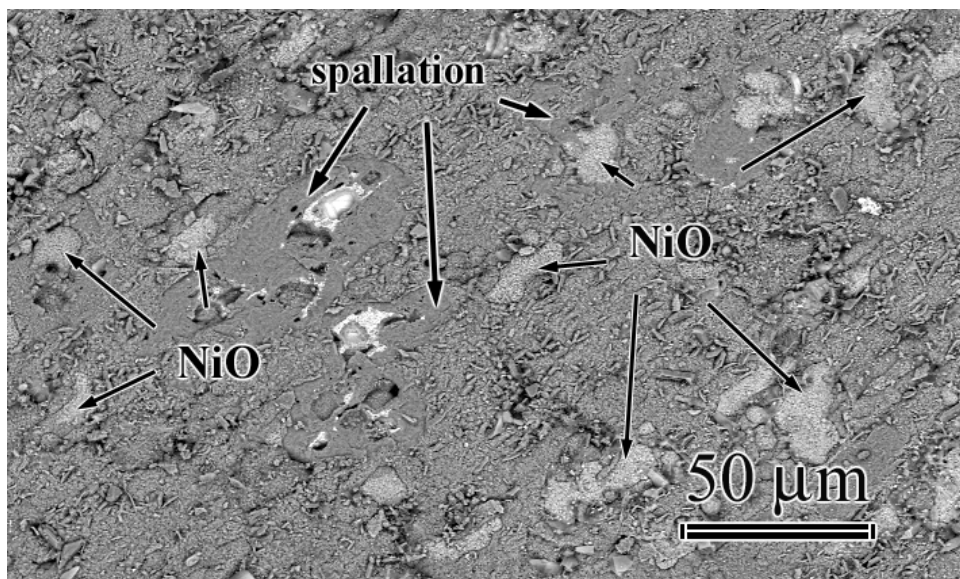


(c)

Figure 6.45: Ni-30Cr-0.1Ce at 900°C in wet air (a) after 99 cycles, (b) after 224 cycles, and (c) after 500 cycles.

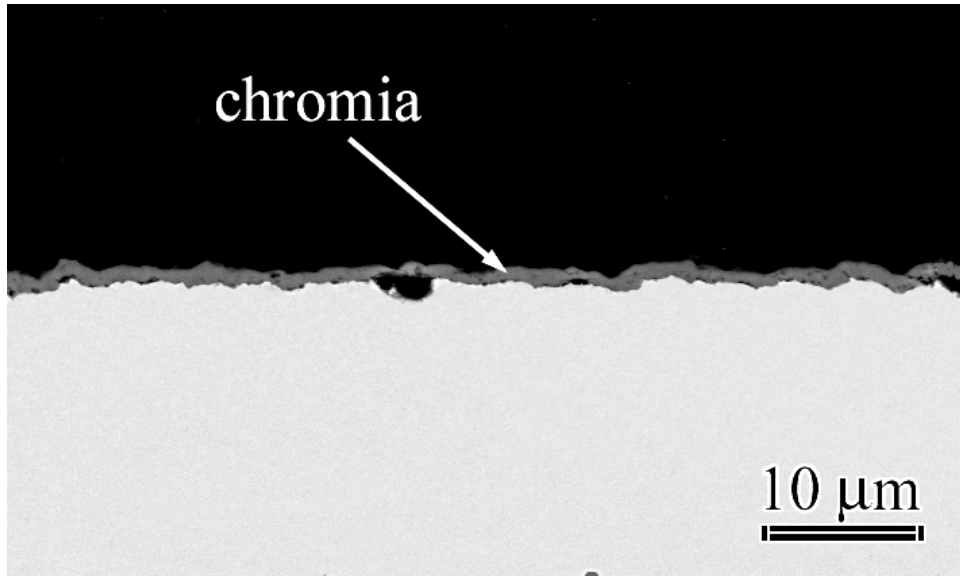


(a)

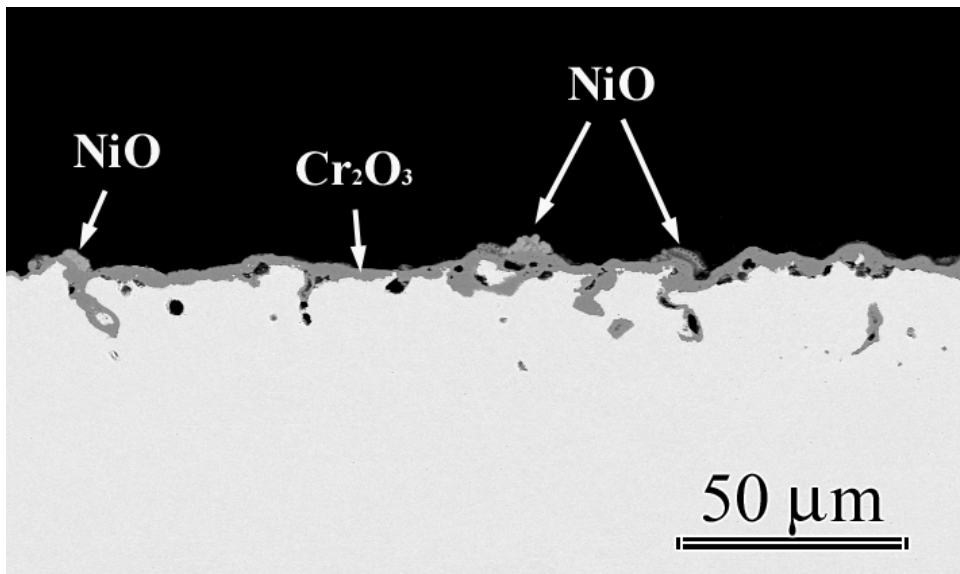


(b)

Figure 6.46: Images show the surface of the oxide scale that developed on Ni-30Cr-0.1Ce at 900°C in wet air (a) after 44 cycles, and (b) after 700 cycles.

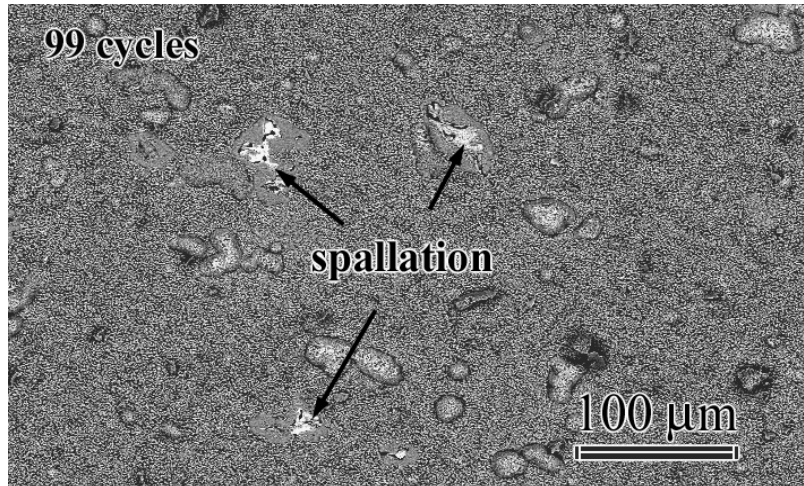


(a)

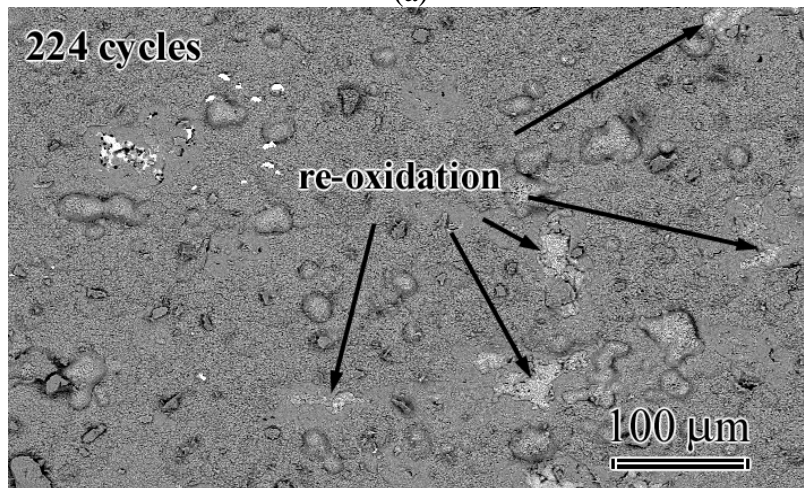


(b)

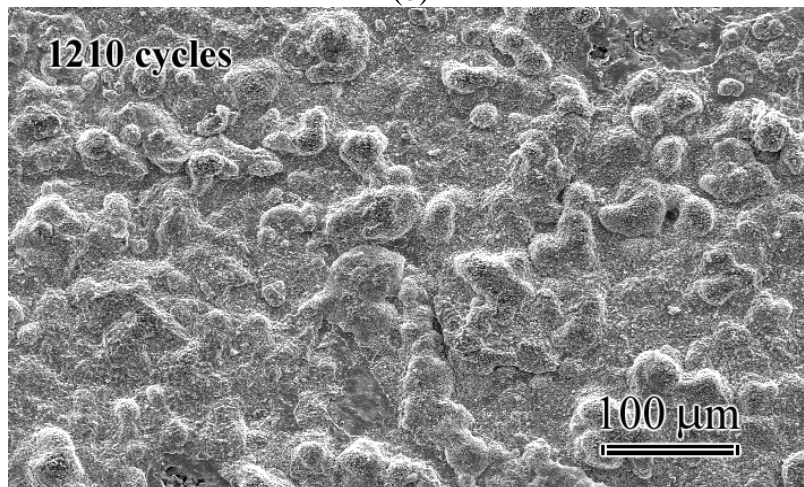
Figure 6.47: Cross-sectional images of Ni-30Cr-0.1Ce at 900°C (a) after 224 cycles, and (b) after 700 cycles in wet air.



(a)

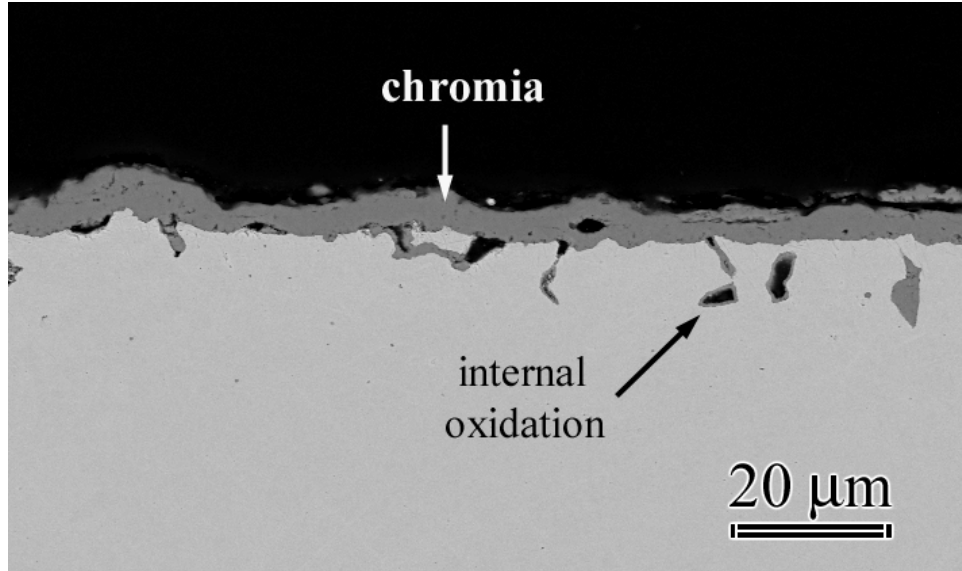


(b)

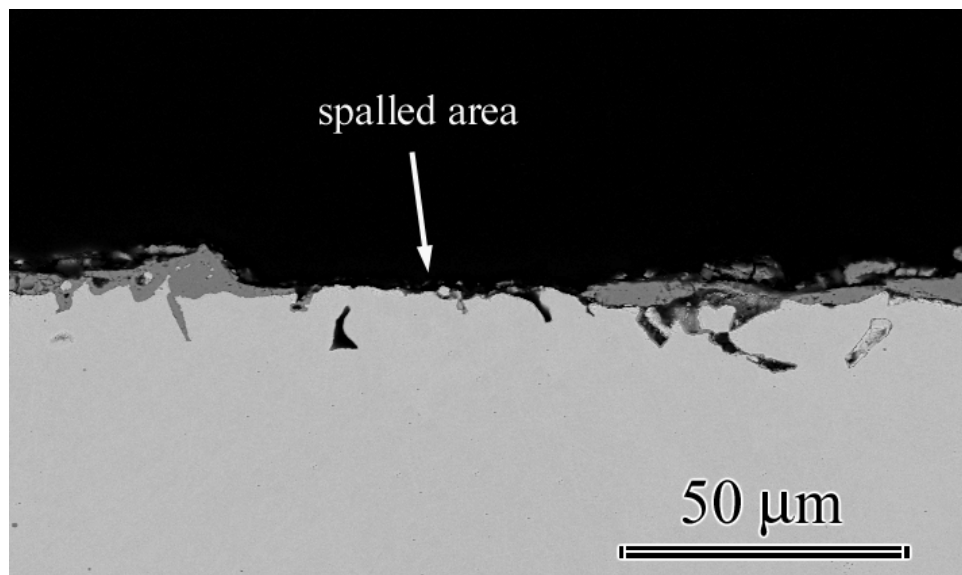


(c)

Figure 6.48: SEM images show the oxide surfaces that developed on Ni-30Cr in dry air at 900°C after (a) 99, (b) 224, and (c) 1210 cycles.

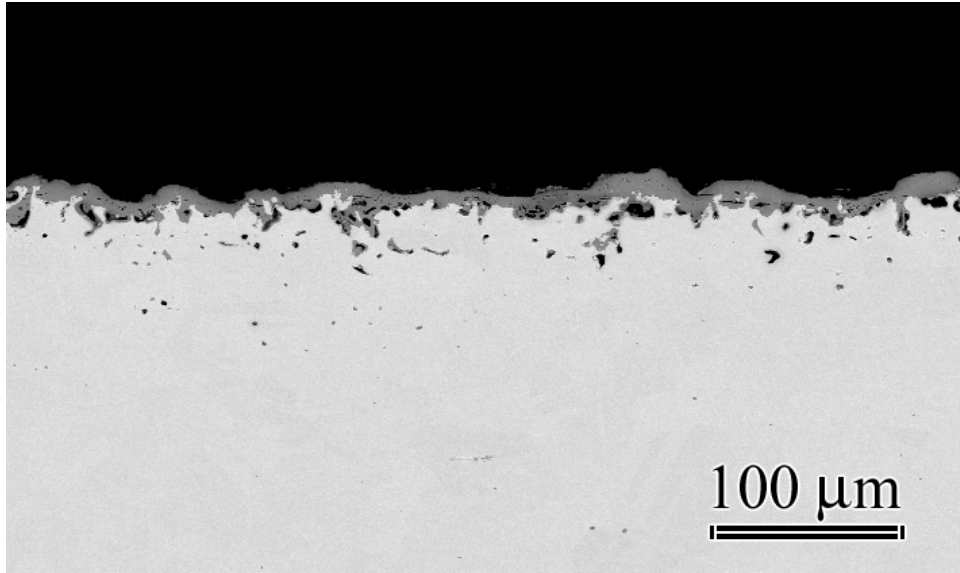


(a)

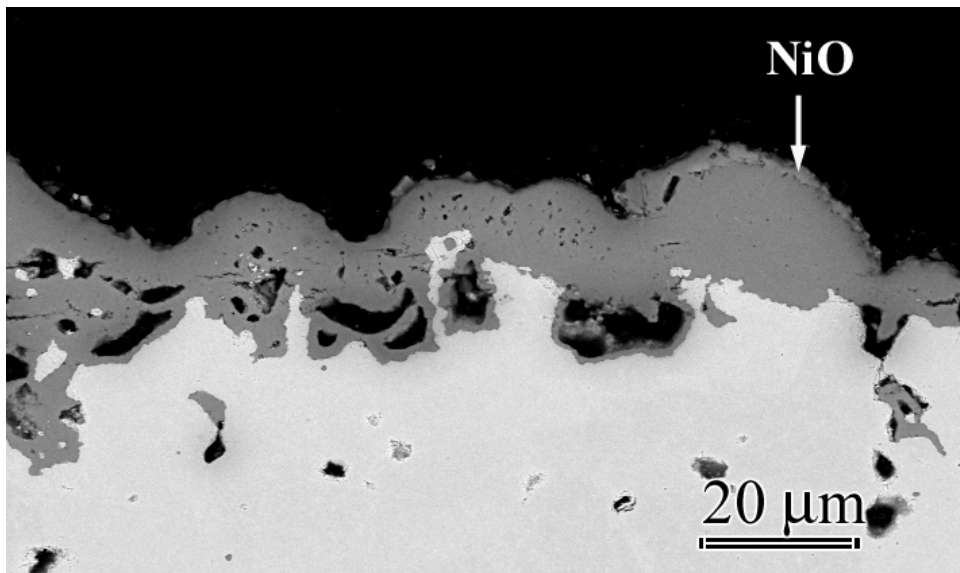


(b)

Figure 6.49: Images show the cross-section of Ni-30Cr at 900°C in dry air after 224 cycles.



(a)



(b)

Figure 6.50: Cross-section of Ni-30Cr at 900°C in dry air after 1210 cycles.

After wet tests, a rather thin scale formed on the alloy surface. Formation of the Cr_2O_3 with the flakey morphology was evident during earlier periods of oxidation. However, at later stages it disappeared as a result of oxide spallation, Figure 6.51. Examination of sample cross-sections showed that a much thinner scale formed in wet air in comparison to dry, Figure 6.49 versus Figure 6.52. Internal oxidation, as well as void formation was evident. The intensity of these features increased with time.

6.1.2 Isothermal tests with Ni-Cr Model Alloys

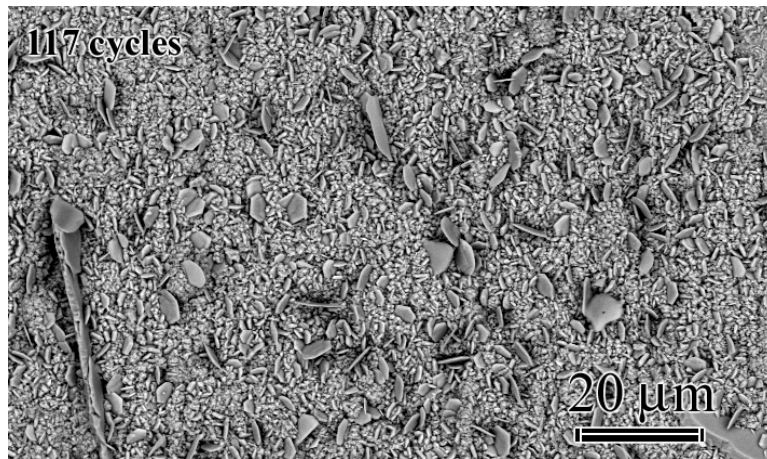
Isothermal tests were designed to see the effects of water vapor on the growth rate of Cr_2O_3 scales and on the formation of vapor species via the reactions between the Cr_2O_3 scale and $\text{O}_{2(g)}$ / $\text{H}_2\text{O}_{(g)}$. For these experiments, the alloy compositions were chosen as Ni-30Cr and Ni-30Cr-0.1Ce, since previous tests have shown that these alloys develop continuous chromia scales in wet and dry air without persistent transient oxidation until scale spallation becomes profuse. Similar to previous studies with the model alloys, the partial pressure of H_2O was set to 0.1 atm in the wet environment. For all experiments the total pressure of gases was 1 atm. Exposures were done at 900°C and 700°C. Emphasis was given to higher temperature studies since vaporization was not expected to be as significant at 700°C.

In addition to the simple alloys, the chromia-forming superalloys IN 738 and X-40 as well as pure Ni were also subjected to testing. These experiments were done at 900°C only.

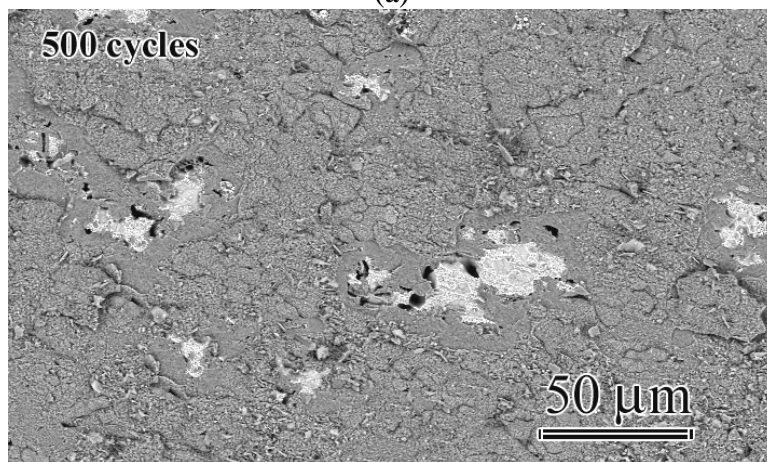
In the following, the results of the tests with the model alloys at 900°C and 700°C will be presented first, followed by the data for the experiments with the superalloys and pure Ni.

6.1.2.1 Isothermal Tests at 900°C: Isothermal TGA tests with the model alloys in dry air have shown that the oxidation reactions for Ni-30Cr and Ni-30Cr0.1Ce followed the parabolic rate law very closely. In Figure 6.53 the data for Ni-30Cr obtained from three specimens in two different TGA apparatuses are shown. The software of the main set-up that was used for the majority of the isothermal tests, which is labeled as equipment-1 in the figure, has an upper time limit of 168 hours. Tests with Ni-30Cr at 900°C in dry air did not show any negative weight changes for 168 hours when the tests were terminated. Therefore, another test was run utilizing different equipment with the capability of collecting data for longer times. This set-up was not chosen as the primary testing equipment because its balance was wired to an analog chart recorder instead of the digital converter. This test served two purposes. The information obtained was used to check the reproducibility and the reliability of the experimentally collected data in different equipment. It also provided information on the longer-term behavior of the system. The control test was run for 535 hours. The weight change data obtained showed good agreement with the former experiments. However, even after over 500 hours no negative weight changes were evident. This showed that the formation of vapor species in dry air was not as profuse at this stage of oxidation. The shape of the curve furthermore suggested that it was not going to become significant for longer times. The data of the control test are presented in Figure 6.53 under the label equipment-2.

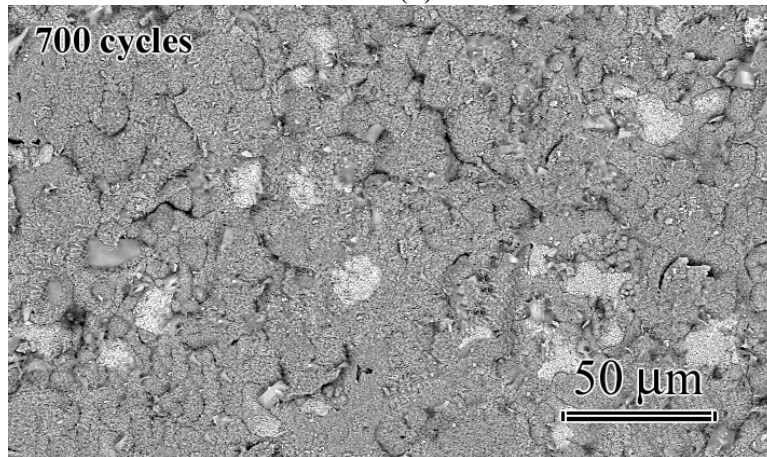
The experimental data were used to estimate the growth rate as well as the vaporization rate of Cr_2O_3 in dry air at 900°C. For the calculations two approaches were used. The results were compared to each other and to the literature values. The starting point for each method was the assumption that the formation of Cr_2O_3 followed the parabolic law, and the vaporization at the



(a)

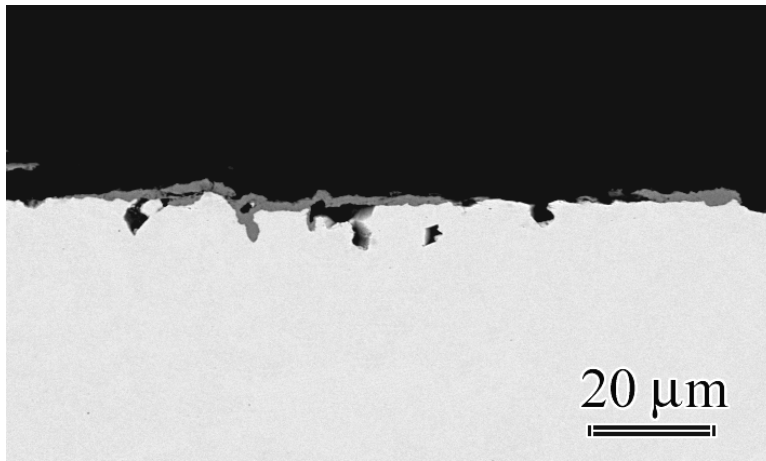


(b)

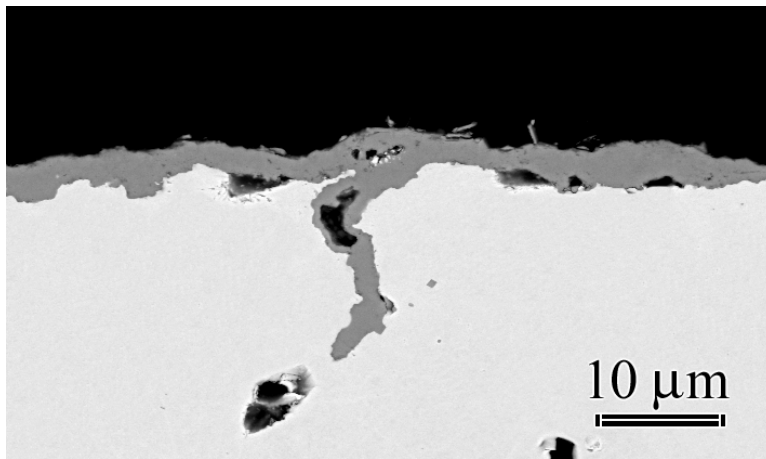


(c)

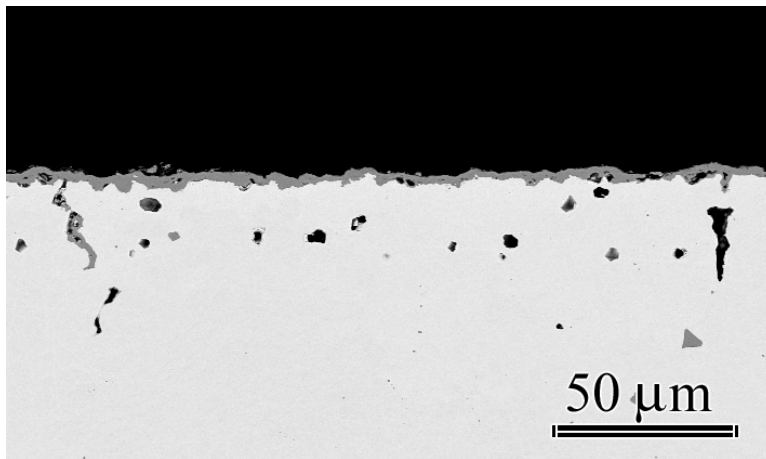
Figure 6.51: Images show the oxide surface that developed over Ni-30Cr at 900°C in wet air after (a) 117 cycles, (b) 500 cycles, and (c) 700 cycles.



(a)



(b)



(c)

Figure 6.52: Cross-section of Ni-30Cr at 900°C (a) after 224 cycles, and (b-c) after 700 cycles in wet air.

oxide/gas interface was independent from chromia formation. The calculations were based on the following relation;

$$\frac{\Delta m}{A} = k'_p \sqrt{t} + k_s t \quad \text{Eqn. 6.1}$$

where $\frac{\Delta m}{A}$ is the weight change per area, t is time, k_s is the linear rate constant, $k'_p = k_p^{1/2}$, and

k_p is the parabolic rate constant. The first method utilized the regression analysis technique.

This approach yielded the value of k_p as $1.13 \times 10^{-8} \text{ g}^2/\text{cm}^4\text{hr}$, and the k_s as $-8.9 \times 10^{-7} \text{ g}/\text{cm}^2\text{hr}$.

The second method assumed that during the early periods of reactions the effects of vaporization would be negligible and the weight changes would originate essentially from the formation of the chromia scales. The value of k_p was calculated using the data between 1 and 40 hours. The

plot of $\ln\left(\frac{\Delta m}{A}\right)$ as a function of $\ln(t)$ in this interval gave a slope of 0.49 which justified the

assumption that the growth rate of Cr_2O_3 was parabolic and the vaporization effects could be

neglected⁴, Figure 6.53(b). The value of k_p was calculated from the change in $\left(\frac{\Delta m}{A}\right)^2$ with time

t as $1.2 \times 10^{-8} \text{ g}^2/\text{cm}^4\text{hr}$. The linear weight change was determined by subtracting the weight

gains due to chromia formation from the total weight change in the system, whereby the weight

gain was determined using the calculated k_p value. This approach yielded the linear rate

constant k_s as $-5.9 \times 10^{-7} \text{ g}/\text{cm}^2\text{hr}$. These numbers were in agreement with some other studies.

The relation developed by Hagel, [89], in 0.1 atm oxygen estimates k_p as 10^{-8} - $10^{-9} \text{ g}^2/\text{cm}^4\text{hr}$,

⁴ The slope of $\ln\left(\frac{\Delta m}{A}\right)$ versus $\ln(t)$ should be 0.5 when the oxidation reaction proceeds according to the parabolic growth law.

and k_s as 10^{-6} - 10^{-7} g/cm²hr. The study by Giggins and Pettit on Ni-Cr alloys estimated the parabolic growth constant in the order of 10^{-7} g²/cm⁴hr in 0.1 atm oxygen at 900°C, [96].

The rate constants obtained from the current study were used to estimate the long-term behavior of the system. The linear weight losses due to oxide vaporization were predicted to start after 8000 hours assuming the growth stresses would not result in the spallation of the chromia layer, and the breakaway oxidation would not start. The experimental data for Ni-30Cr is plotted with the estimated (calculated) weight change in Figure 6.53(c).

Comparison of the cyclic oxidation kinetics to the isothermal reaction kinetics showed that the spallation of the scales due to thermal cycling was very significant in dry air. The data presented in Figure 6.54 reveals that the weight change differences between the thermally cycled and the isothermally tested Ni-30Cr specimens were substantial. Also, thermal cycles resulted in the negative weight changes as early as 150 hours, while isothermal exposures did not display similar trends even after 500 hours, as mentioned above. Similar observations apply to the Ce-added system as well. Differences exist between isothermal and cyclic conditions. However, the addition of the reactive element is still observed to improve the scale adherence and to decrease the Cr₂O₃ formation rate. Weight losses associated with scale spallation rather than vapor species formation were also reported elsewhere for chromia formers in still air, [97].

Literature shows that the reaction rate of the vapor species is not affected by reactive element additions, [19]. As an example, the linear rate constant for chromia vaporization at 1100°C in 0.1 atm oxygen was reported as -7.9×10^{-6} g/cm²hr for TD NiC⁵, [92], and as -7×10^{-6} g/cm²hr for spalled chromia foils, which were grown on Ni-50Cr, [98]. Therefore, the rate

⁵ Ni-20Cr-2 vol % ThO₂,

92. Giggins, C.S. and F.S. Pettit, *The Oxidation of TD NiC (Ni-20Cr-2 vol pct ThO₂) Between 900°C and 1200°C*. Metallurgical Transactions, 1971. 2: p. 1071-1078.

constants for Ni-30Cr-0.1Ce were determined assuming that the linear rate constant for the Ce-doped alloy would be the same as the undoped alloy, i.e. Ni-30Cr, and the chromia growth would follow the parabolic oxidation kinetics. The weight losses associated with the loss of chromia by vaporization were subtracted from the total weight change of the system. The resultant was used to determine the parabolic rate constant, which yielded $3.8 \times 10^{-10} \text{ g}^2/\text{cm}^4\text{hr}$ as k_p . Giggins and Pettit's study estimated the parabolic rate constant as $7.5 \times 10^{-10} \text{ g}^2/\text{cm}^4\text{hr}$ for TD NiC, [92]. Based on the calculated rate constants the onset of negative weight changes due to vapor species formation is predicted to be around 2500 hours at 900°C. The plot is shown in Figure 6.55.

The weight change data for Ni-30Cr obtained from the isothermal tests in air/H₂O mixtures showed an abrupt turn into weight losses with linear kinetics after the initial short period of weight gain due to chromia formation. Similar behavior was also observed with Ni-30Cr-0.1Ce, Figure 6.56. The origin of the weight losses was the formation of the vapor oxide species by the surface controlled reaction between Cr₂O₃ and the oxidizing gases (i.e. O_{2(g)} and H₂O_(g)). The data obtained from the cyclic tests did not display significant deviations from the isothermal ones, Figure 6.57. Unlike the dry case, the reaction rates were very similar. This result showed that scale spallation was not as profuse in the wet environment as it was in dry air. It furthermore suggested that the reason for alloy degradation in wet air was mainly the loss of chromia by the formation of vapor species rather than the loss of the scale by spallation.

The data collected during the TGA tests was used to calculate the reaction rate constants. The approximate value of the linear rate constant (k_s) in wet air was found as $-1.62 \times 10^{-6} \text{ g}/\text{cm}^2\text{hr}$.

The condensation of water vapor on the walls of the furnace tube or possibly on the hang-wire was a concern for the wet exposures. Therefore, a series of isothermal spot tests were done

in the horizontal furnaces to check the accuracy of the TGA data. For this purpose four Ni-30Cr specimens and three Ni-30Cr-0.1Ce samples were prepared. Each specimen was put in a ceramic boat (zirconia). The weight of the specimen in the boat was measured before and after exposures. The purpose of using the boat was to minimize the errors that might result from the possible spallation at the end of the test while the specimen was cooling down to room temperature. During each run only one sample was exposed to the hot gases. The times of exposures were chosen as 5 hr, 16 hr, 68 hr and 118 hr for Ni-30Cr; and as 48hr, 96hr and 112 hr for Ni-30Cr-0.1Ce. Obtained information was compared to the TGA data. It was seen that there was a good match between the tests, Figure 6.58.

Examination of the scale morphologies showed that Ni-30Cr developed continuous chromia scales in wet air. No transient oxides were detected on the specimen surface or in the cross-section of the samples. Formation of the flake-like Cr_2O_3 was evident after the isothermal tests as well, Figure 6.59 (a, c). The scale that formed during dry exposures also consisted of chromia with no transient oxidation, Figure 6.59 (b, d). The thickness of this scale was nearly double the thickness of the former one. This result was in agreement with the kinetic data which showed that the alloys continued to gain weight in the dry environment, while weight losses were dominant in wet air, Figure 6.60. Void formation at the substrate/oxide interface was evident for each condition. They developed preferentially at the substrate grain boundaries, Figures 6.61. The results obtained with the Ce-added version of the alloy were similar to Ni-30Cr. Figure 6.62 shows the SEM images of the sample cross-sections in wet and dry air.

The values of the calculated rate constants indicated that the volatilization was more aggressive in wet air. This was in agreement with the literature information, [71, 72, 93, 99]. The growth rate of Cr_2O_3 could not be determined from the TGA data. However, the

observations on the cyclically tested specimens did not indicate adverse effects on selective Cr oxidation imposed by H₂O. In dry air, the rate of Cr₂O₃ formation was suppressed by the reactive element. Improved scale adherence was also observed on the Ce-added alloy. These results are in agreement with the literature information.

These tests showed that while scale spallation was the main source of system degradation in dry air, the mechanism leading to alloy deterioration in air/H₂O mixtures was primarily the formation of volatile species. No evidence for oxide vaporization was available for the dry tests. However, it is known that in air and in oxygen containing environments Cr₂O₃ reacts with O₂ to form the vapor oxide CrO₃, [65]. This reaction is typically more significant at higher temperatures, i.e. 1000°C and up. The predictions based on the calculated rate constants suggested that weight decreases would eventually become more pronounced assuming that the substrate/oxide interface toughness is high enough and breakaway oxidation does not start before the onset of linear weight losses due to vaporization.

6.1.2.2 Isothermal Tests at 700°C: Experiments at 700°C gave results very similar to 900°C. In dry air oxide vaporization was not evident. Although there was some scale spallation, it was much less in comparison to the higher temperature, Figure 6.63(a). The oxidation kinetics was very close to parabolic for Ni-30Cr and Ni-30Cr-0.1Ce. The chromia growth rate was slower for the latter composition.

During wet exposures, the alloys showed weight losses following an initial increase. The information gathered from the experiments is presented in Figure 6.63(b). For these tests there was significant scatter in the data. Although this information was not reliable for any estimation

of the rate constant for Cr_2O_3 vaporization, it showed tentatively that the phenomenon of vapor oxide formation did occur also at this temperature.

The test results in wet air are compared to the ones in dry air, Figure 6.63(c). The weight gains in the latter environment were larger due to insignificant vapor species formation.

6.2 ISOTHERMAL TESTS WITH OTHER SYSTEMS

6.2.1 Isothermal Tests with IN 738 and X-40

TGA tests were done with the chromia-forming superalloys at 900°C to compare their short term isothermal behavior to the model alloys. Each alloy was exposed to dry air, as well as to wet air for 168 hours. For wet tests, the partial pressure of H_2O was chosen as 0.1 atm, while the total pressure of gases was 1 atm. Dry experiments were done at $P_{\text{total}} = 1$ atm.

The isothermal oxidation kinetics of IN 738 was compared to that for this alloy subjected to thermal cycling. Figure 6.64 shows the data recorded in dry and in wet air. The total weight gains were larger during isothermal exposures. This indicated that oxide spallation was taking place during thermal cycling. The reactions were faster in air/ H_2O mixtures. Mass gain due to oxygen pick-up started at a high rate. After 168 hours the total weight increase was larger for the wet-exposed specimen. This was consistent with the cyclic data, which also showed larger weight gains in air/ H_2O environments. Unlike the model alloys, the weight losses which were associated with vapor oxide formation by the surface controlled reaction between the external chromia layer and the reactive gases did not occur on this system. The oxidation kinetics of the model alloys and IN 738 are compared in Figure 6.65. This plot shows that, while there were very clear indications for Cr_2O_3 vaporization for Ni-30Cr and Ni-30Cr-0.1Ce, IN 738 did not

display the same tendency. Comparisons in dry air showed that the isothermal reaction rate of the superalloy was faster than the reactive element added model alloy Ni-30Cr-0.1Ce, yet slower than Ni-30Cr, Figure 6.66.

Examination of the scale surfaces revealed that the formation of the thin TiO₂ layer, which was observed on the cyclically tested specimens at 700°C and 900°C for longer times, was not a consequence of the loss of protectiveness due to scale spallations. This phase actually developed during the initial stages of oxidation. The SEM images showing the scale in cross-section are given in Figure 6.67. The microstructure of the oxide layer displayed the same characteristics as the specimens subjected to testing for over 3000 cyclic hours. Alumina developed as an internal oxide. Chromia formed as a continuous scale. The total depth of the reaction zone was larger for the alloy tested in the H₂O containing environment. The thin film of TiO₂ was present over both specimens. It is believed that the formation of this thin layer is beneficial for the system, as it seals the surface of the specimen and puts a physical barrier between the Cr₂O₃ layer and the reactive gases. Therefore, the loss of the protective oxide by vaporization is delayed until the scale spalls off when the thermal and growth stresses exceed the critical limit. Once scale spallation starts and exposes the Cr₂O₃ layer, system deterioration begins. This phenomenon will be discussed later again in the “Summary and Discussion” chapter.

The isothermal tests with the second superalloy X-40 at 900°C showed that while rapid weight gains continued in dry air until the end of the exposure, in air/H₂O mixtures weight losses started during very early stages of reactions indicating the evaporation of the Cr₂O₃ layer, Figure 6.68. Examination of the oxide surfaces showed that scale spallation did not occur during the tests, Figure 6.69. The surfaces of the scales displayed morphological differences between wet and dry exposures. In dry air, large islands of chromia with thin Co-oxide layers were detected.

EDX analysis indicated the presence of W in conjunction with the Co-oxide randomly in parts of the scale. The Cr-rich islands developed over a continuous chromia scale. Wet exposures resulted in the formation of a less rugged surface. In this environment different surface features developed instead of the oxide islands observed on the dry-exposed sample. EDX analysis indicated much weaker Co-oxide formation in air/H₂O mixtures. Back scattered electron images showing the sample cross-sections are given in Figure 6.70. Comparison of the scale thicknesses revealed that thinner layers developed after wet tests. This outcome was consistent with the mass change data of the system. Void formation at the substrate/oxide interface was common to both specimens. Observations showed more internal oxidation in the dry-exposed substrate. EDX analysis identified these areas as a mixture of Cr-Co-W and oxygen. This phase mixture of internal oxides developed along the carbide network of the substrate. The Cr-oxide islands with the external Co-oxide scale were located over the areas where internal oxidation took place. This showed that the carbide network provided an easy diffusion path for oxygen, as well as for Cr and Co. Although the internal oxidation was more profuse in dry air, pore formation along the carbide network was more substantial for the wet-exposed specimen. The presence of these pores on this sample suggests that vaporization of the oxides of W might be taking place as well, which would also contribute to the observed weight losses.

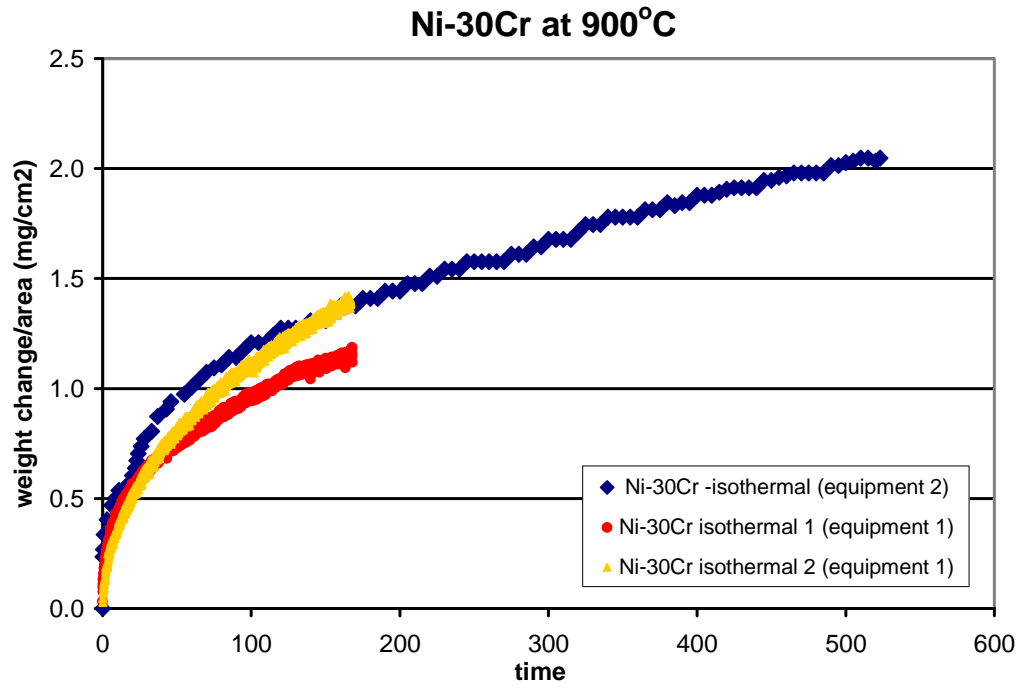
The comparison of the cyclic data to the isothermal ones indicated that the mass gains in dry air were substantially larger for the latter condition, Figure 6.68. This difference was much smaller in wet air. As mentioned, scale spallation was not detected on the isothermally tested specimens. This showed that the difference in the weight change data between the isothermal and cyclic exposures in dry air originated from scale spallation that occurred during thermal cycling. The comparison of the oxidation kinetics of the Co-based superalloy X-40 and the Ni-

Cr alloys showed that in wet air the reaction rates were similar, Figure 6.71. This implied that the vaporization of the externally formed Cr_2O_3 was independent of the substrate composition as long as the stoichiometry of chromia was not significantly disturbed.

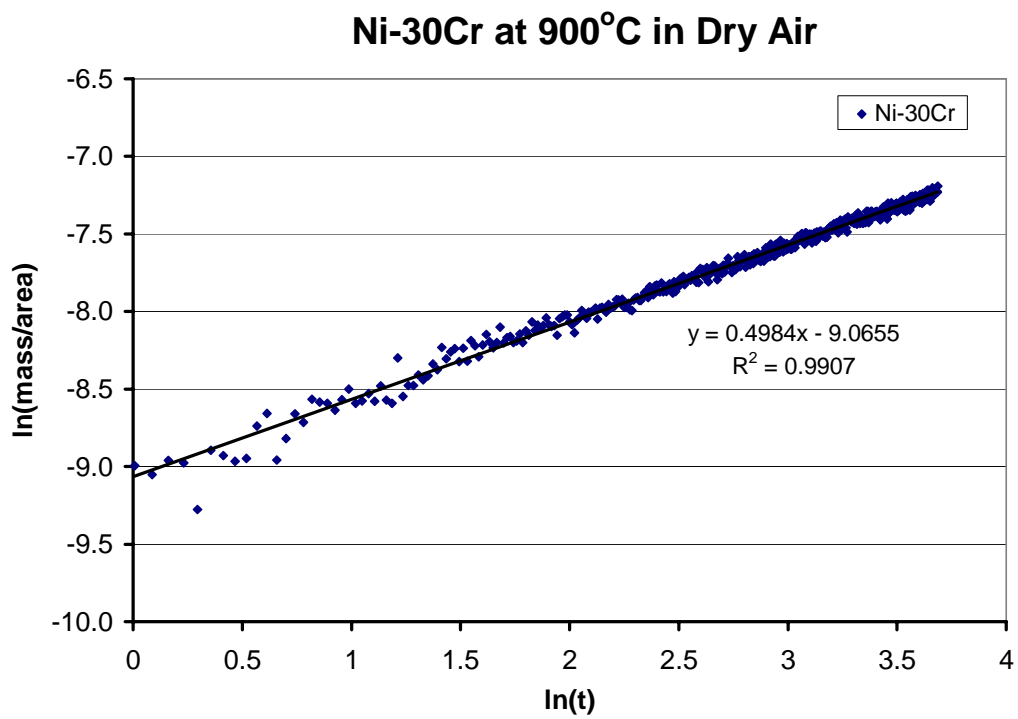
6.2.2 Isothermal Tests with Ni (99.999%)

For the majority of the systems under investigation NiO was the principle transient oxide phase that developed before the establishment of the continuity in the protective layer. Therefore, isothermal tests with pure Ni in air/ H_2O mixtures and in dry air were included in the planning of experiments to gain an understanding in terms of the effect of water vapor on the reaction kinetics of the system. These exposures were done at 900°C only.

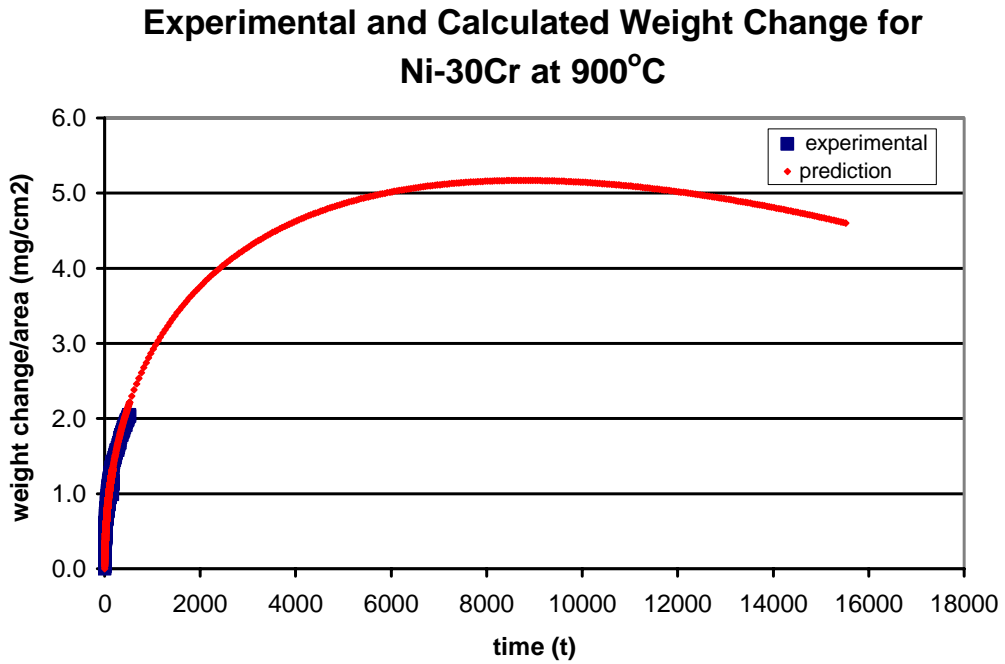
Data recorded during isothermal TGA tests revealed that the reactions advanced faster in dry air, Figure 6.72. However, the differences were not very large. Both reactions followed the parabolic rate law very closely. The parabolic rate constants (k_p) were calculated as approximately $3.8 \times 10^{-7} \text{ g}^2/\text{cm}^4\text{hr}$ in wet air, and $5.9 \times 10^{-7} \text{ g}^2/\text{cm}^4\text{hr}$ in dry air. Examination of the specimen cross-sections confirmed the kinetic data. Slightly thicker scale formation was evident after experiments in dry air, Figure 6.73. The oxide layer that developed in this environment seemed to be more susceptible to cracking and spallation as the low magnification image of the specimen cross-section shows, Figure 6.74. Another difference was the tendency towards void formation. This was observed to be more profuse in the wet environment. The reason for this is unknown. Furthermore, the oxide surfaces indicated morphological differences between wet and dry tests. The scale that developed in dry air consisted of equiaxed NiO grains as shown in Figure 6.75(a). On the other hand, formation of faceted surfaces was observed during wet exposures, Figure 6.75(b).



(a)



(b)



(c)

Figure 6.53: (a) Kinetic plot of Ni-30Cr at 900°C in dry air shows the weight changes as a function of exposure time during isothermal testing. Tests were done in two different types of equipment. (b) The plot of weight change as a function of time on a log-log scale (c) Estimated weight change data for long term exposures plotted together with experimental data.

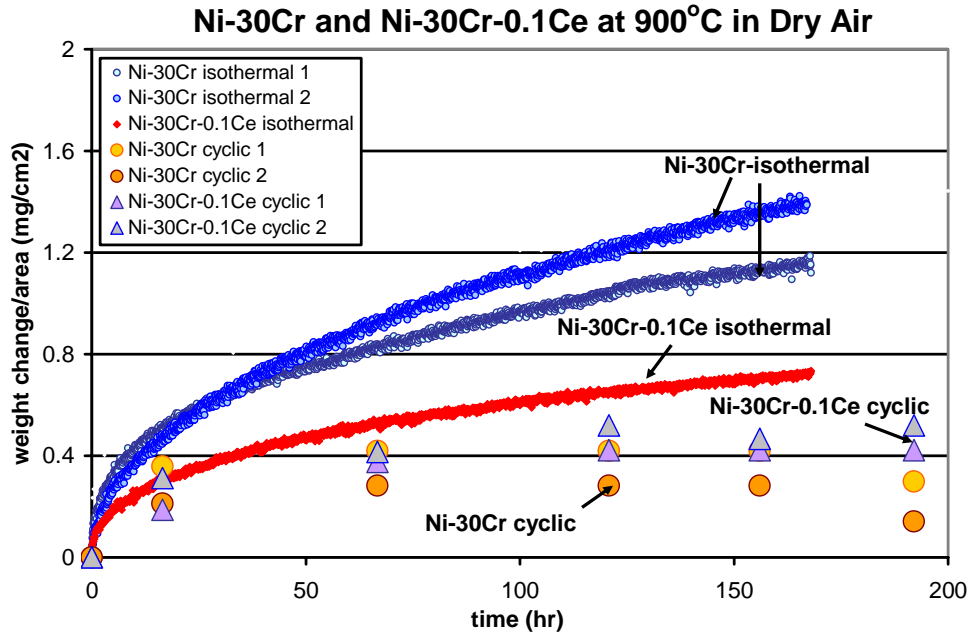


Figure 6.54: The weight changes of Ni-30Cr and Ni-30Cr-0.1Ce after isothermal tests are compared to the same systems after cycling testing. All tests were done at 900°C in dry air.

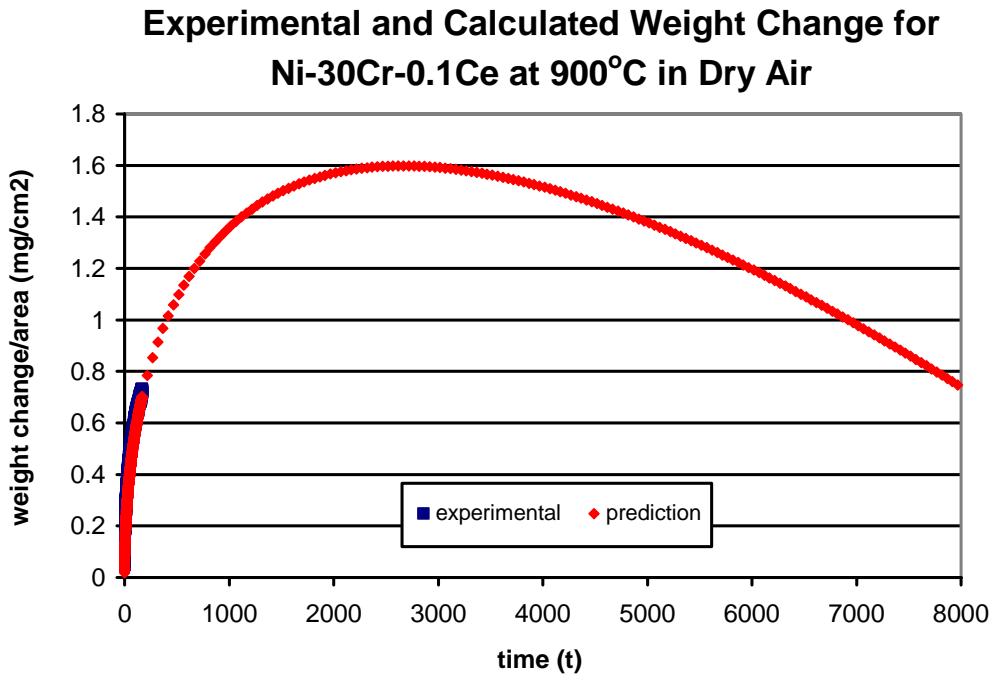


Figure 6.55: The empirical weight change data of Ni-30Cr-0.1Ce at 900C in dry air was used to estimate the long term behavior of the system assuming the chromia growth obeys the parabolic rate law, and the vaporization is linear.

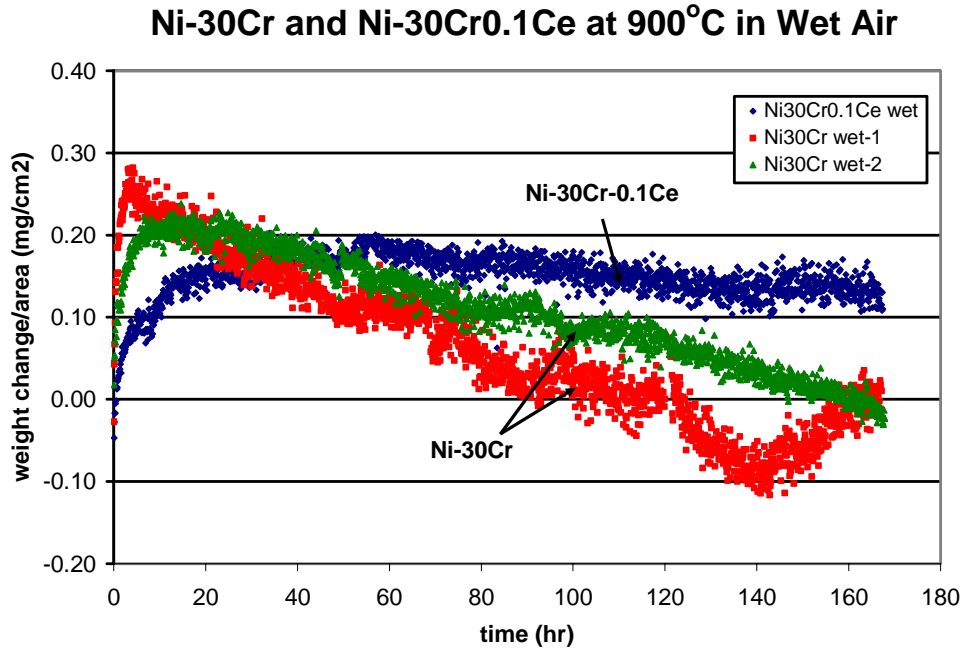


Figure 6.56: The TGA data of Ni-30Cr-(0.1Ce) at 900°C in wet air shows that the system(s) lose weight due to the formation of vapor species. ($P_{H_2O} = 0.1$ atm, $P_{total} = 1$ atm).

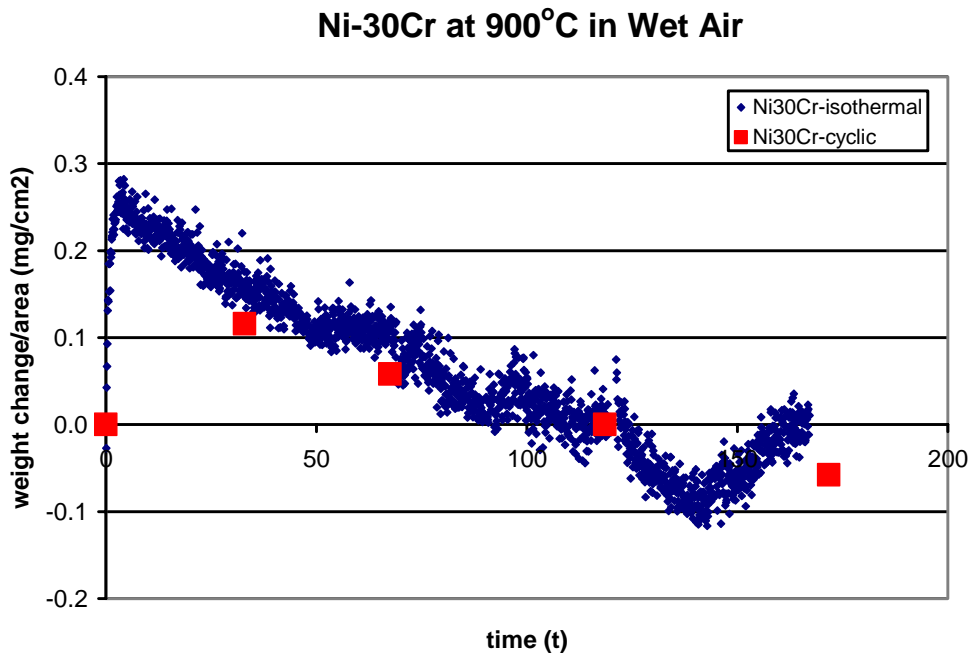


Figure 6.57: The comparison of the weight changes during isothermal tests to cyclic experiments for Ni-30Cr system at 900°C in wet air shows that scale spallation is not very substantial. The weight losses originate essentially from the formation of vapor species.

ISOTHERMAL WET TESTS AT 900°C

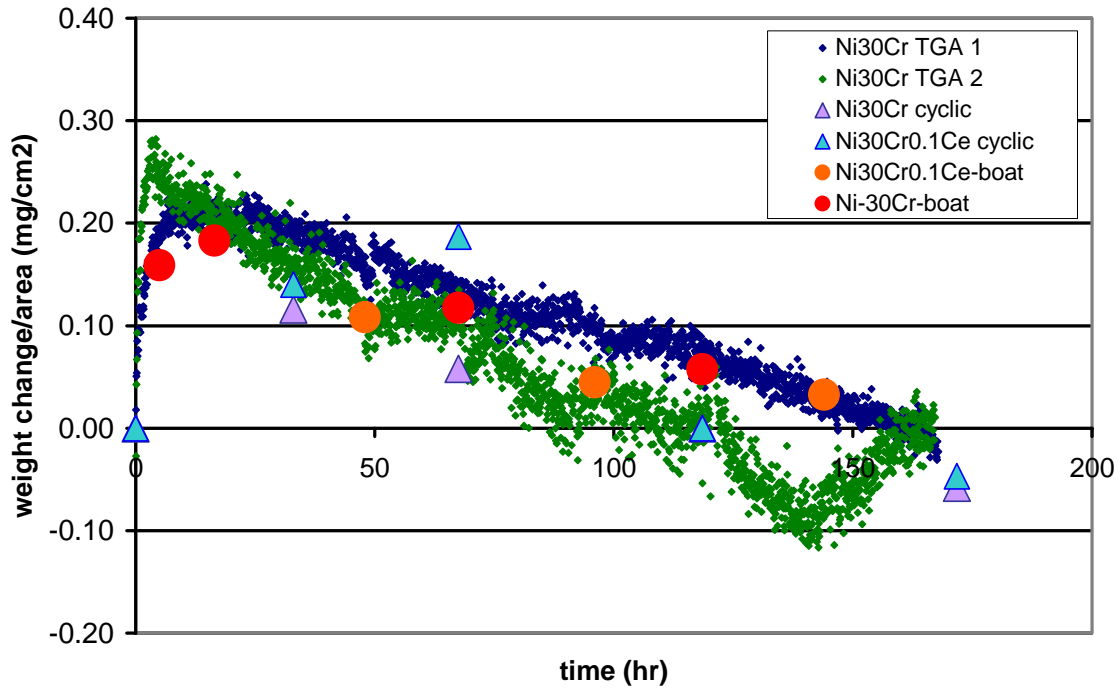
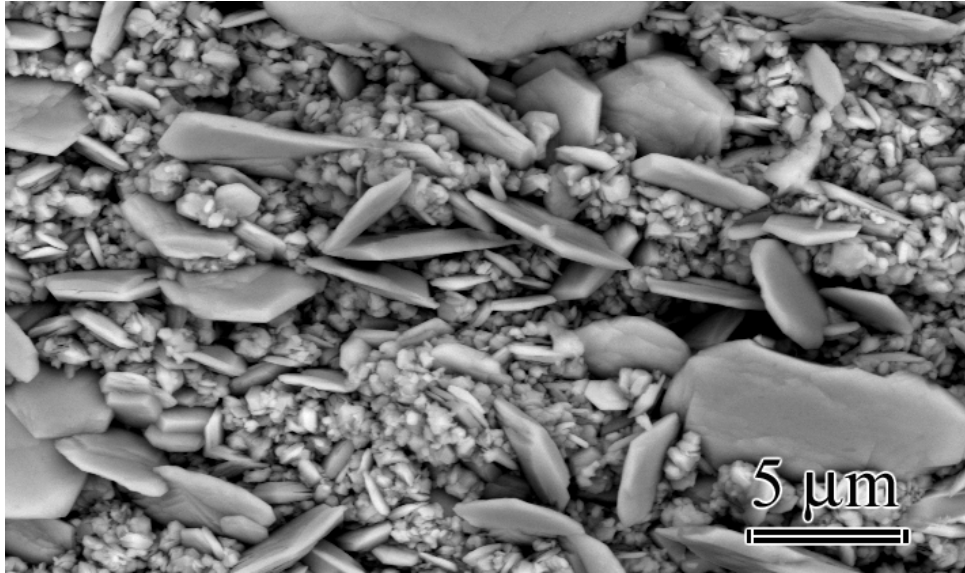
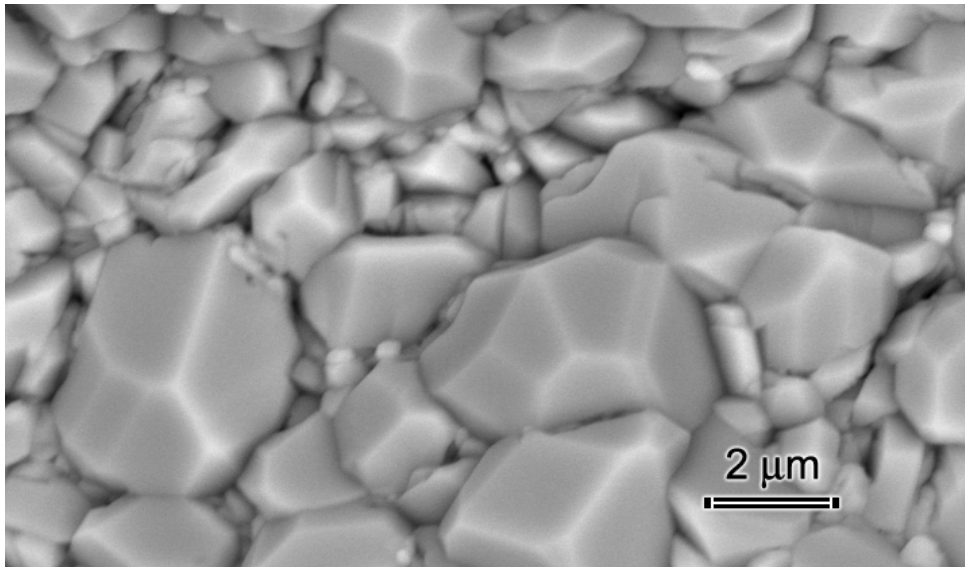


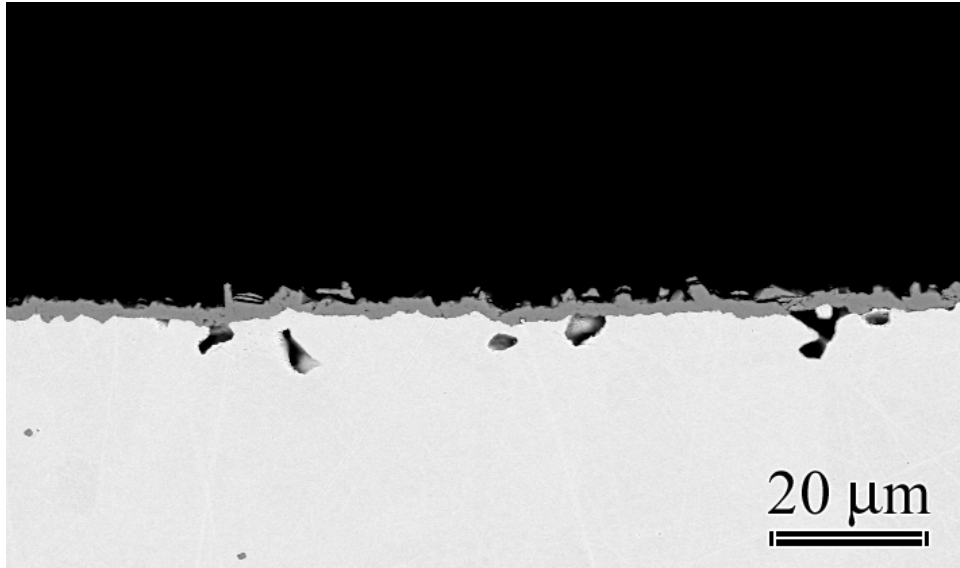
Figure 6.58: The diagram shows the weight changes of Ni-30Cr and Ni-30Cr-0.1Ce at 900°C in wet air. The data obtained from TGA tests is compared to cyclic exposures and to isothermal tests using multiple specimens, each of which was exposed to wet air for a predetermined time in ceramic boats. Results show good agreement between isothermal boat tests and TGA. The cyclic exposures do not result in more pronounced weight losses for Ni-30Cr or Ni-30Cr-0.1Ce. This indicates that the weight losses in this environment are due to vapor species formation rather than scale spallation.



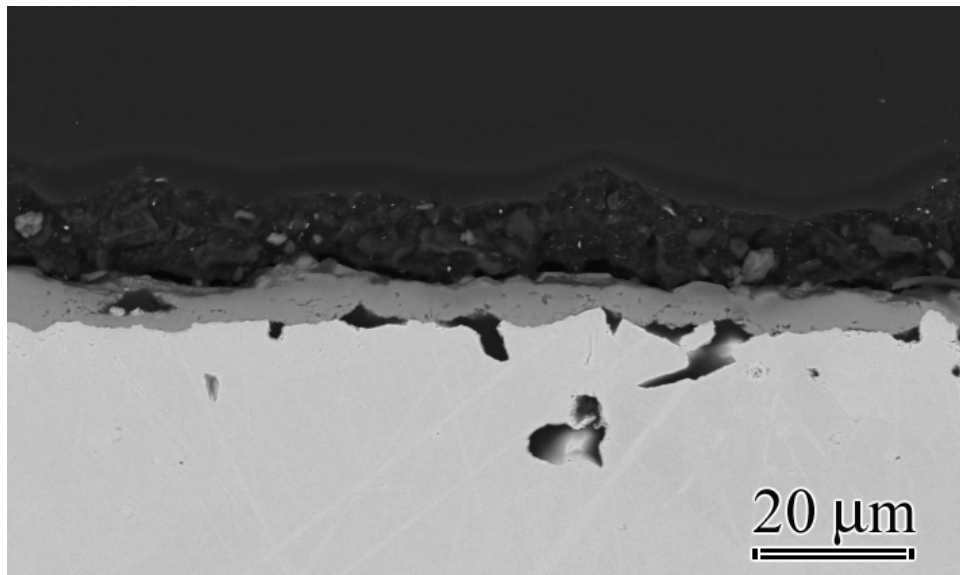
(a)



(b)



(c)



(d)

Figure 6.59: The surface, (a-b), and the cross-sectional, (c-d), images of the alloy Ni-30Cr are shown at 900°C after isothermal TGA tests for 168 hours in wet and dry air. (a) In air/H₂O flakey Cr₂O₃ developed over the continuous chromia layer. (b) High magnification image of chromia that developed in dry air is shown. The chromia flakes were not observed in this environment. (c) SEM image shows the scale that developed in wet air in cross-section. Void formation at the oxide/gas interface was evident. (d) Image shows chromia scale that developed in dry air. The thickness of the layer was twice larger in comparison to wet air. Voids developed at the substrate/oxide interface in this environment as well.

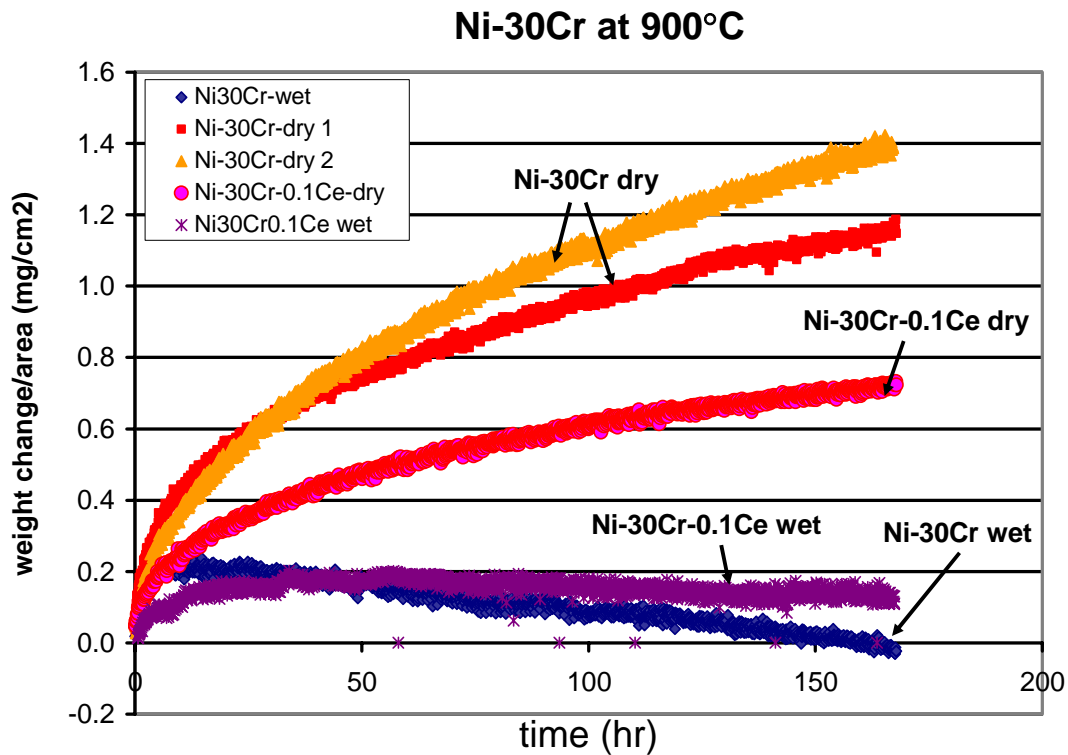
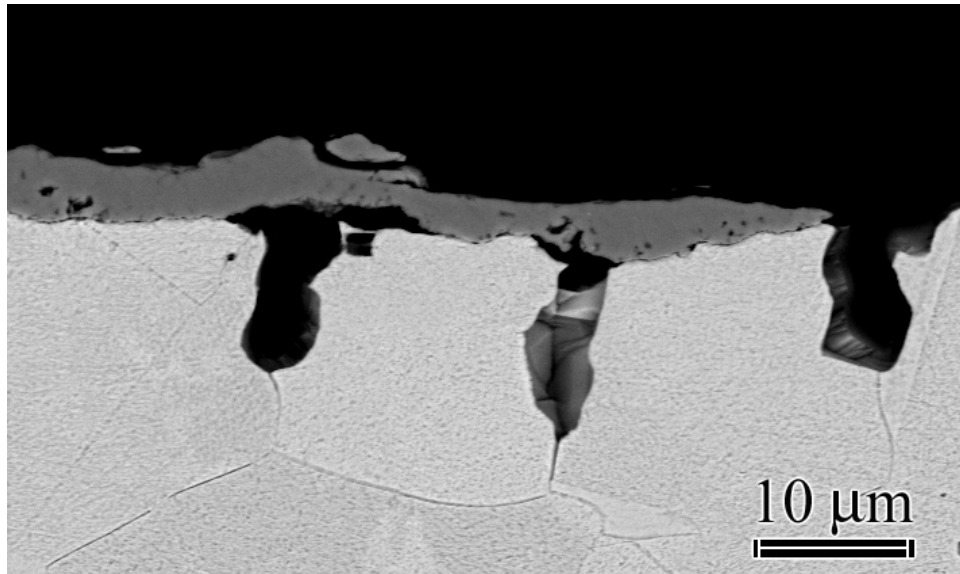
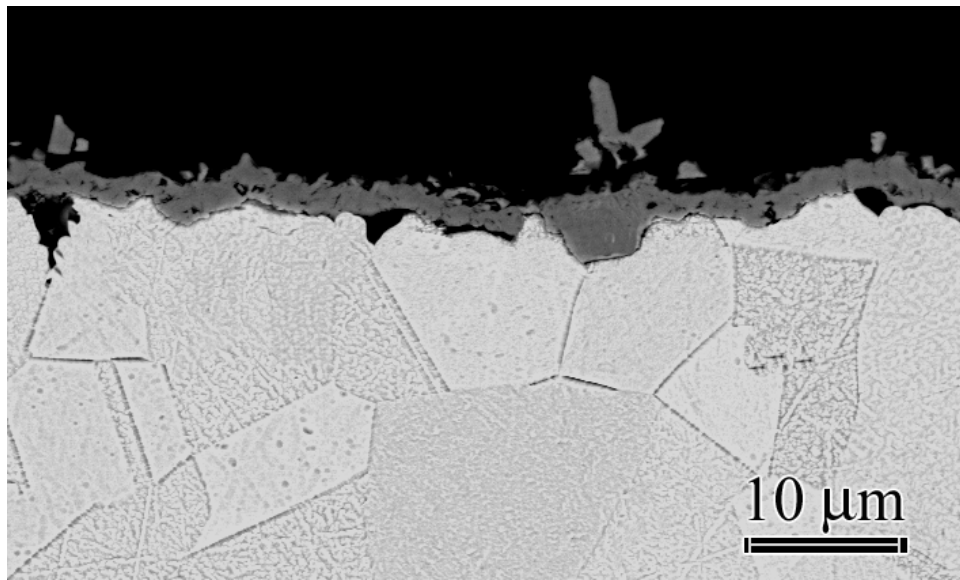


Figure 6.60: The comparison of the TGA data for Ni-30Cr(0.1Ce) in dry air to wet air at 900°C showed that the weight losses were more pronounced for the latter environment. In dry air, the growth rate of chromia was slower for the Ce-doped specimen. The presence of the reactive element did not affect the vaporization rate significantly. These results are in agreement with literature. The deviation between Ni-30Cr and Ni-30Cr-0.1Ce in wet air is experimental.

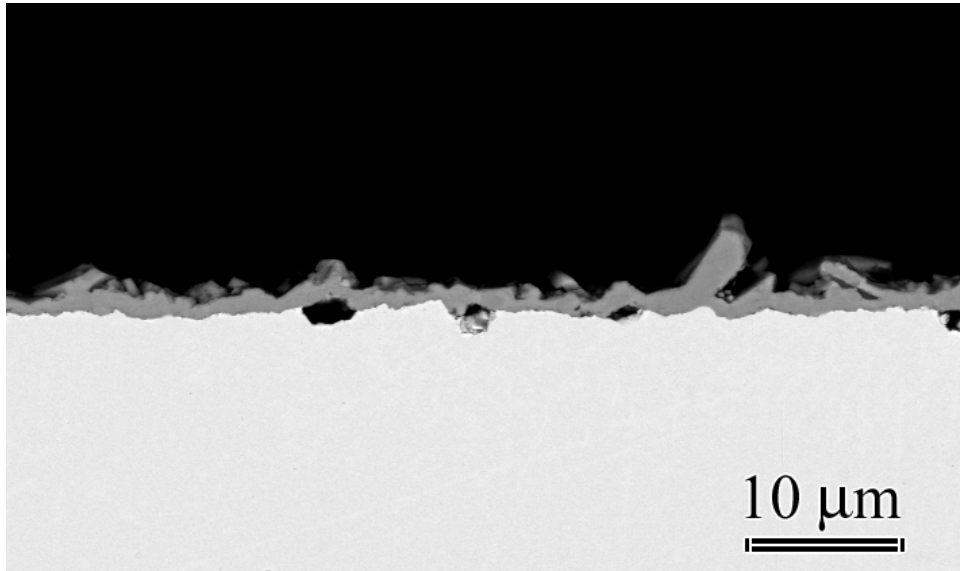


(a)

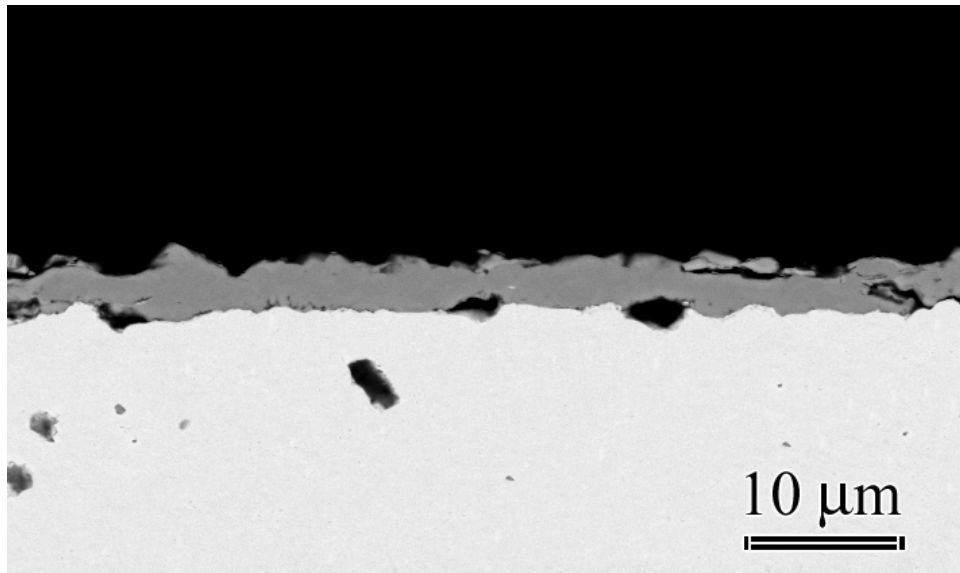


(b)

Figure 6.61: Ni-30Cr at 900°C after isothermal TGA tests for 168 hours. Back scattered electron images show the formation of voids at the alloy grain boundaries (a) in wet air, and (b) in dry air.



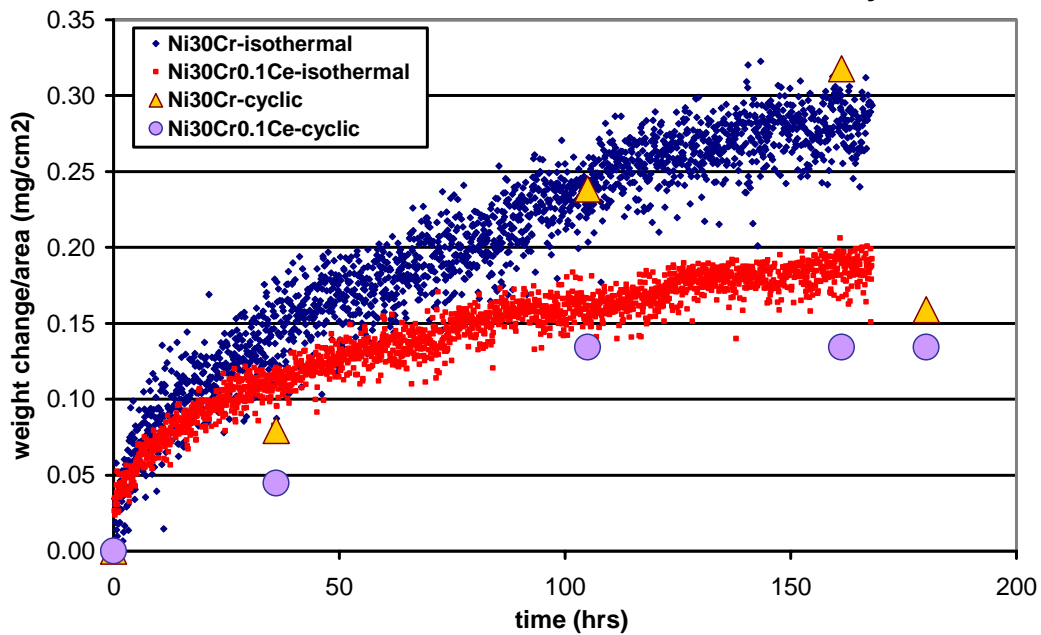
(a)



(b)

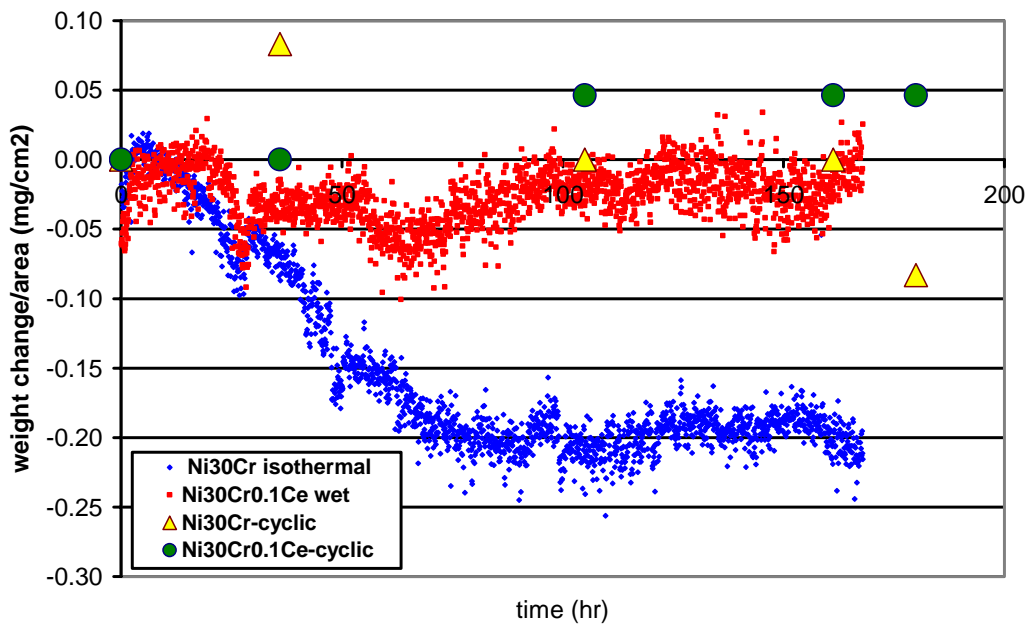
Figure 6.62: Ni-30Cr-0.1Ce at 900°C (a) in wet air, and (b) in dry air after isothermal tests for 168 hours.

Ni-30Cr and Ni-30Cr-0.1Ce at 700°C in Dry Air



(a)

Ni-30Cr and Ni-30Cr -0.1Ce at 700°C in Wet Air



(b)

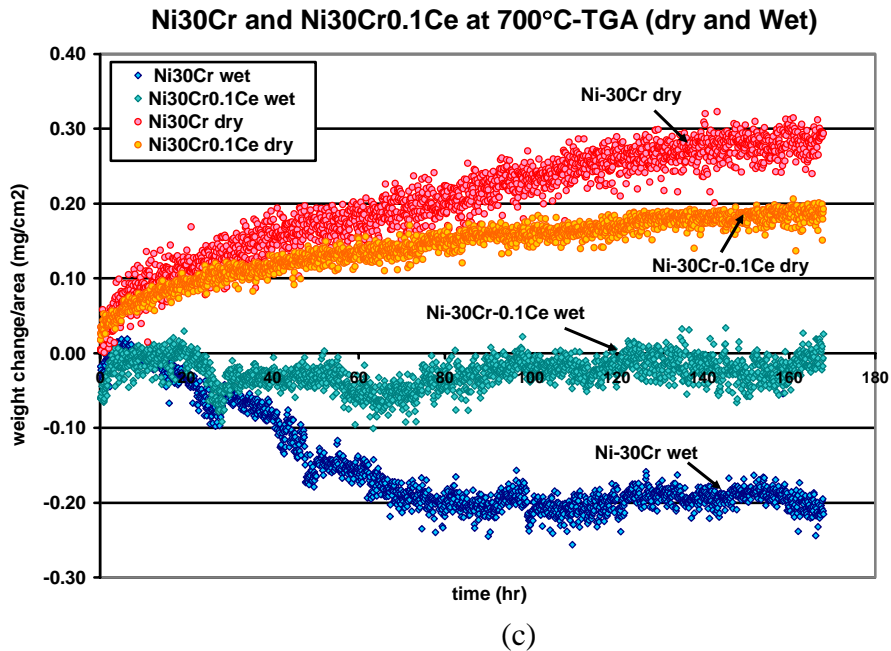


Figure 6.63: The comparison of the TGA data to the cyclic tests at 700°C was in agreement with the results obtained at 900°C. Scale spallation was more pronounced for the tests in dry air, (a), in comparison to wet air (b). The formation of vapor species was evident at this temperature as well. The weight changes in air/H₂O mixtures were more negative compared to dry air, (c).

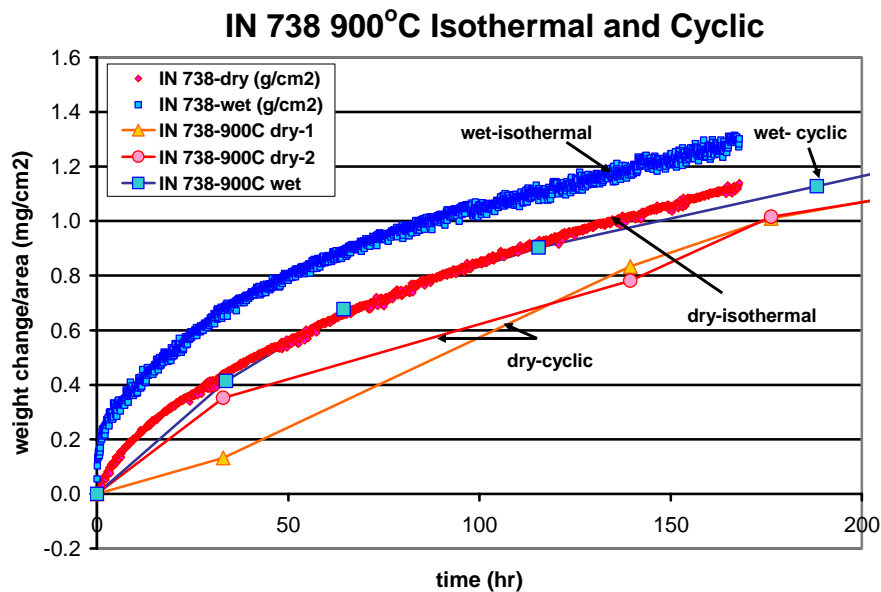


Figure 6.64: Weight losses related to vapor species formation were not evident for IN 738 at 900°C. The comparison of isothermal tests to cyclic experiments showed that the weight changes were smaller for the latter condition. This is related to scale spallation that arises during thermal cycling.

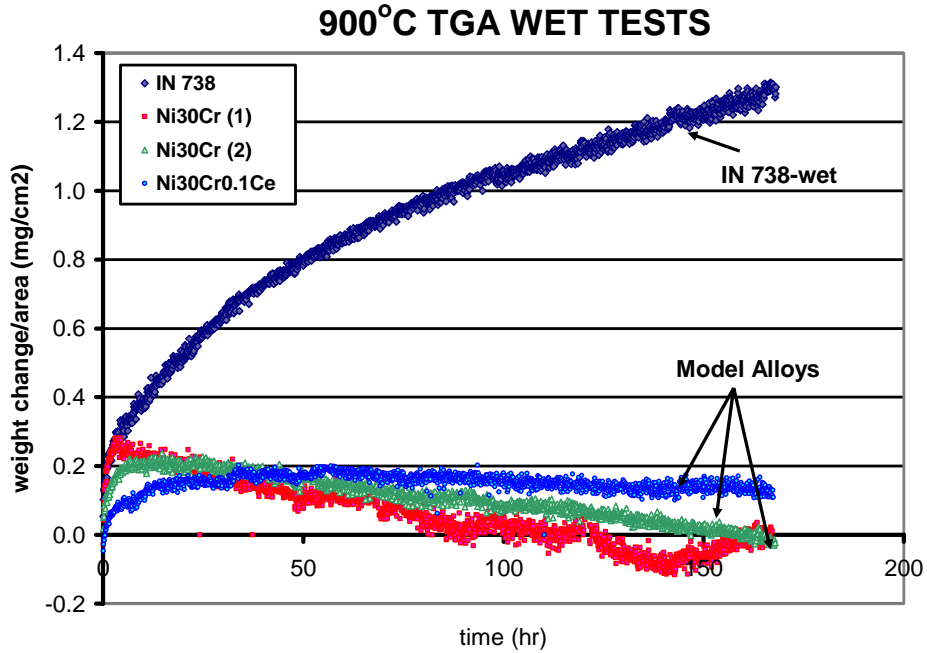


Figure 6.65: The TGA data for IN 738 at 900°C in wet air was compared to the model alloys (i.e. Ni-30Cr and Ni-30Cr-0.1Ce), which were tested under the same conditions. The weight losses associated with the formation of vapor species were not evident for the superalloy.

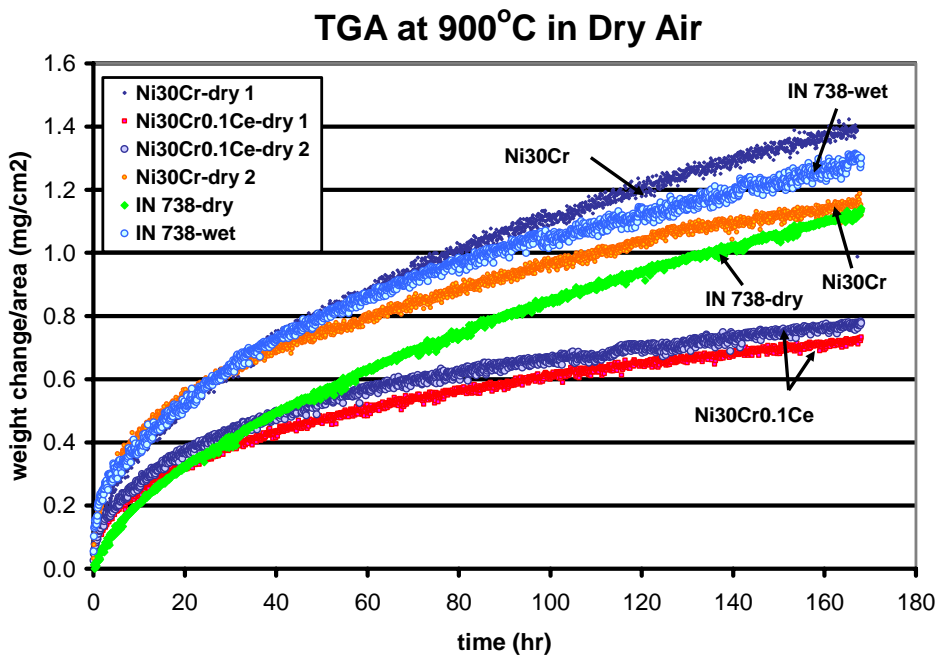
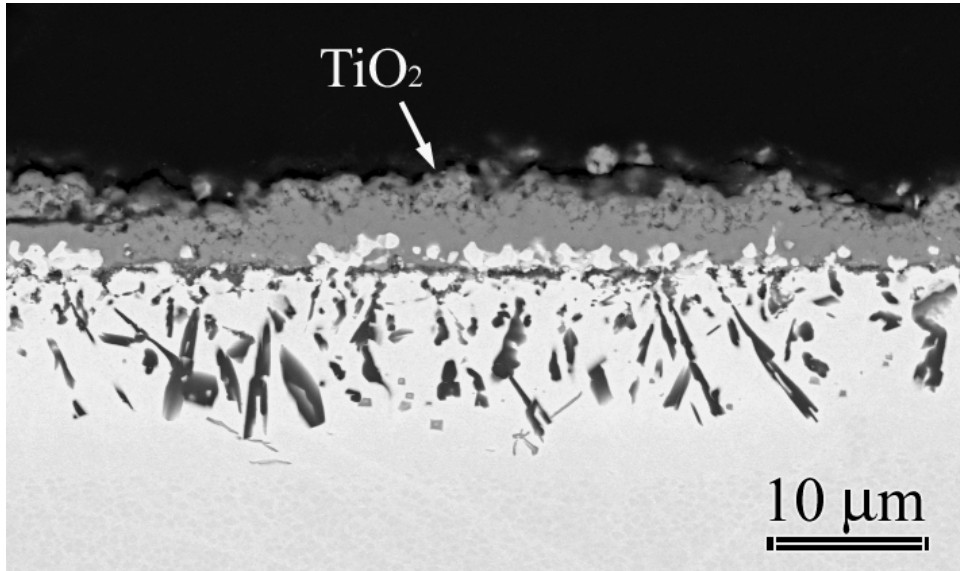
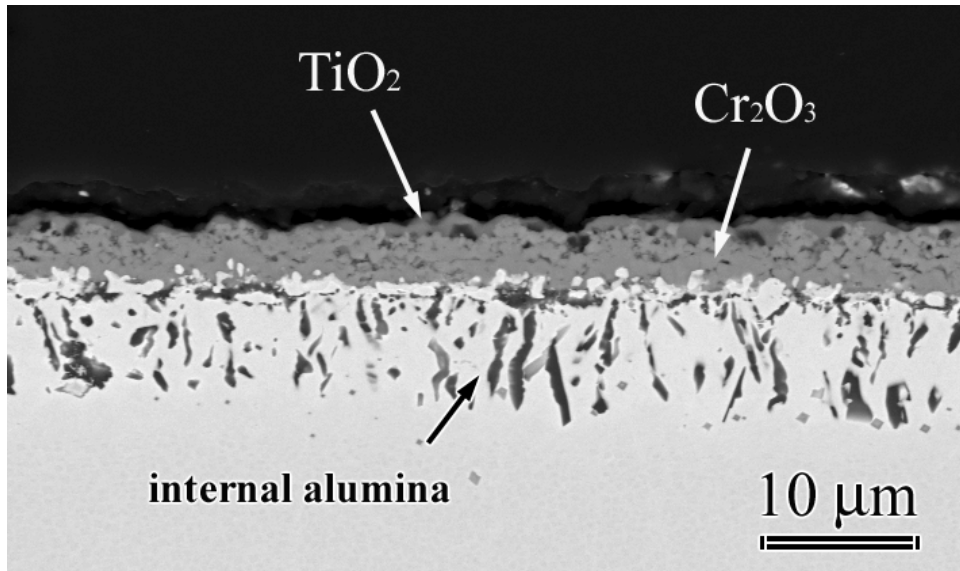


Figure 6.66: Comparison of the isothermal weight change data of IN 738 to the simple alloys at 900°C in dry air showed that the behavior of the superalloy was similar to Ni-30Cr.



(a)



(b)

Figure 6.67: The microscopic examination of IN 738 which was tested isothermally at 900°C showed that Ti developed a thin oxide layer at the oxide/gas interface. This layer was detected in wet air (a), as well as in dry air (b). The existence of this layer put a physical barrier between the chromia scale and the reactive gases. This avoided the loss of the protective layer by the formation of vapor species, which was observed to be more aggressive in air/H₂O mixtures.

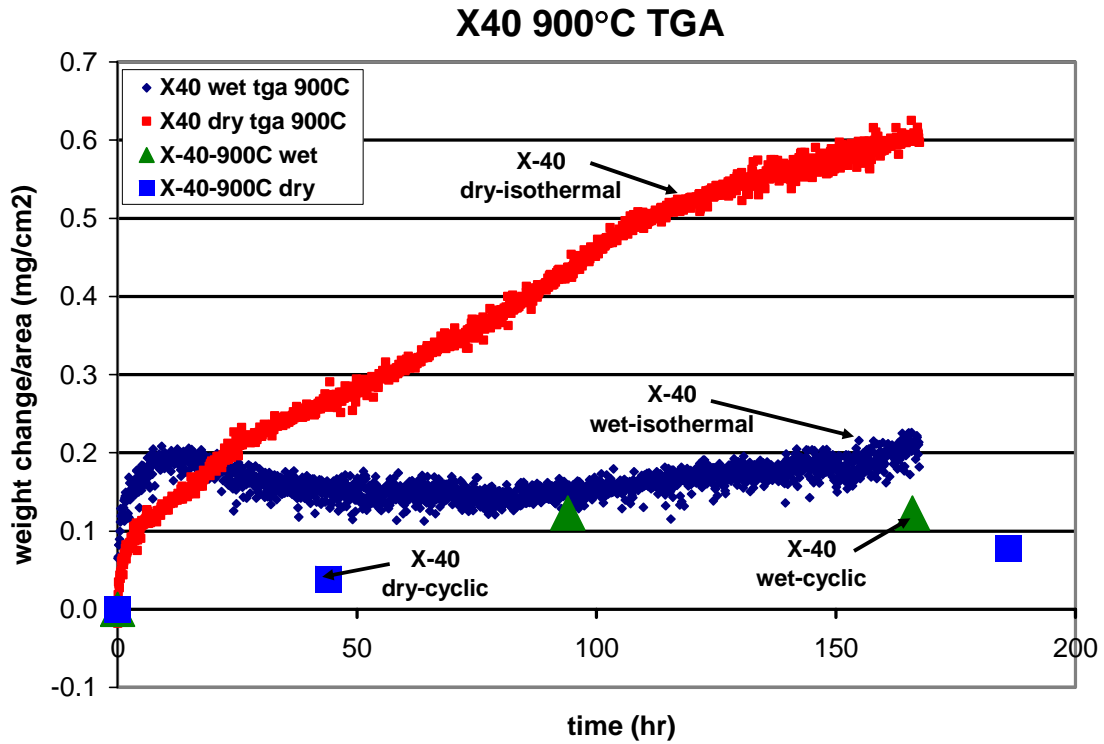
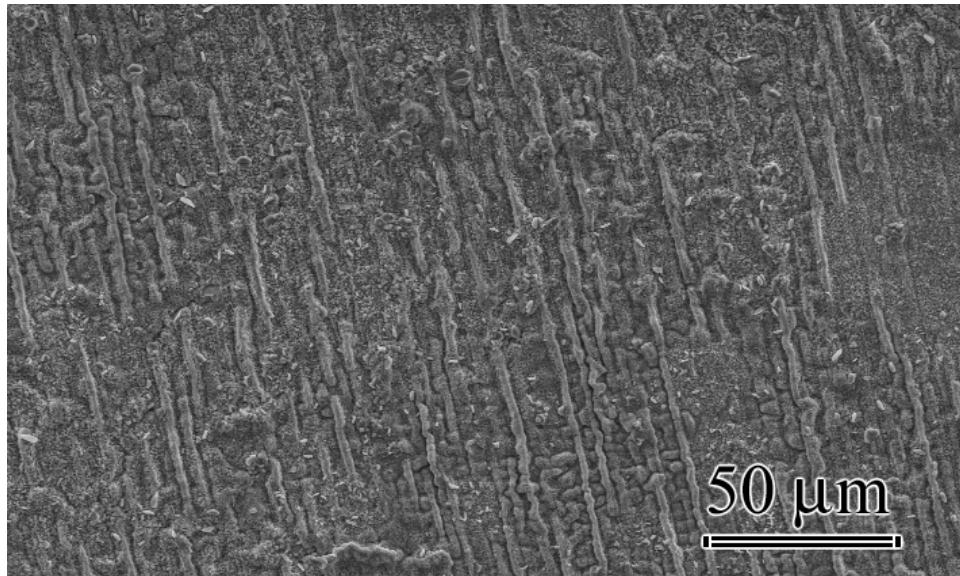
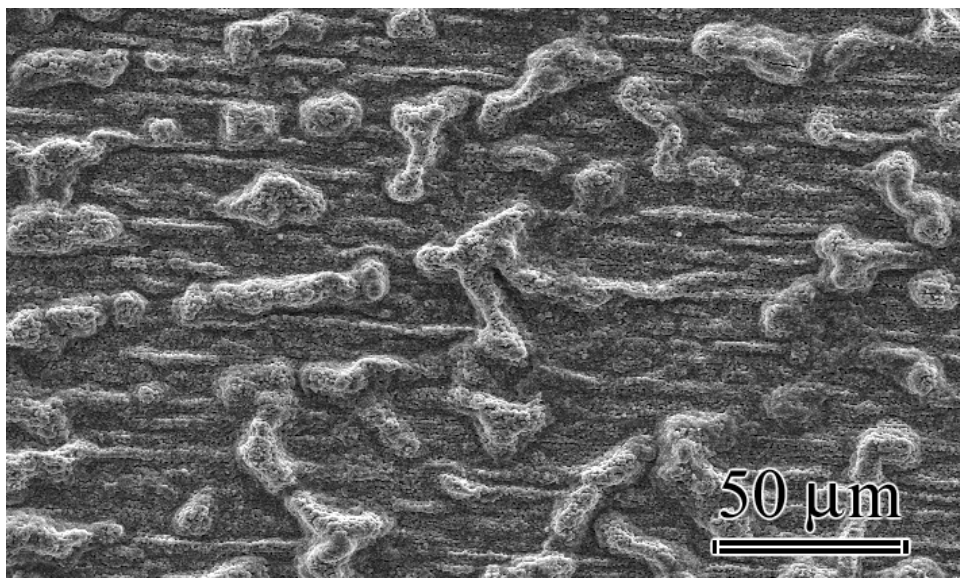


Figure 6.68: The isothermal tests with the superalloy X-40 at 900°C showed that volatile species formation was evident in wet air. The weight changes during cyclic tests were significantly lower for exposures in dry air. This was less pronounced in air/H₂O mixtures.

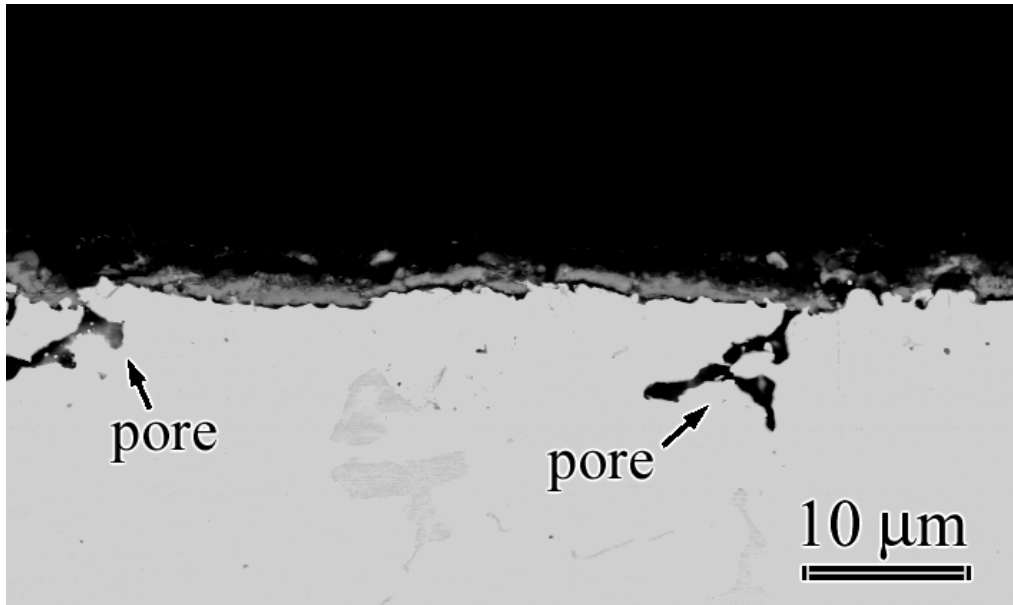


(a)

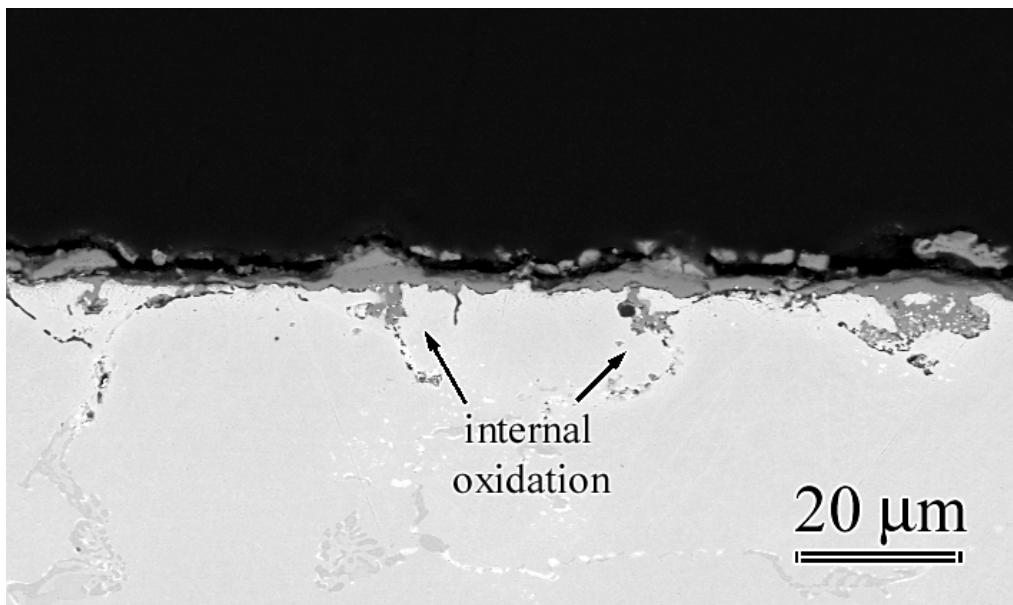


(b)

Figure 6.69: The SEM images of X-40 show the surface of the alloy after isothermal tests, (a), in wet air, and, (b), in dry air for 168 hours at 900°C. EDX analysis indicated the presence of Co and W along with chromia. Co- and W-oxides were more abundant on the specimen tested in dry air. Additionally, the surface morphologies were observed to be different for each environment. The scale was smoother after experiments in wet air, whereas it was rougher for the sample exposed to dry air.



(a)



(b)

Figure 6.70: The back scattered electron microscopy images show the cross-section of the X-40 specimens which were tested isothermally at 900°C for 168 hours, (a) in wet air, and, (b), in dry air. Wet air resulted in the formation of thinner scales with uniform thickness. The scale that developed after exposures in dry air was identified as chromia with transient Co(W)-oxides at the oxide/gas interface. The internal oxidation was more pronounced in dry air. Formation of voids at the oxide/gas interface was evident in wet, as well as in dry air.

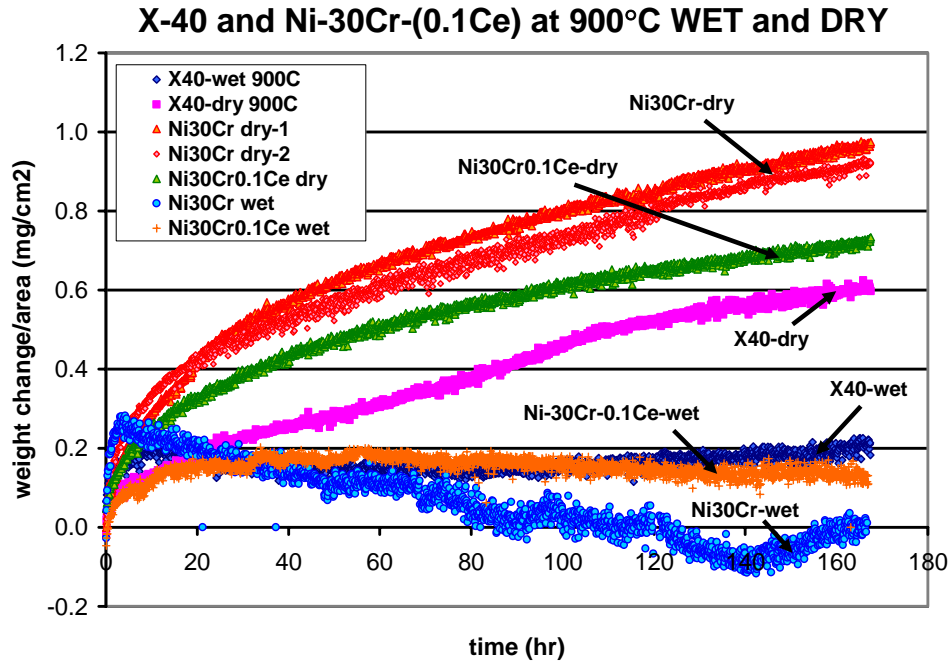


Figure 6.71: The kinetic plot shows the weight changes for model systems and the superalloy X-40 as a function of time at 900°C after TGA tests in dry air and in air/H₂O mixtures.

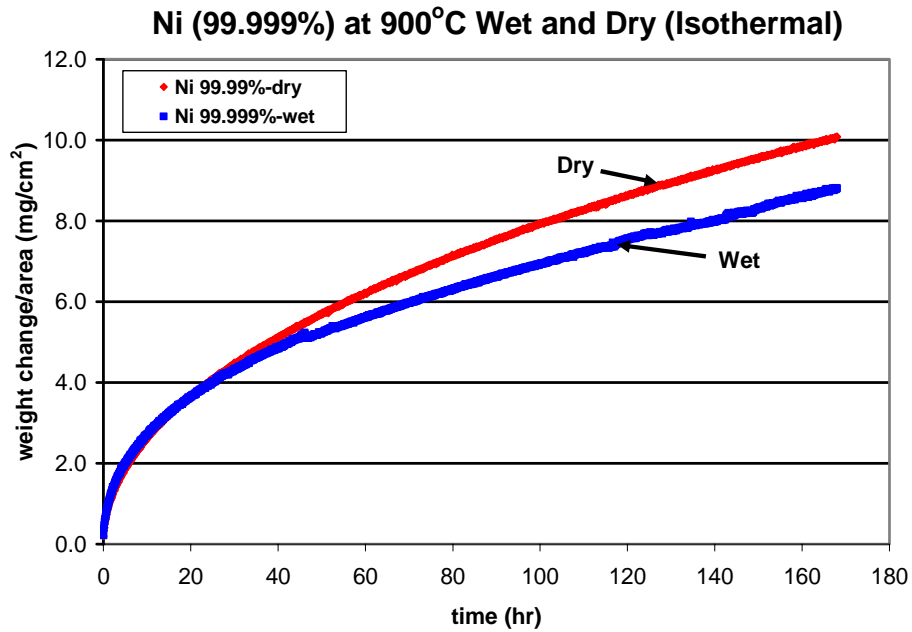
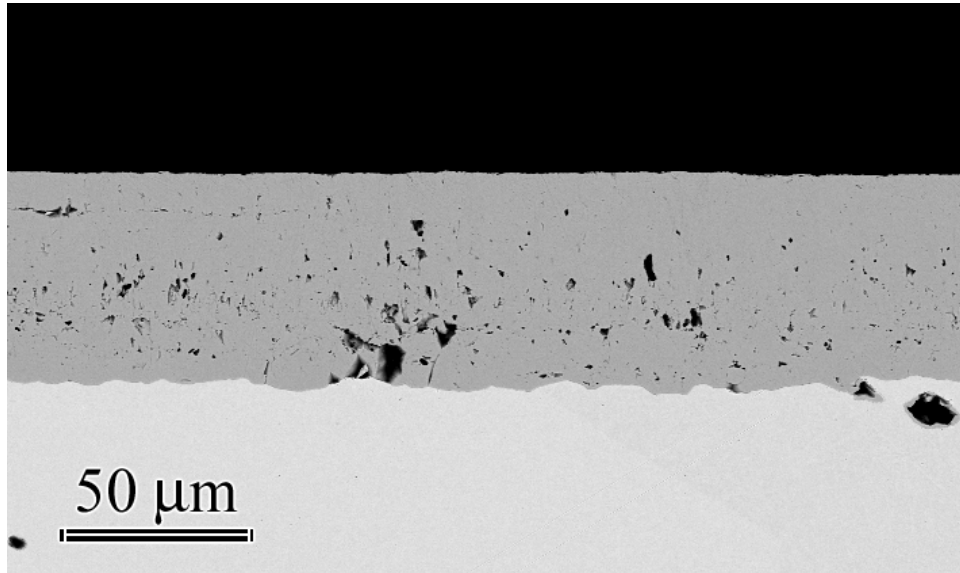
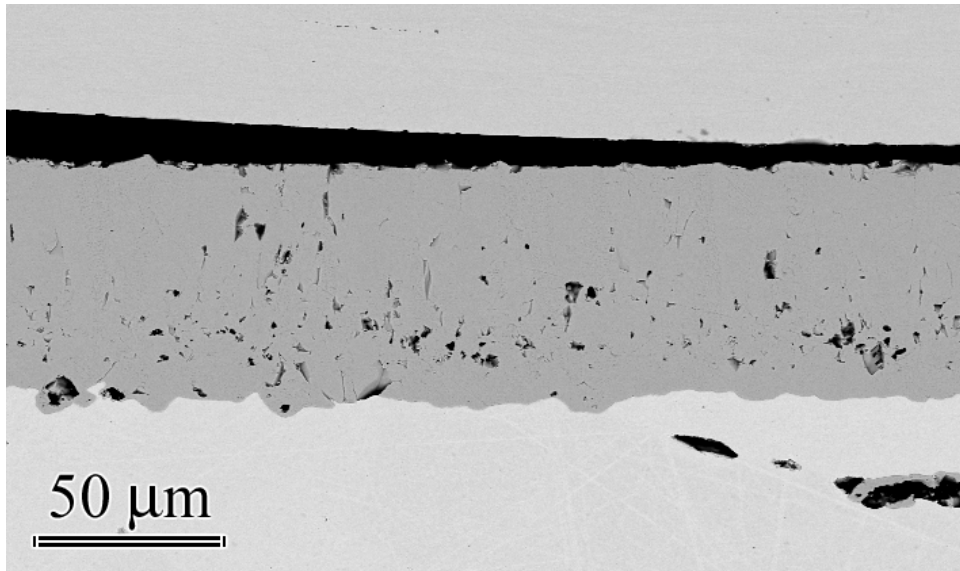


Figure 6.72: The weight change data for Ni(99.999%) at 900°C is shown as a function of exposure time. The metal was subjected to isothermal tests in dry air and in air/H₂O mixtures for 168 hours.

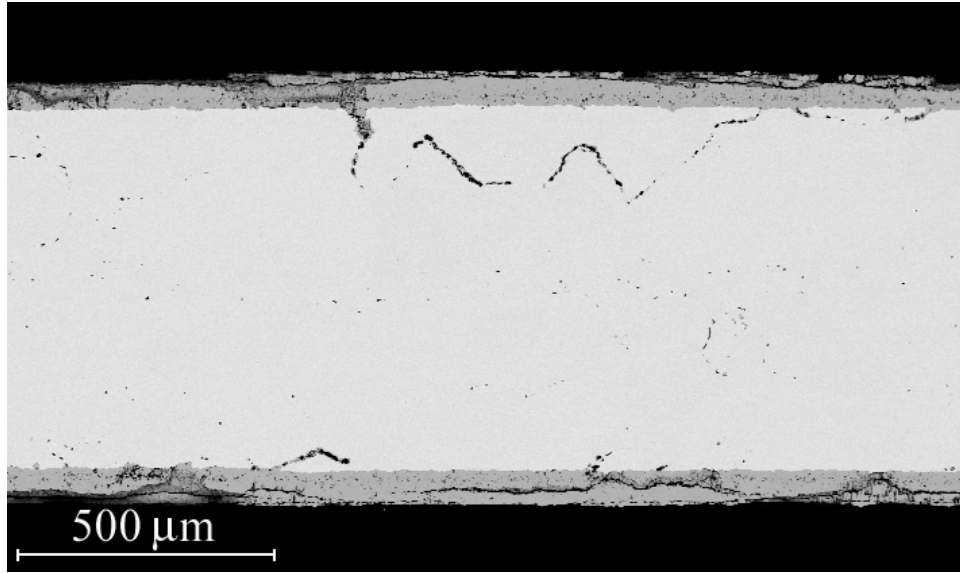


(a)

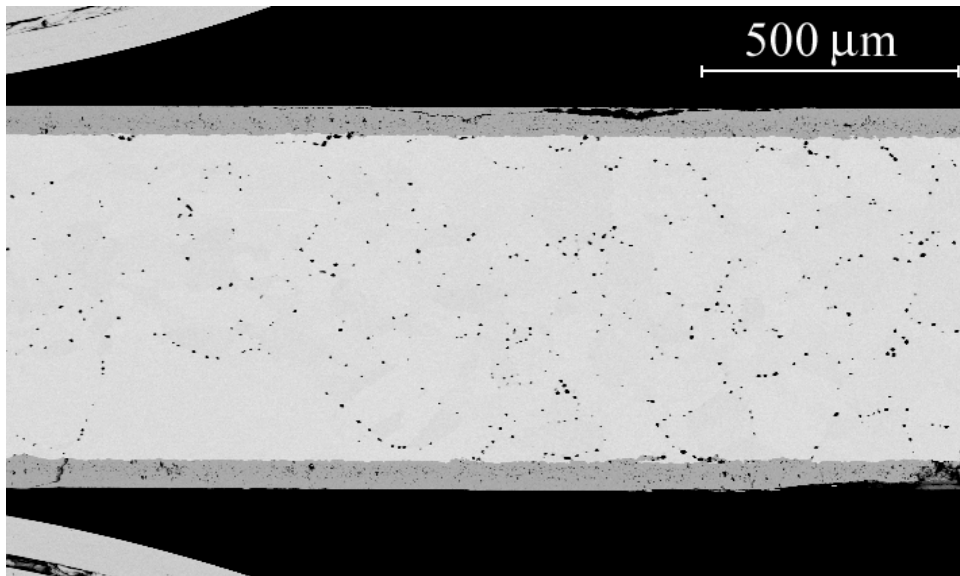


(b)

Figure 6.73: SEM images show the cross-section of pure Ni (99.999%) after isothermal tests at 900°C (a) in air-10% H_2O , and (b) in dry air after 168 hours. The thickness of the NiO layer was found to be slightly larger after exposures in dry air.

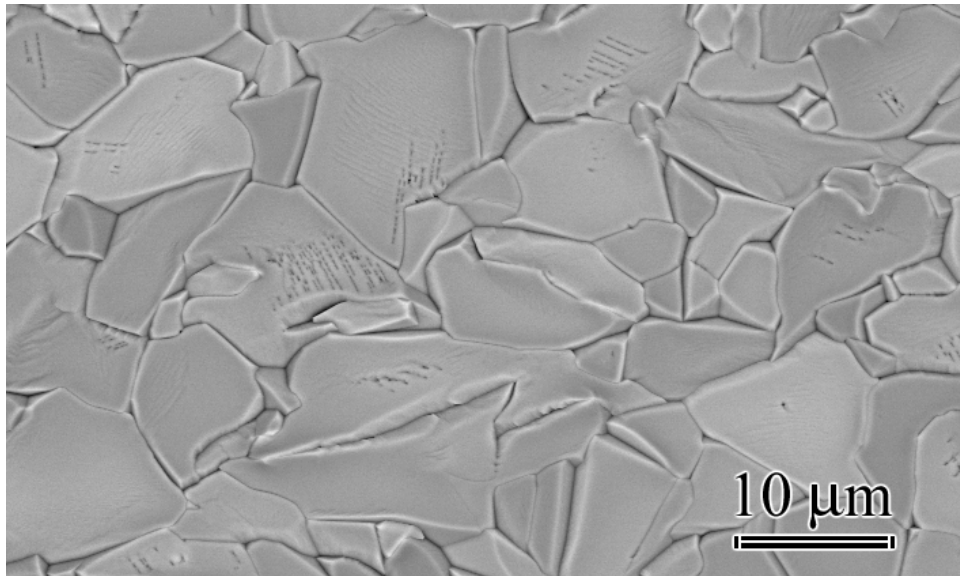


(a)

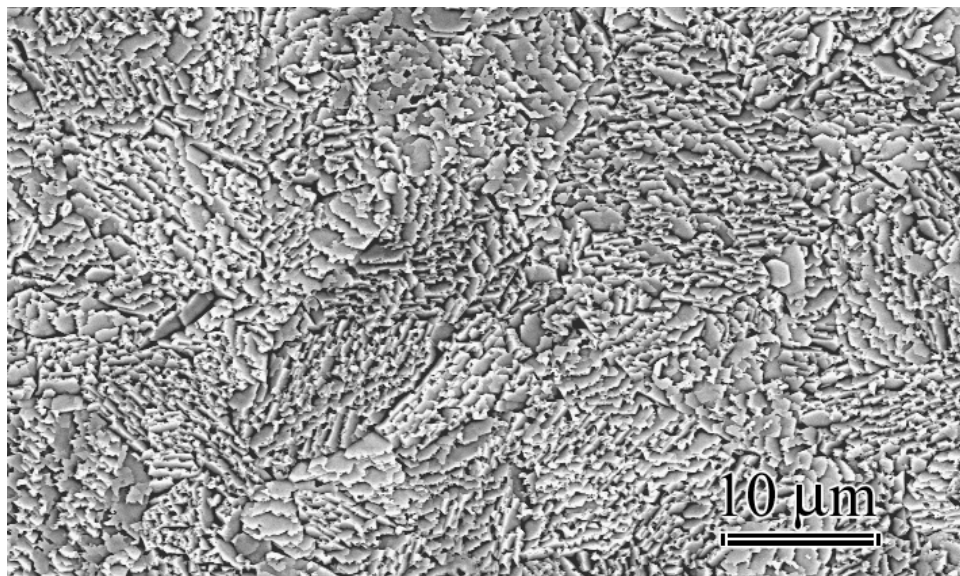


(b)

Figure 6.74: Low magnification SEM images of the Ni(99.999%) sample cross-sections after isothermal tests for 168 hours at 900°C (a) in dry air, and (b) in wet air [$P(\text{H}_2\text{O}) = 0.1 \text{ atm}$, $P_{\text{total}} = 1 \text{ atm}$).



(a)



(b)

Figure 6.75: The images show the surface of NiO that developed on pure Ni(99.999%) after isothermal exposures for 168 hours at 900°C (a) in dry air, and, (b), in wet air. In dry air, equiaxed grains were evident. In wet air faceted surface development was observed.

6.3 FLAKEY-CHROMIA FORMATION IN AIR/WATER-VAPOR MIXTURES

The Cr_2O_3 with the morphology that had been called “flake-like” or “flakey” was unique to tests in environments containing water vapor. Comparison of the x-ray diffraction patterns showed that the same phase developed in dry air and in air/ H_2O mixtures. These oxides did not differ from each other crystallographically. They were identified as $\alpha\text{-Cr}_2\text{O}_3$. To observe the growth kinetics of the flakes, multiple specimens of Ni-30Cr and Ni-30Cr-0.1Ce were exposed to wet air at 900°C . Oxide surfaces were analyzed microscopically after different hold times.

Figure 6.76 shows the surface of Ni-30Cr after 10 minutes, 1 hr, 5hr, 16.5 hr, 67.5 hr, and 168 hr of isothermal testing. Each exposure was done using a fresh specimen from the same batch. Examination of the surfaces showed that after 10 minutes the transition from transient oxidation to chromia formation was not complete, Figure 6.76(a). In the lighter colored areas the scale consisted of Ni-rich oxides. Darker regions were where chromia formation started. After 1 hour, the fraction of the Ni-rich areas decreased, Figure 6.76(b). Formation of granular chromia with grains larger than the rest of the scale was observed in the Cr-rich parts of the surface, Figure 6.76(c). The surface of the specimen exposed for 5 hours consisted of Cr-oxides only, Figure 6.76(d). At this stage, the morphology of Cr_2O_3 was still granular. The formation of the flake-like oxide was first detected on the specimen exposed for 16.5 hr. In time, these features became more distinguished, Figure 6.76(e-f).

Figure 6.77 shows the surface of Ni-30Cr-0.1Ce after 48 hr, 96 hr, 118 hr, and 168 hr of isothermal exposures at 900°C . Examination of the scale showed that the flakey chromia developed more profusely on the Ce-doped alloy. Between 48 hours and 118 hours no substantial changes were evident in terms of the size or frequency of the flakes. However, on the

specimen exposed for 168 hours formation of abnormally big flakes with a different morphology was detected in addition to the smaller sized flakes with the hexagonal geometry, Figure 6.78.

Development of oxides with different morphologies in H₂O containing environments has been reported many times in the literature for several systems [64, 75, 80, 86, 87]. The common observation was the formation of “whiskers” or “blade-like” oxides. The mechanism suggested for their growth was the surface diffusion of cations along a channel that goes through the core of screw dislocations [86, 87]. However, the geometry and the growth direction of the flakes observed over the Ni-Cr alloys are not consistent with this mechanism, Figure 6.79. One possibility for their growth could be the faster cation transport along the grain boundaries of the substrate. During the examination of the scale surfaces it was noticed that the pattern for the pore formation in areas where the scale spalled off of the oxide surface had a close match with the pattern for the flakey Cr₂O₃ formation, Figure 6.80. However, this morphology did not develop in dry air although the pore formation was as profuse, Figure 6.81. It is not clear if there is a connection between the formation of the pores and the flakes. Another possibility is the preferential thermal etching of the oxide during the loss of the Cr₂O₃ scale in the grain interiors while volatile oxide species form combined with the faster cation transport through the defects at the scale/substrate interface. Formation of chromia via vapor transport should also be considered. This phenomenon needs further investigation with more detailed testing and analysis.

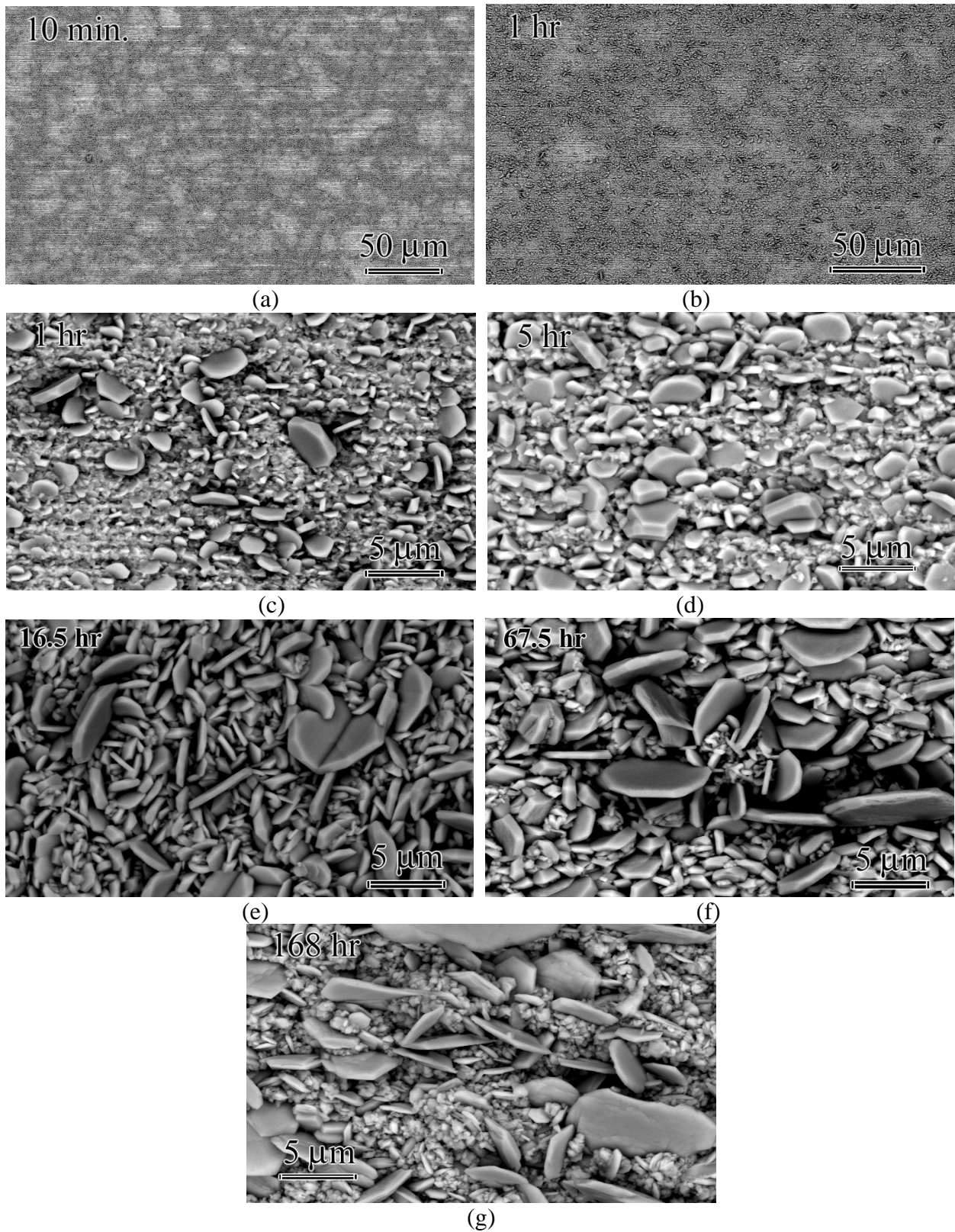


Figure 6.76: SEM images showing the morphology of the chromia scale that developed on Ni-30Cr at 900°C in wet air ($\text{PH}_2\text{O} = 0.1 \text{ atm}$, $\text{P}_{\text{total}} = 1 \text{ atm}$) at different exposure times.

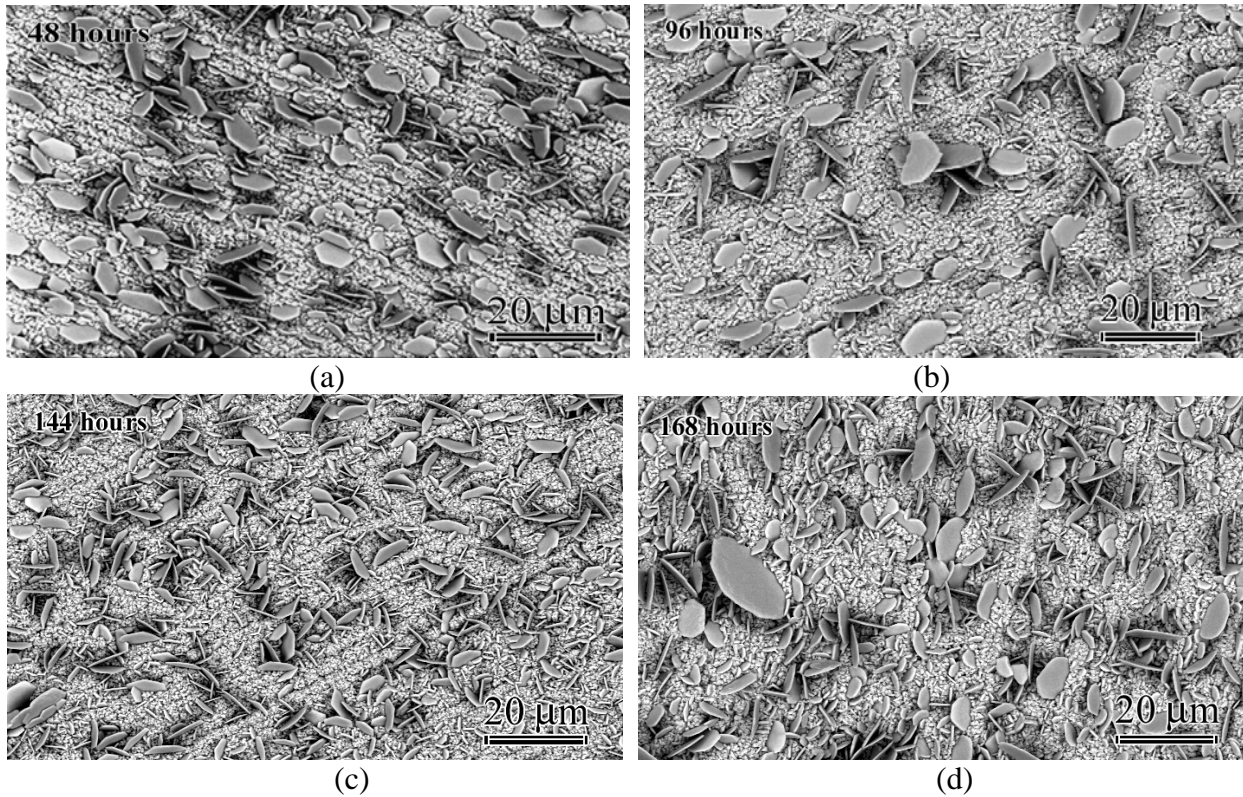


Figure 6.77: Formation of flakey chromia over Ni-30Cr-0.1Ce at 900°C is shown after exposures in air/H₂O mixtures ($P_{H_2O} = 0.1$ atm, $P_{total} = 1$ atm) for different hold times.

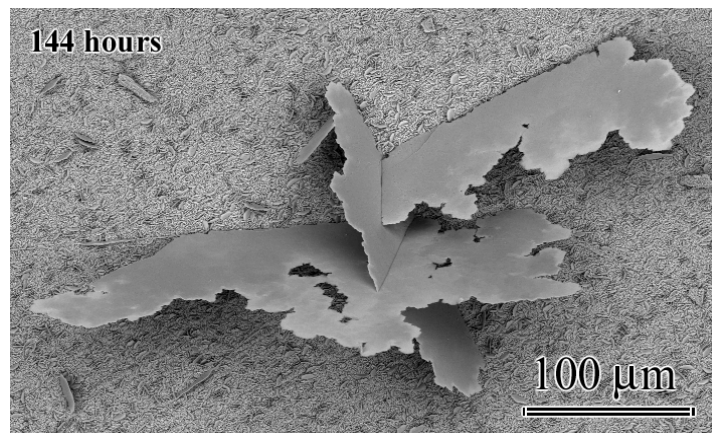
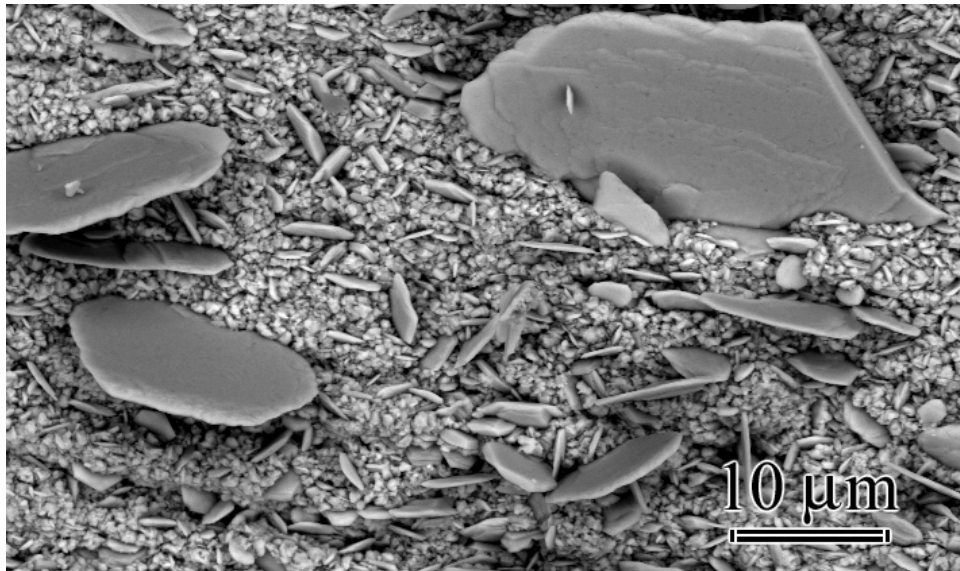
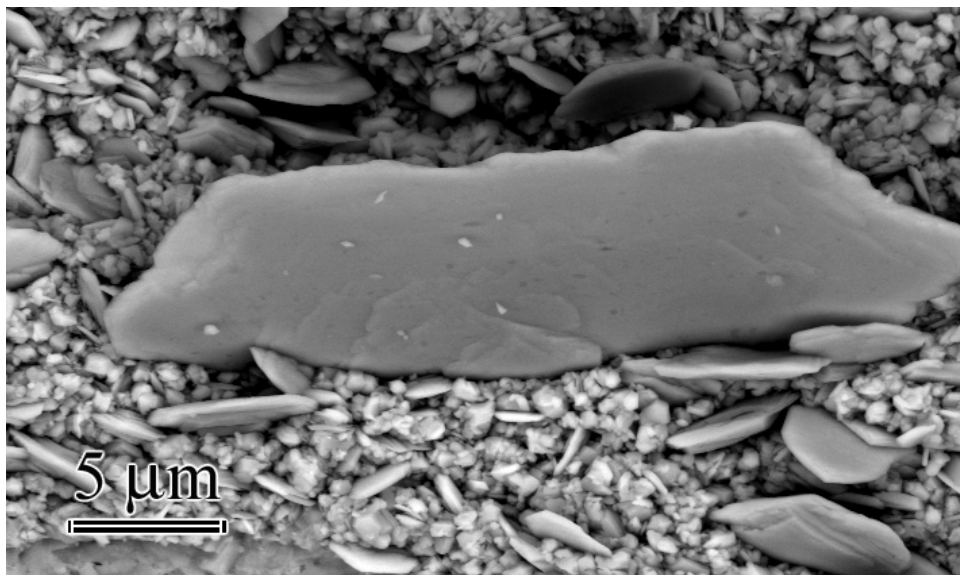


Figure 6.78: SEM image shows Ni-30Cr-0.1Ce after isothermal tests at 900°C for 168 hours in wet air. Formation of abnormally big flakes with a different morphology was detected in addition to the smaller sized flakes with the hexagonal geometry.



(a)



(b)

Figure 6.79: The chromia flakes that are observed on the Ni-Cr alloys after tests in air/H₂O mixtures at 900°C are shown at high magnification.

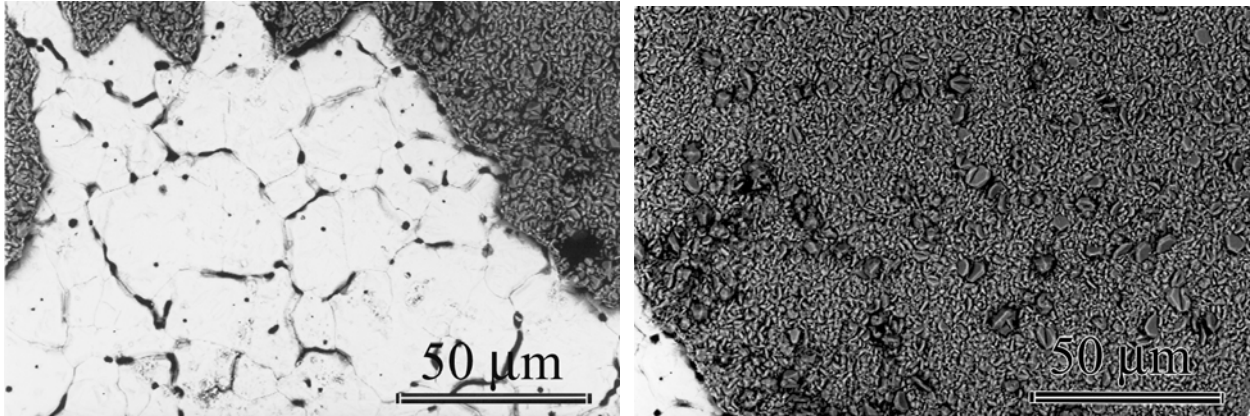


Figure 6.80: SEM images of Ni-30Cr at 900°C in wet air after 16.5 hours. The pattern of the grain boundaries and the pores over the spalled areas displays similarities with the pattern for the formation of chromia flakes.

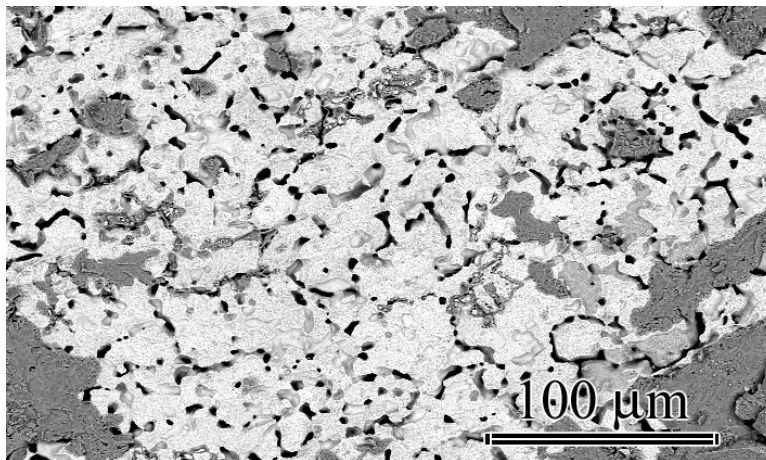


Figure 6.81: Ni-30Cr in dry air at 900°C after 535 hours of isothermal testing. Substantial amounts of scale spallation took place during cooling. Spalled areas revealed pore formation in the substrate.

7.0 SUMMARY AND DISCUSSION OF RESULTS

7.1 ALUMINA FORMATION ON COMPLEX ALLOYS

Tests with the superalloys that are classified as primary alumina formers showed that temperature and water vapor were among the factors that had an adverse effect on selective oxidation of Al. Lower temperature tests, i.e. 700°C, showed that alumina formation was particularly hindered as the diffusion coefficient of Al in the alloy was lower at this temperature. In most systems alumina formed as an internal oxide instead of an externally developed continuous protective layer. This case was more severe in the wet environment. The transient oxide layer was substantially thicker under these circumstances. It was observed that the composition of the underlying alloy was more critical at this temperature. Alloys with smaller Al and Cr additions were affected more severely by the attack of the oxidizing species. The system with the least resistance was PWA 1484, while René N5 displayed the best performance.

Temperature elevations improved the ability of the systems to develop alumina scales remarkably. Generally, protective scale formation was much easier in dry air. The amount of transient oxides varied with the superalloy composition. At 900°C René N5 developed slowly growing scales without significant transient oxidation. Other systems formed various amounts of rapidly growing oxides in proportion with their Al and Cr composition, as discussed earlier. In wet air, transient oxidation was more profuse compared to dry air. However, at 900°C

all systems developed the protective alumina eventually. Upon the formation of this protective layer the reaction rate slowed down significantly for all alloys under investigation. The major effect of increasing the temperature another 100°C, i.e. going from 900°C to 1000°C, was on the adherence of the oxide layer. Tests showed that the systems became more vulnerable to scale spallation at this temperature. This was especially pronounced in wet air.

The general conclusion from the tests with the alumina formers is that water vapor adversely affected selective oxidation of Al. Although other factors were also important such as the temperature, the substrate composition, and the pre-exposed surface condition, it was very clear that the ability of these systems to develop the alumina phase in air/H₂O mixtures was restrained. Additionally, all test results confirmed that the transient oxidation was more profuse in the wet environment. Isothermal tests with the alloy PWA 1484 at 700°C for 4 hours showed that the inward transport of oxygen was faster in wet air, Figures 5.53 and 5.55. The depth of the oxygen-affected zone was substantially larger for the specimen subjected to air/H₂O mixtures. Similar observations were also made for René N5 at 700°C and at 900°C, Figures 5.57-5.60. One of the micrographs showing the cross-section of PWA 1484 at 700°C in wet air is reprinted here as Figure 7.1. The more detailed examination of the internal oxidation zone on this specimen with EDX indicated a concentration gradient along the layer. The atomic percentage of oxygen at the NiO/internal-oxide interface was observed to decrease gradually towards the metal/oxide interface. The internal oxidation zone was found to be depleted in Ni. This showed that the NiO scale developed by the outward diffusion of nickel. The Ni-depleted alloy reacted with the oxygen that was diffusing inwards, which resulted in the development of the zone of internal oxides. EDX analysis did not indicate the presence of oxygen in the alloy beyond this zone. These results suggest that the transport of oxygen species was occurring in the oxide and in

the alloy. However, it is not clear in which form they were being transported. Nevertheless, the net effect is a substantially more aggressive attack when $\text{H}_2\text{O}_{(\text{g})}$ is involved in the process. As mentioned earlier in the background section, there are several mechanisms proposed by different research groups to explain how and in which state water vapor is involved in the oxidation process. Since the observations of most researchers differ from each other, and every study develops the models based on their own findings no consensus has been established. However, one such mechanism suggests that when H_2O is involved in the reaction, the anion transport in the oxide operates by the diffusion of OH^- , which has a smaller ionic radius than O^{2-} ($r_{\text{OH}^-} = 95 \text{ pm}$, $r_{\text{O}^{2-}} = 140 \text{ pm}$), via vacancies [77, 84]. Although this is not a well established theory, it provides some possible explanation to the faster anion transport in wet air observed in the current study. It is possible that the frontline of the oxygen affected zone moves faster via the transport of the OH^- in the oxide and causes thicker transient oxide formation. Another possibility is that the presence of hydrogen species has some doping effects on the transient oxides, and therefore changes the types and/or concentrations of the defects in the system. This might be having an impact on the oxygen activity, and therefore accelerating the inward diffusion of the oxygen species. The faster transport of atomic oxygen in the alloy is another possibility that needs to be considered.

Isothermal TGA tests with pure Ni (99.999%) indicated that the oxidation rate of the metal was not accelerated by water vapor during isothermal exposures at 900°C , Figure 6.70. The differences between the reaction rates were small. The parabolic rate constants (k_p) were calculated as approximately $3.76 \times 10^{-7} \text{ g}^2/\text{cm}^4\text{hr}$ in wet air, and $5.85 \times 10^{-7} \text{ g}^2/\text{cm}^4\text{hr}$ in dry air. Examination of the specimen cross-sections also confirmed the kinetic data. Slightly thicker scales developed on the surface of the dry exposed specimen, Figures 6.71-6.72. The reason for

this slight difference in the oxidation rates is believed to be the partial pressure of oxygen rather than the effect of H₂O. For these tests the value of PO₂ was 0.21 atm and 0.19 atm in dry and in wet air, respectively. The isothermal exposures in high pressure steam (100% H₂O) also showed that the formation of NiO was suppressed under these test conditions, (Section 5.1.2). This is believed to be again the consequence of the lower oxygen partial pressure as NiO formation is very much dependent on PO₂, [95]. Based on these data it is suggested that the reason for more profuse transient oxide formation on the superalloy systems that rely on alumina formation is the side effect of selective Al oxidation rather than the reason for the difficulty in alumina formation. Examination of the kinetic data for the superalloys showed that the transition from non-protective (transient) to protective (steady state) oxidation took place around the same time for CM 186, PWA 1484 and René N5, Figure 7.2. For MarM 247 there is no well defined transition point. However, the reactions follow similar patterns in both environments. These results suggest that at 900°C protective alumina formation is not being delayed in wet air. However, as the short exposures of PWA 1484 and René N5 also showed, because the transport of the oxygen bearing species in the oxide proceeds faster in the H₂O environment, the formation of alumina takes place deeper in the substrate. The frontline of the critical aluminum concentration for alumina formation shifts to the inner parts of the specimen. The layer above this line is being converted to transient oxides. Therefore, the samples tested in wet air develop thicker layers of non-protective oxide phases. This is illustrated in Figure 7.3. These observations suggest that for these systems, the limiting factor is the transport of the metal in the alloy. The oxides of metals that have sufficiently high flux are not affected by H₂O. Upon the development of the continuous alumina layer, the oxygen activity at oxide/alloy interface decreases. Since the diffusivity of aluminum in the superalloy is lower at lower temperatures, this condition becomes

worse at these temperatures. At 1000°C similar conditions take place. Higher temperatures accelerate the diffusion processes, which increases the reaction rates. Therefore thick scales form within shorter periods of time. Scale spallation becomes more aggressive because the strain energy becomes higher due to thicker scale formation and larger ΔT . Additionally, water vapor affects the bond strength at the oxide/substrate interface and decreases the interfacial toughness in this environment. As a consequence, more profuse scale spallation takes place in the presence of H₂O, [46].

Another important parameter is the mode of testing. The results discussed in this study are obtained mostly from cyclic experiments. The thermal cycling of the alloys causes spallation of oxides between each cycle. This has substantial effects on the substrate composition. As the protective scale is being partially lost between each cycle, the superalloy is depleted in Al and Cr. This condition works in favor of the development of the transient oxide phases, while making alumina formation more difficult after each cycle.

The problem at hand is very complicated as there are many factors that affect each other and cannot be isolated. Nevertheless, this study indicated that the selective oxidation of Al in air/H₂O mixtures was adversely affected. This might be related to the diffusion of the metal in the alloy. A comparative study with higher-Al alloys in oxygen and in air/H₂O mixtures could help to understand the phenomenon better.

7.1.1 Some Highlights on Selective Oxidation of Al

The results obtained with the alumina forming superalloys showed that selective oxidation of Al was affected by a number of factors, namely,

- The Cr and Al concentrations in the alloy, with higher Cr and Al concentrations favoring selective oxidation of Al
- The temperature, where the selective oxidation of Al was less favorable as temperature was decreased
- The surface condition of the alloy, where the selective oxidation of aluminum was more favorable on a rough surface
- The presence of water vapor in the gas adversely affecting selective oxidation of aluminum.

Some possible explanations for these observed effects are discussed in the following. The effect of alloy composition is caused by the larger fluxes of Cr and Al to the alloy surface as the concentrations of these elements are increased. The observed effect of temperature is due to the dependence of oxygen and Al diffusion on temperature, in particular, more rapid diffusion of aluminum, and perhaps relatively slower diffusion of oxygen as temperature is increased. The influence of alloy surface condition is probably caused by preferential nucleation of certain oxides on the rougher surfaces. It is also possible that the outward diffusion of Al and Cr is favored on the rough surface. In the presence of water vapor, the internal oxidation zone appears to be thicker in comparison to dry air. This could occur either by the faster inward diffusion of oxygen, or by the slower outward diffusion of Al and/or Cr. Since the latter one is unlikely, the diffusion of oxygen must be more rapid. This could occur by the faster transport of oxygen in the alloy. If oxygen diffuses more rapidly into the alloy, as may occur if atomic oxygen is present, then Al and Cr will be oxidized internally and an external scale of NiO will develop. It is also possible that the initial oxide scale which forms in water vapor grows very rapidly due to some changes in the defect properties of the oxide. This could establish a higher oxygen

potential at the scale/alloy interface. More rapid growth of oxide scales in water vapor has also been observed due to the more rapid movement of OH^- ions compared to the larger O^{2-} ions. These result in the faster inward movement of the oxide/alloy interface, and cause more profuse internal oxidation.

7.2 CHROMIA FORMATION

The aim of this study was to understand the effects of water vapor on the oxidation behavior of the superalloy systems that are designed as chromia formers. As discussed in earlier chapters, first these alloy systems were tested in dry air and in air/water vapor mixtures. Based on the observations, experiments with the model alloys were designed to answer some of the questions that arose after examination of the superalloys. Since some of the phenomena could be explained based on the information obtained from the simple systems, these systems will be reviewed first.

7.2.1 Chromia Formation on Model Alloys

Tests with the model alloys showed that temperature was a very critical parameter in chromia formation. Lower temperatures favored the development and maintenance of the protective oxide. Exposures at 700°C resulted in the formation of chromia scales even on the alloy with the lowest chromium content, i.e. Ni-15Cr. Some transient oxidation was evident on Ni-15Cr, Ni-20Cr and Ni-15Cr-0.1Ce. This was more significant in dry air. The resistance of the alloys to

the formation of these rapidly-growing oxides improved with increasing Cr concentration. At 30% Cr the transient phases did not develop either in wet or in dry air.

At 900°C transient oxidation was more prominent. This time, the Ni-rich oxides developed during wet and dry exposures. Higher Cr concentration was beneficial at this temperature as well. However, the cyclic tests with the alloys Ni-30Cr and Ni-30Cr-0.1Ce still resulted in the formation of NiO. Examination of the specimen surfaces showed that the NiO developed at the spalled areas. The spallations which were induced by thermal cycling were observed to start earlier in dry air. Similar observations on chromia scales were reported also by others[64, 78]. Comparison of the isothermally exposed specimens of the same composition showed that neither scale spallation nor transient oxidation was evident on the surfaces of these samples. The scales consisted of chromia only. These results suggest that the main mechanism leading to the transient oxidation is oxide spallation which exposes the bare metal to the reactive environment. After each spallation the composition of the substrate at the alloy/oxide interface becomes poorer in Cr, which gives rise to the formation of the non-protective oxides. Since the alloys Ni-15Cr, Ni-15Cr-0.1Ce and Ni-20Cr were not isothermally tested the direct comparison for these compositions cannot be done. However, based on the results obtained with Ni-30Cr and Ni-30Cr-0.1Ce it is believed that the transient oxidation for these alloys is also caused mainly by oxide spallation.

As mentioned above, the examination of the scale surfaces of cyclically tested Ni-30Cr and Ni-30Cr-0.1Ce showed that oxide spallation started earlier in dry air. Comparison of the kinetic data of these systems at 900°C also revealed that during the earlier stages of oxidation the weight change differences between cyclic and isothermal exposures were significantly larger in dry air, while this was minimal for the wet exposures. This confirmed that in wet air the major cause for

the degradation was the loss of Cr_2O_3 via the formation of the vapor oxy-hydroxides, while vapor species formation was not that significant in dry air. Instead, the mechanism leading to failure in the latter environment was the loss of the protective oxide by the spalling of the scale. In wet air, the contribution to degradation from scale spallation was much smaller. Comparison of the scale thicknesses also confirmed that wet exposed specimens developed significantly thinner scales. This suggests that the strain energy in these samples was smaller, which prevented the oxide layer from spalling off very drastically. Since the bare metal was not being exposed to the reactive environment as extensively, less transient oxidation occurred. This continued until the substrate depleted in Cr due to the loss of chromia by vaporization and could not maintain the continuity of the protective layer. At this point transient oxidation became profound. A cartoon showing the process schematically is presented in Figure 7.4.

Water vapor was not observed to affect the selective oxidation of Cr. The tests with the simple alloys showed that at 700°C continuous chromia scales developed over the substrate in dry, as well as in wet air. At the higher temperature, i.e. at 900°C , all alloys except for Ni-15Cr were able to develop continuous chromia scales. Unlike the alumina formers, transient oxidation was not observed to be more profuse in air/ H_2O mixtures, as discussed above.

Additions of Ce improved the scale spallation resistance very substantially. The positive effects of the element were especially strong on the alloy Ni-15Cr-0.1Ce and at the higher temperature. At 900°C , Ni-15Cr experienced very severe attack in wet and in dry air. Thick layers of transient oxides developed on the alloy surface. Heavy spallation was pronounced especially in dry air. On the other hand, the Ce-doped version of the alloy developed continuous chromia scales and did not fail dramatically. Improved resistance to scale spallation minimized the tendency for transient oxidation and helped maintain the chromia scale for much longer

exposures. The system benefited from the reactive element in dry air as well as in wet air. Isothermal tests at 900°C with Ni-30Cr and Ni-30Cr-0.1Ce showed that in dry air chromia formation rate was decelerated by the reactive element additions. It is not clear whether the same effect is valid for wet air. However, reactive-element related improvements in the scale adherence were evident in wet as well as in dry air.

The calculated values of the linear rate constants in wet and dry air based on the experimental data suggested that the rate of vapor species formation was faster in air/H₂O mixtures compared to dry air. These results are in agreement with the observations by others, [71, 72, 99].

Void formation at the chromia/substrate interface was common to all Ni-Cr alloys under investigation regardless of the composition of the reactive gases. These features developed preferentially at the alloy grain boundaries, Figure 6.60. Higher temperature exposures resulted in the formation of larger and more frequent void formation. This is characteristic for the oxides that grow by the outward diffusion of cations. In some cases, internal oxidation around the voids or at the grain boundary tips was also observed. This occurs either by the molecular transport of oxygen or H₂O through the cracks or micro-channels in the chromia to the oxide/void interface, or by the dissociation of Cr₂O₃ at the chromia/void interface. New oxide is formed by the alternate oxidation and reduction processes that occur in the vicinity of the pores, [56, 58, 75]. These reactions result in the formation of pocket-like oxides. Some examples are shown in Figure 7.5.

Formation of the flakey chromia was one of the features unique to wet exposures. Closer examination of the flakes indicated lateral oxide growth, which suggested that water vapor was immobilizing some surfaces and favoring growth on certain surfaces, Figure 6.79. The

possibilities considered for their development include vapor transport and the thermal etching of the chromia scales. Further investigation of the phenomenon is needed to identify their formation mechanism more clearly.

7.2.2 Chromia Formation on Complex Superalloys

Tests with the chromia forming superalloys showed that the resistance of these alloys was affected by the exposure temperature significantly. At 700°C the degradation was very slow. Effects of water vapor were also not very pronounced. Chromia developed at the oxide/gas interface and kept its integrity for more than 2500 cyclic hours. However, at and above 900°C, these systems became very vulnerable to attack. The examination of the oxidation kinetics showed that at 900°C breakaway oxidation started around the same time for both of the alloy systems, Figure 7.6. The onset of degradation for wet and dry exposures was also the same. For IN 738, during the breakaway period the weight losses were much more substantial in wet air. In dry air, with the onset of breakaway, the system started to gain weight at a fast (linear) rate for more than 1000 hours; and finally weight losses started to become dominant. As discussed earlier, tests with model alloys showed that the formation of vapor oxide species was more prominent in air/H₂O mixtures compared to dry air. At this temperature, the effect of chromia volatilization in dry air via the formation of CrO_{3(g)} was insignificant. It was also observed that scale spallations were more profuse in the dry atmosphere. These findings suggested that the major reason for the weight losses for IN 738 during wet exposures was oxide vaporization. The formation of the thin TiO₂ layer at the chromia/gas interface prevented the loss of the protective scale by vaporization until the scale started to spall off due to the residual stresses originating from oxide growth and thermal cycling. Once the chromia became exposed to the reactive gases

due to the loss of TiO_2 layer by spallation, vaporization became active. In the mean time internal oxidation continued and possibly even accelerated, because spallation made the ingress of oxygen and other reactive gases, such as nitrogen, much easier. This gave rise to the weight gains observed in dry air. In wet air both of these mechanisms were also operating, i.e. oxide spallation and internal oxidation. However, since the third component of degradation, which is oxide vaporization, was stronger for the wet air than the dry air, the net weight change was negative in contrast to the dry exposed samples. It is not possible to conclude with certainty whether oxide spallation was stronger in wet air or in dry air. However, one can speculate that it was more substantial in dry air. This is based on the examination of the specimen surfaces, the results obtained with the simple alloys, and the observations reported by others. SEM images of the sample cross-sections suggested that the spallations were not as profuse in the wet environment, Figure 5.66(a-b). Nitride formation was also stronger in dry air, which shows that the degree of attack was more severe. Tests with the simple alloys also pointed towards the conclusion that spallations were heavier in dry air. Similar observations were reported elsewhere for chromia scales grown in H_2O containing environments, [64].

Tests with the Co-based superalloy X-40 showed that, unlike IN 738, this alloy was prone to oxide vaporization in wet air beginning at the early stages of oxidation when no thermal cycling was involved. The kinetic data of the isothermally tested sample at 900°C displayed negative weight changes following a short period of weight gains, which occurred at the beginning of the oxidation reactions, Figure 6.68. Here, it is worth mentioning that it is not clear if some fraction of these weight losses were associated with the volatilization of W-oxides, and not only due to the loss of chromia. The cyclic data contradicted the results of the isothermal tests. Assuming that the alloy would continue to lose the oxide scale with the rate determined by the TGA results,

very strong weight losses within shorter times would be expected during cyclic tests. In reality, the system continued to gain weight for approximately 1000 hours, Figure 7.6. This is explained with the formation of the Co-rich transient oxides due to the cracking and spalling of the protective layer between cycles. The weight of the system increases because of the oxygen pick-up during these reactions. In addition to this, these oxides might have similar effects as the TiO_2 phase observed on IN 738. The physical barrier created between chromia and the reactive gases might be slowing down the formation of the vapor oxides.

The comparison of the isothermal tests to the cyclic ones indicated that in dry air scale spallation was very significant. Large differences existed between the isothermal and cyclic weight change data of the system, Figure 6.68. The examination of sample cross-sections also revealed more profuse internal and transient oxidation after isothermal exposures in this environment, Figure 6.70. Similar observations were made for cyclically tested samples as well. After 2050 cycles, the depth of internal oxidation was larger in the dry environment, Figure 5.68. It was not clear if transient oxidation was affected by the composition of the reactive gases at this point. However, more extended exposures caused formation of much thicker transient oxide layers in wet air, Figure 5.69.

The fact that more internal oxidation occurred in dry air even during isothermal exposures confirmed that selective oxidation of Cr was not adversely affected by water vapor. The results even suggested that water vapor improved the ability of the system to form the protective oxide. However, this positive effect was counteracted by the rapid vaporization reactions. The evaporation rate of the alloy was compared to the Ni-based model alloys. Close matches were observed between the Co-based and the Ni-based systems, Figure 6.71. This implied that Cr_2O_3 evaporation was independent of the substrate composition.

7.2.3 Some Highlights on Chromia Formation

In summary, the oxidation reactions were affected by H₂O. These effects were dependent on several factors such as the composition of the substrate, the mode of testing (i.e. cyclic versus isothermal), and the exposure temperature. In general, water vapor did not affect selective oxidation of Cr adversely. In dry air, the vaporization rate of Cr₂O₃ was very small in comparison to its formation rate. To the contrary, air/H₂O mixtures caused significant loss of the oxide by the formation of the vapor species. This effect was much weaker at the lower temperature, i.e. at 700°C.

Additions of the reactive element Ce decreased the formation rate of chromia in dry air. Significant improvements in terms of the scale adherence were observed on the Ce-doped alloys. The same effect was evident in wet air as well.

Scale spallation was more severe in the absence of H₂O. This was due to the development of thinner scales in the wet environment compared to dry. The major cause of system failure in the latter environment was the spalling of the oxides, while in air/H₂O mixtures the loss of the chromia scale by oxide vaporization was a bigger concern. The formation of the thin TiO₂ layer on IN 738 delayed the loss of the protective scale. This showed that applying a coating or alloying the system with elements that would diffuse to the surface and form an external layer would improve the performance of the chromia forming systems substantially.

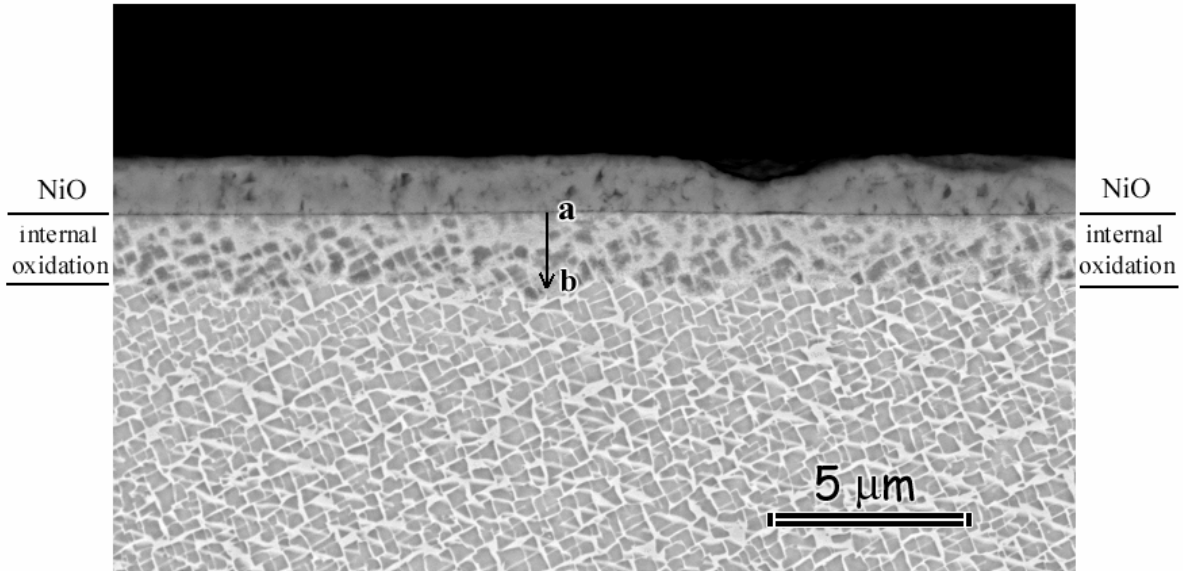
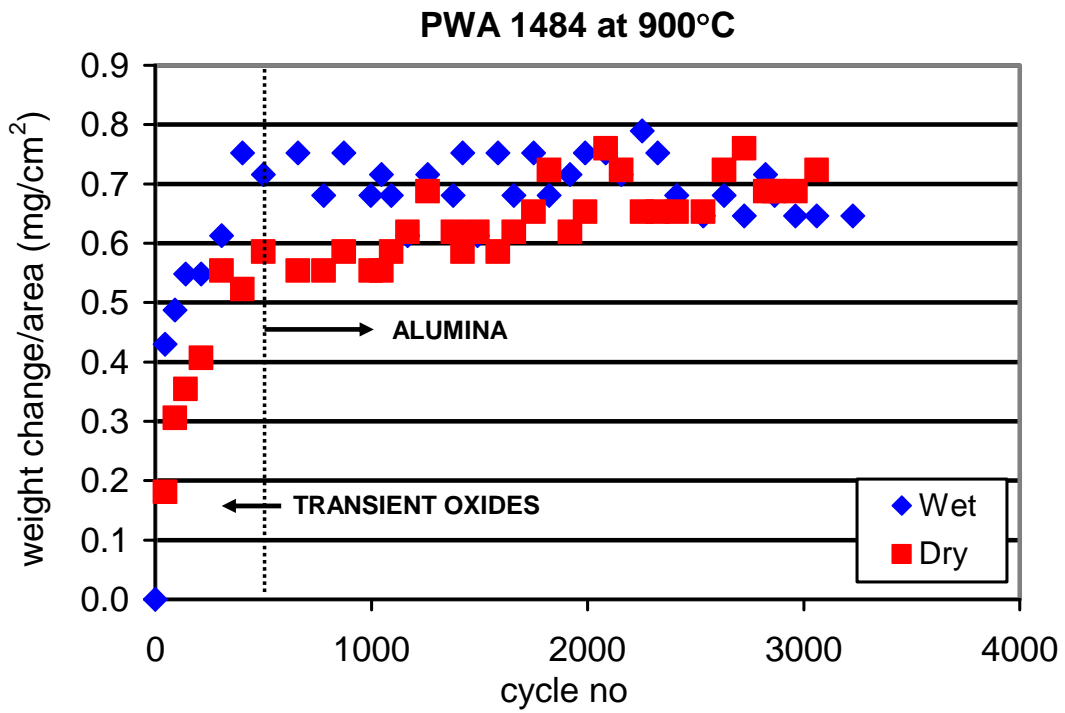
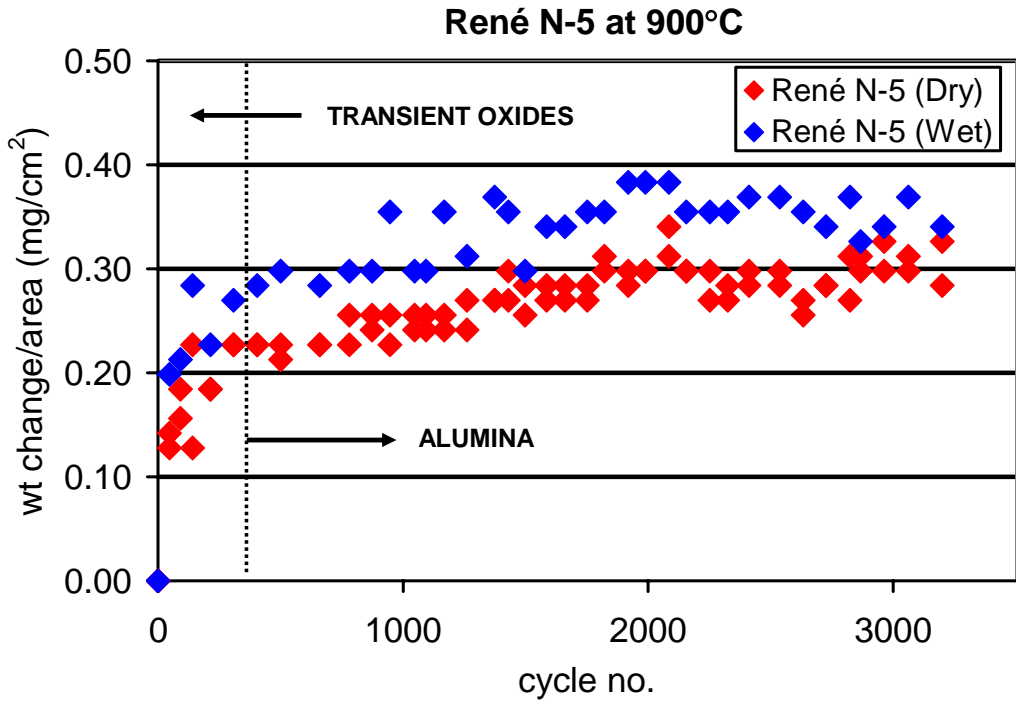


Figure 7.1: PWA 1484 at 700°C after 4 hours of isothermal exposure in wet air, where $P_{H_2O} = 0.3$ atm and $P_{total} = 1$ atm. EDX analysis indicated a concentration gradient in terms of the oxygen in the internal oxidation zone. The atomic percent of oxygen decreased from 50% at the NiO/internal-oxide interface, (labeled as “a”), to 17% at the internal-oxide/alloy interface, (labeled as “b”). Moreover, the Ni concentration was observed to decrease by moving from “b” towards ‘a’. No detectable amounts of oxygen were present below this interface, i.e. in the alloy.



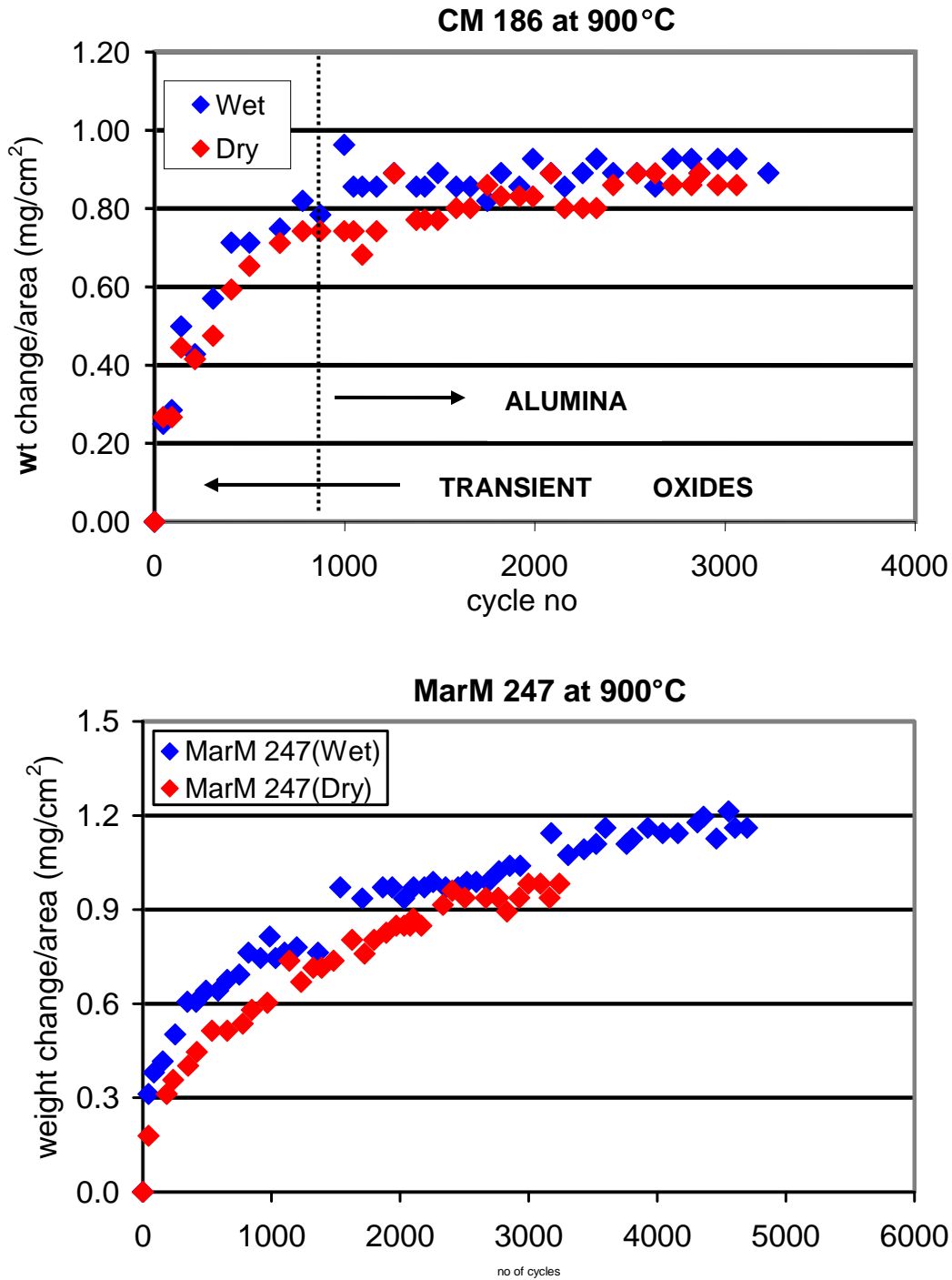


Figure 7.2: Kinetic plots of René N5, PWA 1484 and CM 186 indicate that at 900°C the transition from transient oxidation to steady state oxidation takes places after same exposure times in wet air and in dry air. For MarM 247 no specific transition point is evident. However, the oxidation kinetics follows the same trend in either environment for this system as well.

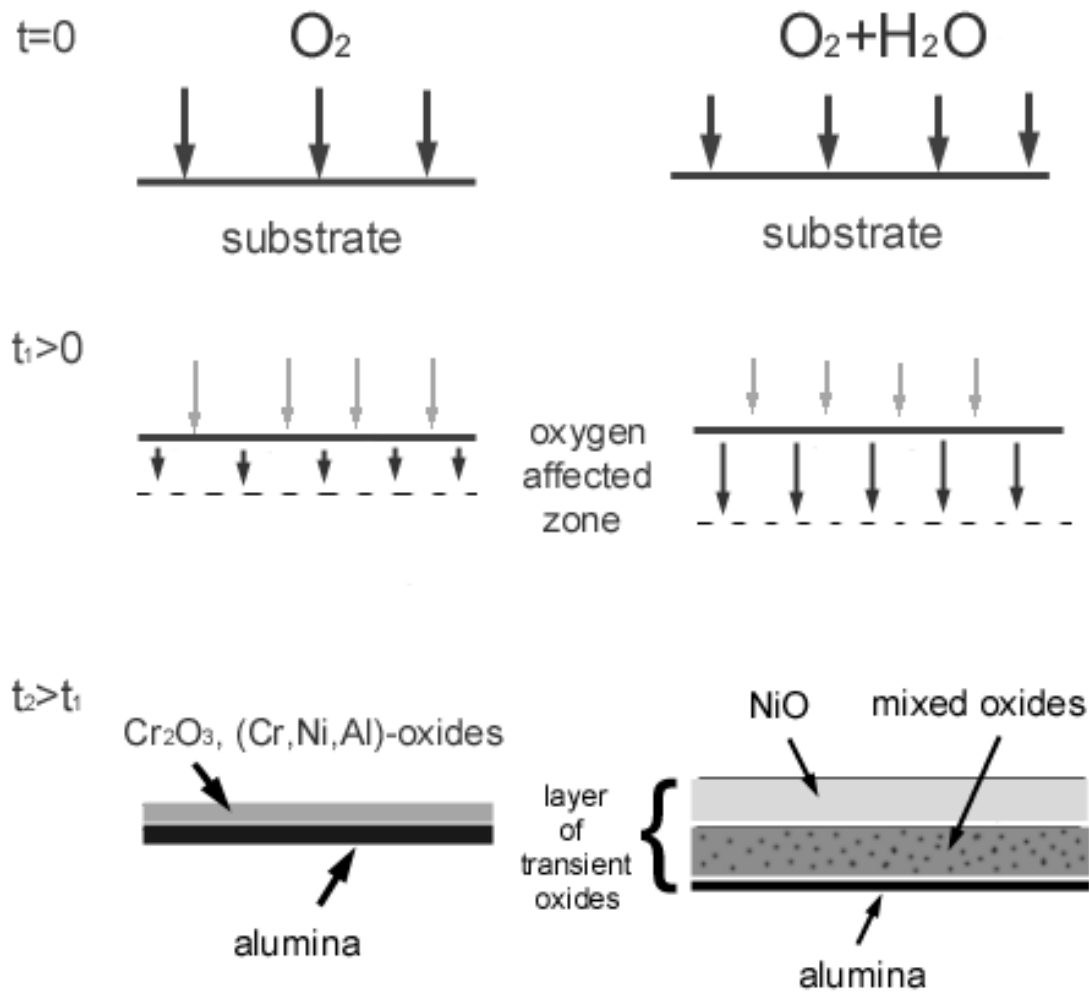


Figure 7.3: In air/H₂O mixtures anion transport in the oxide proceeds faster in comparison to dry air. At time $t > 0$ the depth of the oxygen affected zone is larger in the wet environment. As a result, the protective scale forms deeper in the alloy. Thicker layers of transient oxides develop above the protective alumina scale.

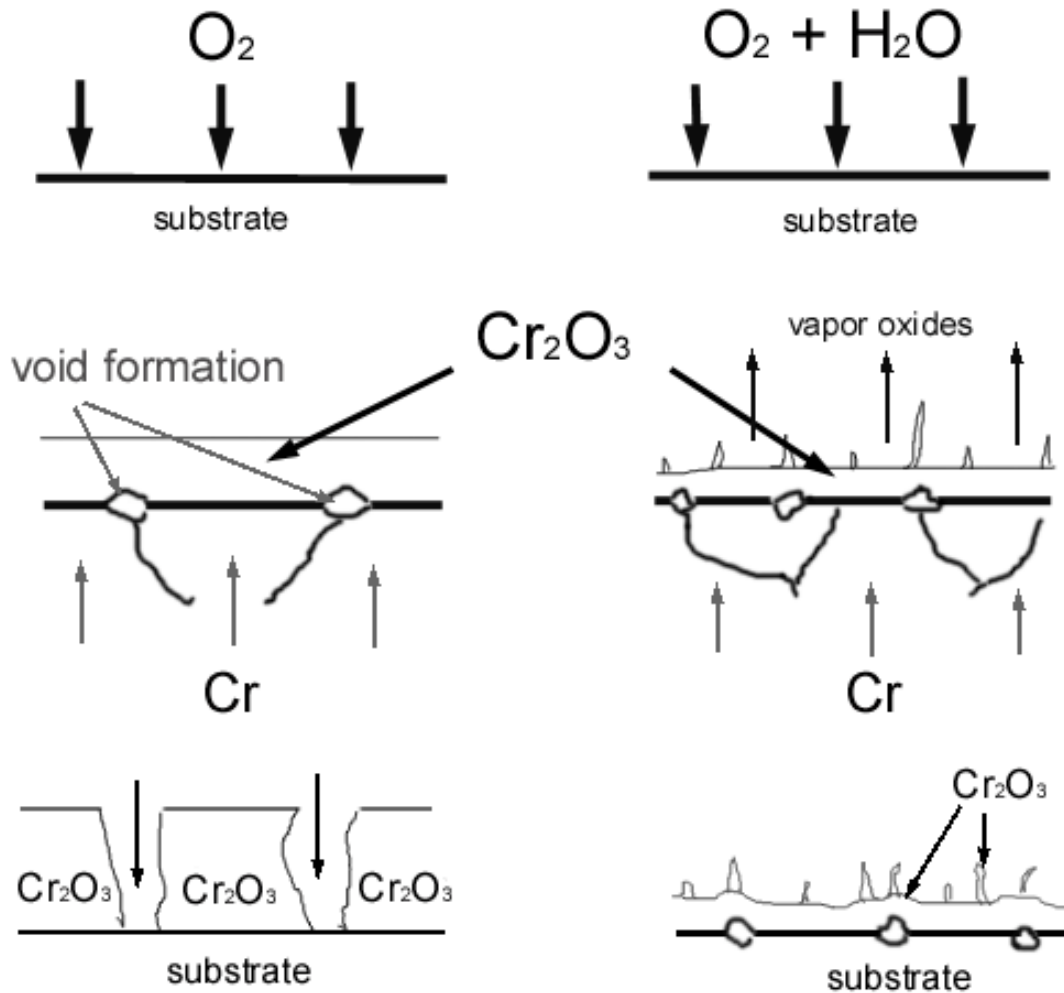


Figure 7.4: When the Ni-Cr alloys are exposed to dry air or to air/H₂O mixtures, chromia scales develop at the substrate surface considering the %Cr in the substrate is sufficiently high. After the formation of the initial thin chromia layer, the scale continues to grow by the outward diffusion of Cr cations. In the mean time, the composition of the substrate changes gradually. The concentration of Cr close to the reaction zone decreases with time. During wet exposures, substantially thinner scales develop due to the loss of the protective Cr₂O₃ by the formation of the vapor oxide species. Therefore, the strain energy for these specimens is less than the ones exposed to dry air. As a result scale detachments and spallations start earlier in the dry environment. When the Cr₂O₃ layer spalls off, the unexposed surface of the substrate material reacts with oxygen. Since the substrate is depleted in Cr, oxides other than chromia form in these spalled areas. Oxygen also diffuses through the cracks and micro-channels in the oxide. The reactions at the oxide/alloy interface give rise to internal oxidation.

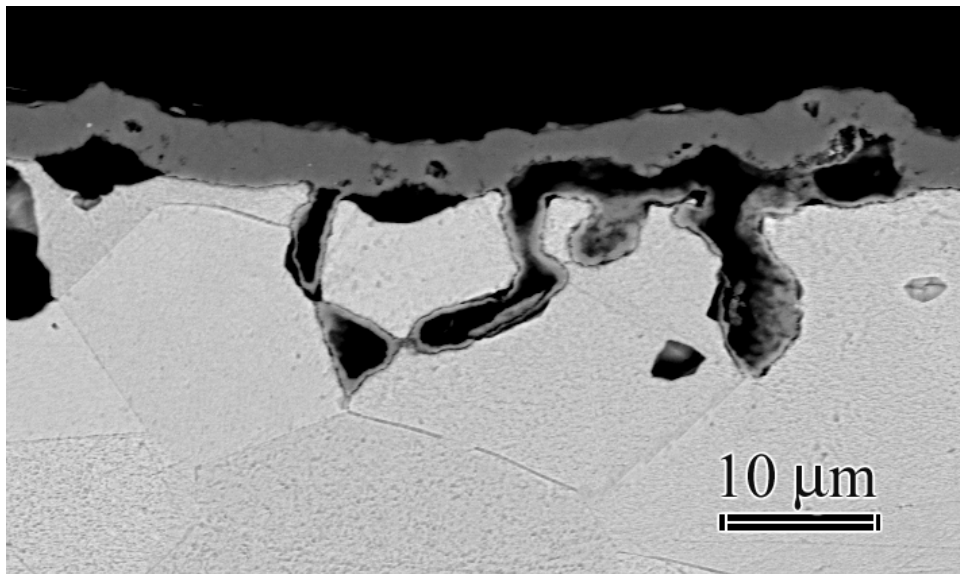
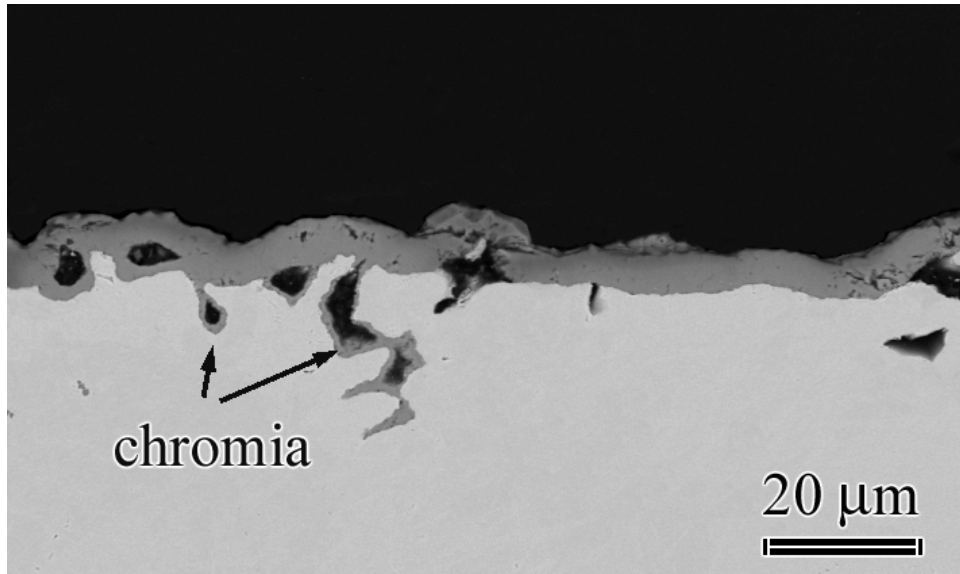


Figure 7.5: SEM image shows Ni-30Cr exposed in dry air at 900°C for 168 hours isothermally. Chromia developed in the substrate by the alternate oxidation and reduction processes.

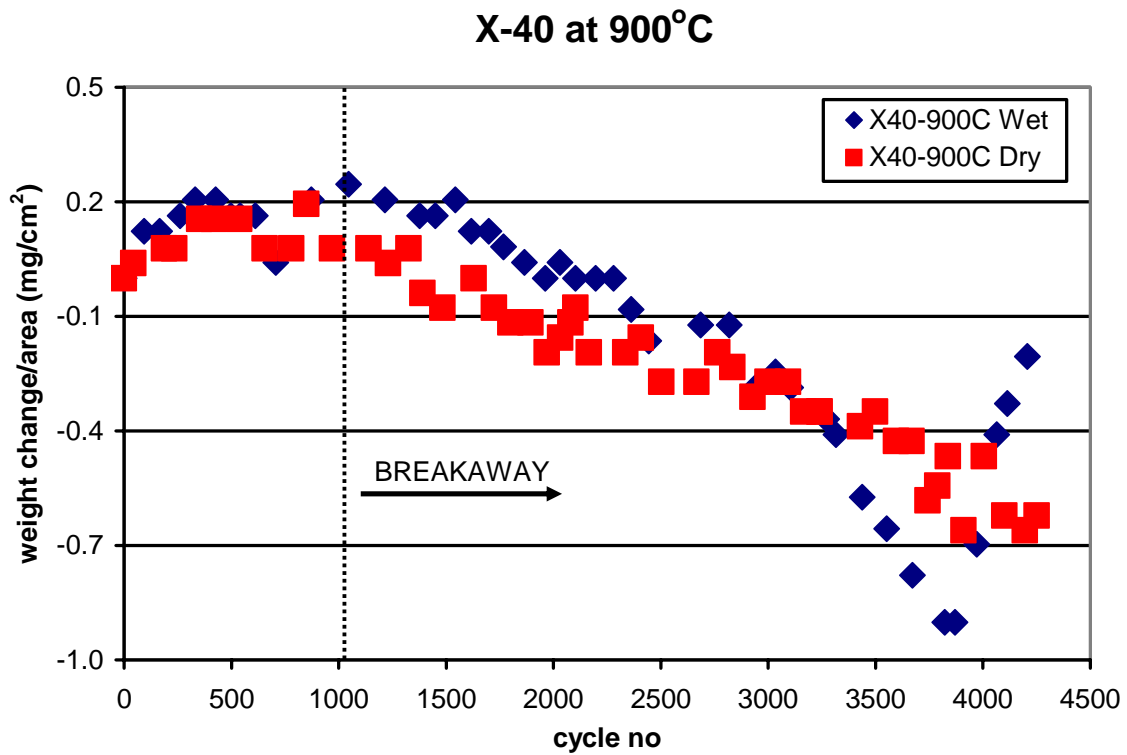
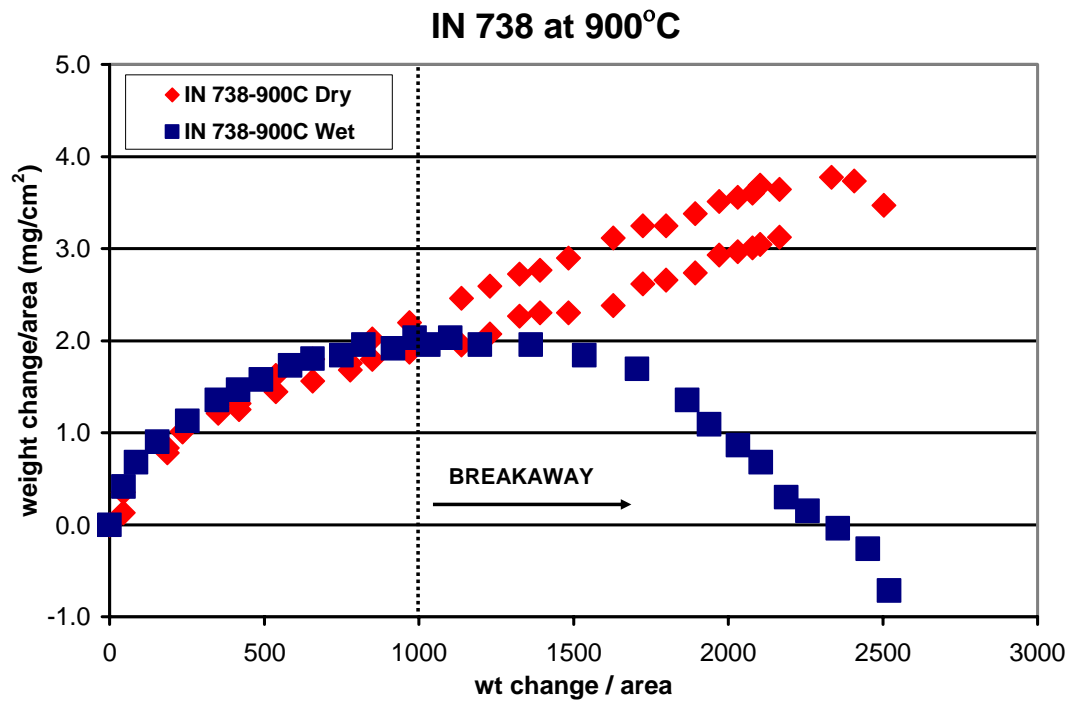


Figure 7.6: Kinetic plots of IN 738 and X-40 at 900°C indicate that the onset of breakaway oxidation is approximately the same time in dry air and in wet air for each system.

8.0 CONCLUSIONS

The studies with various superalloys have shown that water vapor affected the high-temperature oxidation behavior of each system in different ways. These effects were dependent on the primary protective oxide type, i.e. chromia or alumina.

The major effect of H₂O on the development of alumina scales is on the selective oxidation processes. Selective oxidation of Al is not favored in water vapor. This effect is more significant at lower temperatures. Alloys with high concentrations of the element are less vulnerable. The presence of Cr as the getter element also improves the ability of the systems to develop alumina scales.

Transient oxidation is more severe in air/H₂O mixtures compared to dry air. Selective oxidation of Al and the formation of the transient oxides are interrelated. The possibilities considered are the changes in the defect properties of the transient oxides associated with the hydrogen species, and the faster diffusion of the oxygen species in the oxide as OH^- ions as suggested by Wouters et al., [84], or by another mechanism. Under each circumstance, the flux of Al in the alloy is important. When the oxygen species transfer faster, the frontline for continuous alumina formation is forced deeper into the alloy because the concentration of Al cannot reach the critical limit fast enough. Temperature elevations improve the selective

oxidation of Al significantly. Alumina scales can develop easier at higher temperatures. However, the transient oxidation is still more pronounced in air/H₂O compared to dry air.

At 1000°C scale spallation is very significant. At this temperature, water vapor adversely affects the scale adherence. More spallation takes place in air/H₂O mixtures compared to dry air. This occurs by stress corrosion cracking, where H₂O decreases the oxide/alloy interface toughness by altering the bonding between the oxide and the underlying alloy, [46].

Hf additions degrade the performance of alumina formers at 1000°C by inducing internal oxidation. CM 186 and MarM 247, which have significant additions of Hf, show excessive internal oxidation, whereas René N5 and PWA 1484 do not display this behavior owing to their significantly low Hf content.

Exposures in pure H₂O, where the oxygen pressure is very low ($\sim 10^{-5}$ at 700°C, and 10^{-7} at 900°C), result in substantially less NiO formation on the superalloys. Other than the suppressed NiO formation, it is not clear if H₂O by itself affects the oxidation kinetics in a similar manner as in air/H₂O mixtures at higher oxygen pressures, since the exposures times are different for each experiment.

H₂O does not affect the oxidation kinetics of NiO. On the other hand, water vapor-related morphological differences in the oxide scale are evident. In this environment, faceted surfaces develop by the lateral growth of the oxide. This issue needs further investigation.

The condition of the pre-exposed specimen surface is an important experimental parameter. Short term exposures indicate that the specimens with more worked surfaces can develop the protective scales easier. More testing is necessary to observe the long term effects and to understand the mechanisms better.

Unlike Al, the selective oxidation of Cr is not affected by water vapor. There are some indications that chromia formation might be even improved in air/H₂O mixtures. This is due to the high Cr concentration in the underlying alloy. The major effect of water vapor on chromia scales is the rapid reactions at the chromia/gas interface leading to the formation of vapor Cr species. At 900°C and below, these reactions are not significant in oxygen or in dry air. However, the presence of water vapor accelerates the loss of chromia, making the underlying alloy very vulnerable to further attack. The thickness of the chromia layer that develops in wet air is significantly less compared to dry air due to more excessive oxide vaporization for the former case.

The spallation of chromia scales is more profound in dry air compared to air/H₂O. Thermal cycling combined with thicker scale formation increase the strain energy for these systems, which leads to detachment and spallation of the chromia layers. Additions of Ce improve the adherence of the oxides to the underlying alloy in air as well as in wet air.

Another beneficial effect of the reactive element is the decelerated reaction rate in dry air. It is not clear if this occurs in wet air as well.

Exposures in air/H₂O mixtures cause morphological changes in the chromia scales. Flakes of Cr₂O₃ develop over granular chromia. This structure emerges only during wet exposures. This is a complicated issue. However, water vapor is involved in the process possibly by providing vapor transport. More detailed investigation is needed to understand the phenomenon better.

IN 738 develops a thin layer of TiO₂ at the gas/chromia interface upon exposure to high temperatures. This occurs in dry air and in air/H₂O. The formation of the thin TiO₂ layer is beneficial especially in wet air as it delays the loss of the chromia by putting a physical barrier

between the volatile oxide and the reactive environment. This indicates that providing a barrier layer between the oxidizing environment and Cr_2O_3 would improve the performance of chromia formers substantially.

The use of chromia formers at temperatures above 900°C is impractical. Reactions leading to the loss of chromia by the formation of volatile Cr species become more aggressive at such temperatures.

The effect of pure H_2O at low PO_2 on the oxidation behavior of chromia formers needs to be investigated further.

BIBLIOGRAPHY

1. Hindam, H. and D.P. Whittle, *Microstructure, Adhesion and Growth Kinetics of Protective Scales on Metals and Alloys*. Oxidation of Metals, 1982. **18**: p. 245-284.
2. Kofstad, P., *High Temperature Corrosion*. 1988, New York: Elsevier Science Publishing Co., Inc.
3. Birks, N. and G.H. Meier, *Introduction to High Temperature Oxidation of Metals*. 1983: Edward Arnold Ltd.
4. Kofstad, P., *Defects and Transport Properties of Metal Oxides*. Oxidation of Metals, 1995. **44**(1/2): p. 3-27.
5. Kroeger, F.A., *Defects and Transport in SiO₂, Al₂O₃, and Cr₂O₃*, in High Temperature Corrosion, National Association of Corrosion Engineering, Houston, Texas, 1981, p. 89-100.
6. Park, J.-H. and K. Natesan, *Electronic Transport in Thermally Grown Cr₂O₃*. Oxidation of Metals, 1990. **33**(1/2): p. 31-54.
7. Kofstad, P., *Oxides of Group VIA Elements*, in *Diffusion and Electrical Conductivity in Binary Metal Oxides*. 1972, John Wiley and Sons, Inc. p. 203-211.
8. Tolpygo, V.K., *The Morphology of Thermally Grown α -Al₂O₃ Scales on Fe-Cr-Al Alloys*. Oxidation of Metals, 1999. **51**(5/6): p. 449-477.
9. Uran, S., et al., *Effect of Surface Roughness on Oxidation: Changes in Scale Thickness, Composition and Residual Stress*. Oxidation of Metals, 2000. **54**(1/2): p. 73-85.
10. Goedjen, J.G. and D.A. Shores, *The Effect of Alloy Grain Size on the Transient Oxidation of an Alumina-Forming Alloy*. Oxidation of Metals, 1992. **37**(3/4): p. 125-142.
11. Ahmad, B. and P. Fox, *STEM Analysis of a Ni-20Cr Alloy at High Temperature*. Oxidation of Metals, 1999. **52**: p. 113-138.
12. Birks, N., G.H. Meier, and F.S. Pettit, *Forming Continuous Alumina Scales to Protect Superalloys*. JOM, 1994(December): p. 42-46.

13. Rapp, R.A., *The Transition from Internal to External Oxidation and the Formation of Interruption Bands in Silver-Indium Alloys*. Acta Metallurgica, 1961. **9**: p. 730-741.
14. Giggins, C.S. and F.S. Pettit, *The Effect of Alloy Grain Size and Surface Deformation on the Selective Oxidation of Chromium in Ni-Cr Alloys at Temperatures of 900C and 1100C*. Transactions of the Metallurgical Society, 1969. **245**: p. 2509-2514.
15. Wlodek, S.T., *The Oxidation of Rene 41 and Udimet 700*. The Metallurgical Society of AIME, 1964. **230**: p. 1078-1090.
16. Onal, K., et al., *Water Vapor Effects on the Cyclic Oxidation Resistance of Alumina Forming Alloys*. Materials at High Temperatures, 2003. **20**(3): p. 327-337.
17. Onal, K., et al. *Effects of Water Vapor on the Oxidation of Nickel-Base Superalloys and Coatings at Temperatures from 700°C to 1100°C*. in *10th International Symposium on Superalloys*. 2004. Champion, PA.
18. Prescott, R. and M.J. Graham, *The Formation of Aluminum Oxide Scales on High-Temperature Alloys*. Oxidation of Metals, 1992. **38**(3/4): p. 233-254.
19. Stringer, J., B.A. Wilcox, and R.I. Jaffee, *High Temperature Oxidation of Ni-20wt%Cr Chromium Alloys Containing Dispersed Oxide Phases*. Oxidation of Metals, 1972. **5**(1): p. 11-47.
20. Golightly, F.A., G.C. Wood, and F.H. Stott, *The Early Stages of Development of α -Al₂O₃ Scales on Fe-Cr-Al and Fe-Cr-Al-Y Alloys at High Temperature*. Oxidation of Metals, 1980. **14**(3): p. 217-234.
21. Ramanarayanan, T.A., et al., *The Influence of Yttrium on Scale Growth and Adherence*. Oxidation of Metals, 1988. **29**(5/6): p. 445-472.
22. Brady, M.P., B. Gleeson, and I.G. Wright, *Alloy Design Strategies for Promoting Protective Oxide Scale Formation*. JOM, 2000. **January**: p. 16-21.
23. Giggins, C.S. and F.S. Pettit, *Oxidation of Ni-Cr-Al Alloys Between 1000°C and 1200°C*. J. Electrochemical Society: Solid State Science, 1971. **118**(11): p. 1782-1790.
24. Rakowski, J., in *Materials Science and Engineering*. 1994, University of Pittsburgh: Pittsburgh.
25. Choudhury, N.S., H.C. Graham, and J.W. Hinze. *Oxidation Behavior of Titanium Aluminides*. in *Properties of High Temperature Alloys*. 1976. Las Vegas, NV: Electrochem. Soc., Inc., Princeton, NJ.
26. Murriss, I., et al., *High Temperature Oxidation Behavior of Chromium: Effect of Different Batches*. Oxidation of Metals, 2001. **55**: p. 307-331.

27. Han, S. and D.J. Young, *Simultaneous Internal Oxidation and Nitridation of Ni-Cr-Al Alloys*. Oxidation of Metals, 2001. **55**(3/4): p. 223-153.
28. Hiramatsu, N. and F.H. Stott, *The Effects of Molybdenum on the High-Temperature Oxidation Resistance of Thin Foils of Fe-20Cr-5Al at Very High Temperatures*. Oxidation of Metals, 2000. **53**(5/6): p. 561-576.
29. Smialek, J.L., J. Doychak, and D.J. Gaydos, *Oxidation Behavior of FeAl+Hf, Zr, B*. Oxidation of Metals, 1990. **34**(3/4): p. 259-275.
30. Ramanarayanan, T.A., M. Raghavan, and R. Petkovich-Luton, *Metallic Yttrium Additions to High Temperature Alloys: Influence on Al₂O₃ Scale Properties*. Oxidation of Metals, 1984. **22**(3/4): p. 83-100.
31. Czyska-Filemonowicz, A., et al. *The Effect of Ytria Content on the Oxidation Resistance of ADS Alloys Studied by TEM*. in *Microscopy of Oxidation 2*. 1993. Selwyn College, University of Cambridge.
32. Philibert, J. and A.M. Huntz. *Microstructural and Diffusional Studies in α -aluminas and Growth Mechanism of Alumina Scales*. in *Microscopy of Oxidation 2*. 1993. Selwyn College, University of Cambridge.
33. Golightly, F.A., F.S. Stott, and G.C. Wood, *The Relationship Between Oxide Grain Morphology and Growth Mechanism for Fe-Cr-Al-Y Alloys*. J. Electrochem. Soc., 1979. **126**: p. 1035-1042.
34. Tawancy, H.M. and N. Sridhar, *High Temperature Oxidation Behavior of a Ni-Cr-Al-Fe-Y Alloy*. Oxidation of Metals, 1992. **37**(3/4): p. 143-166.
35. Loudjany, M., A.M. Huntz, and G. Petot-Evans, *Science of Ceramics*. Suppl. to J. Phys., 1986. **47**: p. 323.
36. Petot-Ervans, G., et al. in *Proc. 3rd Int. Conf. on Transport in Nonstoichiometric Compounds*. 1986.
37. Allam, I.M., D.P. Whittle, and J. Stringer, *Improvements in Oxidation Resistance by Dispersed Oxide Additions: Al₂O₃-Forming Alloys*. Oxidation of Metals, 1979. **13**(4): p. 381-401.
38. Green, A. and B. B. *The Effect of Reactive Element Additions upon Alloy Depletion from the Preferential removal of the Less Noble Metal during Alloy Oxidation 2*. 1993.
39. Cotell, C.M., et al., *The Influence of Grain-boundary Segregation of Y in Cr₂O₃ on the Oxidation of Cr Metal*. Oxidation of Metals, 1990. **34**(3/4): p. 173-200.
40. Ecer, G.M. and G.H. Meier, *The Effect of Cerium on the Oxidation of Ni-50Cr Alloys*. Oxidation of Metals, 1979. **13**: p. 159-180.

41. Weinbruch, S., et al., *On the Mechanism of High-Temperature Oxidation of ODS Superalloys: Significance of Yttrium Depletion within the Oxide Scales*. Oxidation of Metals, 1999. **51**(1/2): p. 111-128.
42. Smeggil, J.G., A.W. Funkenbusch, and N.S. Bornstein, *A Relationship Between Indigeneous Impurity Elements and Protective Oxide Scale Adherence Characteristics*. Metallurgical Transactions A, 1986. **17A**: p. 923-932.
43. Hou, P.Y. and J. Stringer, *The Effect of Aluminum as an alloying Addition or as an Implant on the High Temperature Oxidation of Ni-25Cr*. Oxidation of Metals, 1990. **34**(3/4): p. 299-321.
44. Siegers, M., H.J. Grabke, and H. Viefhaus. *Initial Stage of Oxidation of Fe₀20Cr-5Al Single Crystals with and without Additions of yttrium*. in *Microscopy of Oxidation 2*. 1993. Selwyn College, University of Cambridge.
45. Jayne, D.T. and J.L. Smialek. *A Sulfur Segregation Study of PWA 1480, NiCrAL, and NiAl using X-ray Photoelectron Spectroscopy with in-situ Sample Heating*. in *Microscopy of Oxidation 2*. 1993. Selwyn College, University of Cambridge.
46. Janakiraman, R., G.H. Meier, and F.S. Pettit, *The Effect of Water Vapor on the Oxidation of Alloys that Develop alumina Scales for Protection*. Metallurgical and Materials Transactions A, 1999. **30A**: p. 2905-2913.
47. Lees, D.G., *On the reasons for the effects of dispersion of stable oxides and additions of reactive elements on the adhesion and growth-mechanisms of chromia and alumina scales- the "sulfur effect"*. Oxidation of Metals, 1987. **27**(1/2): p. 75-81.
48. Melas, I. and D.G. Lees, *Factors Effecting Adhesion of Chromia Scale on Chromium*. Materials Science and Technology, 1988. **4**: p. 455-456.
49. Fox, P., et al. *Alumina and Chromia Scales Formed at High Temperature*. in *Microscopy of Oxidation*. 1993. Selwyn College, University of Cambridge.
50. Dond, W., et al. *An Investigation of Sulfur on the Adhesion and Growth Mechanism of Chromia Formed on Low-S Chromium*. in *Microscopy of Oxidation 2*. 1993. Selwyn College, University of Cambridge.
51. Smialek, J.L., *Maintaining Adhesion of Protective Al₂O₃ Scales*. JOM, 2000: p. 22-25.
52. Hou, P.Y. and J. Stringer, *Effect of Internal Oxidation Pretreatments and Si Contamination on Oxide-Scale Growth and Spalling*. Oxidation of Metals, 1990. **33**(5/6): p. 357-369.
53. Clemens, D., W.J. Quadackers, and L. Singheiser. *High Temperature Corrosion and Materials Chemistry*. in *Electrochemical Society*. 1998. Pennington, Nj.

54. Boulam, M., G. Beranger, and M. Lambertin. *Oxidation of an Alumina Forming Alloy: Morphological and Structural Study*. in *Microscopy of Oxidation*. 1993. Selwyn College, University of Cambridge.
55. Fuji, C.T. and R.A. Meussner, *Journal of Electrochemical Society*, 1964. **111**: p. 1212.
56. Rahmel, A. and J. Tobolski, *Einfluss von Wasserdampf und Kohlendioxyd auf die Oxydation von Eisen in sauerstoff bei hohen Temperaturen*. *Corrosion Science*, 1965. **5**: p. 333-346.
57. Tuck, C.W., M. Odgers, and K. Sachs, *The Oxidation of Fe at 950C in Oxygen/Water Vapor Mixtures*. *Corrosion Science*, 1969. **9**: p. 271-285.
58. Kvernes, I., M. Oliveira, and P. Kofstad, *High Temperature Oxidation of Fe-13Cr-xAl Alloys in Air/H₂O Vapor Mixtures*. *Corrosion Science*, 1977. **17**: p. 237-252.
59. Liu, H., S.B. Lyon, and M.M. Stack, *The Partial Ionic-Electronic Conductivity of Y-Containing and Y-Free Chromia Scales*. *Oxidation of Metals*, 2001. **56**(1/2): p. 147-161.
60. Maeda, M., K. Nakamura, and T. Ohkubo, *Oxidation of Silicon Carbide in a Wet Atmosphere*. *J. of Materials Science*, 1988. **23**(11): p. 3933-3938.
61. Rakowski, J. and B. Pint, *Observations of the Effect of Water Vapor on the Elevated Temperature Oxidation of Austenitic Stainless Steel Foil*. *Corrosion* 2000, 2000.
62. Passier, F., et al., *Thermal Oxidation of Metallic Niobium by Water Vapor*. *Oxidation of Metals*, 2001. **55**(1/2): p. 153-163.
63. Rabbani, F., L.P. Ward, and K.N. Strafford, *A Comparison of the Growth Kinetics and Scale Morphology for three Superalloys at 930C in Air and Low P(O₂) Environments*. *Oxidation of Metals*, 2000. **54**(1/2): p. 139-153.
64. Quadackers, W.J., et al. *Hot stage Microscopy of the Nucleation and Growth of Oxide Scales on Cr and Cr-Based Alloys*. in *Microscopy of Oxidation 3*. 1996. Trinity Hall, University of Cambridge.
65. Hilpert, K., et al., *Chromium Vapor Species over Solid Oxide Fuel Cell Interconnect Materials and Their potential for Degradation Processes*. *J. Electrochem. Soc.*, 1996. **143**(11): p. 3642-3647.
66. Gindorf, C., L. Singheiser, and K. Hilpert, *Cr vaporization from Fe, Cr base alloys used as interconnect in fuel cells*. *Steel Research*, 2001. **72**(11+12): p. 528-533.
67. Tai, W.-P., T. Watanabe, and N.S. Jacobson, *High-Temperature Stability of Alumina in Ar and Ar/Water-Vapor Environments*. *J. Am. Ceram. Soc.*, 1999. **82**(1): p. 245-248.

68. Tveten, B., G. Hultquist, and D. Wallinder, *Hydrogen and Yttria in Chromium: Influence on the High Temperature Oxidation Kinetics in O₂, Oxide Growth Mechanisms and Scale Adherence*. *Oxidation of Metals*, 2001. **55**(3/4): p. 279-289.
69. Hultquist, G., B. Tveten, and E. Hornlund, *Hydrogen in Chromium: Influence on the Oxidation Kinetics in H₂O, Oxide Growth Mechanism, and Scale Adherence*. *Oxidation of Metals*, 2000. **54**(1/2): p. 1-10.
70. Hultquist, G., et al., *Self-Repairing Metal Oxides*. *Oxidation of Metals*, 2001. **56**(3/4): p. 313-346.
71. Asteman, H., et al., *Influence of Water Vapor and Flow Rate on the High Temperature Oxidation of 304L; effect of Chromium Oxide Hydroxide Vaporization*. *Oxidation of Metals*, 2000. **54**(1/2): p. 11-26.
72. Asteman, H., et al., *Indication of Chromium Oxide Hydroxide Evaporation During Oxidation of 304L at 873K in the Presence of Water Vapor*. *Oxidation of Metals*, 1999. **52**(1/2): p. 95-111.
73. Sato, Y. and D.J. Young, *High Temperature Corrosion of Iron at 900C in Atmospheres Containing HCl and H₂O*. *Oxidation of Metals*, 2001. **55**(3/4): p. 243-260.
74. Hayashi, S. and T. Narita, *Competitive Effect of Water Vapor and Oxygen on the Oxidation of Fe-5 wt% Al Alloy at 1073K*. *Oxidation of Metals*, 2001. **56**(3/4): p. 251-270.
75. Jianian, S., Z. Longjiang, and L. Tiefan, *High Temperature Oxidation of Fe-Cr Alloys in Wet Oxygen*. *Oxidation of Metals*, 1997. **48**(3/4): p. 347-356.
76. Galerie, A., Y. Wouters, and M. Caillet, *The Kinetic Behavior of Metals in Water Vapor at High Temperatures: Can General Rules be Proposed?* *Materials Science Forum*, 2001. **369-372**: p. 231-238.
77. Henry, S., A. Galerie, and L. Antoni, *Abnormal Oxidation of Stabilized Ferritic Stainless Steels in Water Vapor*. *Materials Science Forum*, 2001. **369-372**: p. 353-360.
78. Henry, S., et al., *Characterization of Chromia Scales Grown on Pure Chromium in Different Oxidizing Atmospheres*. *Materials at High Temperatures*, 2000. **17**: p. 231-234.
79. Fukumoto, M., et al., *Effect of Water Vapor on the Oxidation Behavior of Fe-1.5Si in Air at 1073 and 1273K*. *Oxidation of Metals*, 2001. **55**(5/6): p. 401-422.
80. Buscail, H., et al., *Water-Vapor-Effect on the Oxidation of Fe-21.5wt%Cr-5.6wt%Al at 1000°C*. *Oxidation of Metals*, 1997. **47**(5/6): p. 445-464.
81. Fritscher, K. and Y.T. Lee, *Effect of Water Vapor on Oxidation and Creep Behavior of Incoloy 800 at Temperatures Between 850 and 980C*. *Oxidation of Metals*, 1989. **32**(3/4): p. 295-317.

82. Honda, K., et al., *Oxidation Behavior of SUS430 Stainless Steel in Moist Atmospheres at 873K*. *Oxidation of Metals*, 1992. **38**(5/6): p. 347-363.
83. Tveten, B., G. Hultquist, and T. Norby, *Hydrogen in Chromium: Influence on the High-Temperature Oxidation Kinetics in O₂, Oxide-Growth Mechanisms, and Scale Adherence*. *Oxidation of Metals*, 1999. **51**(3/4): p. 221-233.
84. Wouters, Y., A. Galerie, and J.-P. Petit, *Thermal Oxidation of Titanium by Water Vapor*. *Solid State Ionics*, 1997. **104**: p. 89-96.
85. Haensel, M., W.J. Quadackers, and D.J. Young, *Role of Water Vapor in Chromia-Scale Growth at Low Oxygen Partial Pressure*. *Oxidation of Metals*, 2003. **59**(3/4): p. 285-301.
86. Raynaud, G.M. and R.A. Rapp, *In Situ Observation of Whiskers, Pyramids and Pits During the High Temperature Oxidation of Metals*. *Oxidation of Metals*, 1984. **21**(1/2): p. 89-102.
87. Rapp, R.A., *The High Temperature Oxidation of Metals Forming Cation-Diffusing Scales*. *Metallurgical Transactions A*, 1983. **15A**: p. 765-782.
88. Asteman, H., Svensson, J.-E., Johansson, L.-G., and Norell, M., *Oxidation of Metals*, 1999. **52**: p. 161.
89. Hagel, W.C., *Factors Controlling the High-Temperature Oxidation of Chromium*. *Transactions of the ASM*, 1963. **56**: p. 583-599.
90. Tedmon, C.S.J., *The Effect of Oxide Volatilization on the Oxidation Kinetics of Cr and Fe-Cr Alloys*. *Journal of Electrochemical Society*, 1966: p. 766-768.
91. Bailey, J., *Volatile Cr Contamination Reduction in Atmospheric Pressure Chemical Vapor Deposition Systems by Selective Alloy Oxidation*. *J. Electrochem. Soc.*, 1997. **144**(10): p. 3568-3571.
92. Giggins, C.S. and F.S. Pettit, *The Oxidation of TD NiC (Ni-20Cr-2 vol pct ThO₂) Between 900°C and 1200°C*. *Metallurgical Transactions*, 1971. **2**: p. 1071-1078.
93. Asteman, H., J.-E. Svensson, and L.-G. Johansson, *Evidence for Chromium Evaporation Influencing the Oxidation of 304L: The Effect of Temperature and Flow Rate*. *Oxidation of Metals*, 2002. **57**(3/4): p. 193-216.
94. Pettit, F.S. and G.H. Meier., *Interaction of Steam-Air Mixtures with Turbine Airfoil Alloys and Coatings*, Research Progress Report, Submitted to the South Carolina Research and Development Center, 2003: Pittsburgh.
95. Harris, A.W. and A. Atkinson, *Oxygen Transport in Growing Nickel Oxide Scales at 600-800C*. *Oxidation of Metals*, 1990. **34**(3/4): p. 229-258.

96. Giggins, C.S. and F.S. Pettit, *Oxidation of Ni-Cr Alloys Between 800°C and 1200°C*. Transactions of the Metallurgical Society of AIME, 1969. **245**: p. 2495-2507.
97. Lowell, C.E., *Cyclic and Isothermal Oxidation Behavior of Some Ni-Cr Alloys*. Oxidation of Metals, 1973. **7**(2): p. 95-115.
98. Ecer, G.M. and G.H. Meier, *The Effect of Cr₂O₃ Volatilization on the Oxidation Kinetics of a Ni-Cr Alloy*. Scripta Metallurgica, 1973. **7**: p. 1189-1194.
99. Yamauchi, A., K. Kurokawa, and H. Takahashi, *Evaporation of Cr₂O₃ in Atmospheres containing H₂O*. Oxidation of Metals, 2003. **59**(5/6): p. 517-527.